Reclamation of polymer-containing produced water via electrodialysis

From process and membrane characterization to improved operation

Paulina Abigail Sosa Fernández

Propositions

1. Polymer-flooding produced water can be reclaimed after reducing its salinity through electrodialysis.
   (this thesis)

2. Polymer-flooding produced water desalination via electrodialysis requires adequate control on hydrodynamics.
   (this thesis)

3. Partially hydrolyzed polyacrylamide is more problematic than crude oil when electrodialyzing produced water.
   (this thesis)

4. Experiment over-simplification leads to irrelevant results.

5. Science skepticism is at least partially due to lack of effort of scientists to reach out to the general public.

6. Conscious consumption can beat unsustainable production.

7. Covid-19 type of crises are opportunities to mitigate the ongoing ecological disaster.

Propositions belonging to the thesis, entitled

"Reclamation of polymer-containing produced water via electrodialysis, *From process and membrane characterization to improved operation.*"

Paulina Abigail Sosa Fernández

Leeuwarden, September 11th, 2020

Reclamation of polymer-containing produced water via electrodialysis

From process and membrane characterization to improved operation

Paulina Abigail Sosa Fernández

Thesis committee

Promotor

Prof. Dr H.H.M. Rijnaarts
Professor of Environmental Technology
Wageningen University & Research

Co-promotors

Dr J.W. Post
Deputy Program Director
Wetsus, European Centre of Excellence for Sustainable Water Technology,
Leeuwarden

Dr H. Bruning
Assistant Professor, Environmental Technology
Wageningen University & Research

Prof. Dr F.A.M. Leermakers
Personal chair, Physical Chemistry and Soft Matter
Wageningen University & Research

Other members

Prof. Dr A. van der Padt, Wageningen University & Research
Dr S.G. Velizarov, Universidade Nova de Lisboa, Portugal
Prof. Dr D.C. Nijmeijer, Eindhoven University of Technology
Prof. Dr A. Nijmeijer, University of Twente, Enschede

Reclamation of polymer-containing produced water via electrodialysis

From process and membrane characterization to improved operation

Paulina Abigail Sosa Fernández

Thesis
submitted in fulfilment of the requirements for the degree of doctor
at Wageningen University
by the authority of the Rector Magnificus,
Prof. Dr A.P.J. Mol,
in the presence of the
Thesis Committee appointed by the Academic Board
to be defended in public
on Friday 11 September 2020
at 1:30 p.m. in De Harmonie, Leeuwarden.

Para mi familia

Table of contents

Chapter 1

Introduction

1.1 About oil, enhanced oil recovery, and polymer-flooding

To present date, crude oil remains the largest source of energy for humanity, accounting for nearly 34% of the primary energy consumed worldwide (**Figure 1.1**) [1]. Despite global concerns about the use of fossil fuels and climate change, in 2018 oil consumption grew 1.5%, while forecasts by the International Energy Agency (IEA) predict that oil demand will keep growing at least until 2024, with no peak in sight [1,2]. Meanwhile, environmental and societal pressure is increasing to come up with more sustainable solutions to meet this increasing demand. Since finding and exploiting new oil fields becomes more challenging and expensive, it is then necessary to maximize oil recovery from currently producing reservoirs [3]. By employing primary or conventional recovery methods, only 30% of the oil in a reservoir can be extracted, so most part of the oil potentially available is left behind [3,4]. Consequently, it is increasingly necessary to employ secondary (waterflooding or gas reinjection) and tertiary (thermal, gas injection, or chemical injection) oil recovery processes, which can increase the oil recovery to reach 50 to 80% [4].
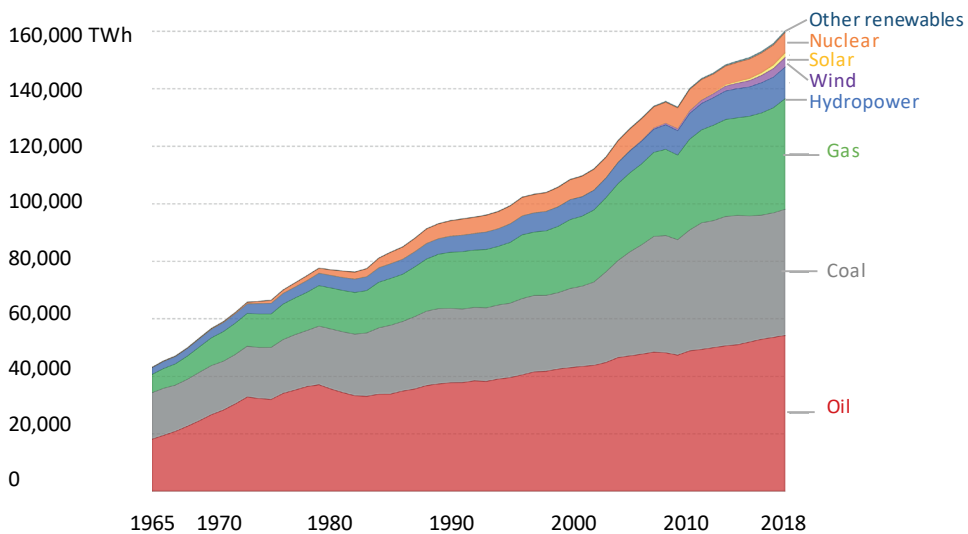
Figure 1.1. *Global primary energy consumption by source. Adapted from [5].*

Tertiary methods, most commonly known as enhanced oil recovery (EOR), work by increasing oil mobility in the matrix of the subsurface reservoir. These are mainly applied for recovering heavy and extra heavy crudes, oil sands, bitumen and shale oil. It is estimated that 3.6 % of the worldwide oil production in 2012 came from fields that utilize some form of EOR technique [6]. There are three kinds of EOR: gas injection, thermal, and chemical techniques. The latter, chemical enhanced oil recovery (cEOR), consists of injecting external fluids, containing polymers, surfactants and other chemicals, to increase oil mobility and improve its overall

flow. Although there are different kinds of cEOR methods (surfactant flooding, alkaline flooding, etc.), the most employed is polymer flooding, comprising 55% of the total EOR market in 2012 [4].

As shown in **Figure 1.2**, polymer flooding consists in injecting an aqueous viscous solution through an injector well to increase the oil recovery from existing oilfields [3]. The technique was implemented in numerous pilots and field injection tests mostly in the USA in last century during the 70-80s following the 70s oil crisis [7]. Today, it is considered a mature cEOR technique that has re-emerged due to a combination of increased demand, improvement of the polymers and chemicals available, and a better understanding of the process mechanisms. It has been recently applied in multiple projects around the world, including the USA, Canada, China, India, Angola, Brazil, and Oman, in most cases yielding successful results [4,6–8].
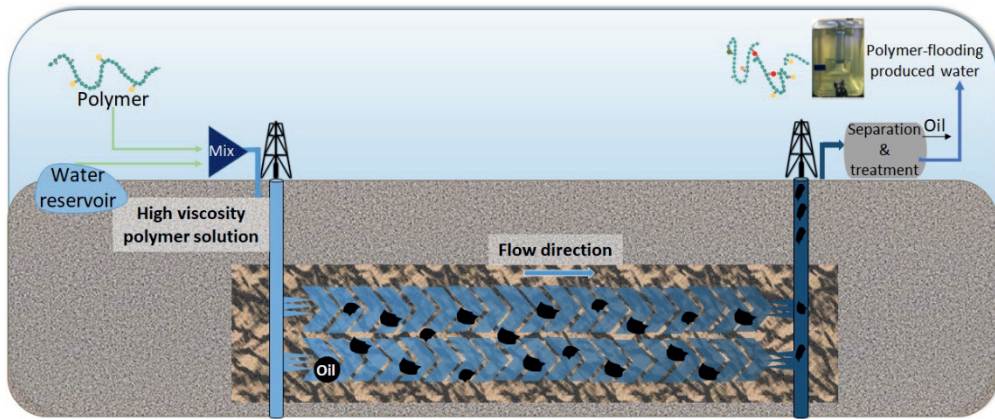

Figure 1.2. Scheme of a polymer flooding process. A viscous polymeric solution is injected through an injector well, and the mix of fluids is recovered in a production well.

1.2 Water cycle for EOR?

Besides chemicals, polymer flooding and most EOR processes require large amounts of water. It is usually estimated that to produce one barrel of oil with EOR, 4 to 8 barrels of water are needed [4]. In terms of absolute volume, the daily water demand can be estimated as 12 to 24 million barrels per day (BPD), equivalent to 2 to 4 million m3/day. The estimation considers the world average oil production in 2012 was 86 million BPD [1] and the fraction of oil production by EOR from section 1.1. This water can be obtained from different sources, depending on the location of the project. As shown in **Figure 1.3A**, for EOR projects performed inland, water sources are surface water (rivers, lakes), underground water, or produced water, the latter referring to water co-produced together with oil. Meanwhile, for the few projects developed offshore, the main water sources are seawater and produced water [9].

1
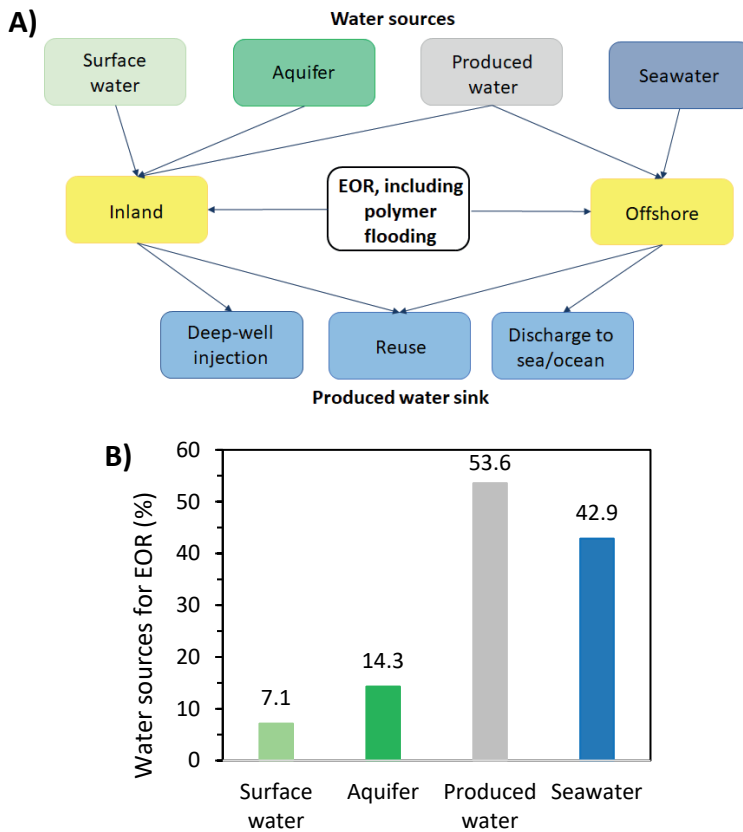
Figure 1.3. A) Schematic representation of the main water sources and produced water sinks depending on the location of the EOR project. B) Type of source water for EOR projects, adapted from [9].

Due to increased water demand for human consumption, general water scarcity, and stricter regulations, most EOR projects currently rely on produced water (inland) and seawater (offshore) to operate (**Figure 1.3B,** [9]). Furthermore, reusing produced water might soon become the only option to operate EOR projects in countries where legislation forbids the use of fresh potable water for oil well injection, like in Oman [10]. In terms of volume, reusing produced water makes much sense since oil and gas industry usually co-produces 3 to 10 barrels of water with each barrel of oil, depending on the age and location of the wells [11,12]. All these reasons point out towards produced water being the ideal water source for EOR treatments, at least in quantitative terms. However, there are also some constraints, as will be elucidated after explaining the working principle of polymer flooding and the parameters that influence the viscosity of the solutions.

1.3 About viscous solutions for polymer flooding and how they are influenced by salinity, ion composition, and temperature

It has been mentioned that polymer flooding utilizes viscous solutions to increase oil production. The viscous solutions operate at two scales: macro- and micro-scale. In the macro-scale, polymer flooding improves the sweep efficiency by reducing the mobility ratio between the displacing phase and the displaced phase through increasing water viscosity. Meanwhile, at the micro-scale, polymer flooding improves oil displacement efficiency due to the decreased elasticity of the solution due to the presence of the polymer [13,14]. The viscous solutions used in polymer flooding are prepared by adding high molecular weight polymers, mostly partially hydrolyzed polyacrylamide (HPAM) and its derivatives or, in selected cases, biopolymers, like xanthan gum [3,7,13].

HPAM is a copolymer of polyacrylamide (PAM) and poly(acrylic acid), obtained by partial hydrolysis of PAM or by copolymerization of sodium acrylate with acrylamide (**Figure 1.4**). HPAM and its derivatives have been extensively used in industry as flocculants, dispersants, retention aids, steric stabilizers, and associate thickeners in areas like wastewater treatment, mineral flotation, paper making, oil and coal refineries, and emulsion polymerization reactions [15]. When used in EOR, the degree of hydrolysis of the acrylamide monomers, which is also the fraction of carboxyl groups, is preferred to be between 25 and 35%. In this range, the HPAM solution has the right balance between viscosity gain on one hand, and sensitivity to the salinity and hardness of the solvent on the other [13], hardness being defined as the concentration of calcium and magnesium ions in a water-based solution [9].
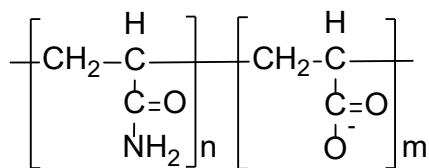
Figure 1.4. Partially hydrolyzed polyacrylamide (HPAM) molecule

The sensitivity to salinity, among many other factors, can be explained by considering that HPAM is a polyelectrolyte, that is, when dissolved in water its counterions may dissociate. However, attractive interactions between the poly-ion chain and the counterions still remain [16]. The counterions balance most of the charge inside the polymer coil, so their osmotic pressure makes the chain expand to larger sizes, resulting in the increased solution viscosity. Consequently, any factor that affects the charge distribution or the electrostatic interaction, can also influence the polyelectrolyte configuration and its global size or structure. For most polyelectrolytes, these factors include the degree of hydrolysis, the ionic strength,

the solvent quality, the solution pH value, the polyelectrolyte concentration, and the solution temperature [17]. All these factors, plus the molecular weight of the polyelectrolyte and its structure (linear, branched) influence the rheology of the aqueous solutions into which these polymers are dissolved.

To understand how these factors affect the viscosity of HPAM solutions, it is important to realize that the viscosity is a measurement of the intra- and inter-molecular interactions, that is, the interactions within the same molecule and with others. In solutions with low polymer concentration, intramolecular associations dominate, which is known as the dilute region. The hydro-dynamic volume is reduced and therefore the viscosity of the subsequent polymer solutions. When the polymer concentration is increased the solution moves to the semi-dilute region where intermolecular associations dominate. This leads then to network-like formations (transient networks) which substantially increase the viscosity of the solution [13]. The transition from the dilute to the semi-dilute regime is known as the critical overlap concentration (C*), defined as the concentration at which individual polymer molecules begin to interact (see **Figure 1.5**). This explains why solutions with higher viscosities are obtained when using higher concentrations of HPAM, HPAM with large molecular weights (MW), or branched HPAM derivatives [18–21].
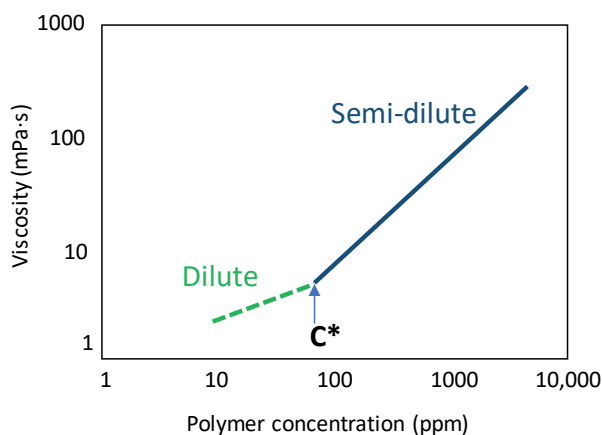
Figure 1.5. *Scheme representing the critical overlap concentration C*, with the transition between the dilute and semi-dilute regimes. Based on Figure 7 in [20].*

The effect of ionic strength, commonly referred as salinity, in the rheology of HPAM solutions has been also addressed in several studies [19,21–28]. All of them confirm the inverse relationship between viscosity and ionic strength, so the higher the ionic strength, the lower the viscosity of an HPAM solution with fixed concentration. Furthermore, the type of salts dissolved in the solution also have a great influence in the viscosity. Multivalent cations present in the water affect the properties of

HPAM solutions much stronger than monovalent cations. Depending on the salt concentration and shear rate, the viscosity of HPAM solutions with multivalent salts can have one order of magnitude lower viscosity compared to solutions with the same ionic strength of monovalent ions [9,21,28,29]. There are two reasons to explain this behavior: multivalent ions have a stronger charge shielding effect, and they also act as cross-linking agents that interconnect two or more polymer molecules or two regions of the same one through covalent bonds, further influencing the conformation and rheological behavior of HPAM solutions [28].

1.4 Produced water must be treated before reused to confect viscous polymer-flooding solution

As can be inferred from the previous section, polymer flooding requires water of certain characteristics, which do not correspond to those of produced water. In terms of quality, produced water can contain high salinity and diverse pollutants, so for most applications it must be treated before being reused [30–32]. If produced water is to be reinjected in conventional waterflooding (secondary recovery), it must be only partially treated before being injected back in the subsoil [33]. However, when EOR techniques are to be applied, higher water quality is required, as explained in section 1.3. Thus, to be reused, produced water should to go through a series of treatment steps, which may vary depending on its characteristics. At large, the water must pass by a primary stage (hydrocyclone, corrugated plate separator, API separator, or similar) followed by a secondary treatment, which can be a floater or a nutshell filter. Finally, for certain cases, polishing and desalination steps are also needed [33,34].

If water with high salinity or with high content of multivalent cations is used to prepare a viscous solution for injection, either larger amounts of polymer need to be added or more specialized (and expensive, and sometimes less environmentally friendly) polymer formulations are needed [9,13]. In that case, additional to the economic impact of using more chemicals, there is an environmental impact due to increased polymer contamination in the produced streams.

Furthermore, there are also arguments for performing EOR with water that is low in sulfate and other divalent anions. Sulfate present in produced water can be converted to hydrogen sulfide (H_2S) by thermophilic sulfate-reducing bacteria, causing reservoir souring problems. In addition, water with high carbonate and sulfate content is prone to cause scaling, which occurs normally in the form of calcium or strontium salts. These salts can precipitate in surface facilities, injection or production wells, or downhole in the reservoir, triggering miscellaneous operational problems [35–37].

Given the aforementioned reasons, polymer flooding solution should be prepared with soft and/or low-salinity water, preferably with TDS in the range of 500 to 1000 ppm [35]. Regarding hardness, just 500 ppm of calcium decreases in half the viscosity of the solution [9]. However, low-salinity water is rarely available on location. As shown in **Figure 1.6**, nearly 90% of the EOR projects recently surveyed used water with salinities above 1,000 mg/L, most of them above 10,000 mg/L [9]. Produced water can have even higher salinities, in the range between 2,600 and 360,000 mg/L [11]. Even though high-salinity water (TDS above 80,000 mg/L) has been employed to prepare viscous polymer solution [7], nowadays it can be more cost-competitive to include a desalination step in the process and to prepare the polymer flooding solution in low-salinity water [35]. In that case, seawater desalination is a relatively standard procedure, while produced water desalination becomes more challenging due to its complex composition and variability, so treatment schemes are being still investigated.
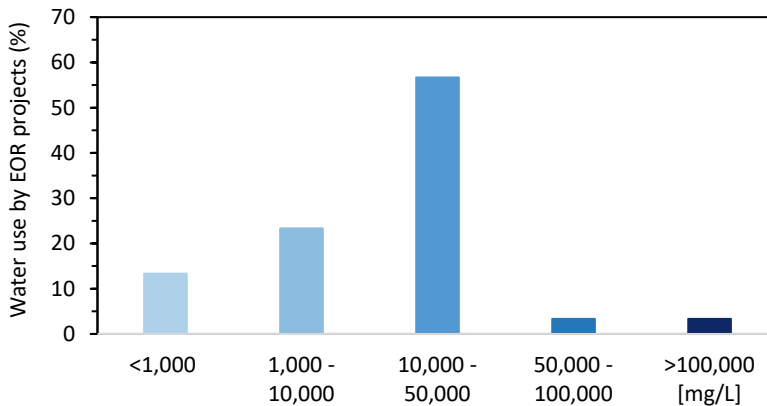
Figure 1.6. Approximate salinity of the source water for EOR projects. Figure adapted from [9].

1.5 Technologies for produced water softening and desalination

Advanced treatments for produced water include softening (the focus is on removing multivalent cations) and desalination, and their application depend on the intended use of the water. Softening is mainly performed to avoid scaling, that could otherwise plug the reservoir and/or damage injection equipment [4], while desalination can be performed to comply for criteria for discharge to surface waters, or to reuse the water for irrigation, for low-salinity waterflooding, or for EOR applications.

There are several technologies currently available to reduce the salinity and hardness of conventional produced water (PW). The mature technologies that can be used either for desalination or softening purposes are i) thermal processes like evaporation, multistage flash distillation, mechanical vapor compression (MVC),

and multi-effect distillation; ii) pressure-based membrane treatments: reverse osmosis (RO) and nanofiltration (NF), iii) electrodialysis (ED) and similar electro-membrane processes, and iv) other mature softening processes, like ion exchange and chemical precipitation [4,33,38]. Since it would be very extensive to describe all these technologies, only those with recent developments reported recently in the scientific literature (<10 years), are compared in **Table 1.1** (as a reference, 1 bbl = 0.159 m^3). Further information about these and other treatments can be found in recent literature reviews [11,30–33,38–40].

When performing the mentioned literature review, two technologies stood out due to the elevated number of mentions: forward osmosis (FO) and membrane distillation (MD) [41,42]. Although they are still under development, they have been identified as potentially applicable for PW desalination. Hence, their main characteristics are summarized in **Table 1.2**.

Yet, it must be considered that in most cases, a single technology cannot supply a water product with the desired quality, so many technology-providing companies offer treatment processes that make use of two or more softening/desalination technologies [33].

Table 1.1. Comparison of selected mature technologies suitable for produced water softening and desalination

Technology	Applicability	Advantages	Disadvantages	Energy use
MVC [39,43]	TDS removal up to 200,000 mg/L	Modular design, lower capital costs, reduced operating costs, less prone to fouling by oil and grease, less intensive pre-treatment, recycling reduces the need for disposal, highly reliable and efficient for desalination of PW.	High energy requirements and high operational costs associated with improvements of heat transfer coefficient	10.4−13.6 kWh/m^3
RO [30,44,45]	TDS removal (<40,000 mg/L)	Robust technology for monovalent salts removal, high pH tolerance, automated operation, no chemicals used, potential for energy reduction through process modifications, treatment of	Sensitive to organics and inorganics in the feed stream, vulnerable to membrane fouling, sensitive to high temperature (>40°C),	0.46 – 0.67 kWh/bbl and 0.02 – 0.13 kWh/bbl for seawater and brackish water

1

		concentrate not needed, water recovery of 30% – 60% for seawater and 60% - 85% for brackish water.	intensive pre-treatment required for PW desalination.	desalination respectively.
NF [30,31]	TDS removal (500-25,000 mg/L)	Removes multivalent ions at a lower pressure than RO, high pH tolerance, easily automated operation, no solid waste generation, lower energy costs by use of energy recovery subsystems, water recovery between 75% and 90% is possible.	Prone to membrane fouling, secondary waste production, highly sensitive to organic and inorganic pollutants in the feed, vulnerable to high operational temperature, requires backwashing	0.08 kWh/bbl.
ED [30,46]	TDS removal (500-160,000 mg/L)	Cost-effective for the treatment of produced waters with relatively low TDS. Robust technology for water reclamation. Desalination % can be easily adjusted. Membranes less sensitive to fouling compared to other processes. Selective removal of ions and small charged molecules.	High operation costs for treatment of concentrated produced waters. Relatively high CAPEX. Process requires periodic maintenance. Membranes prone to fouling.	0.31-0.44 kWh/kg of NaCl equivalents removed

Table 1.2. Comparison of technologies under development for produced water desalination

Technology	Applicability	Advantages	Disadvantages	Energy use
FO [43,44,47]	TDS (500 – 175,000) mg/l and dissolved organics removal	Low applied pressure thus lower fouling potential, inexpensive, high water recovery, simple, no need for pre-treatment, high rejection of all	Re-concentration of the draw solution is needed thus extra cost, membrane	0.46 – 0.67 kWh/bbl for seawater desalination.

		contaminants, membrane fouling is reversible, the potential for regeneration of draw solution.	cleaning often required.	
MD [43,44]	Salts and hydrocarbons removal (TDS up to 300,000 mg/l)	Highly saline water desalination is possible, lower membrane fouling, no applied pressure, lower operating temperatures, e.g., in VMD, high TDS rejection, non-volatiles removal, a modular design utilizing plastics thus avoiding corrosion, feed salt concentration does not affect performance, different energy sources can be employed.	Membrane fouling in the case of hydrophobic membrane, mineral scaling, pre-treatment of feed water is required, low flux.	Energy use depends on configuration. On average, its 6.83 kWh/bbl without waste heat and 1.63 kWh/bbl with waste heat.

1.6 Suitability of desalination technologies for treating polymer-flooding produced water

All the desalination technologies enlisted in the previous section have been applied to desalinate conventional produced water. However, when EOR technology is applied, the chemicals added to the injected solution are also recovered with the produced water, increasing its complexity. Since polymer-flooding is the most employed cEOR technique, and most of the polymers employed are not easily biodegradable, "polymer flooding-produced water" (PFPW) should receive special attention [48].

In principle, PFPW could be treated with the same technologies used to desalinate conventional produced water. For example, when thermal methods are applied, the presence of polymer does not have a large influence, since these are robust technologies with little sensitivity to the presence of organics, most of which are degraded by physical-chemical processes that are enhanced at high temperatures. Moreover, the desalinated stream consists basically of demineralized water, free from salts and polymers, and thus would need to be partially salted again, and fresh polymer added in order to be used as viscous flooding solution. Hence, this method is less resource-efficient in terms of polymer recovery and reuse.

Another mature technology for desalination is nanofiltration. Here the main problem is that the membranes are sensitive to fouling, and that extensive pre-treatments such as ultrafiltration must be applied, often repeatedly [49]. Moreover, it has been reported that considerable amounts of polymer pass the ultrafiltration membranes [50], leaving the NF membranes still exposed to fouling [51]. Furthermore, the NF water products would be i) a partially desalted stream for reuse and reinjection, still needing fresh polymer to be added, and ii) a rejected solution that would still contain polymer plus salts, which is not useful for reuse and reinjection, and thus becomes as waste stream that needs to be treated before being discharged into the environment. Something similar would be expected in the case of applying reverse osmosis, but since even trace amounts of oil and grease can cause membrane fouling [11], very intensive pre-treatment methods would be needed.

Electrodialysis (ED) is another technology emerging in the field of PFPW desalination [52]. As presented in **Figure 1.7**, ED works by applying an electric potential through two electrodes situated at the sides of a stack composed of anion and cation exchange membranes arranged in an alternate form. The imposed potential drives the cations towards the cathode (-, a negative potential), while anions go towards the anode (+, a positive potential), which combined with the stack configuration causes the depletion of ions in some channels and their concentration in others. Compared to other desalination technologies, it offers two advantages for treating PFPW:

a) Since it is an ion-selective technology, salts are transported through the membranes while the polymer remains in the desalinating solution, reusing the polymer could be a possibility.

b) ED allows the degree of desalination to be easily controlled. Thus, the product is obtained already containing the desired salinity, avoiding the step of partially mineralizing the stream.

Being able to reuse the back-produced polymer instead of spending energy and resources to degrade it results a very attractive option, which makes electrodialysis a very suitable desalination process. Furthermore, this option results beneficial since it would minimize the pollution caused by produced water disposal while assuring a reliable supply of water for the EOR projects [53]. If less polymer is required, the impact is also favorable in terms of chemical procurement, transportation, storage and handling (mixing and hydration) requirements and operating costs.
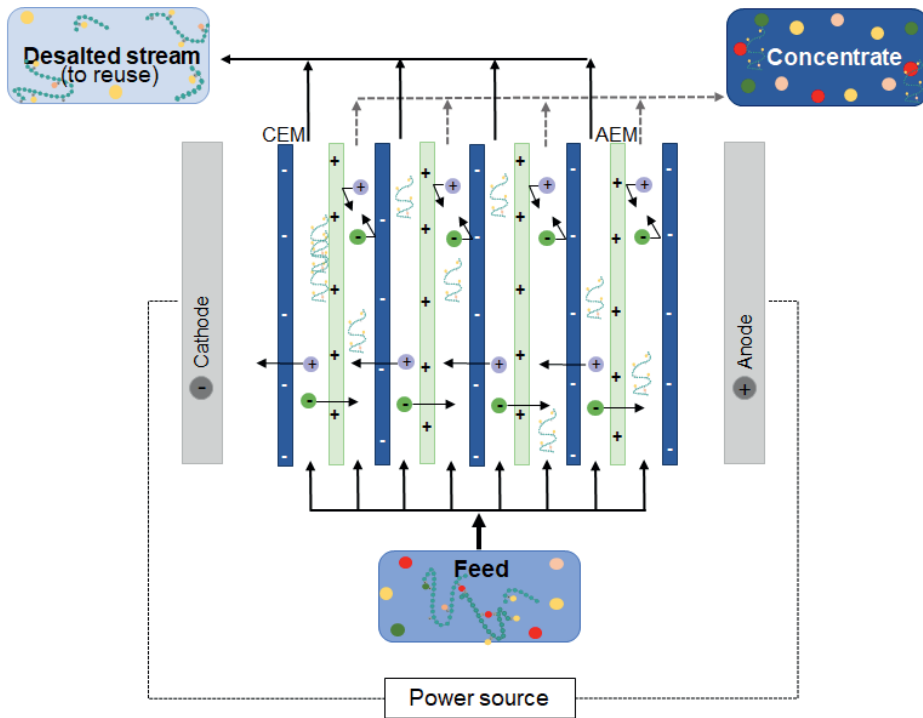
Figure 1.7. *Electrodialysis for (polymer-flooding) produced water desalination.*

1.7 Current state of art and challenges for electrodialysis of polymer-flooding produced water

Although the first reported application of electrodialysis to desalinate PFPW dates to a few years ago, it has already been proven to be a promising option for desalting PFPW. In China, where the largest polymer-flooding project in the world is being developed, an ED pilot plant has been operating for a few years [54]. However, there are still several issues to be investigated and solved, which can be grouped in five areas:

a) Influence of PFPW composition and conditions. Until now, most of the available literature about PFPW electrodialysis refers to the Daqing filed, in China. However, PFPW composition and temperature varies enormously in ionic composition, salt concentration, and temperature from place to place [55]. Would electrodialysis still be applicable for all these cases with different compositions and temperatures? And, would the treated water with polymer, for all these cases, be suitable for reuse? Since scarce literature reports on the effectivity of ED desalination and polymer recovery as function of PFPW ionic

composition and temperature, this has been identified as a relevant knowledge gap.

b) Removal of multivalent ions. It has been stated that complete desalination of the stream is generally not required for PFPW reuse for reinjection. However, multivalent ions cause the most severe problems in terms of scaling and lost polymer viscosity activity, so these ions should be preferentially removed. In the literature, insufficient and contradictory information is available on the possibilities to tailor ED for the specific removal of multivalent ions, hence this is also an important knowledge gap.

c) Fouling. From the available scientific literature and information from practice (personal communication with the members of the Wetsus Desalination theme), this is the biggest problem to be addressed. Most of the polymers added to prepare the viscous solution are polyelectrolytes, that is, they are, in overall, negatively charged in solution, which attracts them towards the also charged ion-exchange membranes, especially the positively charged anion exchange membranes. Again, considering that PFPW composition would vary depending on the geographical location and specific case conditions, it is desirable to know how the ionic composition of the feed water would influence fouling. Important questions to be resolved are which membrane characteristics would make the membranes less prone to fouling by PFPW and which operational conditions should be applied to the ED-system to minimize fouling.

d) Preservation of the polymer integrity and its viscosifying activity during and after electrochemical treatments like ED.

e) Overall energy and material efficiency in terms of resource utilization and minimization of negative impacts to the environment.

1.8   Aim and outline

The objective of this work is to improve the scientific understanding of the desalination of synthetic polymer flooding produced water via electrodialysis and the practical conditions relevant for its reuse to prepare viscous flooding solution. To summarize, from the state of art and knowledge gaps addressed in the previous paragraph, the following research questions were identified:

1) How do PFPW composition and temperature influence the electrodialysis performance?

2) Would it be possible to preferentially remove multivalent ions from PFPW without completely desalinating it? Under which conditions?

3) What kind of fouling is formed on the ion-exchange membranes when desalting PFPW and how is it affected by its composition?

4) Which methods are the most suitable to minimize fouling by PFPW?

5) Which operational conditions result in improved electrodialysis performance?

6) What is the overall energy and material efficiency of ED PFPW treatment in terms of resource efficiency and sustainability?

These questions leaded to the outline of the thesis (**Figure 1.8**) which is now presented.
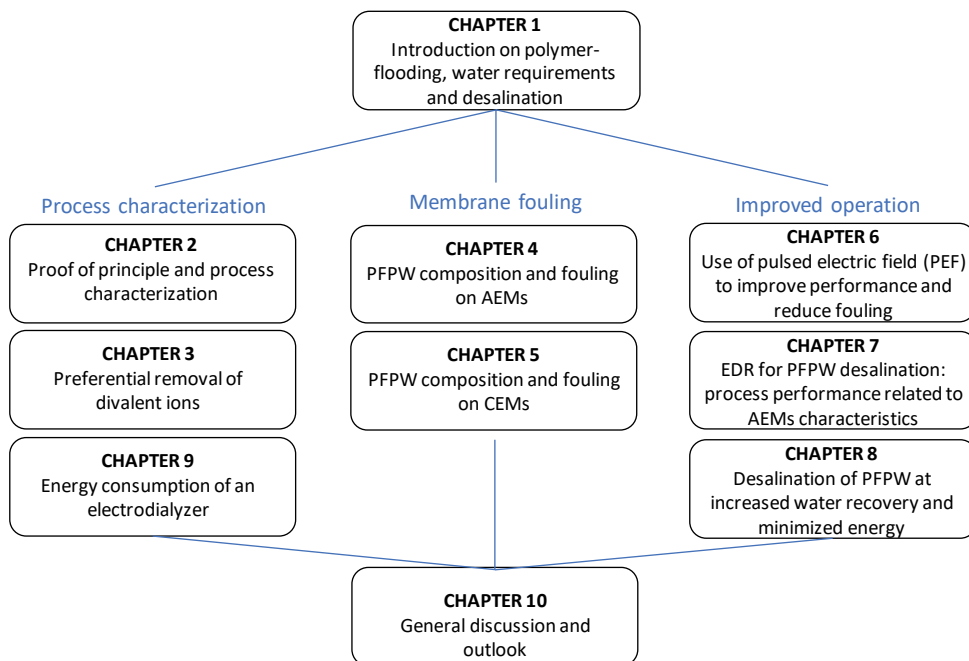
Figure 1.8. Structure of this thesis.

First, considering that PFPW composition and temperature differ greatly from location to location, **Chapter 2** explores PFPW desalination and reuse at selected conditions (RQ1). In this chapter, we aimed to find out which were the most challenging conditions to perform electrodialysis of PFPW, and how suitable would it be to prepare fresh viscous solution with the desalinated PFPW.

In **Chapter 3**, we evaluate the possibility of preferentially removing divalent ions from synthetic PFPW conditioned at different temperatures by varying the applied current density (RQ2).

In **Chapters 4 and 5**, we investigate the effects of polymer-flooding produced water composition and the fouling mechanism for the anion and cation exchange membranes, respectively (RQ3).

Chapters 6, 7, and 8 explore different options to minimize fouling (RQ4) and improve the electrodialysis performance (RQ5) when desalinating PFPW. In **Chapter 6**, we utilize a relatively new mode of operation, pulsed electric field, which has been positively evaluated in the literature to minimize concentration polarization and fouling. In **Chapter 7**, we analyze how the use of AEMs with specific properties would impact the desalination performance when operated in ED reversal mode. Later, in **Chapter 8**, we use the knowledge gathered along previous chapters to propose an improved operation mode that considers the water recovery-energy-membrane area tradeoff.

In addition, since the application of electrodialysis to desalinate viscous solutions is unusual, **Chapter 9** investigates the energetic consequences of working with this kind of feed streams in terms of desalination and pumping energy consumption (RQ6).

Finally, **Chapter 10** includes a general discussion about the findings presented in this thesis, and an outlook of the application of electrodialysis to desalinate industrial water containing charged polymers.

References

[1]   BP, BP Statistical Review of World Energy, 2019. https://www.bp.com/content/dam/bp/business-sites/en/global/corporate/pdfs/energy-economics/statistical-review/bp-stats-review-2019-full-report.pdf.

[2]   International Energy Agency (IEA), Oil 2019. Analysis and forecast to 2024, 2019. www.iea.org.

[3]   M.S. Kamal, A.S. Sultan, U.A. Al-Mubaiyedh, I.A. Hussein, Review on Polymer Flooding: Rheology, Adsorption, Stability, and Field Applications of Various Polymer Systems, Polymer Reviews. 55 (2015) 491–530. doi:10.1080/15583724.2014.982821.

[4]   J.A. Herschell, Water and Wastewater Treatment for Enhanced Oil Recovery, Mahon, Cork, Ireland, 2016.

[5]   H. Ritchie, M. Roser, Fossil fuels, Our World in Data. (2020). https://ourworldindata.org/fossil-fuels (accessed February 2, 2020).

[6]   L. Henthorne, W. Standard, J. Walsh, V. Llano, W. Standard, Water Management for EOR Applications - Sourcing , Treating, Reuse and Recycle, SPE Offshore Technology Conference. (2013) 1–13.

[7]   D.C. Standnes, I. Skjevrak, Literature review of implemented polymer field projects, Journal of Petroleum Science and Engineering. 122 (2014) 761–775. doi:10.1016/j.petrol.2014.08.024.

[8]   J.J. Sheng, B. Leonhardt, N. Azri, Status of Polymer-Flooding Technology, Journal of Canadian Petroleum Technology. 54 (2015) 116–126. doi:10.2118/174541-PA.

[9]   L. Henthorne, G.A. Pope, U. Weerasooriya, V. Llano, Impact of Water Softening on Chemical
        Enhanced Oil Recovery, in: Proceedings - SPE Symposium on Improved Oil Recovery 2014,
        SPE, Tulsa, Oklahoma, 2014.

[10]   S. of O. Ministry of Oil & Gas, Oil & Gas Law, 2011.
        http://www.oman.om/wps/wcm/connect/f5b459d2-584d-42a9-b766-
        f8f555567763/10Oil+and+Gas+Law+%28Royal+Decree+No.+4274%29.pdf?MOD=AJPERES.

[11]   A. Fakhru'l-Razi, A. Pendashteh, L.C. Abdullah, D.R.A. Biak, S.S. Madaeni, Z.Z. Abidin, Review
        of technologies for oil and gas produced water treatment, Journal of Hazardous Materials.
        170 (2009) 530–551. doi:10.1016/j.jhazmat.2009.05.044.

[12]   R. Arnold, D.B. Burnett, J. Elphick, T.J. Feeley III, M. Galbrun, M. Hightower, Z. Jiang, M.
        Khan, M. Lavery, F. Luffey, P. Verbeek, Managing Water - From Waste to Resource, Oilfield
        Review. 16 (2004) 26–41.
        http://www.slb.com/~/media/Files/resources/oilfield_review/ors04/sum04/04_managing_
        water.pdf.

[13]   D.A.Z. Wever, F. Picchioni, A.A. Broekhuis, Polymers for enhanced oil recovery: A paradigm
        for structure-property relationship in aqueous solution, Progress in Polymer Science
        (Oxford). 36 (2011) 1558–1628. doi:10.1016/j.progpolymsci.2011.05.006.

[14]   B. Wei, L. Romero-Zerón, D. Rodrigue, Oil displacement mechanisms of viscoelastic
        polymers in enhanced oil recovery (EOR): a review, Journal of Petroleum Exploration and
        Production Technology. 4 (2014) 113–121. doi:10.1007/s13202-013-0087-5.

[15]   K. Lewandowska, Comparative Studies of Rheological Properties of Polyacrylamide and
        Partially Hydrolyzed Polyacrylamide Solutions, Journal of Applied Polymer Science. 103
        (2007) 2235–2241. doi:10.1002/app.25247.

[16]   M. Ullner, K. Qamhieh, B. Cabane, Osmotic pressure in polyelectrolyte solutions: cell-model
        and bulk simulations, Soft Matter. 14 (2018) 5832–5846. doi:10.1039/c8sm00654g.

[17]   J. Kanatharana, J. Sukpisan, A. Sirivat, S.Q. Wang, On the correlation between the viscosity
        of partially hydrolyzed polyacrylamide solution and the diffusion coefficient in the
        semidilute concentration regime, Polymer Engineering and Science. 36 (1996) 2986–2995.
        doi:10.1002/pen.10701.

[18]   D.A.Z. Wever, F. Picchioni, A.A. Broekhuis, Comblike polyacrylamides as flooding agent in
        enhanced oil recovery, Industrial and Engineering Chemistry Research. 52 (2013) 16352–
        16363. doi:10.1021/ie402526k.

[19]   J.C. Jung, K. Zhang, B.H. Chon, H.J. Choi, Rheology and polymer flooding characteristics of
        partially hydrolyzed polyacrylamide for enhanced heavy oil recovery, Journal of Applied
        Polymer Science. 127 (2013) 4833–4839. doi:10.1002/app.38070.

[20]   L.F. Lopes, B.M.O. Silveira, R.B.Z.L. Moreno, Rheological Evaluation of HPAM fluids for EOR
        Applications, International Journal of Engineering & Technology IJET-IJENS. 14 (2014) 35–
        41.

[21]   C. Gao, Empirical correlations for viscosity of partially hydrolyzed Polyacrylamide, Journal of
        Petroleum Exploration and Production Technology. (2013) 209–213. doi:10.1007/s13202-
        013-0064-z.

[22]   M. Rashidi, A.M. Blokhus, A. Skauge, Viscosity Study of Salt Tolerant Polymers, Journal of
        Applied Polymer Science. 117 (2010) 1551–1557. doi:10.1002/app.

[23]   A. Aitkadi, P.J. Carreau, G. Chauveteau, Rheological Properties of Partially Hydrolyzed

Polyacrylamide Solutions Rheological Properties of Partially Hydrolyzed Polyacrylamide Solutions, Journal of Rheology. 31 (1987) 537–561. doi:10.1122/1.549959.

[24]   R. Zhang, X. He, S. Cai, K. Liu, Rheology of diluted and semi-diluted partially hydrolyzed polyacrylamide solutions under shear: Experimental studies, Petroleum. 3 (2017) 258–265. doi:10.1016/j.petlm.2016.08.001.

[25]   A.M. Mansour, R.S. Al-maamari, A.S. Al-hashmi, A. Zaitoun, H. Al-sharji, In-situ rheology and mechanical degradation of EOR polyacrylamide solutions under moderate shear rates, Journal of Petroleum Science and Engineering. 115 (2014) 57–65. doi:10.1016/j.petrol.2014.02.009.

[26]   Y. Feng, B. Grassl, L. Billon, A. Khoukh, J. François, Effects of NaCl on steady rheological behaviour in aqueous solutions of hydrophobically modified polyacrylamide and its partially hydrolyzed analogues prepared by post-modification, Polymer International. 51 (2002) 939–947. doi:10.1002/pi.959.

[27]   L. Yang, W. Zhihua, L. Xianli, L. Xinpeng, W. Xiaotong, ASP flooding produced water management: Evaluation, disposal and reuse, Society of Petroleum Engineers - SPE Middle East Health, Safety, Environment and Sustainable Development Conference and Exhibition, MEHSE 2014. (2014) 305–318. doi:10.2118/170396-ms.

[28]   A. Samanta, A. Bera, K. Ojha, A. Mandal, Effects of alkali, salts, and surfactant on rheological behavior of partially hydrolyzed polyacrylamide solutions, Journal of Chemical and Engineering Data. 55 (2010) 4315–4322. doi:10.1021/je100458a.

[29]   K.C. Tam, C. Tiu, Role of ionic species and valency on the steady shear behavior of partially hydrolyzed polyacrylamide solutions, Colloid & Polymer Science. 268 (1990) 911–920. doi:10.1007/BF01469369.

[30]   E.T. Igunnu, G.Z. Chen, Produced water treatment technologies, International Journal of Low-Carbon Technologies. 9 (2014) 157–177. doi:10.1093/ijlct/cts049.

[31]   E. Drioli, A. Ali, Y.M. Lee, S.F. Al-Sharif, M. Al-Beirutty, F. Macedonio, Membrane operations for produced water treatment, Desalination and Water Treatment. 3994 (2015) 1–19. doi:10.1080/19443994.2015.1072585.

[32]   J.M. Dickhout, J. Moreno, P.M. Biesheuvel, L. Boels, R.G.H. Lammertink, W.M. de Vos, Produced water treatment by membranes: A review from a colloidal perspective, Journal of Colloid and Interface Science. 487 (2017) 523–534. doi:10.1016/j.jcis.2016.10.013.

[33]   S. Jiménez, M.M. Micó, M. Arnaldos, F. Medina, S. Contreras, State of the art of produced water treatment, Chemosphere. 192 (2018) 186–208. doi:10.1016/j.chemosphere.2017.10.139.

[34]   J. Guolin, W. Xiaoyu, H. Chunjie, The effect of oilfield polymer-flooding wastewater on anion-exchange membrane performance, Desalination. 220 (2008) 386–393. doi:10.1016/j.desal.2007.03.010.

[35]   S.C. Ayirala, E. Uehara-Nagamine, A.N. Matzakos, R.W. Chin, P.H. Doe, P.J. van den Hoek, A Designer Water Process for Offshore Low Salinity and Polymer Flooding Applications, SPE Improved Oil Recovery Symposium. (2013). doi:10.2118/129926-MS.

[36]   R. Cord-Ruwisch, W. Kleinitz, F. Widdel, Sulfate-reducing Bacteria and Their Activities in Oil Production, Journal of Petroleum TechnologyTechnology. (1987) 10. doi:10.2118/13554-PA.

[37]   M.S.H. Bader, Sulfate removal technologies for oil fields seawater injection operations, Journal of Petroleum Science and Engineering. 55 (2007) 93–110.

1

doi:10.1016/j.petrol.2006.04.010.

[38]   M. Nasiri, I. Jafari, B. Parniankhoy, Oil and Gas Produced Water Management: A Review of Treatment Technologies, Challenges, and Opportunities, Chemical Engineering Communications. 204 (2017) 990–1005. doi:10.1080/00986445.2017.1330747.

[39]   J.M. Estrada, R. Bhamidimarri, A review of the issues and treatment options for wastewater from shale gas extraction by hydraulic fracturing, Fuel. 182 (2016) 292–303. doi:10.1016/j.fuel.2016.05.051.

[40]   J. Zheng, B. Chen, W. Thanyamanta, K. Hawboldt, B. Zhang, B. Liu, Offshore produced water management: A review of current practice and challenges in harsh/Arctic environments, Marine Pollution Bulletin. 104 (2016) 7–19. doi:10.1016/j.marpolbul.2016.01.004.

[41]   C. Murray-Gulde, J.E. Heatley, T. Karanfil, J.H. Rodgers, J.E. Myers, Performance of a hybrid reverse osmosis-constructed wetland treatment system for brackish oil field produced water, Water Research. 37 (2003) 705–713. doi:10.1016/S0043-1354(02)00353-6.

[42]   S. Munirasu, M.A. Haija, F. Banat, Use of membrane technology for oil field and refinery produced water treatment—A review, Process Safety and Environmental Protection. 100 (2016) 183–202. doi:10.1016/j.psep.2016.01.010.

[43]   D.L. Sha, L.H.A. Chavez, M. Ben-Sasson, S. Romero-Vargas Castrillon, N.Y. Yip, M. Elimelech, Desalination and Reuse of High-Salinity Shale Gas Produced Water: Drivers, Technologies, and Future Directions, Environmental Science and Technology. 47 (2013) 9569–9583. doi:10.1021/es401966e.

[44]   A. Subramani, J.G. Jacangelo, Emerging desalination technologies for water treatment: A critical review, Water Research. 75 (2015) 164–187. doi:10.1016/j.watres.2015.02.032.

[45]   S.A. Dastgheib, C. Knutson, Y. Yang, H.H. Salih, Treatment of produced water from an oilfield and selected coal mines in the Illinois Basin, International Journal of Greenhouse Gas Control. 54 (2016) 513–523. doi:10.1016/j.ijggc.2016.05.002.

[46]   L. Dallbauman, T. Sirivedhin, Reclamation of Produced Water for Beneficial Use, Separation Science and Technology. 40 (2005) 185–200. doi:10.1081/SS-200041910.

[47]   P. Jain, M. Sharma, P. Dureja, P.M. Sarma, B. Lal, Bioelectrochemical approaches for removal of sulfate, hydrocarbon and salinity from produced water, Chemosphere. 166 (2017) 96–108. doi:10.1016/j.chemosphere.2016.09.081.

[48]   X. Zhao, L. Liu, Y. Wang, H. Dai, D. Wang, H. Cai, Influences of partially hydrolyzed polyacrylamide (HPAM) residue on the flocculation behavior of oily wastewater produced from polymer flooding, Separation and Purification Technology. 62 (2008) 199–204. doi:10.1016/j.seppur.2008.01.019.

[49]   X. Qiao, Z. Zhang, J. Yu, X. Ye, Performance characteristics of a hybrid membrane pilot-scale plant for oilfield-produced wastewater, Desalination. 225 (2008) 113–122. doi:10.1016/j.desal.2007.04.092.

[50]   H. Guo, L. Xiao, S. Yu, H. Yang, J. Hu, G. Liu, Y. Tang, Analysis of anion exchange membrane fouling mechanism caused by anion polyacrylamide in electrodialysis, Desalination. 346 (2014) 46–53. doi:10.1016/j.desal.2014.05.010.

[51]   R. Zhang, W. Shi, S. Yu, W. Wang, Z. Zhang, B. Zhang, L. Li, X. Bao, Influence of salts, anion polyacrylamide and crude oil on nanofiltration membrane fouling during desalination process of polymer flooding produced water, Desalination. 373 (2015) 27–37. doi:10.1016/j.desal.2015.07.006.

[52]   G. Jing, X. Wang, H. Zhao, Study on TDS removal from polymer-flooding wastewater in crude oil: extraction by electrodialysis, Desalination. 244 (2009) 90–96. doi:10.1016/j.desal.2008.04.039.

[53]   G. Jing, L. Xing, S. Li, C. Han, Reclaiming polymer-flooding produced water for beneficial use: Salt removal via electrodialysis, Desalination and Water Treatment. 25 (2011) 71–77. doi:10.5004/dwt.2011.1766.

[54]   J. Guolin, X. Lijie, L. Yang, D. Wenting, H. Chunjie, Development of a four-grade and four-segment electrodialysis setup for desalination of polymer-flooding produced water, Desalination. 264 (2010) 214–219. doi:10.1016/j.desal.2010.06.042.

[55]   Z. Gu, J. Qiu, Y. Li, G. Cai, Heat pump system utilizing produced water in oil fields, 23 (2003) 1959–1970. doi:10.1016/S1359-4311(03)00143-1.
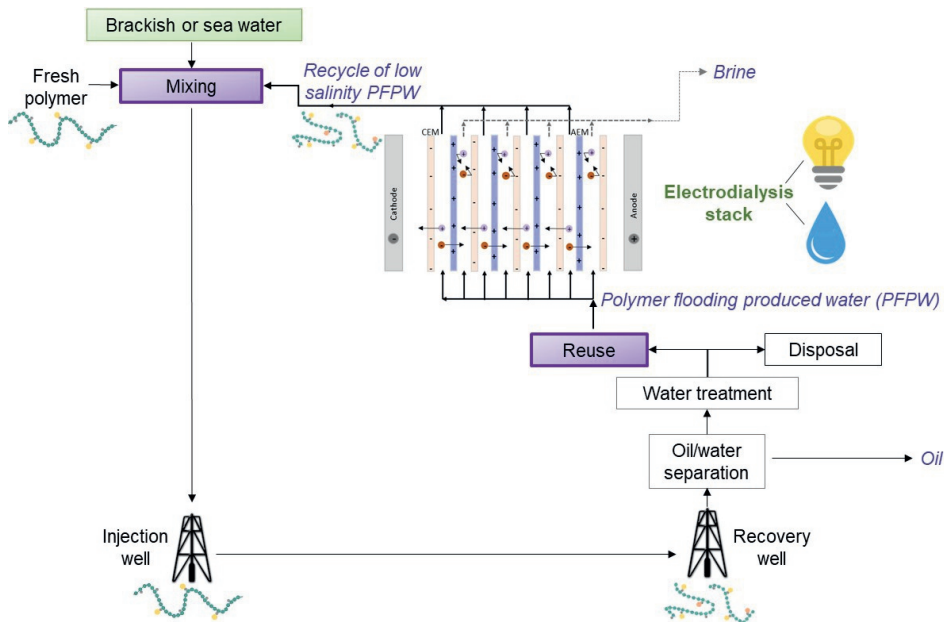
1

Chapter 2

Electrodialysis-based desalination and reuse of sea and brackish polymer-flooding produced water

Abstract

The reuse of polymer flooding produced water (PFPW) generated in oil and gas industry is limited by its salt content, making desalination by electrodialysis a promising treatment option. Therefore, this study aimed to 1) assess the technical feasibility of employing electrodialysis to desalinate PFPW generated in assorted scenarios, and 2) evaluate the reuse of the electrodialysis-desalted water to confect polymer-flooding solution. The experimental work involved desalting two kinds of synthetic PFPW solutions, one with relatively low salinity (TDS=5000 mg/L, brackish PFPW), and another with high salinity (TDS= 32,000 mg/L, sea PFPW), at two different temperatures, and later reusing the desalted solution to prepare viscous solutions. For the electrodialysis runs, the effects of feed composition and temperature on water transport, energy consumption and current efficiency were analyzed. It was found that the presence of polymer did not significantly influence the water transport rate nor the specific energy consumption for the seawater cases, but had a measurable effect when desalting brackish water at 20°C. It was also found that some polymer remained in the stack, the loss occurring faster for the brackish PFPW. Still, both kinds of reused PFPW probed adequate to be employed as a basis for preparing n polymer solution.

2.1   Introduction

2.1.1   Polymer flooding produced water

Polymer flooding is a method for chemical enhanced oil recovery (cEOR) that relies on the use of polymeric solutions to increase the recovery of hydrocarbons from existing oil fields. It is currently applied in several projects around the world – including countries like China, India, Oman, Angola, USA, Canada, United Kingdom, and Brazil– and its use is predicted to increase since both energy and oil demand will keep growing during the following decades, while finding new oil fields becomes increasingly challenging and costly [1–4].

Polymer flooding consists in employing displacing fluids with high viscosity, which consequently reduces the mobility of the aqueous phase and the water/oil mobility ratio, and finally leads to an increase in the macroscopic displacement efficiency [5]. In practice, this means that large volumes of water viscosified with polymers are pumped through an injector well in order to sweep the remaining oil and increase its recovery. The produced stream is later recovered in a production well and split in a gas, an oil and a water stream; the latter better called polymer-flooding produced water (PFPW) so to distinguish it from other produced water without polymers.

Depending on the geographic location of each project, the water for preparing the polymeric solution can be taken from different sources, therefore varying extremely in composition and salinity. As a rule, offshore projects rely on seawater as main water source, while onshore projects can have access to a variety of water sources. Recently, Henthorne et al. [6] published a survey about the source of injection water for over fifty EOR projects, including besides polymer addition, other chemical and thermal methods: most common source of water used was produced water itself (over 50% of the cases) followed by seawater (40%). The authors also reported that the salinity range of the water employed (57% of cases) was between 10,000 to 50,000 total dissolved solids (TDS), followed by lower salinity waters in the range of 1,000 to 10,000 TDS (23%). For the specific case of polymer flooding projects, Standnes & Skjevrak [7] summarized the characteristics and results of 72 polymer flooding projects implemented around the world. Considering only the projects for which the polymer injection water quality is clearly stated, more than 50% reported employing fresh water for the polymer preparation, 22% reported using produced water and 15% made use of high salinity water. Even though fresh water appeared as the preferred option, it must be considered that many of the evaluated projects were carried on during the 1960's to 1980's, but in contemporary conditions of growing water-scarcity and increasingly stringent legislation, it is foreseen that present and future EOR projects will become more dependent on produced water as a main supply source for their daily operation, including the make-up of polymer solutions. For example, state regulation in Oman forbids oil and gas companies to use fresh

water reservoirs (including shallow aquifers) for oilfield development, so the operators in the country currently rely on deep groundwater and produced water as supply sources [8,9].

Legislation and environmental concerns do not only play an increasingly important role in the accessibility to water sources, but also in the selection of disposal methods for EOR produced water. Even in non-water-stressed regions, the discharge of PFPW has to adhere to progressively stringent regulations, making reuse a more and more appealing option [10]. For example, according to the United Kingdom law, the most commonly employed EOR polymer does not pass the standard biodegradation test, so the base case for any polymer flooding project in the country is currently that water that potentially contains traces of polymers cannot be disposed of and needs to be re-injected [11]. With more stringent regulations, it could be even possible that the practice of EOR produced water discharge may be phased out, forcing closed loop recycling [1]. Consequently, the reuse of produced water and PFPW in different EOR applications is being assiduously evaluated [1,12].

Among the different reuse options, the use of PFPW to confect new polymer solution results threefold beneficial since it would minimize fresh water consumption, reduce the pollution caused by PFPW discharge and guarantee a reliable supply of water for the EOR projects [13]. In order to serve for reuse purposes, produced water is required to go through a series of operations to remove reuse hindering contaminants. Compared with the conventional produced water, PFPW contains not only crude oil, minerals, and bacteria, but also residual polymer. This makes treatment with commonly used methods difficult. Even after treatments such as flotation, coagulation, sedimentation, sand filtration and ultrafiltration, PFPW still contains residual organics and relatively high salinity (ranging from 2,000 to 150,000 ppm), the latter making the mixture inadequate for reuse in EOR [14,15]. This is because the most employed viscosifying polymers are high molecular-weight polyelectrolytes – like partially hydrolyzed polyacrylamide (HPAM, **Figure 1.4**) and its derivatives – which are sensitive to the presence of ionic species in solution – salt, alkali, or ionic surfactants. These ionic species have the effect of shielding the natural repulsion between the negative charges of the carboxylate groups of the HPAM, reducing the hydrodynamic size of the polymer molecule [16], and consequently lowering the viscosity of the solution. Thus, for produced water to be reused to confect polymeric solution, reduction of the salinity is highly desirable. Indeed, it has been suggested that the ideal water salinity for this purpose is in the range of 500 to 1000 ppm, due to potential swelling and incompatibility with the reservoir formation [17].

2.1.2   Electrodialysis to desalinate PFPW

Currently, two types of processes are relevant for the desalination of produced water: thermally-driven processes – that include multistage flash evaporation, multiple-effect distillation and vapor compression evaporation,– and pressure-driven processes such as reverse osmosis (RO) and nanofiltration [18–20]. While each method possesses its own advantages and drawbacks, in this case they all share one inconvenience: production of a water stream very low in TDS, and a rejected stream concentrated in salts and organic matter. While the latter is problematic because it still poses disposal issues, the former does not have the adequate salinity to be reused in EOR, as previously explained.

This explains why electrodialysis (ED), a salt selective technology, has been recently proposed to reduce the salinity of the PFPW stream [21]. In the reuse scheme, this would have the highly desirable effect of reducing the amount of fresh polymer and chemicals required to reach the target injection viscosity. Other potential benefits of including a partial desalination step are the reduction of scaling along the injection system, a decreased risk of reservoir souring, and a diminished polymer contamination in the produced streams [22].

As stated before, the application of electrodialysis to desalinate PFPW is relatively recent (first documented ten years ago), and has been focused in PFPW from the Daqing field in China [21,23]. Until now results seem promising, leading to the construction of a 9600 t/d water treatment ED setup [24] and further studies addressing fouling of the ED membranes [24,25]. However, as EOR and polymer flooding are being applied in increasingly diverse scenarios, the variety of the generated PFPW is therefore also growing. For example, PFPW of salinities between 5000 TDS to seawater levels are abundant streams whose treatment with ED has not been reported. Therefore, the reuse of these new varieties of PFPW also needs to be considered as a genuine option over the traditional injection and discharge practices. This requires having actual experimental data and understanding of both: the ED desalination process of PFPW and the factors that control the quality of the reclaimed solution, leading to the objectives of this study.

2.1.3   Objectives

Accordingly, the two objectives of this work are:

i) To assess the technical and energetic feasibility of employing electrodialysis to desalinate PFPW generated in assorted and relevant cEOR scenarios, i.e. with different compositions and temperatures. The assessment is to be performed in a way that allows identifying opportunity areas as well as potential implementation issues.

ii) To evaluate the reuse of the electrodialysis-desalted water to confect polymer flooding solution.

The variables, salinity and temperature, were specifically chosen because they are an obvious and unavoidable consequence of the variety of locations on which polymer-flooding is being implemented. Still, both can have important repercussions on the performance of ED and the characteristics of the treated water.

2.2 Materials and methods

2.2.1 Materials

2.2.1.1 *Solutions for ED runs*

Two different PFPW solutions were selected for this study, one with relatively low salinity (TDS= 5,000 mg/L, from now on referred as brackish PFPW), and another with high salinity (TDS= 32,000 mg/L, referred as sea PFPW). Their compositions are specified in **Table 2.1**.

Brackish and sea PFPW synthetic solutions were prepared at a concentration of 1.0 g/L of HPAM with MW=5-8 million Da. The size and concentration of the polymer were chosen considering reported values of polymer being back-produced with 50% of its original molecular size [26] and at a lower concentration of what originally injected.

Table 2.1. *Measured composition of solutions. Prepared based on values reported by [28] and [10].*

	Sea water (SW)	Brackish water (BW)
	g/L	g/L
Na^+	9.500	1.761
K^+	0.331	0.021
Ca^{2+}	0.350	0.014
Mg^{2+}	0.952	0.013
Cl^-	17.407	2.009
HCO_3^-	0.447	0.864
SO_4^{2-}	3.051	0.207

For preparing the back-produced polymer solution the procedure was the following. First, 500 mL of previously prepared salt solution were poured in a glass bottle containing a magnetic stirrer. Then, 500 mg of commercial HPAM with MW= 5-8 million Da were weighted in an analytical balance and slowly poured in the vortex formed in the salt solution stirred at 600 rpm by a magnetic stirrer. Once all the polymer was poured in, the agitation was reduced to 150 rpm and the bottle was

sealed. Each polymer solution was left stirring overnight in order to assure complete hydration [27], and was employed within 72 hours of its preparation.

Analytical grade salts (NaCl, CaCl$_2$·2H$_2$O, MgCl$_2$·6H$_2$O, NaHCO$_3$, KCl, and Na$_2$SO$_4$) were purchased from VWR and employed without further purification. Two kinds of HPAM were employed, Flopaam 3230S (MW= 5-8 million Da, 30% hydrolyzed), and Flopaam 3630S (MW= 20 million Da, 30% hydrolyzed), both kindly provided by SNF (France). All the solutions were prepared with demi water.

2.2.1.2 *Solutions for viscosity measurement as a function of polymer concentration*

In order to evaluate the effect of reusing desalted PFPW on the amount of polymer required to attain the desired injection viscosity, a total of eight sets of solutions were prepared, four for each water case. One set of solutions was prepared with the original sea water (TDS ~ 32,000 mg/L), another with the original brackish water (TDS ~ 5,000 mg/L), and the other six sets employed the reused diluates of the ED runs (TDS ~ 500 mg/L). Before preparing some of the viscous solutions, the pH of the ED diluates were adjusted to 8.0 by adding 1.0 M NaOH (**Table 2.2.**).

Table 2.2. *Sets of viscous solution prepared to evaluate the viscosity as function of the concentration of HPAM 20M Da*

| Set	Basis for stock solution	Diluted with
SW or BW no ED	Sea or brackish water	Sea or brackish water (no residual polymer)
Diluate PFPW	Final diluate without polymer	Final diluate with residual polymer
Diluate SW or BW pH=8.0	Final diluate without polymer, pH adjusted to 8.0	Final diluate without polymer, pH adjusted to 8.0
Diluate PFPW pH=8.0	Final diluate without polymer, pH adjusted to 8.0	Final diluate with residual polymer, pH adjusted to 8.0

Each of the eight sets of solutions was prepared from a stock HPAM solution (5.0 g/L), just like in the field procedure in which a concentrated (stock) polymer solution is prepared and then diluted to the desired injection viscosity. To assure proper polymer hydration, all stock solutions were prepared in a basis without residual polymer. The preparation method was like the one described in section 2.2.1.1, but with the necessary adjustments to achieve the design concentration of 5.0 g/L of the MW= 20 million Da HPAM.

After keeping the stock solutions under slow agitation for 24 hours, volumetric dilutions were performed so to obtain solutions with 20 million Da HPAM concentrations ranging between 0.2 and 2.0 g/L. The water employed for diluting

some solutions was the diluate of the ED experiments containing residual HPAM (5-8 million Da). The viscosity of these solutions was measured employing the rheometer and settings specified in section 2.2.2.2.

2.2.1.3   Electrodialysis setup

Experiments were performed in an ED stack containing five repeating cells, each consisting of a cation and an anion exchange membrane. The CEM and AEM employed were Neosepta CMX and Neosepta ANX (Tokuyama Co., Japan), respectively, and had a working area of 104 cm². An additional CEM was placed at the beginning of the stack to close the first cell. The intermembrane distance was fixed by using woven ETFE fabric spacers (Fluortex 09-590/47, Sefar, Switzerland), with reported thickness of 485 μm. Gaskets made of silicone rubber with a thickness similar to the spacer thickness were used to seal all the compartments and to form the alternated flow channels for the diluate and the concentrate. On both sides of the stack, squared titanium electrodes (mesh 1.7, area 96.04 cm²) with a mixed metal oxide coating of Ru/Ir (Magneto Special Anodes BV, The Netherlands) were employed as cathode and anode. The stack was closed with plates made of PMMA (poly(methyl methacrylate)) and 8 bolts (**Figure 2.1**).
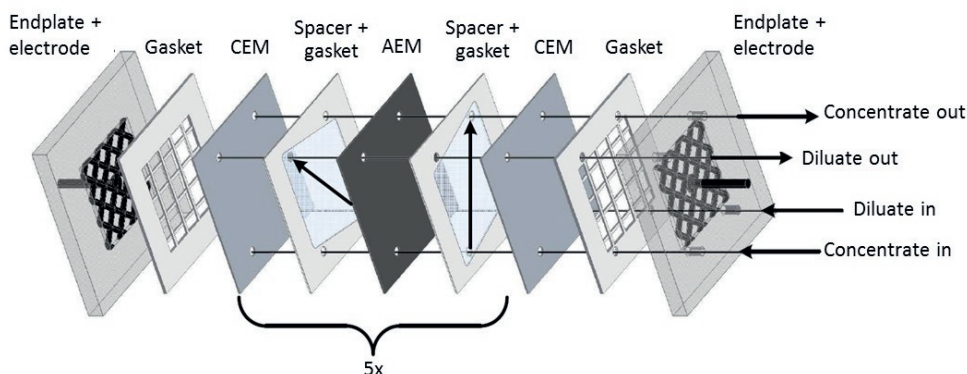
Figure 2.1. *Scheme of the electrodialysis stack employed, which was composed of six cation exchange membranes (CEM) and five anion exchange membranes (AEM). Adapted from Vermaas et al. [29].*

A potentiostat/galvanostat (Ivium Technologies, The Netherlands) was employed to control electrical current and to measure the potential difference. The potential difference over the membrane stack is measured using two reference Ag/AgCl gel electrodes (QM711X, QIS, The Netherlands) placed at the inlet of each electrode compartment.

Conductivities of the diluate and concentrate were measured inline with two conductivity probes (Orion DuraProbe 4-electrode conductivity cell 013005MD) directly before the ED stack. The probes were connected to a dedicated transmitter

box (Orion Versastar Pro), which corrected the measured values to the reference value at 25°C, and this last to a computer, where conductivity data was recorded every 5 seconds. pH of the diluate and concentrate were also measured inline, after the ED cell, with two pH probes (MemoSENS Endress + Hauser, pH range 1 to 12), connected through a transmitter box (P862, QIS) with a data logger (Memograph M RSG30, Endress + Hauser).

The solutions were pumped through the stack with peristaltic pumps (Cole-Parmer, Masterflex L/S Digital drive, USA). Temperature control during the experiments was achieved by employing 1.0 L glass jacketed vessels to store the diluate and concentrate solutions. On the external part of the vessels, water coming from a temperature-controlling recirculation bath was circulated. **Figure 2.2** illustrates the setup configuration.
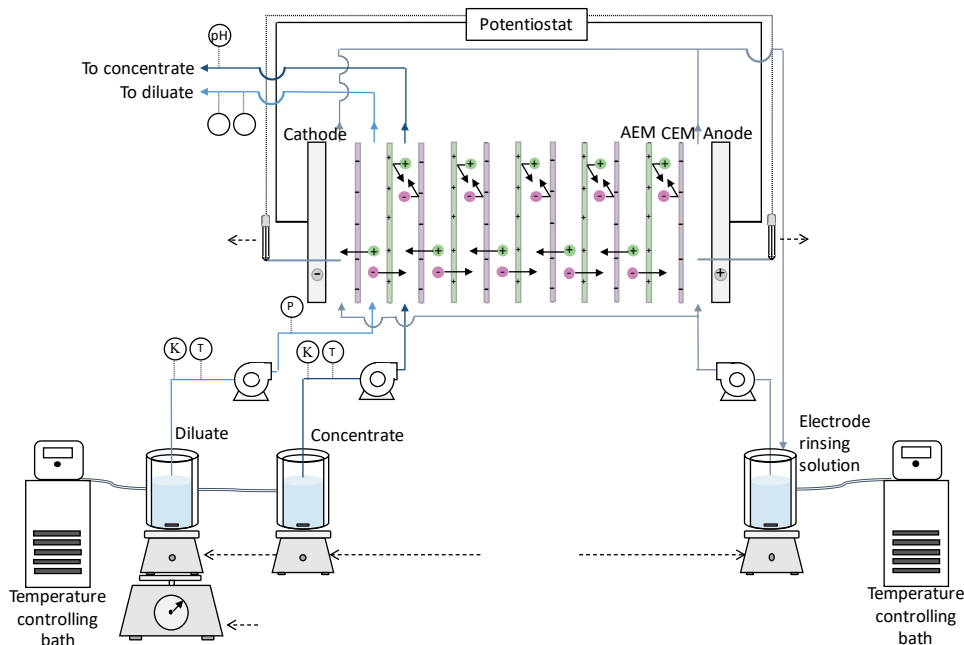
Figure 2.2. Scheme of the setup. The electrodialysis stack was connected to a potentiostat/galvanostat to control the electrical current and measure the potential difference between two reference Ag/AgCl gel electrodes. The temperature of the solutions during the experiments was controlled by two controlling baths.

2.2.2   Methods

2.2.2.1   *Electrodialysis runs*

ED experiments were carried out in a batch operation mode at fixed working temperatures (20°C and 40°C). The diluate and concentrate containing vessels were

pre-conditioned to the desired temperature by circulating water supplied by the temperature-controlling bath. Later, 500 mL of the diluate and concentrate solutions were poured in their corresponding vessels. For all experiments, the initial concentrate consisted on 5.0 g/L of sodium chloride solutions. As diluate, four different kinds of solutions were employed: sea and brackish PFPW with and without HPAM added. Runs with and without polymer were always performed in an alternate pattern.

The electrode rinse solution (2.0 L of sodium sulfate 20 g/L) was conditioned to the experiment working temperature by using another temperature-controlling bath. The concentrate and the diluate were recirculated through the corresponding compartments of the ED stack at a constant flow rate of 120 ml/min, while the electrode solution was re-circulated at a flow rate of 100 ml/min. The solutions were circulated in their correspondent circuits during 10 minutes before starting the experiment, allowing them to stabilize at the desired working temperature.

The experiments were run in constant current mode, at a fixed current density of 24 A/m^2 and switched to constant voltage mode when the limit value of 8.6 V was reached over the work electrodes. All experiments were stopped when the diluate's conductivity dropped to 1.0 mS/cm. During all experiments, stack voltage and current, as well as pH and conductivity were monitored for each circuit. Samples of 1.0 mL were taken periodically from the diluate and concentrate compartments.

During the experiments, the mass of the diluate was monitored by means of a mass balance placed under its vessel. The volume of the solution at each data point was calculated from the mass data using a density value corresponding to the composition of the solution at a reference temperature of 25 °C (1.0075 g/L for the experiments with sea PFPW and 1.00 g/L for the experiments with brackish PFPW). These density values were calculated as the average of measured densities of the solutions before and after being desalinated.

After each experiment with HPAM involved, the membrane stack was cleaned in-place. The procedure consisted in pumping a series of solutions in both the diluate and the concentrate compartments, each solution for a period of 10 minutes. The sequence of solutions was: sodium chloride solution (15 g/L), sodium hydroxide solution (0.1 M), fresh sodium chloride solution (15 g/L), hydrochloric acid solution (0.1 M), and finally fresh sodium chloride solution (15 g/L) [30].

All the experiments were performed by triplicate, and the results shown are the average of the values obtained for each of them.

2.2.2.2 *Viscosity measurements*

The dynamic viscosities of the polymer solutions were measured with a Discovery HR-3 rheometer (TA instruments) with a bob and cup configuration. The cup had an internal diameter of 30.43 mm and the bob an external one of 28.04 mm. The temperature of the solution was controlled by a heating jacket and the viscosity measured at ± 0.1 °C of the specified temperature. The measurements were performed at constant shear rate, starting from 1 s^{-1} to 100 s^{-1}.

2.2.2.3 *Analytical methods*

Samples taken during the ED runs were analyzed to determine their cation and anion content. Cations (Na$^+$, K$^+$, Ca^{2+}, Mg^{2+}) were measured by inductive-coupled plasma optical emission spectroscopy (ICP-OES, Optima 5300DV, Perkin Elmer) and anions (Cl$^-$ and SO$_4$$^{2-}$) by ion chromatography (IC, 761 Compact IC, Metrohm). For all the runs with HPAM involved and selected samples without it, both diluate and concentrate samples were analyzed for total carbon (TC) and total organic carbon (TOC) using a TOC analyzer (Shimadzu TOC-VCPH). With this method, besides monitoring the polymer concentration, it was possible to quantify the inorganic carbon as the difference between the detected TC and the TOC. The inorganic carbon detected was considered in the bicarbonate form (HCO$_3$$^-$) if the pH of solution was above the pK$_a$ of the carbonic acid/bicarbonate pair (pK$_a$= 6.4). Additionally, the diluate samples were analyzed utilizing liquid chromatography followed by an organic carbon detector (LC-OCD) (Doc-Labor, Germany) to get further size and nature information of the organic matter fractions of the polymer [31].

The total dissolved solids (TDS) content of each sample was calculated by adding the obtained concentrations of cations and anions, including the bicarbonate.

2.3 Results and discussion

2.3.1 Electrodialysis performance

ED experiments were carried out at two different temperatures, 20 and 40°C, at a fixed current density of 24 A/m^2, and stopped when the diluate's conductivity reached 1.0 mS/cm. The initial conductivity of the solutions circulating in the diluate circuit was, on average, 49.20 ± 0.6 mS/cm for the sea PFPW and 8.4 ± 0.1 mS/cm for the brackish PFPW, with no significant difference for the solutions with polymer and without polymer. Thus, all experiments performed with seawater had roughly the same duration –400 minutes– despite the presence of polymer, the same happening with all the experiments performed with brackish water, which lasted approximately 56 minutes (see F**igure A2.1).**

As explained in section 2.2.2.3, the TDS of each sample was calculated by adding up the measured concentrations of cations and anions. The values obtained are also represented in Figure A2.1, which shows the decrease in remaining TDS as a function of the measured conductivity. For the case of sea PFPW, the samples taken at the end of the experiment contained in average 405 mg/L of TDS – a removal percentage of 98.7%. This TDS value is slightly below the suggested minimal 500 mg/L to prepare the polymer solution for EOR [17], so it is advisable for future experiments to target a final conductivity above 1.0 mS/cm. Additionally, it was found that at the end of the desalination, the only ions still present in the diluate were Na^+, Cl^-, SO_4^{2-} and HCO_3^-, with a respective mass percentage of 38, 30, 30 and 2%.

Regarding the brackish PFPW, the average TDS of the diluates at the end of the desalination was 450 mg/L. From the initial TDS content of 5,000 mg/L, the percentage of removal is approximately 90.7%. Again, the only ions detected in the final diluate were only Na^+, Cl^-, SO_4^{2-} and HCO_3^-, in this case with a respective mass percentage of 38, 28, 13 and 20%. These results are in agreement with those presented by Jing et al., who reported faster removal of Ca^{2+} and Cl^- compared to the removal of Na^+ and HCO_3^- when desalting Daqing PFPW [21].

Since all the experiments were performed at constant current and only switched to constant voltage for the last minutes, the desalination time ought to be proportional to the amount of salts removed, or more accurately, to the number of molar equivalents that were transferred. In the case of sea PFPW, the average removal rate was 157.8 ± 1.3 meq/h, while in the case of brackish PFPW, a removal rate of 150.2 ± 2.3 meq/h was attained. When statistically compared, both removal rates differ insignificantly ($p > 0.05$).

2.3.1.1 *Water transport*

Together with the ions, water is also transported, consequently influencing the efficiency of the separation process [32–34]. Thus, it is of great interest to understand the implications of water transport when desalting PFPW.

During electrodialysis, water transport can occur either as free or as bound water. Free water transport (osmosis) will take place due to the difference in concentration between the diluate and the concentrate [35]. The relationship between this driving force and the flux of water transported by osmosis J_{osm} (mol m^{-2} s^{-1}) can be characterized by the water transfer or diffusion coefficient D_w (m^2/s), as expressed in equation 1 [33,35]:

$$J_{osm} = D_w \frac{(c_c - c_d)}{\delta} = \frac{\Delta m}{A \cdot t} \qquad\qquad /2.1/$$

where c_c and c_d are, respectively, the molar concentrations in the concentrate and diluate (mol/m³), δ is the membrane thickness (m), Δm is the amount of water transported (mol), A is the membrane area (m²), and t is the time (s).

Transport of water bound to ions, known as electro-osmosis, will take place whenever ions are passing through the membrane, and has a minimum corresponding to the water in the primary hydration sphere of the ions [32,36]. The amount of water transported by electro-osmosis is highly related to the membrane structure and properties, to the nature of the electrolyte solution and its concentration, and to the current density [33,34,37–39]. The water flux due to electro-osmosis is proportional to the flux of ions as expressed by:

$$J_{eosm} = t_w \sum_i J_i \qquad\qquad /2.2/$$

Here, J_{eosm} is the electro-osmotic water flux (mol m⁻¹ s⁻¹), t_w is the average water transport number for a specific membrane pair (-), and J_i is the flux of positive and negative ions (mol m⁻¹ s⁻¹). It is important to notice that t_w is calculated as the average water transport number across a membrane pair, thus comprising the water carried by anions and cations combined [40].

As can be inferred, water transport through ion-exchange membranes is a complex topic which can be addressed at many detail levels. For our study, the main interest is to have a general outlook of the impact of the chosen variables – salinity, temperature and polymer presence – on the observed water transport and finally on the overall process efficiency. Of special interest is the assessment of the effect of viscosifying polymer in the diluate stream. After all, the osmotic water transport is thermodynamically defined as a function of the difference in water activities across the membrane [41], and it is known that the addition of a solute to water always lowers its thermodynamic activity [42]. From this perspective, lower water transport could be expected for the viscosified solutions. And although electrodialysis has been widely employed to desalinate multicomponent solutions with viscosities higher than water – like meat extract [43], maple sap [44] and crude glycerol [45], – the impact of the viscous component regarding the observed water transport was not quantified.

During our study, the diluate's mass was recorded and from this data, the volume of solution was calculated (section 2.2.2.1). The computed volume decrease for all the studied PFPWs is presented in **Figure 2.3**. The conductivity of the diluate is presented in the x axis instead of time to facilitate the comparison of the amount of salts present at a given moment in the sea and brackish cases. For the sea water PFPW, the water transport profile of all the studied cases was quite similar, showing

only a larger volume drop in the last two data points of the experiments without polymer running at 40°C. Thus, at the end of the desalination, the largest water transport was recorded for the referred set of experiments, from which the recovered volume was 81.3 ± 0.3% of the initial one. In contrast, for the runs at the same temperature but with polymer, the water loss was slightly less severe (83.4 ± 0.9% recovered volume).
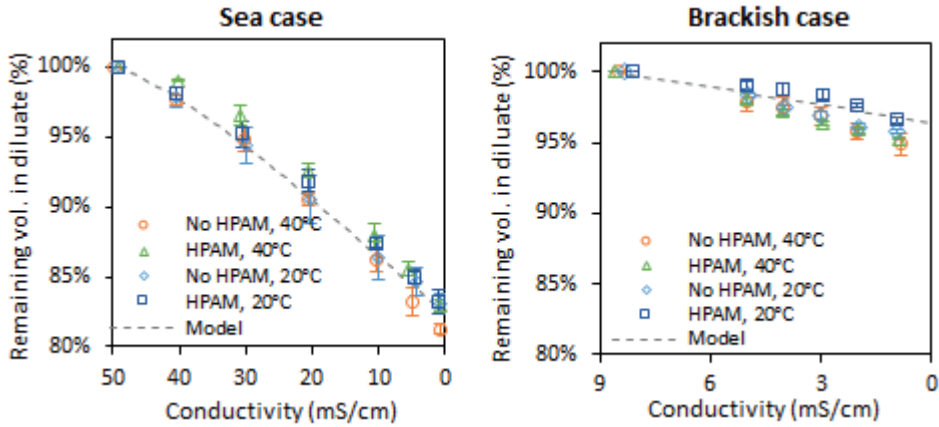
Figure 2.3. Remaining volume in the diluate as function of the measured conductivity. Experimental data points are represented by markers and modelled results by continuous dashed lines. Model calculated employing process efficiency of 90% (see section 2.3.1.2), t_w= 8, and D_w= 2.0 × 10^{-10} m²/s.

Although with a smaller volume decrease, the experiments performed with brackish water showed a tendency like the one observed in the seawater ones. In the brackish case, the highest volume recovery was registered in the runs with polymer at 20°C. Meanwhile, the runs at 40°C without polymer showed again the smallest volumetric recovery (94.9 ± 0.8 %), while for the runs with polymer at the same temperature the recovery was 96.6 ± 0.6 %. Although the statistical analysis showed that neither the differences in the sea water nor in the brackish water cases are significant ($p > 0.05$), the potential recovery of an extra 2.0% volume of water could be large enough to draw the attention towards the differences when desalting solutions in the presence or absence of viscosifying polymer.

To assess the role of osmotic and electro-osmotic water transport in the observed volume reductions, equations *2.1* and *2.2* were employed to calculate the projected volume changes as a function of t_w and D_w. Since the values of these parameters may vary depending on the actual experimental conditions, they were calculated by performing a regression analysis of the experimental data obtained at 20°C and without HPAM. By setting a target to minimize the difference between the calculated and the measured diluate volumes, an optimal combination of t_w= 8.0 and D_w=2.0 × 10^{-10} m²/s was found. Both parameters are in agreement with other values

reported in the literature, where t_w values of 8.2 and 8.0 for the same membrane pair have been recently reported [40,46]. In a similar way, the calculated transfer coefficient D_w is in the same order of magnitude that the value reported by Galama for a similar membrane pair [33]. Finally, these t_w and D_w values reveal that the electro-osmotic water transport had the largest influence in the total amount of transported water. It was calculated that, respectively, 94 and 95% of the effective water transport in the sea and brackish cases, was attributable to the electro-osmotic mechanism.

2.3.1.2   *Energy use and current efficiency*

Since the desalination experiments were run at constant current and stopped at similar desalination degrees, the effects of the presence of polymer and the variation in temperature were reflected in the energy use. The first indication of energy consumption tendencies are the voltages supplied to the cell during the runs, shown in **Figure 2.4**. In the case of sea PFPW, the initial voltages are around 0.5V, and all of them increase slowly and steady as the desalination progress. They all show a sharp increase around the minute 360, the time at which the diluate's conductivity had decreased to approximately 5.0 mS/cm. It is also noteworthy that the experiments running at the same temperature behave in similar way, despite the presence or absence of HPAM. On contrary, in the case of the brackish PFPW results, there were larger differences between the experiments with and without polymer, especially for the runs at 20°C. These differences again can be explained as the result of the different viscosities of the solutions, which affect the diffusion rate of the ions and influence the thickness of the ion depletion layer.

Furthermore, to assess the energy costs of desalting the different types of water studied, and to compare the results with available data, the energy requirement per unit of diluate volume (*W*) was calculated. For that, the following equation can be employed [33]:

$$W_{desalination} = \frac{\int I \cdot E_{stack} dt}{V_d} \qquad /2.3/$$

where *I* is the current (A), E_{stack} is the measured voltage in the stack (V), *t* is the time period (s), and V_d is the measured diluate volume (m³). It is important to notice that this equation only accounts for the stack's energy use; electrode losses and pumping energy are not included.
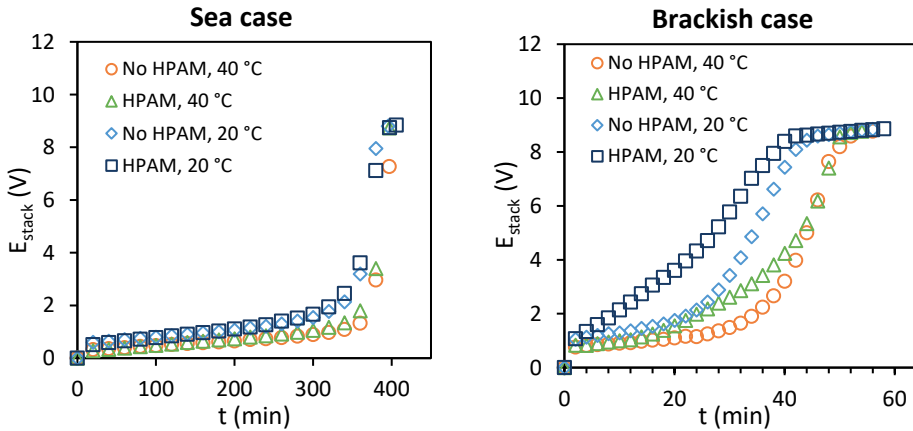
Figure 2.4. Measured voltages over the 5-cell pair stack. For the sea cases, there was a slow and steady increase in potential until approximately minute 340, when presumably the limiting current was reached, and from there on the voltage increases rapidly. For the brackish case, the sharp increase in voltage occurred around the minute 30 for the solutions at 40°C and before for the solutions at 20°C. Lower voltages were recorded for the sea cases than for the brackish ones; for the experiments running at 40°C, and for the experiments running without HPAM.

Since the required desalination degree of PFPW would depend on the location and type of reservoir, the energy necessary to reach two different TDS concentrations: 1000 and 500 mg/L (**Figure 2.5**) was calculated using Eq. *2.3*. As expected, the specific energy consumption for desalting seawater was larger than for desalting brackish water, experiments running at 40°C consumed less energy than the ones running at 20°C, and the presence of polymer also increased the energy use, most notoriously for the desalinations reaching 500 TDS and the runs at lower temperature. It should be emphasized that although the process parameters were not optimized, the energy consumption for the seawater case falls within the values reported by other authors [47].
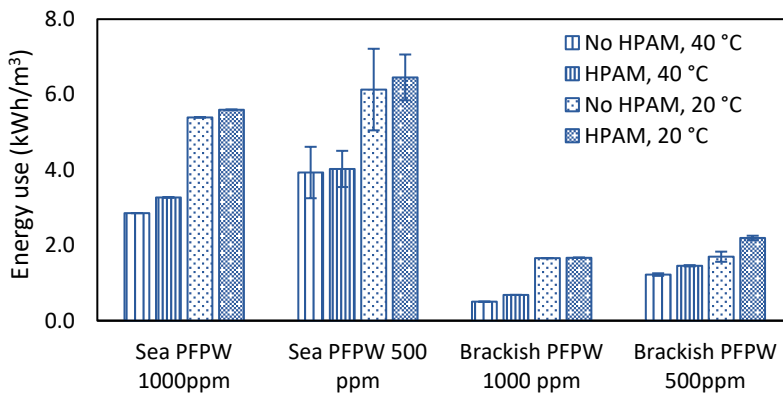
Figure 2.5. Specific energy consumption for desalting sea and brackish PFPW in kWh per m³ of desalted product.

As in all desalination processes, not all energy supplied to an ED system is used effectively. In a large extent, the efficiency of electrodialysis is determined by the properties of the membranes. Phenomena like back-diffusion of ions or co-ion transport can occur due to their non-perfect selectivity [33]. Additionally, electrodialysis efficiency is also affected by the process and system design, which determine the limiting current density, the current utilization, the concentration polarization, etc. In order to quantify the effectiveness of current utilization, the coulombic efficiency is extensively used, defined as the total amount of electric charge transported by ions, divided by the electric charge applied to the system [33,48]. This is shown in Eqs. 2.4-2.6.

$$\eta = \frac{Q_{transported}}{Q_{applied}} \times 100 \qquad\qquad /2.4/$$

$$Q_{transported} = F \sum_i z_i \Delta n_i \qquad\qquad /2.5/$$

$$Q_{applied} = N_{cell} \int_0^t I dt \qquad\qquad /2.6/$$

Where η is the coulombic efficiency (%), Q the electric charge (C), F is Faraday constant (C/eq), z_i is the valence of the ion (eq/mol), Δn_i, the moles of ions transported (mol), and N_{cell} the number of cell pairs (-). It must be noted that eq. 2.5 can be employed either for the cations or for the anions, but not both simultaneously. Thus, the efficiency for each experiment was reported as the average of the efficiencies calculated independently for the cations and for the anions.

In general, the calculated current efficiencies were higher for the brackish water experiments, ranging between 89 to 97%, while for the seawater ones it was found to in the range of 84 to 90% (**Figure 2.6**). The most surprising finding is that in 3 of the 4 cases, the runs without polymer presented a lower current efficiency than the same run with polymer. This can possibly be explained as an effect of the lower diffusivity of the ions when the viscosity of the solvent increases, which causes the back-diffusion phenomena to happen at a lower rate.
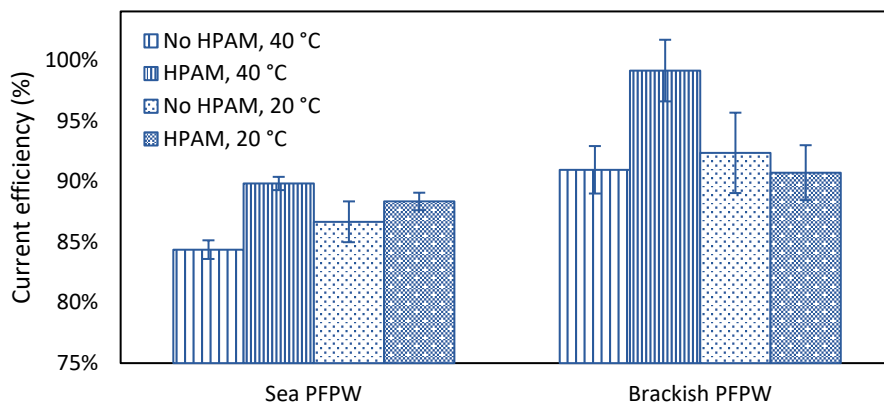
Figure 2.6. *Current efficiency for the desalination of PFPW.*

2.3.2 Evaluation of the PFPW solutions

As explained, the final goal of desalting the PFPW is to reuse it to confect fresh polymer solution. Thus, as important as analyzing the process feasibility in energetic terms, it is to make sure that the desalted stream can be reused in the polymer-flooding process. Of special attention is its readiness to confect viscous solutions, as it will be further studied in this section.

It has been stated that in polymer flooding, the oil recovery is increased by lowering the mobility of the displacing phase (water) compared to the mobility of the displaced phase (oil). This mobility reduction of the water phase is achieved by increasing its viscosity through the addition of water-soluble polymers [4,5]. The type of polymers employed and their concentration vary for each reservoir and project, but in general it is preferred to use polymers with high molecular weight, and in concentrations between 1000 ppm to 3000 ppm [5]. The viscosity of the polymer solution must be evaluated at least at two temperatures, reservoir and environmental, to ensure that the fluid viscosity remains within the desired range at downhole conditions, but that it is also reasonably viscous to be pumped at surface conditions [5]. And even though steady and dynamic rheological properties of the polymer solution are important for cEOR applications [5,49,50], the initial evaluation of a solution consists on performing a viscosity curve at different shear rates, with special attention given to the viscosity obtained at a shear rate of 7.3 s^{-1} or similar.

Accordingly, this study relied on steady shear measurements to characterize the polymer solutions. The viscosities of the synthetic sea and brackish PFPW solutions were measured before and after the desalination, at 20 and 40°C at various shear rates (section 2.2.2.2). To facilitate the analysis, the viscosities recorded at shear rate of 6.3 s^{-1} are summarized in **Table 2.3**, but the complete set of measurements is available in the supplementary material (Figure A2.3).

Table 2.3. *Viscosities of sea and brackish water solutions (in mPa.s).*

	Sea water		Sea PFPW (HPAM)[c]		Brackish water		Brackish PFPW (HPAM)[c]	
	20°C	40°C	20°C	40°C	20°C	40°C	20°C	40°C
Before desalination	1.059[a]	0.694[a]	3.331	2.233	1.010[b]	0.659[b]	9.027	6.080
After desalination	1.002	0.653	6.033	4.172	1.002	0.653	32.01	22.93

[a] Viscosity of solutions of salinity 30 g/kg [51]

[b] Calculated as the average viscosity of water with 10 g salt/kg solution [51] and the viscosity of pure water

[c] Viscosities of solutions with HPAM reported at a shear rate of 6.30 s^{-1}.

Focusing on the values before the desalination, it is possible to notice that the sea and brackish PFPW had, respectively, viscosities 3 to 9 times higher than same solutions without polymer. It is also apparent that the viscosity of the solutions at 40°C is approximately 30% lower compared to that of the same solution at 20°C, which is also normally observed in HPAM solutions [52]. Finally, when comparing the viscosities of the different PFPW's, the values measured for sea PFPW were found to be 2 to 3 times lower than those for the brackish PFPW, something that was expected due to the differences in salinity. Indeed, this difference in viscosity as a function of salinity is similar to the one reported by Levitt for solutions of the same polymer, Flopaam 3230S, although his measurements were performed with higher polymer concentration and only using NaCl [27].

Then, after desalting the sea and brackish PFPW to a similar TDS content and composition, one might expect the viscosity values to be higher and alike. Remarkably, this was not the case. As presented in **Table 2.3.** (and in **Figure A2.3.**) both, sea and brackish PFPW, showed an increase in viscosity after treated with ED. However, the change in the sea PFPW was moderate, while for the brackish case it was much more substantial. The viscosity of the sea PFPW at 40°C increased almost twofold, from 2.23 to 4.17 mPa·s, while the viscosity of the brackish PFPW measured at the same temperature increased nearly four times, from 6.08 to 22.93 mPa·s. This meant that even after the desalination, the properties of both solutions still differ. Thus, before trying to reuse them to prepare fresh polymer-flooding solution, the cause(s) of these differences in viscosity were further scrutinized.

2.3.2.1   *HPAM content during the electrodialysis runs*

Viscosity is highly dependent of the polymer concentration. Thus, the actual polymer content of the solutions during the desalination process was monitored through TOC analyses, which were carried on for both the diluate and the

concentrate compartments. Initially, the sea and brackish PFPW solutions registered an average of 381 and 360 mg/L TOC, respectively, while the analysis of the concentrate solution showed zero TOC content. For all the subsequent concentrate measurements, the TOC measurement always resulted below the detection limits (1.0 mg/L), indicating that the polymer was not able to pass through the IEMs.

The TOC measurements for the diluate sides of the sea and the brackish PFPW are shown in **Figure 2.7**. In the case of the sea PFPW, it is observed that the TOC values are practically constant since the beginning of the desalination process until the conductivity reached 20 mS/cm, decreasing slightly in the three last measurements. For the case of the brackish PFPW, it results noticeable that there is a larger decrease of the TOC values in a much shorter desalination time. Furthermore, since water was being transported from the diluate to the concentrate and the polymer was not passing through the membranes, it was expected to detect an increase in the polymer concentration in the diluate as the desalination occurred. The increase did not happen, as shown with the dashed lines in the graphs, which represent the expected TOC concentration when considering the water transported during the process. Since organic carbon was never detected in the concentrate solution, the only explanation would be that the missing polymer got adsorbed and/or precipitated on the IEMs and spacers and stayed in the stack. This is a plausible explanation since it is known that the charged polymer has affinity for the ion-exchange membranes, as already reported in previous studies [24,25]. Additionally, when performing the cleaning protocol, it was possible to observe some polymer and small solids precipitating in the solutions, mainly in the basic one.

Considering the recovered volumes of the diluates and the measured TOC concentrations, it is possible to quantify the amount of polymer remaining in the stack. For the sea PFPW desalination runs at 40 and 20°C, it was calculated that 28.2 and 21.6%, respectively, of the initial mass of polymer in solution was left behind. This represents a 14% (40°C) and 6% (20°C) reduction in the polymer concentration measured by TOC. In the case of the brackish PFPW, 25.5 and 30.1% of the HPAM remained in the stack during the runs at 40 and 20°C, respectively. This was reflected as 22% (40°C) and 28% (20°C) reduction in the polymer concentration. Thus, despite both kinds of water suffered similar polymer losses in terms of mass, for the brackish case the loss occurred in a much shorter time. This observation, together to the accelerated decrease rate on the sea PFPW when reaching a conductivity of 10 mS/cm, suggests that the polymer loss is closely related with the ionic strength (salinity) of the solution. It seems that this variable affected the polymer loss more than the temperature or processing time. As measured in the sea cases, the polymer tends to remain in solution while the salinity is high, but once the salinity reaches a certain level its attachment on the stack increases. This can be explained by the shielding of the charges on the polymer. When the stream has high salinity, the

charges on the polymer are effectively covered, so it is not substantially affected by the electric forces on the stack. However, as the salinity decreases its intrinsic charges become less shielded, making it more susceptible to have electrostatic interactions with the stack elements.
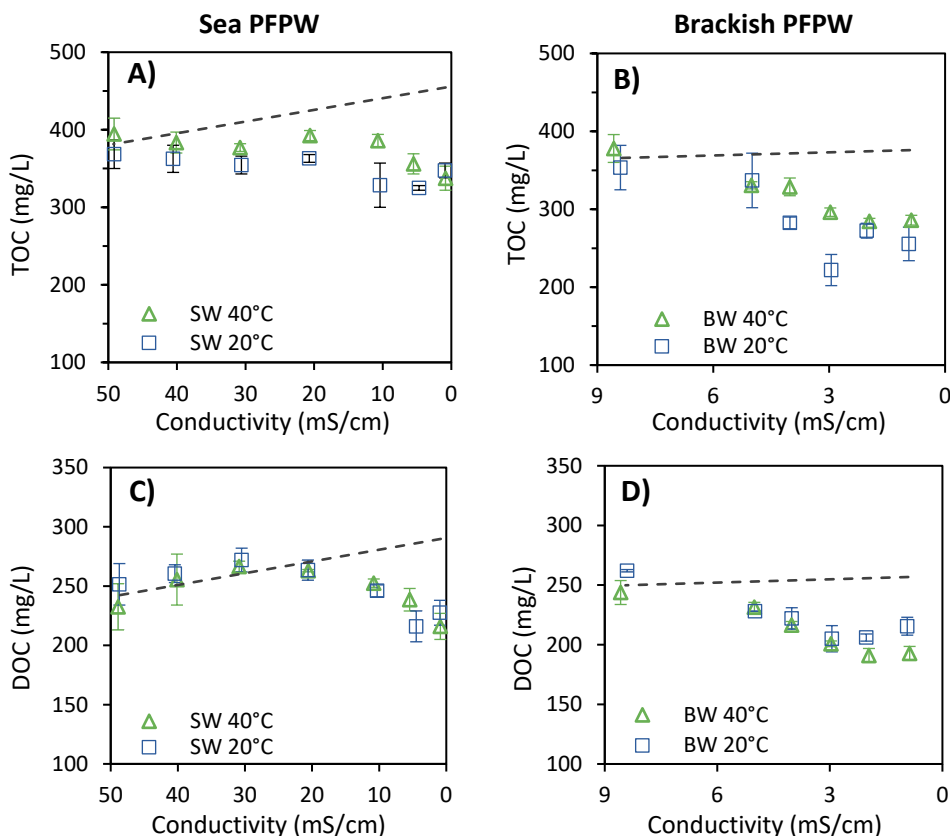
Figure 2.7. Measured and calculated TOC (A, B) and DOC (C, D) in the diluate's of desalted solutions. The TOC quantifies all the polymer present in solution, while the DOC can be regarded as the concentration of small polymer particles which could pass through a 0.45 μm PES filter. Each data point indicates the average concentrations of samples taken from at least three different experiments. The dashed lines represent the expected TOC and DOC concentrations considering volume reduction due to water transport.

Additional to the TOC analysis, all the diluate samples were also analyzed with LC-OCD. One of the parameters that can be evaluated by this technique is the concentration of dissolved organic carbon (DOC), which is all the organic carbon still in solution after filtering the sample through a 0.45 μm PES filter. The results for the sea PFPW (**Figure 2.7C**), show initial DOC values for both temperatures around 240 mg/L, which is approximately 60% of the initial TOC concentrations, meaning that 40% of the polymer particles in solution were large enough to be retained by the filter. At this point it is important to emphasize that when filtering an HPAM or any

other polymeric solution, the hydrodynamic radius of the particles in solution plays a significant role in their filter retention. The hydrodynamic radius of a HPAM molecule depends not only on its molecular weight and hydrolysis degree [53], but it is also highly sensitive to the ionic strength of the solution [27], pH [53,54], polymer concentration [54], and to the presence of multivalent cations [55]. Regarding this last point, it has been demonstrated that when calcium ions are present in the solution, intrachain and interchain complexes are formed, so a particle is not a single polymer molecule, but a cluster of molecules [55].

Further on, it is interesting that the two subsequent data points of the sea PFPW analysis showed a small increase in DOC, and still the samples taken at 20 mS/cm contained nearly the expected DOC concentration given the volume change of the solution (dashed line). Since this tendency was not observed in the TOC analysis, a plausible explanation is that while larger polymer molecules get adsorbed as soon as the desalination starts, the smaller polymer molecules remain in solution for a longer time. However, the initial tendency reverts and, from the 10 mS/cm reading until the end of the desalination, the DOC values decrease proportionally to the TOC values, suggesting that there was no more distinction between small and big particles. Still, the final ratio of DOC to TOC was around 0.65, slightly larger than the initial one.

Meanwhile, the DOC analysis of the brackish PFPW experiments and its comparison with the TOC evolution (**Figure 2.7B, D**) suggests that, for this case, the temperature plays a more significant role than for seawater. Although the overall DOC tendency seems similar to the one of TOC, when closely examining it results clear that while the DOC to TOC ratio is practically the same before and after the 40°C runs (0.67), it increases from 0.72 up to 0.85 for the ones at 20°C. At first glance this result is counter-intuitive: as the viscosity of the solution increased, one would expect small particles to uncoil during the process, thus reducing the ratio of DOC to TOC. Apparently, this effect was small compared to the larger loss of the bigger HPAM particles in solution, as can be understood from the decrease in TOC.

It must be added that although the LCD-OCD analysis also included the chromatographic separation of the dissolved organics, the results only indicated that all the organics remaining in solution had an estimated molecular weight above 20,000 Da.

Another variable that was analyzed to explain the viscosity change during the process was the pressure difference in the diluate stream. Although the analysis was not conclusive, it is included as Appendix B.

In summary, the results presented in this section gave a good insight into the differences when desalting sea and brackish PFPW, but some questions remain. Why after removing 31,500 mg/L TDS, the viscosity of the sea PFPW only had a light increase, especially when compared against the change in the brackish PFPW? And why does a solution with less polymer concentration show a higher viscosity? A logical explanation for both questions would be that since the sea PFPW was desalted for a longer time, the polymer in solution suffered more degradation (chain breaking), which was not possible to detect with the TOC/DOC analyses. However, yet another parameter might also be playing an important role in the observed behavior: the pH.

2.3.2.2 *The role of pH*

One of the key parameters to consider when evaluating HPAM solutions is their pH. The carboxyl groups along the backbone chain of the molecule are pH-sensitive, so the viscosity of HPAM solutions is strongly dependent on the hydrolysis degree (content of carboxyl groups) and the variation of pH. These carboxyl groups can exchange protons with dissolved salts in water, depending on pH conditions. At high pH, the carboxyl groups dissociate and are negatively charged. Still, counter-ions balance most of the charge inside the coil, so their osmotic pressure makes the chain expand to larger sizes, resulting in the increased solution viscosity. On the other hand, low pH causes all carboxyl groups to be protonated with hydrogen ions, resulting in no charges on the polymer chain. The polymer molecules are now in a coiled state which decreases viscosity [53]. Experimental results of this viscosity dependence on the pH of solution [52,53], as well as on the addition of hydroxide [52], have been previously reported.

Accordingly, the pH of the diluate solutions exiting the ED cell was constantly monitored. For the sea PFPW the initial pH was 7.9, slightly basic, due to the presence of bicarbonate ions in the solution. However, as the desalination progressed the pH decreased, reaching average values of 4.5 and 3.8 for the runs at 40 and 20°C, respectively (**Figure 2.8**). It was also noted that there was a large pH variability among the runs, especially in the readings between 20 and 5 mS/cm.

On the other hand, the brackish PFPW had an initial pH of 8.4, consequence of a higher bicarbonate concentration (**Table 2.1**). The pH of these solutions also decreased during the desalination, but in a less extent and with almost no variability, consistently reaching a final pH of 6 regardless of the temperature.
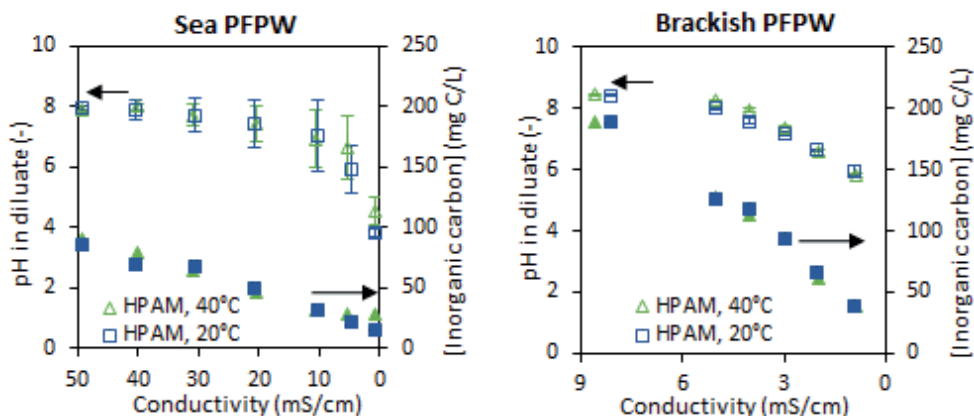
Figure 2.8. pH (open symbols) and inorganic carbon (filled symbols) evolution in the diluate solution. The largest pH drop (from approximately 8 to 4) was observed for the sea PFPW, which had a low initial inorganic carbon content (derived from a low bicarbonate content). Meanwhile, the brackish PFPW had a moderate pH change (from 8.4 to 6), which could be related to a higher initial inorganic carbon content.

These observations can be explained as combination of several factors. First, it must be recalled that the bicarbonate ion is removed from the diluate together with the other anions, so its concentration was decreasing over time. This is apparent from the inorganic carbon results, which are also presented in **Figure 2.8**. It must be noticed that the inorganic carbon value encompasses several inorganic molecules, including carbonate, bicarbonate, carbonic acid, and carbon dioxide. Initially, the main component of both kinds of solutions was bicarbonate, since their pH was higher than the pK_a of the carbonic acid/bicarbonate pair ($pK_a = 6.4$). However, as the desalination progressed, the bicarbonate was removed, so the solution had less buffering capacity. This made the solutions more sensitive to any H^+ entering the diluate, which can be coming from the anode reactions and/or from water splitting happening within the cell. It is worth to notice that, despite the apparently large change in pH, the concentration of protons went from 0.01 µmol/L (pH=8) to about 100 µmol/L (pH=4). Seen from this point of view, the net increase of protons in the diluate becomes less outstanding. In case that most of the extra protons were originated in the anode, it is considered that an increase in the number of cell pairs and in the flow rate of the electrode rinse would be enough to minimize the pH variation.

However, there is evidence suggesting that the pH change was also enhanced by water splitting within the membrane stack. When comparing the pH evolution of the solutions with HPAM (**Figure 2.8**) and without it (data not shown), it was noted that the HPAM containing solutions had a faster pH decrease, and their final pH value was slightly lower than for the solutions without polymer. Since the relation diluate/electrode rinse was the same in all cases, the most feasible explanation is that

water splitting was occurring as consequence of membrane fouling. It is known that water splitting occurs when the concentration in charged species is not enough to ensure the current transport at the membrane interface in the electrodialysis cell [29]. When this limiting current density is reached, water dissociation occurs in the interface of the AEMs [36,37,56]. The phenomenon causes the generation of H$^+$ at the AEM diluate interface and OH$^-$ at the AEM concentrate interface. From this study (section 2.3.2.1) and from others before it is known that HPAM tends to foul the ion exchange membranes [24,25]. And when fouling occurs, the conditions for splitting water become more ideal, which may even keep triggering the fouling formation [5,30,31]. Indeed, from the fast voltage increase in the last minutes of the desalination (**Figure 2.4**), it can be deduced that the limiting current density was reached during this part of the ED treatment.

Since the desalted sea PFPW had higher polymer concentrations and even less ions than the brackish PFPW one might, at least partially, attribute the minimal change in viscosity of the former to its lower pH. In that case, the restoration to (nearly) neutral pH might result useful to uncover the viscosifying potential of the remaining HPAM in solution.

2.3.3   Preparation of viscous flooding water with desalted solution

Finally, the desalted solutions were employed together with 20 million Da HPAM to prepare polymer flooding viscous solutions with different polymer concentrations (section 2.2.1.2). For comparison purposes, two sets of viscous solutions were also prepared with original sea and brackish water. The viscosities were evaluated at 40°C, close to the median temperature of 46°C of many polymer flooding projects [4].

All the measured curves confirm that the viscosity of the viscous solution is highly dependent of the concentration of polymer (**Figure 2.9**). For both studied cases, sea and brackish, the desalted solutions showed higher viscosities than the non-desalted for same added polymer concentration.

As elucidated in the previous section, the low pH of the seawater diluates was probed to be partially responsible for their lower viscosity compared to the desalted brackish PFPW. In **Figure 2.9** it is shown that, by adjusting the pH of the PFPW diluate from its final value of 4.9 to 8.0, the viscosity increased from 4 to 10 mPa·s. However, the effect of correcting the pH of the reused solutions is only noticeable at low HPAM concentrations (below 1.5 g/L for the sea case and under 1.0 g/L for the brackish case). This occurs because the addition of fresh HPAM also has the outcome of increasing the pH of the solution, so even without initial pH control, the PFPW diluates with 2.0 g/L HPAM reached a pH close to neutral. When the salinity and

pH are similar, the viscosities of the sea and brackish PFPW diluates should be alike, as found in the measurements for the 2.0 g/L HPAM concentration.

It is also interesting to compare the viscosities achieved by reusing PFPW with residual polymer vs using desalted water, both being in neutral pH conditions. In the sea case, the presence of residual polymer made the reused PFPW up to four times more viscous that its equivalent, diluate SW, without residual polymer. In the case of brackish water, the viscosity differences were smaller, but still 50% larger when residual polymer is present. For both kinds of water, the viscosifying effect of the residual polymer is noticeable only when the fresh HPAM concentration was below 1.5 g/L.

To finalize with the discussion about the differences in viscosity between the desalted sea and brackish water, it can be pointed out that although the restoration to neutral pH duplicated the viscosity of the sea PFPW diluate, it did not equalize it to the one of the desalinated brackish PFPW. Since it has already been established and explained that the sea diluate contained even a higher concentration of polymer, it can be concluded that the polymer suffered some form of degradation. This could be attributed to two factors, shear degradation due to the relatively long pumping time, and chemical degradation due to the acidic conditions. The validation of these hypotheses would need to be addressed in further studies.

Lastly, a hypothetic polymer flooding design with desired viscosity of 20 mPa.s at 40°C was considered (**Figure 2.9**). For the sea water case, the use of desalted water would mean polymer savings of approximately 75%, while the use of desalted PFPW with residual polymer and pH=8 could use less 10 times less polymer. These results fully agree with the estimations of Ayirala et al., who indicate 5-10 times lower consumption of polymer in low salinity water compared to seawater [17]. Regarding the brackish case, it is estimated that 60 to 100% less fresh polymer would be needed, depending on the presence of residual polymer. Riethmuller et al. projected a slightly lower (50%) reduction in the consumption of polymer and associated stabilizing agents for brackish water desalted to 1000 ppm, but when considering a viscosity goal of 55 mPa·s [9].
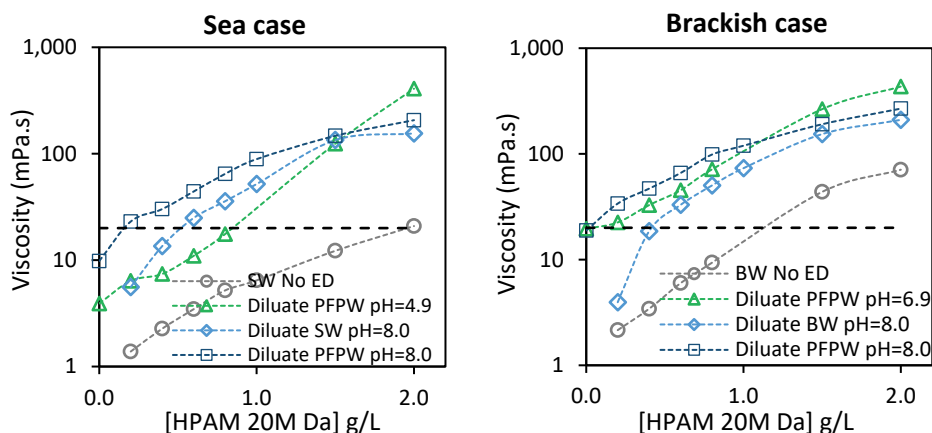
Figure 2.9. *Comparison of the viscosities of polymeric solution as a function of HPAM 20M Da concentration and the type of water employed for their preparation. A hypothetical viscosity goal of 20 mPa·s is represented by the horizontal black line. All values reported were measured at 40°C and shear rate of 7.3 s^{-1}.*

2.4 Conclusions

Electrodialysis is a suitable desalination process to treat PFPW of different salinities and compositions. It was possible to reduce the salinity of synthetic PFPW (containing 1.0 g/L of commercial 5-8 million Da HPAM) with two different salinity levels (32,000 and 5,000 TDS in ppm) to approximately 500 ppm, the optimal salinity to confect new polymer solution.

Water transport during the desalination was substantial, especially for the sea water cases, for which only 81-83% of the initial volume was recovered. Slightly lower water transport rates were measured for the runs with polymer at 20°C, but the differences were not significant. The volume decrease was a consequence of osmotic and electro-osmotic transport, the last being the most prominent. Yet, since osmotic transport is a function of process time, lower volume losses could be attained by employing higher current densities, at least for the initial part of the desalination, with its consequent lower process time.

In terms of energy use, it was found that the presence of polymer did not significantly influence the specific energy consumption for the desalination runs on seawater nor brackish water at 40°C, but indeed it had a measurable effect when desalting brackish water at 20°C. These results are thought to be related to the higher viscosity of the latter stream, which restricts the movement of ions and results in an accelerated arrival to the limiting current. It is noticeable that despite the process conditions are not yet optimized, the energy consumption for the sea case at 40°C was approximately 4.0 kWh/m³ when aiming to retain only 500 ppm of salt, and

even 3.0 kWh/m^3 if the desalination is stopped when 1000 ppm are still in solution. Regarding the energy efficiency, the presence of polymer seemed to have a beneficial effect for achieving higher energy efficiencies, most likely due to hampering the back-diffusion of ions.

Concerning the analysis of the desalted PFPW, it was found that 20 to 30% of the initial mass of polymer in the diluate stream remained on the stack, most likely adsorbed/precipitated on the membranes and spacers. The polymer loss was faster on the brackish cases than on the sea ones, and for the latter the decrease rate accelerated when reaching certain salinities. Thus, the decrease was associated to the ionic strength of the solution. This variable seems to be more critical than temperature or processing time regarding polymer adsorption/precipitation, an observation that may result valuable when studying fouling (and associated loss and degradation processes in the stack) for this type of polymers.

The desalted solutions presented an immediate and moderate increase in viscosity. Even though the final salinity in all studied cases was similar, the final viscosities of the sea and brackish PFPW differed significantly. It was verified that this was partially due to the pH decrease during the desalination, and most likely also due to partial degradation of the residual polymer. However, when fresh polymer was added, all desalted solutions showed higher viscosities compared to the non-desalted ones. The viscosifying effect of the residual polymer is also tangible, so it has been demonstrated that by reusing PFPW the consumption of fresh polymer could be reduced, resulting beneficial in environmental and economic terms.

References

[1]   J.A. Herschell, Water and Wastewater Treatment for Enhanced Oil Recovery, Mahon, Cork, Ireland, 2016.

[2]   Internacional Energy Agency (IEA), World Energy Outlook 2016, Paris, 2016. http://www.iea.org/publications/freepublications/publication/WEB_WorldEnergyOutlook2015Exec utiveSummaryEnglishFinal.pdf.

[3]   A. Muggeridge, A. Cockin, K. Webb, H. Frampton, I. Collins, T. Moulds, P. Salino, Recovery rates, enhanced oil recovery and technological limits, Philos. Trans. R. Soc. A Math. Phys. Eng. Sci. 372 (2013) 20120320–20120320. doi:10.1098/rsta.2012.0320.

[4]   J.J. Sheng, B. Leonhardt, N. Azri, Status of Polymer-Flooding Technology, J. Can. Pet. Technol. 54 (2015) 116–126. doi:10.2118/174541-PA.

[5]   M.S. Kamal, A.S. Sultan, U.A. Al-Mubaiyedh, I.A. Hussein, Review on Polymer Flooding: Rheology, Adsorption, Stability, and Field Applications of Various Polymer Systems, Polym. Rev. 55 (2015) 491–530. doi:10.1080/15583724.2014.982821.

[6]   L. Henthorne, G.A. Pope, U. Weerasooriya, V. Llano, Impact of Water Softening on Chemical Enhanced Oil Recovery, 2014.

[7]   D.C. Standnes, I. Skjevrak, Literature review of implemented polymer field projects, J. Pet. Sci. Eng. 122 (2014) 761–775. doi:10.1016/j.petrol.2014.08.024.

[8]   S. of O. Ministry of Oil & Gas, Oil & Gas Law, 2011. http://www.oman.om/wps/wcm/connect/f5b459d2-584d-42a9-b766-f8f555567763/10Oil+and+Gas+Law+%28Royal+Decree+No.+4274%29.pdf?MOD=AJPERES.

[9]   G. Riethmuller, A. Abri, N. Al Azri, G. Stapel, S. Nijman, W. Subhi, R. Mehdi, Opportunities and Challenges of Polymer Flooding in Heavy Oil Reservoir in South of Oman, SPE EOR Conf. Oil Gas West Asia. (2014). doi:10.2118/169737-MS.

[10]   A. Fakhru'l-Razi, A. Pendashteh, L.C. Abdullah, D.R.A. Biak, S.S. Madaeni, Z.Z. Abidin, Review of technologies for oil and gas produced water treatment, J. Hazard. Mater. 170 (2009) 530–551. doi:10.1016/j.jhazmat.2009.05.044.

[11]   Oil & Gas Authority United Kingdom, Polymer Enhanced Oil Recovery, London, 2017.

[12]   Y. Liu, E.B. Kujawinski, Chemical composition and potential environmental impacts of water-soluble polar crude oil components inferred from esi FT-ICR MS, PLoS One. 10 (2015) 1–18. doi:10.1371/journal.pone.0136376.

[13]   G. Jing, L. Xing, S. Li, C. Han, Reclaiming polymer-flooding produced water for beneficial use: Salt removal via electrodialysis, Desalin. Water Treat. 25 (2011) 71–77. doi:10.5004/dwt.2011.1766.

[14]   E. Drioli, A. Ali, Y.M. Lee, S.F. Al-Sharif, M. Al-Beirutty, F. Macedonio, Membrane operations for produced water treatment, Desalin. Water Treat. 3994 (2015) 1–19. doi:10.1080/19443994.2015.1072585.

[15]   R. Zhang, W. Shi, S. Yu, W. Wang, Z. Zhang, B. Zhang, L. Li, X. Bao, Influence of salts, anion polyacrylamide and crude oil on nanofiltration membrane fouling during desalination process of polymer flooding produced water, Desalination. 373 (2015) 27–37. doi:10.1016/j.desal.2015.07.006.

[16]   A. Samanta, A. Bera, K. Ojha, A. Mandal, Effects of alkali, salts, and surfactant on rheological behavior of partially hydrolyzed polyacrylamide solutions, J. Chem. Eng. Data. 55 (2010) 4315–4322. doi:10.1021/je100458a.

[17]   S.C. Ayirala, E. Uehara-Nagamine, A.N. Matzakos, R.W. Chin, P.H. Doe, P.J. van den Hoek, A Designer Water Process for Offshore Low Salinity and Polymer Flooding Applications, SPE Improv. Oil Recover. Symp. (2013). doi:10.2118/129926-MS.

[18]   C. Murray-Gulde, J.E. Heatley, T. Karanfil, J.H. Rodgers, J.E. Myers, Performance of a hybrid reverse osmosis-constructed wetland treatment system for brackish oil field produced water, Water Res. 37 (2003) 705–713. doi:10.1016/S0043-1354(02)00353-6.

[19]   E.T. Igunnu, G.Z. Chen, Produced water treatment technologies, Int. J. Low-Carbon Technol. 9 (2014) 157–177. doi:10.1093/ijlct/cts049.

[20]   S. Munirasu, M.A. Haija, F. Banat, Use of membrane technology for oil field and refinery produced water treatment—A review, Process Saf. Environ. Prot. 100 (2016) 183–202. doi:10.1016/j.psep.2016.01.010.

[21]   G. Jing, X. Wang, H. Zhao, Study on TDS removal from polymer-flooding wastewater in crude oil: extraction by electrodialysis, Desalination. 244 (2009) 90–96. doi:10.1016/j.desal.2008.04.039.

[22]   E.C.M. Vermolen, M. Pingo-almada, B.M. Wassing, D.J. Ligthelm, S.K. Masalmeh, H. Mohammadi, G.R. Jerauld, M. Pancharoen, IPTC 17342 Low-Salinity Polymer Flooding : Improving

2

Polymer Flooding Technical Feasibility and Economics by Using Low-Salinity Make-up Brine, SPE Imroved Oil Recover. Symp. (2014) 15. doi:10.2118/153161-MS.

[23]   G. Jing, Y. Liu, T. Zhao, C. Han, Reclamation of the polymer-flooding produced water, 2nd Int. Conf. Bioinforma. Biomed. Eng. iCBBE 2008. (2008) 3240–3243. doi:10.1109/ICBBE.2008.1138.

[24]   T. Wang, S. Yu, L. an Hou, Impacts of HPAM molecular weights on desalination performance of ion exchange membranes and fouling mechanism, Desalination. 404 (2017) 50–58. doi:10.1016/j.desal.2016.10.007.

[25]   H. Guo, L. Xiao, S. Yu, H. Yang, J. Hu, G. Liu, Y. Tang, Analysis of anion exchange membrane fouling mechanism caused by anion polyacrylamide in electrodialysis, Desalination. 346 (2014) 46–53. doi:10.1016/j.desal.2014.05.010.

[26]   H. Al Kalbani, M.S. Mandhari, H. Al-Hadhrami, G. Philip, J. Nesbit, L. Gil, N. Gaillard, Treating Back Produced Polymer To Enable Use Of Conventional Water Treatment Technologies, (n.d.). doi:10.2118/169719-MS.

[27]   D.B. Levitt, The Optimal Use of Enhanced Oil Recovery Polymers Under Hostile Conditions, The University of Texas at Austin, 2009.

[28]   J. Zheng, B. Chen, W. Thanyamanta, K. Hawboldt, B. Zhang, B. Liu, Offshore produced water management: A review of current practice and challenges in harsh/Arctic environments, Mar. Pollut. Bull. 104 (2016) 7–19. doi:10.1016/j.marpolbul.2016.01.004.

[29]   D.A. Vermaas, M. Saakes, K. Nijmeijer, Doubled power density from salinity gradients at reduced intermembrane distance, Environ. Sci. Technol. 45 (2011) 7089–7095. doi:10.1021/es2012758.

[30]   H. Guo, F. You, S. Yu, L. Li, D. Zhao, Mechanisms of chemical cleaning of ion exchange membranes: A case study of plant-scale electrodialysis for oily wastewater treatment, J. Memb. Sci. 496 (2015) 310–317. doi:10.1016/j.memsci.2015.09.005.

[31]   S.A. Huber, A. Balz, M. Abert, W. Pronk, Characterisation of aquatic humic and non-humic matter with size-exclusion chromatography - organic carbon detection - organic nitrogen detection (LC-OCD-OND), Water Res. 45 (2011) 879–885. doi:10.1016/j.watres.2010.09.023.

[32]   H. Strathmann, Electromembrane Processes: Basic Aspects and Applications, Compr. Membr. Sci. Eng. (2010) 391–429. doi:DOI: 10.1016/B978-0-08-093250-7.00048-7.

[33]   A.H. Galama, M. Saakes, H. Bruning, H.H.M. Rijnaarts, J.W. Post, Seawater predesalination with electrodialysis, Desalination. 342 (2014) 61–69. doi:10.1016/j.desal.2013.07.012.

[34]   C. Jiang, Q. Wang, Y. Li, Y. Wang, T. Xu, Water electro-transport with hydrated cations in electrodialysis, Desalination. 365 (2015) 204–212. doi:10.1016/j.desal.2015.03.007.

[35]   T. Sata, Ion Exchange Membranes; Preparation, Characterization, Modification and Application, Royal Society of Chemistry, 2004.

[36]   V.K. Indusekhar, N. Krishnaswamy, Water transport studies on interpolymer ion-exchange membranes, Desalination. 52 (1985) 309–316. doi:10.1016/0011-9164(85)80040-0.

[37]   A.G. Winger, R. Ferguson, R. Kunin, The electroosmotic transport of water across permselective membranes, J. Phys. Chem. 60 (1956) 556–558. doi:10.1021/j150539a010.

[38]   N. Berezina, N. Gnusin, O. Dyomina, S. Timofeyev, Water electrotransport in membrane systems. Experiment and model description, J. Memb. Sci. 86 (1994) 207–229. doi:10.1016/0376-7388(93)E0075-U.

[39]   L. Han, S. Galier, H. Roux-de Balmann, Ion hydration number and electro-osmosis during electrodialysis of mixed salt solution, Desalination. 373 (2015) 38–46. doi:10.1016/j.desal.2015.06.023.

[40]   S. Porada, W.J. van Egmond, J.W. Post, M. Saakes, H.V.M. Hamelers, Tailoring ion exchange membranes to enable low osmotic water transport and energy efficient electrodialysis, J. Memb. Sci. 552 (2018) 22–30. doi:https://doi.org/10.1016/j.memsci.2018.01.050.

[41]   G.M. Geise, D.R. Paul, B.D. Freeman, Fundamental water and salt transport properties of polymeric materials, Prog. Polym. Sci. 39 (2014) 1–24. doi:10.1016/j.progpolymsci.2013.07.001.

[42]   M.J. Blandamer, J.B.F.N. Engberts, P.T. Gleeson, J.C.R. Reis, Activity of water in aqueous systems; A frequently neglected property, Chem. Soc. Rev. 34 (2005) 440. doi:10.1039/b400473f.

[43]   S. Shi, S. Cho, Y. Lee, S. Yun, J. Woo, S. Moon, Desalination of fish meat extract by electrodialysis and characterization of membrane fouling, 28 (2011) 575–582. doi:10.1007/s11814-010-0375-4.

[44]   L. Bazinet, D. Lavigne, N. Martin, Partial demineralization of maple sap by electrodialysis : impact on syrup sensory and physicochemical characteristics, 1698 (2007) 1691–1698. doi:10.1002/jsfa.

[45]   P. Vadthya, A. Kumari, C. Sumana, S. Sridhar, Electrodialysis aided desalination of crude glycerol in the production of biodiesel from oil feed stock, Desalination. 362 (2015) 133–140. doi:10.1016/j.desal.2015.02.001.

[46]   W.J. van Egmond, U.K. Starke, M. Saakes, C.J.N. Buisman, H.V.M. Hamelers, Energy efficiency of a concentration gradient flow battery at elevated temperatures, J. Power Sources. 340 (2017) 71–79. doi:10.1016/j.jpowsour.2016.11.043.

[47]   Y. Ghalavand, M.S. Hatamipour, A. Rahimi, A review on energy consumption of desalination processes, Desalin. Water Treat. 54 (2015) 1526–1541. doi:Doi 10.1080/19443994.2014.892837.

[48]   H. Strathmann, Ion-Exchange Membrane Processes in Water Treatment, Elsevier, 2010. doi:10.1016/S1871-2711(09)00206-2.

[49]   D. Wang, J. Cheng, Q. Yang, G. Wenchao, L. Qun, F. Chen, Viscous-Elastic Polymer Can Increase Microscale Displacement Efficiency in Cores, (2000). doi:10.2118/63227-MS.

[50]   R. Zhang, X. He, S. Cai, K. Liu, Rheology of diluted and semi-diluted partially hydrolyzed polyacrylamide solutions under shear : Experimental studies, Pet. Xxx. (2016) 1–10. doi:10.1016/j.petlm.2016.08.001.

[51]   J.D. Isdale, C.M. Spence, J.S. Tudhope, Physical properties of sea water solutions: viscosity, Desalination. 10 (1972) 319–328. doi:10.1016/S0011-9164(00)80002-8.

[52]   J.C. Jung, K. Zhang, B.H. Chon, H.J. Choi, Rheology and polymer flooding characteristics of partially hydrolyzed polyacrylamide for enhanced heavy oil recovery, J. Appl. Polym. Sci. 127 (2013) 4833–4839. doi:10.1002/app.38070.

[53]   S. Choi, pH Sensitive polymers for novel conformance control and polymer flooding applications, The University of Texas at Austin, 2008.

[54]   M.P.S. Gomes, M. Costa, Determination of the critical concentration of partially hydrolyzed polyacrylamide by potentiometry in an acidic medium, J. Appl. Polym. Sci. 128 (2013) 2167–2172. doi:10.1002/app.38310.

2

[55]   S. Peng, C. Wu, Light Scattering Study of the Formation and Structure of Partially Hydrolyzed Poly(acrylamide)/Calcium(II) Complexes, Macromolecules. 32 (1999) 585–589.

[56]   Y. Tanaka, Concentration polarization in ion-exchange membrane electrodialysis: The events arising in an unforced flowing solution in a desalting cell, J. Memb. Sci. 244 (2004) 1–16. doi:10.1016/j.memsci.2004.02.041.

Appendix 2A. Supplementary material
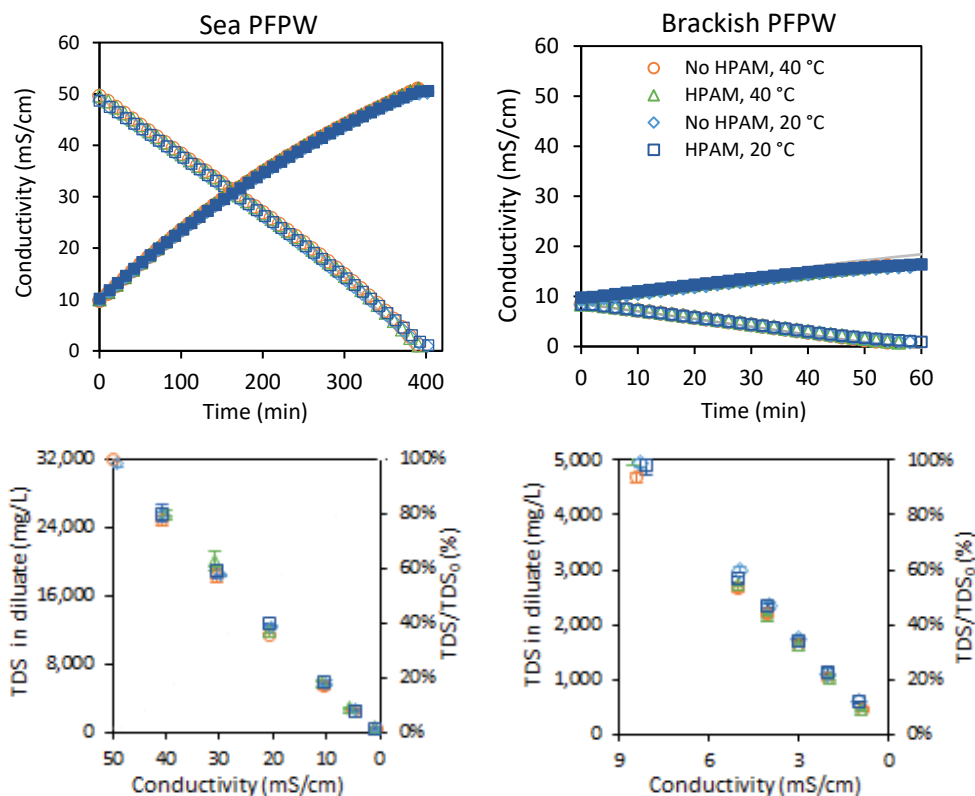
Figure A2.1. *Top) Measured conductivity vs time for diluate and concentrate of ED runs performed. Continuous lines indicate calculated conductivities considering an efficiency of 90% and water transport (see section 2.3.1). Bottom) Measured TDS remaining on the diluate related to the conductivity in ED experiments at different temperatures and compositions.*
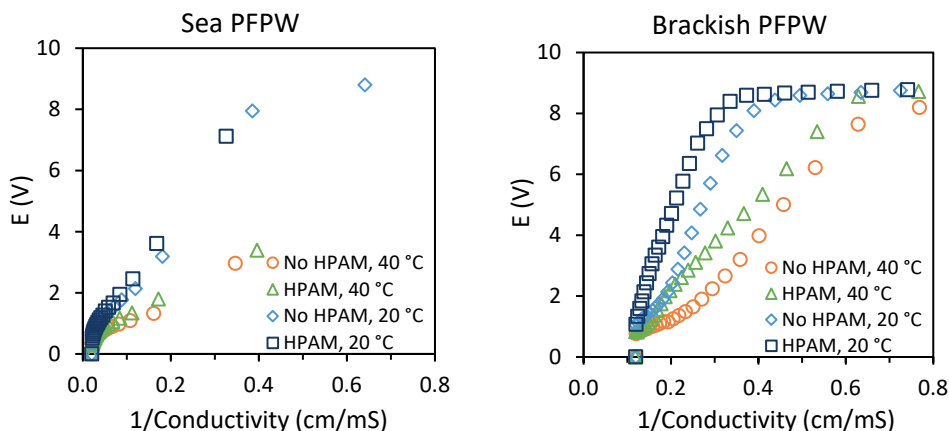
Figure A2.2. *Measured voltages over the 5-cell pair stack represented as a function of the inverse of the conductivity of the diluate. A straight line indicates that the dominant resistance is that from the diluate, as can be observed in part of the brackish PFPW plot. For the sea PFPW, the shape of the curves is not linear, indicating that the total resistance is not controlled by a single factor (from Ohm's law E=I*R with R=R$_0$ + B/conductivity).*
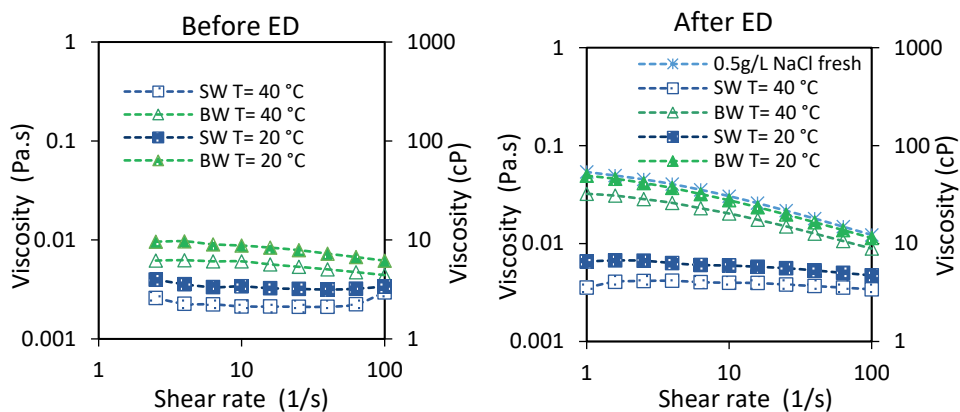
Figure A2.3. *Viscosities of synthetic sea (TDS~ 32,000 g/L) and brackish (TDS~ 5,000 g/L) PFPW (HPAM concentration of 1.0 g/L) at 20 and 40°C before and after the electrodialysis treatment. For most cases, the viscosities decrease with increasing shear rate, a behavior known as shear thinning, characteristic of HPAM and other polymer solutions [52]. The viscosity curve of a 0.5g/L NaCl +1.0 g/L HPAM solution in the "After ED" plot is a reference of the expected viscosity.*

## Appendix 2B. Pressure drop measurements

A parameter that could be useful to assess the contrasts while desalting sea and brackish PFPW was the pressure drop of the diluate stream, since it can be easily related with the apparent viscosity of the solution. It is known that the pressure drop for an uniform and laminar flow in an infinite wide channel can be calculated by using a momentum balance containing the pressure gradient and the wall friction [29]:

$$\Delta p = \frac{12\mu \cdot L \cdot \phi}{d^3} \qquad\qquad /2.7/$$

Where Δp is the differential pressure (Pa), ϕ is the volumetric flowrate of the diluate (m³/s), L is the length of the flow path (m), and d is the height of the flow path (m). As expressed in the equation, the pressure drop at a specific time is directly proportional to the viscosity of the medium, in this case the brackish or the sea PFPW. Supposing that the values of the rest of the parameters represented in Eq. 7 remain constant during the desalination, any change in pressure drop could be related to a change in the viscosity of the solution.

As an example, one can observe that when desalting either sea or brackish solution without polymer, the differential pressure Δp remained practically constant (**Figure A2.4**). This was expected since the viscosity of salt solutions is not sensitive to the amount of dissolved salts, especially at low to moderate concentrations, as also reported in **Table 2.2**. In a similar way, it was expected that the Δp during the desalination of both sea PFPW runs would remain nearly constant. When applying **Eq. 7** and the measured viscosities from Table 2.3, the calculated Δp increase at the end of the sea runs at 20 and 40°C were around 0.9 and 0.6 kPa, respectively. As shown on **Figure A2.4.** , these projected changes in Δp were not observed, and even during the run at 20°C the opposite trend was recorded.

Regarding the brackish PFPW desalination, the calculated Δp increases were larger, 3.9 and 2.8 kPa for the runs at 20 and 40°C, respectively. However, as in the sea case, the Δp during the 40°C experiment remained practically constant. The only polymer-containing stream that displayed a Δp increase during the desalination process was the run at 20°C on brackish PFPW, and in this case the measured increase of 4 kPa was consistent with the calculated value of 3.9 kPa.
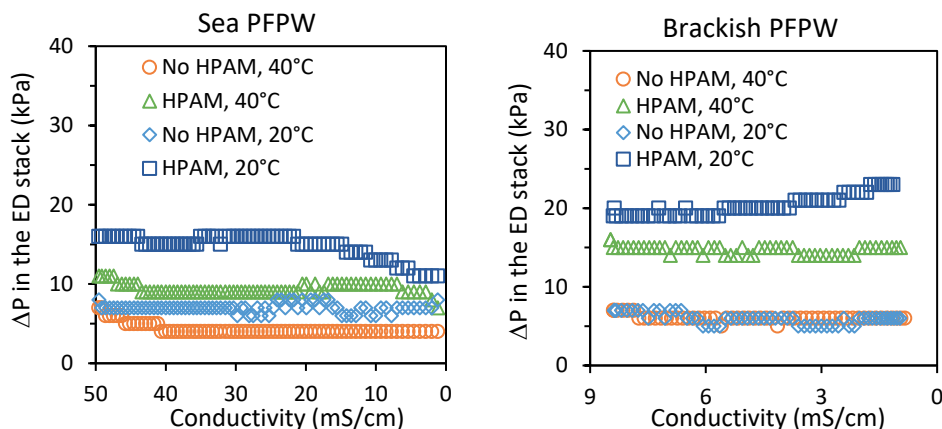
Figure A2.4. *Pressure difference measured between the inlet and the outlet of the ED stack for the diluate stream. According to these results, the only stream that increased its viscosity during the desalination was brackish PFPW running at 20°C with HPAM.*

Nevertheless, the fact that only certain runs behaved according to the presented equation forbids us from reaching conclusions regarding the change in viscosity during the desalination of the PFPW. A possible explanation for the inconsistent data is that the assumption of constant dimensions for the flow is not accurate, since flow dead zones might arise. Another option, especially for the runs at 40°C, is that the cell temperature was still changing when the desalination started.
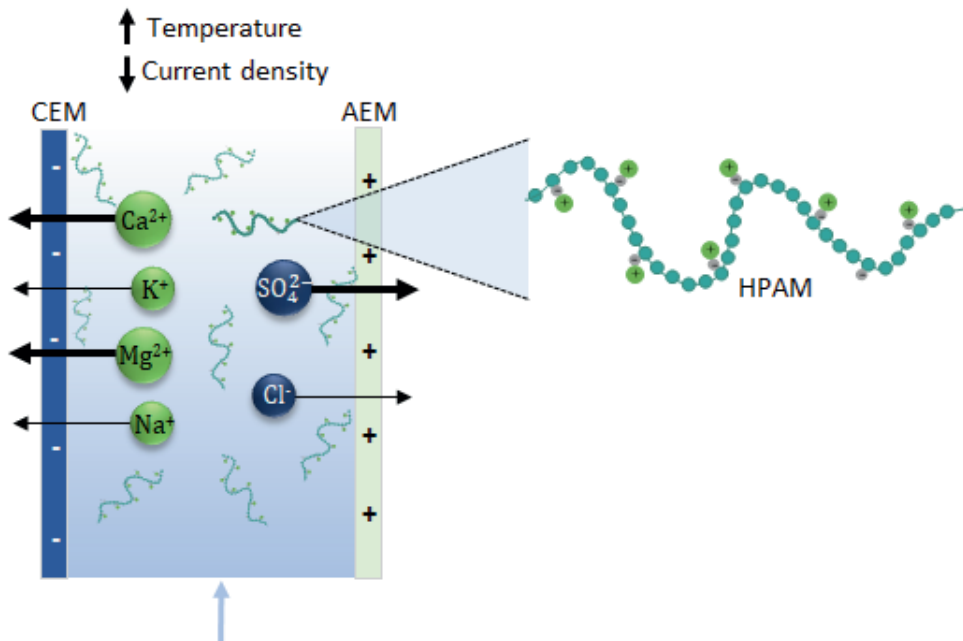
Chapter 3

Removal of divalent ions from viscous polymer-flooding produced water and seawater via electrodialysis

Abstract

The presence of multivalent ions in polymer-flooding produced water (PFPW) hampers its recycling mainly because i) they increase the risk of scaling and reservoir souring (sulfate), ii) they interfere with the viscosifying effect of the fresh polyelectrolyte. It is desirable to achieve the removal of most multivalent ions without completely desalting the stream. With the adequate process conditions, electrodialysis could help to achieve this goal, so this work focused on evaluating the removal of divalent ions from synthetic PFPW through varying operational conditions. The experimental work consisted on batch experiments run in an electrodialysis-stack composed of strong Neosepta ion-exchange membranes. Synthetic PFPW solutions containing a mixture of monovalent and divalent ions were desalted at four different current densities, and three different temperatures. Additionally, the effect of the dissolved polymer on the removal was assessed by performing half of the experiments on polymer-containing solutions and half of them on solutions without it. Our results demonstrate that it is possible to achieve preferential removal of divalent cations (calcium and magnesium) through electrodialysis, especially when employing low current densities (24 A/m^2) and high temperature (40°C). The removal of sulfate, a divalent anion, is also accelerated in these conditions. The presence of polyelectrolyte did not significantly affect the removal rate of divalent ions. Thus, it is concluded that meticulous application of ED to minimize concentrations of divalent ions in PFPW is a potential effective way for water and polymer recycling in enhanced oil recovery situations, as an alternative to the use of other non-selective desalination technologies.

3.1   Introduction

Electrodialysis was first applied at industrial scale to desalinate brackish water, more than 50 years ago [1]. Driven by the need of producing sodium chloride from concentrated sea water, Japanese scientists developed a few years later ion exchange membranes with permselectivity for monovalent ions [2], which eventually enabled electrodialysis to be applied in various new fields [3,4]. However, a similar selective process only allowing passage of multivalent ions seems more difficult to achieve: yet no membranes with permselectivity for multivalent ions are reported. Alternatively, some investigations have suggested that at adequate process conditions, electrodialysis can be used to preferentially remove multivalent ionic species from a stream [5–7]. This is of practical and economic importance for treating and reusing waters produced by enhanced oil recovery and particularly from polymer flooding, as later detailed. Therefore, this article is focused on achieving preferential multivalent ion removal from saline water containing significant polymer concentrations.

Polymer flooding is a chemical enhanced oil recovery (cEOR) method that consists on the injection of large amounts of aqueous viscous solutions to increase the oil recovery from existing oilfields [8]. Given the increasing energy and oil demand together with the difficulty to find new oil fields, the technology has re-emerged and it is currently applied in numerous projects around the world [9,10]. However, two constraints still limit the use of polymer flooding and cEOR in general: little water accessibility and/or restrictions for the disposal of the produced water (water recovered together with the oil). Both restraints could be overcome when the water can be reused in a closed loop [11], for which it must be treated. A process for reusing produced water usually consist on primary and secondary treatments that strip it of the excess of dissolved oil, and subsequent tertiary (or polishing) steps [12], often designed to reduce the salinity and hardness of the produced water [13]. For the specific case of reusing produced water to prepare polymer flooding solution, the desalination step appears to be desirable for technical, economic, and environmental reasons. This is because polymer flooding solution is usually brought to adequate viscosity by adding high molecular weight polyelectrolytes, like partially hydrolyzed polyacrylamide (HPAM) and its derivatives. Its viscosity enhancing effect is extremely sensitive to the salinity of the water in which they are dissolved. Thus, when low salinity water is employed, less polymer is required to reach the design viscosity [14], and thus both the operational costs and the environmental impact of the produced streams are reduced.

Nevertheless, not all salt ions are equally disadvantageous for the preparation of a viscous polyelectrolyte solution (see Figure A3.1). The viscid properties of HPAM solutions are significantly affected by the presence of multivalent cations, [15–19] being calcium and magnesium (hardness), the most common ones. Solutions

intended for cEOR applications must contain as less sulfate as possible to minimize the risk of reservoir souring problems and the deposition of scaling [14,20,21]. Since polymer flooding solution should not be prepared with wholly desalted water [14], partial desalination of the produced water stream with preferential removal of divalent ions would make the water fit for reuse in the make-up of viscous flooding solution to be injected into the subsurface.

Compared to other options available to desalinate produced water (like thermal and pressure-based membrane treatments) [12,22–24], electrodialysis offers two main advantages: 1) the desalination target can be easily adjusted; and 2) since only ions are removed, the remnant polymer in the desalted solution contributes to attain the viscosity needed, i.e. savings on fresh polymer additions [25]. Moreover, it has been reported that through varying operation parameters, like current density and flowrate, preferential removal of a number of ionic species can be achieved [5,26]. Thus, electrodialysis could be employed to desalinate water generated from polymer flooding applications –better referred as polymer-flooding produced water (PFPW)–, to enable its reuse. The first step would be to select the adequate type of membranes and process parameters.

3.1.1   Factors affecting permselectivity for specific ions: affinity, differences in migration speed, and process conditions

The core of an electrodialysis assembly are the ion-exchange membranes (IEMs), which selectively allow the passage of oppositely charged ions (counter-ions), while obstructing similarly charged ions (co-ions). However, for PFPW desalination and other applications, it is also desirable to have permselectivity between counter-ions of different valence [4], like Na^+ and Ca^{2+}. The topic has been investigated by Sata [2], who found that the permselectivity for specific ions in ion exchange membranes is only governed by the affinity of the ions to the membrane (ion exchange equilibrium constant) and the differences in the migration speed of the ions in the membrane phase. However, this affirmation is conditioned to the elimination of the effect of the diffusion boundary layer, which is usually not realistic. Hence, the transport of counter-ions also depends on the operational conditions, explicitly, on the current density and fluid dynamics. These parameters directly influence the concentration polarization phenomena, controlling the formation of diffusion boundary layers close to the membrane, and thus affect its selectivity [4,27,28]. This and most findings regarding the selectivity of monopolar membranes can be found in a recent review by Luo et al. [4], so we limited our literature overview to the most relevant cases for the application.

Most studies related to competitive ion transport have been focused on the cation exchange membranes (CEMs). According to Kim et al., the competitive transport is governed mainly by two factors: the CEM selectivity and the boundary layer thickness [29]. While studying the separation of K^+ and Ca^{2+}, they observed an increase in the transport number of K^+ ions with an increase in current density (or cell pair potential drop). They concluded that despite the CEM has a higher affinity towards Ca^{2+} due to the greater ionic charge, the boundary layer facilitates a higher K^+ transport number due to its higher diffusivity. Zabolotsky et al. also had calculated that as a consequence of boundary layer development, the transport number of Ca^{2+} ions decreased if the current density was increased [30]. Thus, both studies coincide that divalent transport number is increased with lower current densities, when the boundary layers are less pronounced. Later, Galama et al. desalinated synthetic seawater and found that indeed the application of low current densities enhanced the transport numbers of both, divalent cations and divalent anions [5]. Other authors have also reported enhanced transport numbers of divalent cations by applying lower current densities[7] and temperature gradients [6].

However, most of the publications on competitive transport utilized aqueous solutions with diverse salts, in absence of other components. In case charged polymers are added, i.e. residual polymers in produced EOR waters, it is unclear how these would affect the processes in the boundary layers and thereby the permselectivities of salt ions.

3.1.2   Potential effects of polymer presence in selectivity

The presence of polymer may affect the transport of ions due to three main reasons. Firstly, it may alter the removal of all ions in general because it affects the macroscopic viscosity of the solution, which directly influences the attained turbulence of the fluid, concentration polarization, and thickness of the diffusion boundary layers [6,31].

Then, considering that the most common viscosifying polymer is HPAM, its presence in solution could affect the effective diffusion coefficient of ions, particularly of cations. The charged segments of the anionic polyelectrolyte may interact with the diffusing ions and give rise to some retardation of the diffusivity. Furthermore, there is a known affinity between the divalent cations and HPAM [32,33], and it has been described how Ca^{2+} and Mg^{2+} can interact with the acrylic anion in a polyacrylamide derivative [34]. If these cations remain bound to the polymer instead of being free in solution, they may stay longer in the diluate.

The presence of HPAM could also trigger some differences in the removal rate of anions, in this case due to the adsorption and concentration polarization of negatively charged HPAM on the surface of the AEM [35,36], as represented in **Figure 3.1**. It has been reported that the adsorption of an anionic polyelectrolyte on the surface of strongly basic AEMs can decrease the transport number of SO_4^{2-} relative to that of Cl^- due to stronger electrostatic repulsion between the anionic surface layer and the SO_4^{2-} ions [37]. Concentration polarization is enhanced because the HPAM molecules tend to move towards the anode under the influence of the electric field [36], creating a gel layer that might hinder the transport of (certain) ions.
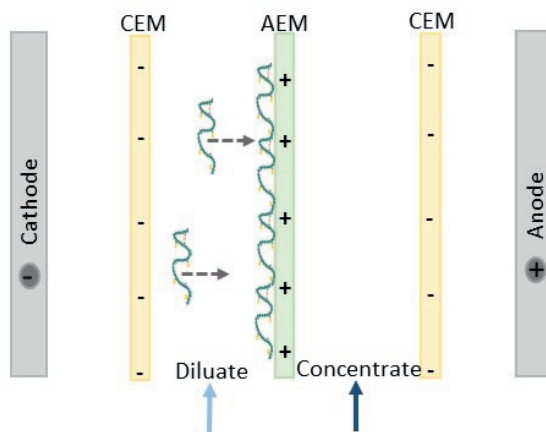
Figure 3.1. *Representation of the adsorption of HPAM to the AEM during the desalination process.*

3.1.3   Objectives

The objective of this work was to achieve and evaluate the preferential removal of divalent ions from synthetic PFPW through varying operational conditions, namely current density and temperature. It must be emphasized that the selection of this last variable followed two main reasons: 1) the temperature of PFPW is highly dependent on the location where the EOR process is carried out [38], and 2) its variation can influence the results of an electrodialysis run in several ways, because many relevant parameters (including the diffusion coefficients of ions, the viscosity of the fluids, and the membrane properties) are temperature dependent [6,39,40].

Additionally, the effect of the dissolved polymer on the removal was assessed by performing half of the experiments on polymer-containing solutions and half of them on solutions without polymer. The effect of achieving preferential removal of divalent ions over the monovalent ones was assessed by measuring the viscosity attained when a fixed amount of fresh polymer is added to prepare viscous polymer solution from the desalinated water.

3.2   Materials and methods

3.2.1   Materials

3.2.1.1   *Electrodialysis setup*

Experiments were performed in an ED stack and setup like the one previously described [25]. The stack contained five repeating cells, each consisting of a cation exchange membrane (Neosepta CMX) and an anion exchange membrane (Neosepta AMX), both from Tokuyama Co. (Japan). This membrane pair has been characterized elsewhere [41]. The working area of the membranes was 104 cm². An additional CEM was placed at the beginning of the stack to close the first cell. The intermembrane distance was fixed by using woven ETFE fabric spacers (Fluortex 09-590/47, Sefar, Switzerland), with reported thickness of 485 µm. Gaskets made of silicone rubber with a thickness similar to the spacer thickness were used to seal all the compartments and to form the alternated flow channels for the diluate and the concentrate. On both sides of the stack, squared titanium electrodes (mesh 1.7, area 96.04 cm²) with a mixed metal oxide coating of Ru/Ir (Magneto Special Anodes BV, The Netherlands) were employed as cathode and anode. The stack was closed with plates made of PMMA (poly(methyl methacrylate)) and 8 bolts.

A potentiostat/galvanostat (Ivium Technologies, The Netherlands) was employed to control electrical current and to measure the potential difference. The potential difference over the membrane stack was measured using two reference Ag/AgCl gel electrodes (QM711X, QIS, The Netherlands) placed at the inlet of each electrode compartment. Conductivities of the diluate and concentrate were measured inline with two conductivity probes (Orion DuraProbe 4-electrode conductivity cell 013005MD) directly before the ED stack. The probes were connected to a dedicated transmitter box (Orion Versastar Pro), which corrected the measured values to the reference value at 25°C, and this last to a computer, where conductivity data was recorded. pH of the diluate and concentrate were also measured inline with two pH probes (MemoSENS Endress + Hauser, pH range 1 to 12), connected through a transmitter box (P862, QIS) with a data logger (Memograph M RSG30, Endress + Hauser).

The solutions were pumped through the stack by using peristaltic pumps (Cole-Parmer, Masterflex L/S Digital drive, USA). Temperature control during the experiments was achieved by employing 1.0 L glass jacketed vessels to store the diluate and concentrate solutions. On the external part of the vessels, water coming from a temperature-controlling recirculation bath was circulated. The electrolyte was also kept at the working temperature by means of a second temperature control bath.

3.2.1.2   *Solutions*

The diluate consisted of salt solutions with an initial composition specified in **Table 3.1** (TDS~32,000 mg/L), plus 1.0 g/L of commercial HPAM. To prepare the synthetic PFPW, 500 mL of previously prepared salt solution were poured in a glass bottle containing a magnetic stirrer. Next, 500 mg of commercial HPAM (MW= 5-8 million Da, 30% hydrolyzed) were slowly poured in the vortex formed in the salt solution stirred at 600 rpm. Once all the polymer was added, the stirring rate was reduced to 200 rpm and the bottle was closed. Each polymer solution was mixed overnight to assure complete hydration and employed within 72 hours of its preparation.

Table 3.1. *Measured mineral composition of diluate solutions. Prepared according to values in [25,42].*

Cations	C (mM)	Anions	C (mM)
Na^+	425.08	Cl^-	482.95
K^+	8.54	HCO_3^-	6.36
Ca^{2+}	8.74	SO_4^{2-}	32.57
Mg^{2+}	38.82		

For comparative purposes, ED runs without any added polymer (using as diluate the salt solution described in Table 1) were also performed. In all experiments, the initial concentrate consisted on solutions containing 5.0 g/L of sodium chloride. For the electrolyte compartments, solutions of 20 g/L sodium sulfate were circulated.

Additional solutions were prepared with each of the salts and 1.0 g/L of high molecular weight HPAM (MW= 20 million Da, 30% hydrolyzed) to characterize their influence on the viscosity of the flooding solution.

Analytical grade salts (NaCl, $CaCl_2 \cdot 2H_2O$, $MgCl_2 \cdot 6H_2O$, $NaHCO_3$, KCl, and Na_2SO_4) were purchased from VWR and employed without further purification. The HPAM employed were Flopaam 3230S (MW= 5-8 million Da, 30% hydrolyzed) and Flopaam 3630S (MW= 20 million Da, 30% hydrolyzed), both kindly provided by SNF (France). All the solutions were prepared with demi water.

3.2.2   Methods

3.2.2.1   *Electrodialysis runs*

ED experiments were carried out in a batch operation mode at fixed working temperatures (10, 20, and 40°C). The diluate and concentrate containing vessels were pre-conditioned to the desired temperature by circulating through their heating jacket water from the temperature-controlling bath. Later, 500 mL of the diluate and

concentrate solutions were poured in their corresponding vessels. The electrode rinse solution (2.0 L of sodium sulfate 20 g/L) was also conditioned to the experiment working temperature by immersing the container in a second temperature-controlling bath. The concentrate and the diluate were recirculated through the corresponding compartments of the ED stack at a flow rate of 120 mL/min (linear velocity of 1.03 cm/s), while the electrode solution was recirculated at a flow rate of 100 mL/min. The solutions were circulated in their correspondent circuits during 10 minutes before starting the experiment, allowing them to stabilize at the desired working temperature.

The experiments were run in constant current mode, with current densities values ranging 24 to 96 A/m² and switched to constant voltage mode when the limit value of the potentiostat of 8.8 V was reached. All experiments were stopped when the diluate's conductivity dropped to 1.0 mS/cm. During the experiments, stack voltage, electric current, pH, conductivity and the mass of the diluate were monitored. Samples of 1.0 mL were taken periodically from the diluate and concentrate reservoirs.

After each experiment with HPAM involved, the membrane stack was cleaned in-place. The procedure consisted in pumping a series of solutions in both the diluate and the concentrate compartments, each solution for a period of 10 minutes. The sequence of solutions was: sodium chloride solution (5 g/L), sodium hydroxide solution (0.1 M), fresh sodium chloride solution (5 g/L), hydrochloric acid solution (0.1 M), and finally fresh sodium chloride solution (5 g/L). This last solution would remain in the stack until a new experiment was performed.

All the experiments were performed at least in duplicate, and the results shown are the average of the values obtained for each case.

3.2.2.2 *Viscosity measurements*

The dynamic viscosities of the polymer solutions were measured with an Anton Paar MCR 102 rheometer, with the standard measuring system CC27/T200/SS (bob and cup configuration). The measurements were performed at constant shear rate, from 1.0 to 100 s⁻¹, at a controlled temperature of 40°C.

3.2.2.3 *Charge density*

The charge density of Flopaam 3230S was determined by colloid titration using a Mütek Particle Charge Detector (PCD03), as described elsewhere [43]. In brief, a 0.1 g/L polymer solution was prepared in MiliQ water (section 3.2.1.2) and later diluted to obtain a concentration of 1 mg/L. Then, a 10 mL sample with unadjusted pH (~6.5) was titrated against a complexing agent of opposite charge (0.01 mN poly-

diallyldimethylammonium chloride, pDADMAC), using an automatic titrator (Metrohm titrando 888). To perform the titration, the titrant was added in steps of 0.02 mL to the PCD measuring cell, while simultaneously recording the streaming potentials (mV). The specific charge quantity was then determined based on the titrant consumption in mL.

3.2.2.4   *Analytical methods*

Samples taken during the ED runs were analyzed to determine their cation and anion content. Cations (Na^+, K^+, Ca^{2+}, Mg^{2+}) were measured by inductive-coupled plasma optical emission spectroscopy (ICP-OES, Optima 5300DV, Perkin Elmer) and anions (Cl^- and SO_4^{2-} by ion chromatography (IC, 761 CompactIC, Metrohm). For the runs with HPAM involved, both diluate and concentrate samples were analyzed for total carbon (TC) and total organic carbon (TOC) using a TOC analyzer (Shimadzu TOC-VCPH). The total dissolved solids (TDS) content of each sample was calculated by adding the obtained concentrations of cations and anions.

3.2.2.5   *Evaluation of permselectivity*

The ion selectivity between divalent and monovalent ions of the same sign was quantified in terms of the ratio P_{monov}^{div}, which is defined as [4,44]:

$$P_{monov}^{div} = \frac{t_{div}/t_{monov}}{C_{div}/C_{monov}} \tag{/3.1/}$$

Where t represents the transport number of either divalent (*div*) or monovalent (*monov*) ions (-), and C their concentrations in the diluted compartment (eq/m^3). The transport number t is defined as [44]:

$$t_k = J_k / \sum [J_s] \tag{/3.2/}$$

Where J_k denotes the ion flux (eq/m^2h) of ion or group or ions k and $\sum[J_s]$ is the total ion flux. In order to focus on the monovalent vs divalent effect, a single transport number t and concentration C were calculated for monovalent cations (comprising $Na^+ + K^+$) and another for divalent cations ($Ca^{2+} + Mg^{2+}$). Ion fluxes were obtained from the ion concentration time courses in the diluted compartment during each experiment.

3.3 Results and discussion

3.3.1 General electrodialysis performance

ED experiments were carried out at three different temperatures: 10, 20 and 40°C, and four different current densities: 24, 48, 72, and 96 A/m². The initial conductivity of the solutions circulating in the diluate circuit was, on average, 49.7 mS/cm when only salts were present, and 49.1 mS/cm when 1.0 g/L of HPAM was dissolved in the solution. The corrected conductivities (section 3.2.1.1) did not show any significant variation for experiments running at different temperatures. Experiments running at a lower temperature had longer durations than the ones running at higher temperatures due to an earlier reaching of the limiting potential of 8.8 V and the consequent switching to the constant voltage mode. Detailed information is provided in **Table A3.1**.

The amount of TDS at different moments of the process was calculated by adding the measured concentrations of cations and anions from the samples taken (section 3.2.2.4). By plotting the TDS values against the diluate's conductivity, a constant linear relationship between these two parameters was confirmed, regardless of the different experimental conditions e.g. temperature and polymer presence (**Figure A3.2**). This is emphasized because later in the document comparisons are made for samples taken at analogous moments based on the conductivity in the diluate. Thus, these comparisons will not only refer to samples taken at same conductivity, but also at similar TDS content.

3.3.2 Removal of cations

The CEM used in this study, Neosepta CMX, is a strong membrane with fixed sulfonic groups. For this type of membranes, a general transport order has been recently described as: $Ca^{2+} > Mg^{2+} > K^+ > Na^+$ regarding the cations presently involved [4]. Additionally, the reported permeability of sodium over calcium ($P_{Ca^{2+}}^{Na^+}$) for the mentioned membrane is 0.64 (measured at 150 A/m² for a equimolar solution of both ions) [45]. At these conditions, the membrane is intrinsically more selective towards calcium, or in other words, it will permit the preferential removal of the divalent cations, presuming operational conditions allow the minimization of the effects of the boundary layers.

3.3.2.1 *Effect of current density on the removal of cations*

The results concerning ion removal at 20°C in absence of polymer are first discussed to facilitate the linking to the literature. Plot A on **Figure 3.2** shows the measured decrease of divalent cations (C_{div}, mM) and monovalent cations (C_{monov}, mM) versus the extent of desalination (presented as decreasing conductivity of the diluate), for the experiments performed on seawater at different current densities. Firstly, it must be noticed that the cation concentration decrease is linear for monovalent and

slightly curved for divalent ions. Additionally, the curvature is more pronounced for experiments ran at lower current densities. The curves indicate a faster decrease in ion diluate concentration for the divalent cations compared to that of the monovalent ones. This can be better visualized in plot C of the same figure, which shows the permeability of divalent over monovalent cations, calculated as described in section 3.2.2.5. Most of the obtained values are above 1, indicating preferential removal of divalent over monovalent cations. Indeed, the average value is 1.3, which is close to the value reported by [45]. In addition, it is possible to distinguish some differences in transport behavior depending on the applied current densities. While the experiments performed at 96 A/m^2 maintain an almost constant permeability during their entire duration, the values calculated for the runs carried on at 24 A/m^2 change during the desalination, peaking between 30 and 20 mS/cm. This variation in permeability suggests that the transport of ions is governed by different processes during the desalination, as will be further analyzed.

A further analysis of the transport of each cation for the two extreme current density cases is presented in plots E and G of **Figure 3.2**. The different profiles obtained in plots E and G, show the effect of the applied current density on the transport of cations, which is noteworthy for Ca^{2+} and Mg^{2+}, and in less obvious for Na$^+$. This can be explained considering that at low current densities the competitive transport is governed by the CEM selectivity, which prefers Ca^{2+} and Mg^{2+} over the monovalent ions [5,6,45,46]. On contrary, for higher current densities, the diffusion boundary layer becomes thicker [47] becoming the rate-limiting region [29], favoring the transport of monovalent cations due to their smaller hydrated size and faster diffusion rates. The exception is the K$^+$ profile, independent of the applied current density, which is in line with its high mobility/diffusivity, i.e. the boundary layer was not a limiting factor to the transport of this ion. The observed divalent ion transport order [Ca^{2+} > Mg^{2+} > Na$^+$] is in agreement with the ion-exchange and selectivity hierarchies reported in the literature [4]. Actually, a previous study [40] already reported a selectivity reversal for the [K$^+$/Ca^{2+}] system, finding in ion-exchange equilibrium experiments that the CMX membrane is more selective for potassium than for calcium, which seems to be the case for the initial part of the runs at 24 A/m^2 in plot E.
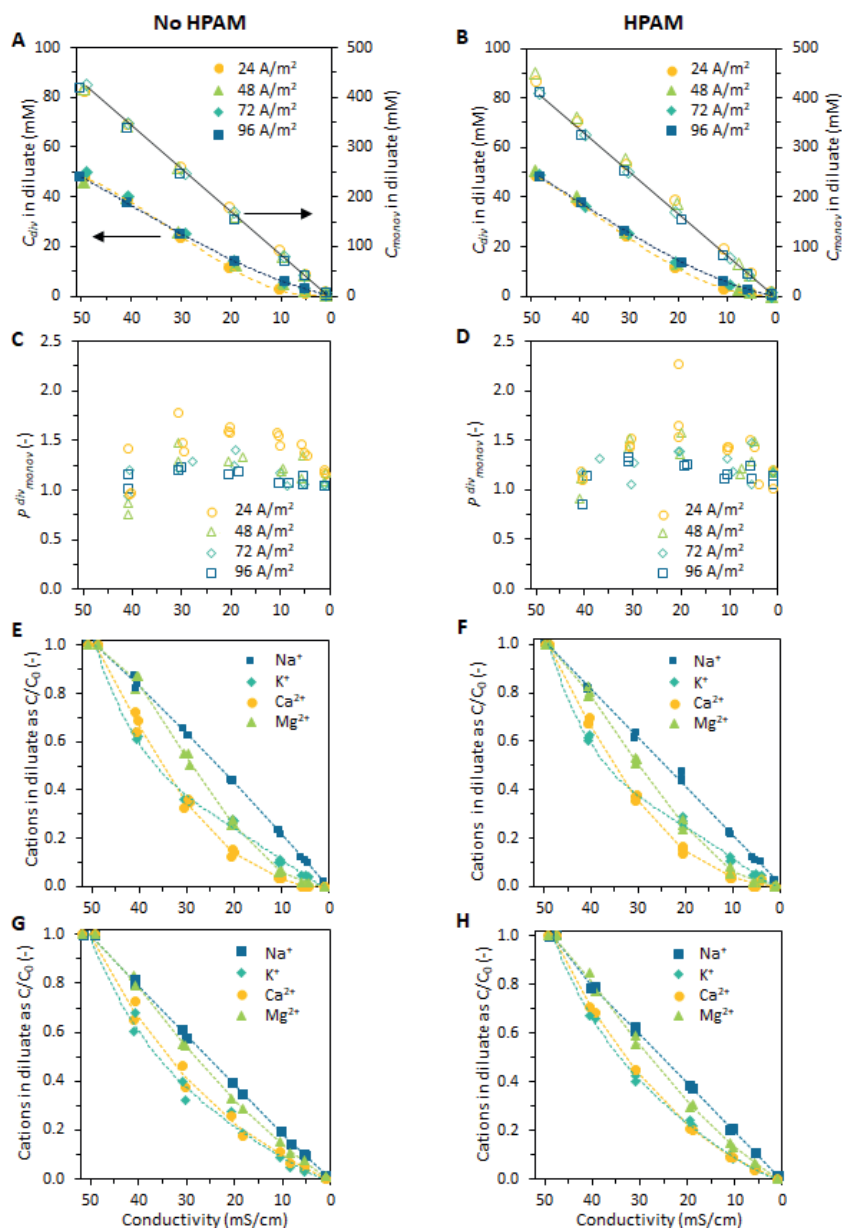
Figure 3.2. *Experiments performed at 20°C. **A, B)** Concentration of Ca^{2+} + Mg^{2+} (C_{div}, mM) (filled symbols) and Na^+ + K^+ (C_{monov}, mM) (open symbols) vs conductivity in the diluate during the electrodialysis at different current densities and 20°C. Continuous lines are presented to guide the eye. **C, D)** Permeability of divalent over monovalent cations (Eq. 1) vs conductivity in the diluate. **E, F)** Normalized concentrations of cations remaining in the diluate for experiments performed at 24 A/m^2, and **G, H)** 96 A/m^2. For **E, F, G,** and **H** the results of individual experiments are shown with the markers, while the trend lines indicate the median values of the measurements. **A, C, E,** and **G** refer to experiments without HPAM, while **B, D, F,** and **H** to experiments with HPAM*

Overall, the observed preferential removal of divalent cations is in agreement with other studies [13,29,48–50], and especially with the one of Galama et al. [5], who also focused on the desalination of seawater at 20°C when applying similar current densities (30 and 100 A/m^2) in a stack containing Neosepta CMX membranes. Similar composition profiles were obtained for the mentioned current densities despite having differences in the experimental conditions (like initial composition of the concentrate and linear fluid velocity), and slightly different feed composition (they had 10% higher TDS). Thus, the influence of the applied current density over other process variables results noteworthy. These results show that the transport of divalent cations is favored over the transport of the monovalent ones, for conditions with less pronounced diffusive boundary layers, such as at low current densities.

3.3.2.2 *Effect of polymer presence on the removal of cations*

The addition of HPAM increased the viscosity of the solution. For the experiments at 20°C, the seawater solution with 1.0 g/L of polyelectrolyte had an average viscosity of 4.8 mPa·s, calculated from the initial (3.33 mPa·s) and final (6.03 mPa·s) viscosities measured with the rheometer, as reported in our previous study [25]. This value is approximately 4.6 times the viscosity of the seawater solution without polymer [25]. However, it must be remarked that a rheometer reports the macroscopic viscosity, which may deviate significantly from the microscopic viscosity experienced by the ions in the solution due to their friction with the solvent [51]. The microscopic viscosity is not affected much because the solvent is still water plus a very low concentration of dissolved polymer segments at 20°C. This means that the diffusion coefficients of the ions should remain the same despite the changes in macroscopic viscosity. This was validated by the conductivity readings, which were practically the same for solutions with and without HPAM (section 3.3.1), and is also reported in the literature for other solutions viscosified with polymers [31,52]. Thus, the presence of HPAM could only influence the selectivity by changing the fluid dynamics in the electrodialyzer, and by interacting with the ions in solution.

Regarding the change of fluid dynamics on the electrodialyzer, we drew on the potential requirement during the experiments to find out if there was an impact on concentration polarization. The data is included in **Figure 3.3**, from which two main facts can be noticed. The first is that, no matter the experimental conditions, the voltage kept increasing since the start of the experiments, indicating continuous increase of resistance in the stack (according to Ohm's law). However, during the first half of our desalination experiments, the ohmic resistance was supposed to decrease, given that the resistivity of the initial concentrate solution was five times higher than the one of the diluate (95 vs 20 Ω·cm, respectively). The continuous increase thus suggests that the dominating resistance was in the diluate compartment, possibly due to the progressive development of concentration polarization in the diffusion boundary layer [6,47].

The second remark for **Figure 3.3** is the similarity of the curves obtained for the experiments with and without polymer. For the experiments run at lower current densities (24 and 48 A/m²) the presence of polymer was not a determining factor in the potential needed to sustain the fixed currents densities. However, for the experiments performed at 72 and 96 A/m², the presence of HPAM resulted to a higher voltage in the cell, a sooner reaching of the limiting voltage in the potentiostat, and slightly longer experiments (Table A3.1). This could be caused by the lower turbulence in the cell when the diluate is viscosified, which affects the mass transfer from the bulk of the fluid to the surface of the membrane [31]. However, it appears that the changes in fluid viscosity, and presumably in concentration polarization, were not severe enough to affect the "ordinary" selectivity for cationic species. **Figure 3.2** shows that there was practically no difference between the concentration profiles for experiments performed at the same current density, disregarding the presence of polymer.
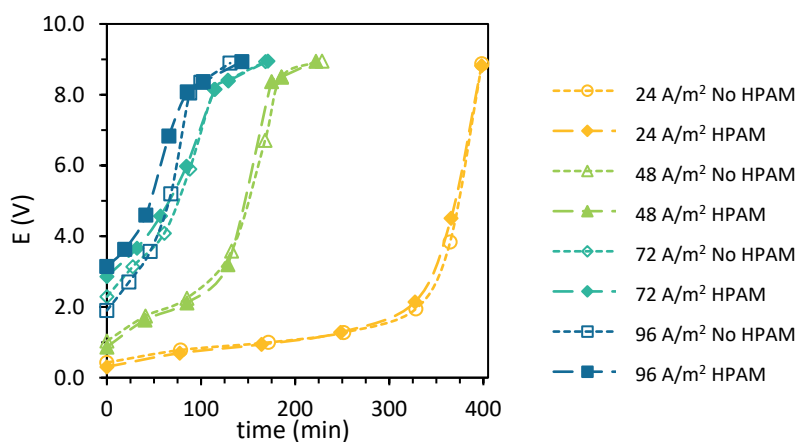
Figure 3.3. Voltage applied to the stack as a function of time for experiments at 20°C.

Concerning the interaction of HPAM with the cations, again **Figure 3.2** shows that the composition profiles and permeabilities of divalent over monovalent cations are alike the ones obtained for the solutions without polymer (left vs right side in the figure). The main difference is the presence of small amounts of divalent cations (0.1 mM of Mg^{2+}) in the last samples taken from the experiments run with HPAM at 24 A/m², while for the analogues without HPAM no divalents were detected. These results were somewhat surprising because, as mentioned in section 3.1.2, HPAM has a special affinity to divalent cations [32,33], and its acrylic group bonds particularly well with calcium [34]. However, the plots show that the transport rate of both divalent and monovalent ions is only affected by the applied current density and not by the presence of polymer. The charge density of HPAM in solution was experimentally determined (section 3.2.2.3) to a value of 5.62 meq/g. Thus,

considering the polymer concentration in the diluate bulk (1.0 g/L), approximately 5.62 meq/L of the cations could remain bound to the polymer instead of being free in solution, being retained in the diluate. The initial solution contained approximately 95 meq/L of divalent cations (17 meq/L of Ca^{2+} and 78 meq/L of Mg^{2+}) and 433 meq/L of monovalent cations, so they were present in excess. However, the remaining part of divalent ions was much less than 5.62 meq/g (a maximum of 0.74 meq/g Mg^{2+}, and 0 meq/g Ca^{2+}), hence the forces of the imposed electric field on the cations appear to overrule the electrostatic attractive forces in solution between divalent cations and polymers.

3.3.2.3   *Effect of temperature on removal of cations*

Let us next consider the removal of divalent cations at different temperatures, 10 and 40°C, in the presence of HPAM. Again, the effect of having a viscous diluate in the formation of a boundary layer can be extracted from the information in Table A3.1. At 40°C, we observed that for runs at the same current density, the switching points and total durations were practically indifferent to the presence of HPAM. On the contrary, for 10°C, the presence of HPAM significantly affected the behavior of runs at current densities above 24 A/m². In the most extreme case (96 A/m²), the limiting potential was reached when only 1.68×10^3 C had been transported, half the amount that theoretically passed in the absence of polymer.

To explain these observations, as well as the removal of divalent cations, it must be considered that the difference in temperature can influence the boundary layers by two mechanisms: by affecting the diffusion coefficient of the ions [53,54], and by changing the macroscopic viscosity of the fluid [25]. Both factors contribute to make ion mobility less susceptible to diffusion limitation due to thinner boundary layers. Therefore, the differences in experimental results in presence and absence of HPAM (evaluated at the same current density and temperature) are attributed to the changes in flow conditions and its effect in concentration polarization. Then, as shown in **Figure 3.4**, most of the normalized concentrations for experiments at same temperature and current density fall within the same trend lines, indicating that the transport of divalent cations was practically unaltered by the different flow conditions attained within the cell. Indeed, even the results obtained at different temperatures were very similar. **Figure 3.4** highlights by means of tendency lines the two most extreme cases regarding experimental conditions: the experiments performed at 40°C without HPAM (low viscosity and high diffusion coefficients) and the ones at 10°C with HPAM (high viscosity and low diffusion coefficients). Yet, even between these two extremes the differences in transport of divalent cations are only perceptible for the runs performed at 24 and 48 A/m². This can be explained by considering that at high current densities the boundary layer is already so significant that the selective transport is governed by the diffusion of the ions through it [29].

At this point, the changes in temperature and hydrodynamic conditions are not enough to make a difference in the observed selectivity. In contrast, when lower current densities are applied, the differences in diffusivity can still impact the thickness of the boundary layer, so the membrane properties can still exert influence on the removal. However, it is also noted that the early reaching of the maximum voltage for the experiments at 72 and 96 A/m^2 and 10°C limits the data points available for comparison, and therefore extensive mechanistic interpretations.
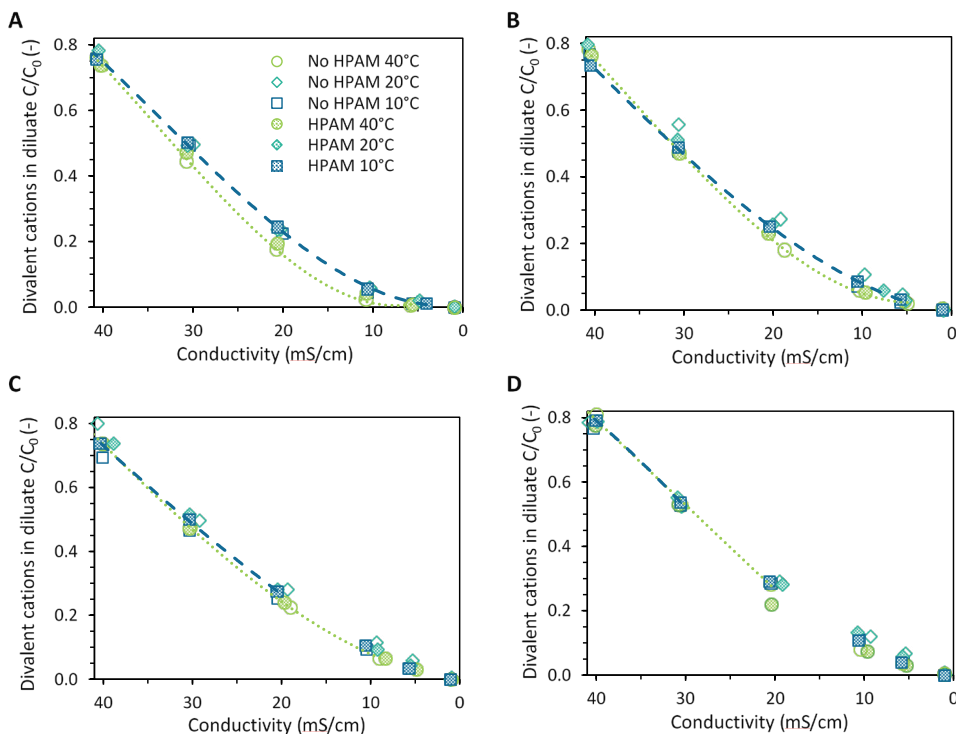
Figure 3.4. Normalized concentrations of divalent cations remaining in the diluate for experiments performed at different temperatures, with and without HPAM, at fixed current densities A) i= 24 A/m^2, B) i= 48 A/m^2, C) i= 72 A/m^2 and D) i= 96 A/m^2. Data from the initial part of the runs is not shown to give visibility to the final stage. Discontinuous lines for the most extreme cases are included for guiding the eye and to indicate when the system got voltage limited.

However, **Figure 3.4** also shows that the concentration of divalent cations for experiments performed at 40°C was always lower than for the other temperatures, no matter the current density nor the presence of HPAM. There is another factor to be considered when discussing the effect of temperature on the competitive transport: its influence on the membrane properties. It was already mentioned that at 25°C, the CMX membrane has a larger permeability for calcium over sodium [45]. Furthermore, it has been reported that the selectivity coefficient of the CMX for Ca^{2+} over Na$^+$ increases with temperature, doubling when measured at 40°C instead of

10°C [40]. Even if Mg^{2+} was not included in the referred study, its similarity with Ca^{2+} and our own observations indicate that the enhanced selectivity of the CMX membrane at higher temperatures is probably also applicable for the system $[Mg^{2+}/2Na^+]$.

Thus, for the system studied, a combination of factors was shown to be beneficial to achieve higher removal of divalent cations: i) low current densities which allow the intrinsic selectivity of the membrane to dominate the process, and ii) higher temperatures which reduce the thickness of the boundary layer and increase the selectivity of the CMX membrane towards the divalent species. This can be better visualized in **Figure 3.5**, which shows the percentage of divalent cations remaining in the diluate for the samples taken at conductivities 10.5 and 5.5 mS/cm (corresponding to approximately 83 and 91% of TDS removal). In all cases, the experiments at 24 A/m² and 40°C retained a lower amount of Ca^{2+} and Mg^{2+} compared to experiments run at higher current densities and lower temperatures, as expected from the previous analysis. In addition, it is shown that the effect of the low current density is less pronounced when HPAM is present, which is thought to be related to the viscosity of the fluid increasing during the last part of the process.

### 3.3.3   Removal of anions

3.3.3.1   *Effect of current density on the removal of anions*

Following a similar scheme as for the transport of cations, **Figure 3.6** shows the concentration of anions in the diluate during the experiments run at 20°C at different current densities. It must be considered that given the minimal concentration of bicarbonate (6.36 mM) compared to that of chloride (490 mM) in the feed water, the removal of the first was not monitored. Then, **Figure 3.6A** shows that, for the experiments without HPAM, the concentration of chloride decreased in a fast and constant mode, while sulfate ions tended to stay longer in the diluate, without much apparent influence of the applied current density. Only when the concentration of chloride had dropped to around 150 mM, the sulfate decreases more meaningfully. This can be better observed in **Figure 3.6C**, which shows how the permeability of sulfate over chloride started in low values (around 0.3) and kept increasing during the experiment, finalizing around 0.9 for all current densities. This means that the removal of sulfate was always lower than that of chloride, so at the end of the desalination the molar concentration of both anions was nearly the same. Regarding the influence of the current density, only one of the experiments performed at 24 A/m² (out of 3) slightly deviated from the general behavior of the rest of the experiments, so a possible explanation for this observation is explored further in the text.
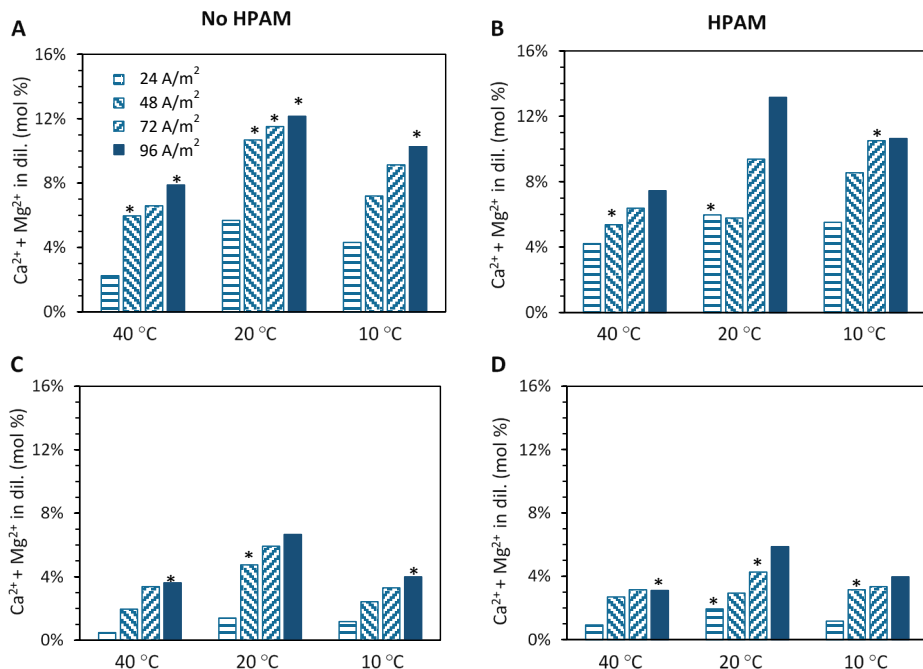
Figure 3.5. *Percentage of Ca^{2+} + Mg^{2+} remaining in the diluate.* **A)** *Samples taken at 10.5 mS/cm from experiments without HPAM;* **B)** *Samples at 10.5 mS/cm with HPAM;* **C)** *Samples taken at 5.5 mS/cm from experiments without HPAM;* **D)** *Samples at 10.5 mS/cm from experiments with HPAM. Each bar is the average calculated from 2 independent experiments, and the star (*) indicates that the individual values differed above 10%.*

The transport tendencies for the anions agree with the results of Galama et al. [5], who reported a constant reduction of chloride while the removal of sulfate accelerated after approximately two thirds of the salts had been removed, although in their study they found differences in transport rate depending on the applied current density. Sirivedhin et al. [13] also reported different removal rates of anions depending on the initial salinity of the water to be desalted. For waters with high salinity (TDS above 62,000 mg/L), chloride was preferentially removed, most probably due to its higher feed concentration. Meanwhile, for low salinity waters (TDS ~5,000 mg/L) the removal of sulfate was faster than for the other anions, especially when a low voltage was applied [13]. Indeed, the expected removal order of anions passing through a strong AEM is Cl^- > SO_4^{2-} [4,37], although it has also been reported that the AMX membrane is more selective for sulfate than for chloride ($P_{Cl^-}^{SO_4^{2-}} = 1.3$) when evaluated for a equimolar solution of chloride and sulfate at 30°C and 20 A/m² [44]. Thus, our results together with the literature indicate that the competitive transport of chloride and sulfate ions through the AMX membrane is highly dependent on the concentration of the bulk solutions and the process operational conditions.
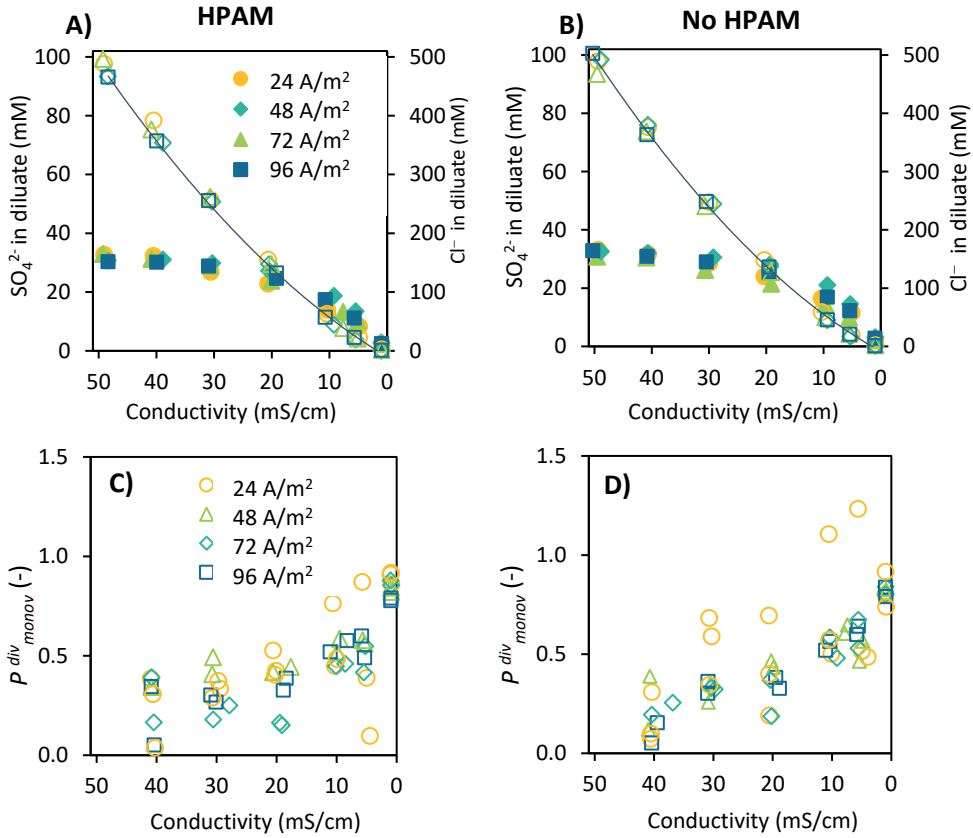
Figure 3.6. A, B) *Concentration of anions in the diluate during the electrodialysis at different current densities and 20°C. The concentration of divalent anions (filled symbols) can be read in the left axis, while the concentration of the monovalent ones (non-filled symbols) can be read in the right axis. Continuous lines are presented to guide the eye.* ***C, D)*** *Ratio of monovalent over divalent anions.* ***A*** *and* ***C*** *refer to experiments without HPAM, while* ***B*** *and* ***D*** *to experiments with HPAM*

### 3.3.3.2   *Effect of polymer presence on the removal of anions*

Regarding the influence of HPAM in the removal of anions, **Figure 3.6** shows that there were no significant differences between the experiments performed with and without HPAM. In both cases, chloride was preferentially removed, the final diluates contained equimolar amounts of both anions, and there was no distinction regarding the applied current density. This similarity can be explained by considering that the concentration polarization of HPAM on the membranes only occurs mainly in the final stage of the experiments, when the ionic strength of the solution has diminished considerably, as observed in our previous study [25]. Thus, during most part of the experiments the polyelectrolyte remains free in solution, not interfering with the normal electrodialysis performance.

Additionally, one of the triplicates of the experiment at 24 A/m^2 presented again a slightly higher permeability of sulfate over chloride (**Figure 3.6D**). Both observations are thought to be due to a higher pH of the diluate stream, particularly when the last sample was taken, which was the only anomaly in common for both experiments. While for the two referred cases the final pH of the diluate was around 5, for most of the experiments the pH reached a value of 4. This was most probably caused by an incomplete removal of the acidified solution during the washing procedure.

3.3.3.3 *Effect of temperature on anions removal*

The effect of temperature on the removal rate of sulfate was more substantial that the one measured for the divalent cations, as can be seen on **Figure 3.7**. While for the experiments performed at 10°C the sulfate removal was like the one obtained at 20°C, experiments at 40°C showed a faster transport of the referred anion. This faster removal at increasing temperature could be due to two factors: i) the faster diffusion coefficient of the sulfate anion, which would increase its concentration near the membrane, and ii) the increased affinity of the AMX membrane towards sulfate with higher temperature [39]. In this regard, Guesmi et al. it reported that the selectivity coefficient of the AMX membrane for SO_4^{2-} over $2Cl^-$ increases almost tenfold for experiments at 40°C compared to the one measured at 10°C, this as a consequence of an increase of the equilibrium extent of reaction mounting with temperature [39].

Figure 3.7 also shows that the presence of polymer did not affect the transport tendencies of sulfate, as had been already observed for the experiments at 20°C. However, contrary to those, the runs at 40°C indicated an effect of the applied current densities on the removal of sulfate. The faster removal of sulfate at lower current densities is perceptible when comparing the removal at specific salinities. A feasible explanation is that at low temperatures, the transport through the AMX membrane is limiting the removal of sulfate, so varying current density does not have any effect on its removal. At higher temperatures, the transport of sulfate through the membrane is facilitated, so now the limiting process would be the transport from the bulk solution to the surface of the membrane, which is affected by concentration polarization and current density.

A

B

C

D
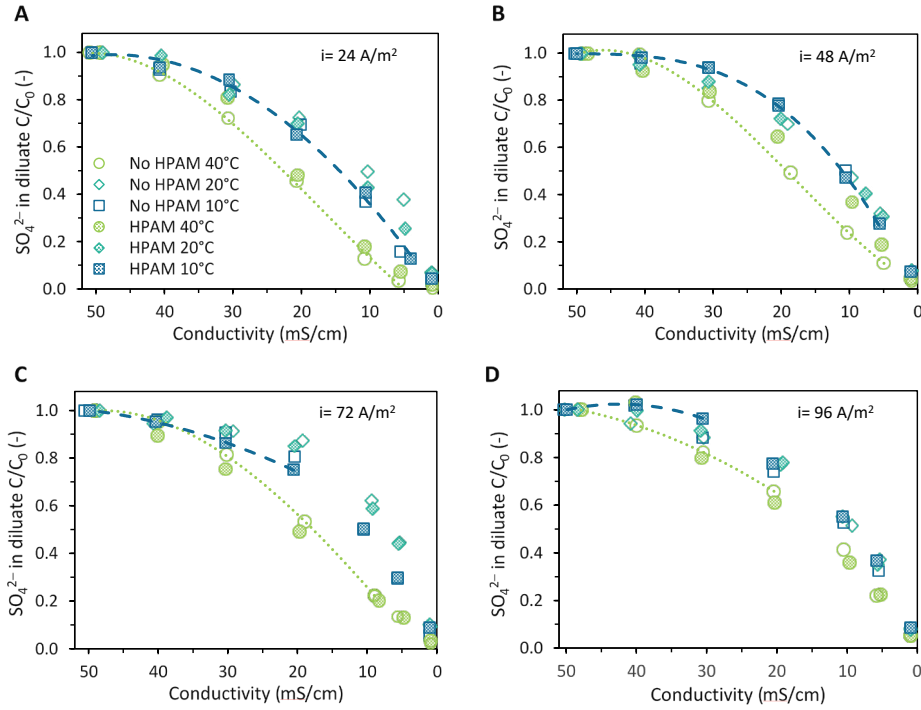
Figure 3.7. *Normalized sulfate remaining in the diluate for experiments performed at different current densities and temperatures, with and without HPAM. **A)** 24 A/m², **B)** 48 A/m², **C)** 72 A/m², **D)** 96 A/m². Discontinuous lines for the most extreme cases are included for guiding the eye and to mark the period for which the constant current was maintained.*

To close this section, we include **Figure 3.8**, which shows the percentage of sulfate remaining in the partially desalted diluate (10.5 and 5.5 mS/cm) for the different experimental conditions. The percentages of sulfate are significantly higher than the ones presented in **Figure 3.4** for the divalent cations, so it becomes clear that this anion was transported with more difficulty. For instance, when the diluate solutions had a conductivity of 10.5 mS/cm, most of them still had 50% of the initial amount of sulfate, while roughly 80% of the other ions had already been removed. Thus, the only conditions that allowed the preferential removal of sulfate were 40°C and 24 A/m², coinciding with the best settings for the removal of divalent cations. Our results indicate that in the presence of HPAM the removal of sulfate was slightly decreased, although the differences are minimal.

A No HPAM

B HPAM

3

C

D
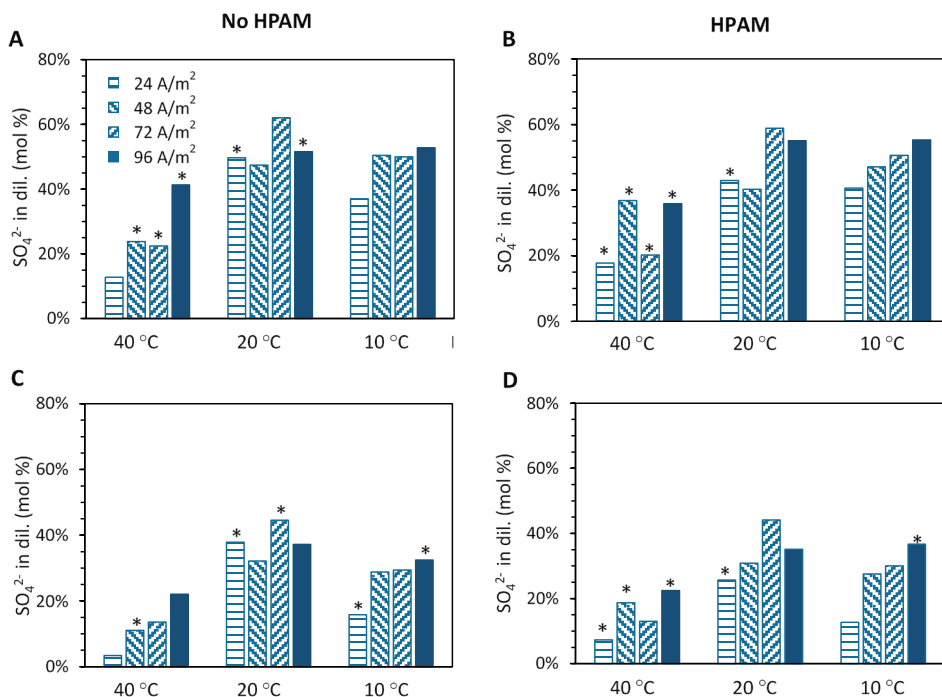
*Figure 3.8. Percentage of sulfate remaining in the diluate. **A)** Samples taken at 10.5 mS/cm from experiments without HPAM; **B)** At 10.5 mS/cm with HPAM; **C)** At 5.5 mS/cm from experiments without HPAM; **D)** At 5.5 mS/cm from experiments with HPAM. Each bar is the average calculated from 2 independent experiments, and the star (*) indicates that the individual values differed above 10%.*

3.3.4   Water reuse after desalination

As a final evaluation, we include a comparison of the properties of viscous solutions obtained when using electrodialysis versus a non-selective desalination. To represent the electrodialysis case, salt solutions were prepared with the compositions obtained in the best preferential removal case, this is, when the sea water was desalted at 40°C and 24 A/m². The no-preferential removal solution was prepared by adding demi water to the synthetic seawater until reaching the conductivity goal. Then, for both cases, high MW polymer was added and hydrated as described in section 3.2.1.2, and their viscosities measured at 40°C.

As shown in **Figure 3.9**, the four solutions prepared with water desalted through electrodialysis presented higher viscosities than the solutions prepared with diluted seawater, the differences ranging between 22 and 43%. These results demonstrate that even though the preferential removal of multivalent ions seemed minor, it can have measurable effects in the properties of the viscous solution, which would be potentially reflected as savings of fresh polymer and chemicals. If less polymer is required, the impact is also favorable in terms of chemical procurement,

transportation, storage and handling (mixing and hydration) requirements and operating costs [14].

Regarding the sulfate removal, the desulphation level needed to minimize the scaling would greatly depend on the amount of hardness in solution. As a reference, a sulfate reduction plant based on nanofiltration can decrease sulfate concentrations from 3000 to 40 mg/L, but even at this concentration there may still be a scaling potential [55]. However, it is also known that $SrSO_4$ precipitation is inhibited when $[SO_4]$ is below 1000 mg/L; and for $[Ba]$=80 mg/L, like in seawater [42], the precipitation of $BaSO_4$ starts when $[SO_4]$>175 mg/L [55]. Then, since the experiments run at 24 A/m² and 40°C achieved a final sulfate concentration under 10 mg/L when no HPAM was present (and 60 mg/L when it was), obtained results also seem promising in this aspect.
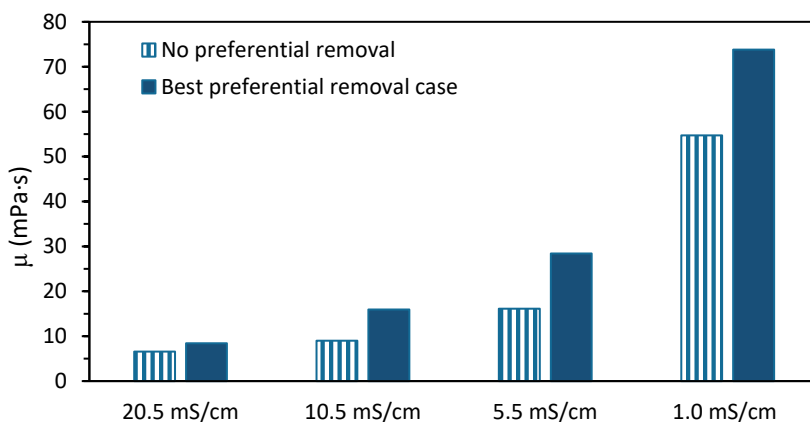
Figure 3.9. *Viscosity of HPAM solutions prepared with desalted water. For the "no preferential removal" case, the sea water solution was diluted with demi water until reaching the desired conductivity. The "best preferential removal case", was prepared according to the ionic compositions attained during the runs at 40°C, 24 A/m² and without polymer. All solutions were prepared with 1.0 g/L of high MW HPAM, and their viscosities measured at 40°C and 7.3 s⁻¹. Values measured at other shear rates are included in the Supplementary material.*

3.4   Conclusions

To be reused, polymer-flooding produced water needs to be partially desalted, and desirably stripped of its multivalent ions. For the composition studied in this article, it was identified that divalent cations, accounting for less than 10% of all the cations in solution, have the most significant effect in reducing the viscosity of polymer-flooding solutions.

Our results demonstrate that it is possible to achieve preferential removal of divalent cations through electrodialysis, especially when employing low current densities (24

A/m²) and high temperature (40°C). The removal of sulfate, a divalent anion, is also accelerated in these conditions. The presence of the polyelectrolyte HPAM does not significantly affect the removal rate of divalent ions. Thus, meticulous application of ED to minimize concentrations of divalent ions in PFPW is a potential effective way for water and polymer recycling in cEOR situations, as an alternative to the use of other non-selective desalination technologies. However, understanding permselectivity of ions and the phenomena affecting it, including the effects of the boundary layers, remains a topic for further clarifying research.

3

References

[1]   H. Strathmann, Electrodialysis, a mature technology with a multitude of new applications, Desalination. 264 (2010) 268–288. doi:10.1016/j.desal.2010.04.069.

[2]   T. Sata, Studies on ion exchange membranes with permselectivity for specific ions in electrodialysis, J. Memb. Sci. 93 (1994) 117–135. doi:10.1016/0376-7388(94)80001-4.

[3]   V.A. Shaposhnik, K. Kesore, An early history of electrodialysis with permselective membranes, J. Memb. Sci. 136 (1997) 35–39. doi:10.1016/S0376-7388(97)00149-X.

[4]   T. Luo, S. Abdu, M. Wessling, Selectivity of ion exchange membranes: A review, J. Memb. Sci. 555 (2018) 429–454. doi:10.1016/j.memsci.2018.03.051.

[5]   A.H. Galama, G. Daubaras, O.S. Burheim, H.H.M. Rijnaarts, J.W. Post, Seawater electrodialysis with preferential removal of divalent ions, J. Memb. Sci. 452 (2014) 219–228. doi:10.1016/j.memsci.2013.10.050.

[6]   A.M. Benneker, J. Klomp, R.G.H. Lammertink, J.A. Wood, Influence of temperature gradients on mono- and divalent ion transport in electrodialysis at limiting currents, Desalination. 443 (2018) 62–69. doi:10.1016/j.desal.2018.05.005.

[7]   N. Kabay, H. Kahveci, Ö. Ipek, M. Yuksel, Separation of monovalent and divalent ions from ternary mixtures by electrodialysis, Desalination. 198 (2006) 74–83. doi:10.1016/j.desal.2006.09.012.

[8]   M.S. Kamal, A.S. Sultan, U.A. Al-Mubaiyedh, I.A. Hussein, Review on Polymer Flooding: Rheology, Adsorption, Stability, and Field Applications of Various Polymer Systems, Polym. Rev. 55 (2015) 491–530. doi:10.1080/15583724.2014.982821.

[9]   J.A. Herschell, Water and Wastewater Treatment for Enhanced Oil Recovery, Mahon, Cork, Ireland, 2016.

[10]   Internacional Energy Agency (IEA), World Energy Outlook 2016, Paris, 2016. http://www.iea.org/publications/freepublications/publication/WEB_WorldEnergyOutlook2 015ExecutiveSummaryEnglishFinal.pdf.

[11]   G. Jing, L. Xing, S. Li, C. Han, Reclaiming polymer-flooding produced water for beneficial use: Salt removal via electrodialysis, Desalin. Water Treat. 25 (2011) 71–77. doi:10.5004/dwt.2011.1766.

[12]   S. Jiménez, M.M. Micó, M. Arnaldos, F. Medina, S. Contreras, State of the art of produced water treatment, Chemosphere. 192 (2018) 186–208.

doi:10.1016/j.chemosphere.2017.10.139.

[13]   T. Sirivedhin, J. McCue, L. Dallbauman, Reclaiming produced water for beneficial use: Salt removal by electrodialysis, J. Memb. Sci. 243 (2004) 335–343. doi:10.1016/j.memsci.2004.06.038.

[14]   S.C. Ayirala, E. Uehara-Nagamine, A.N. Matzakos, R.W. Chin, P.H. Doe, P.J. van den Hoek, A Designer Water Process for Offshore Low Salinity and Polymer Flooding Applications, SPE Improv. Oil Recover. Symp. (2013). doi:10.2118/129926-MS.

[15]   K.C. Tam, C. Tiu, Role of ionic species and valency on the steady shear behavior of partially hydrolyzed polyacrylamide solutions, Colloid Polym. Sci. 268 (1990) 911–920. doi:10.1007/BF01469369.

[16]   A. Samanta, A. Bera, K. Ojha, A. Mandal, Effects of alkali, salts, and surfactant on rheological behavior of partially hydrolyzed polyacrylamide solutions, J. Chem. Eng. Data. 55 (2010) 4315–4322. doi:10.1021/je100458a.

[17]   C. Gao, Empirical correlations for viscosity of partially hydrolyzed Polyacrylamide, J. Pet. Explor. Prod. Technol. (2013) 209–213. doi:10.1007/s13202-013-0064-z.

[18]   L. Henthorne, G.A. Pope, U. Weerasooriya, V. Llano, Impact of Water Softening on Chemical Enhanced Oil Recovery, 2014.

[19]   L.F. Lopes, B.M.O. Silveira, R.B.Z.L. Moreno, Rheological Evaluation of HPAM fluids for EOR Applications, Int. J. Eng. Technol. IJET-IJENS. 14 (2014) 35–41.

[20]   R. Cord-Ruwisch, W. Kleinitz, F. Widdel, Sulfate-reducing Bacteria and Their Activities in Oil Production, J. Pet. Technol. (1987) 10. doi:10.2118/13554-PA.

[21]   M.S.H. Bader, Sulfate removal technologies for oil fields seawater injection operations, J. Pet. Sci. Eng. 55 (2007) 93–110. doi:10.1016/j.petrol.2006.04.010.

[22]   C. Murray-Gulde, J.E. Heatley, T. Karanfil, J.H. Rodgers, J.E. Myers, Performance of a hybrid reverse osmosis-constructed wetland treatment system for brackish oil field produced water, Water Res. 37 (2003) 705–713. doi:10.1016/S0043-1354(02)00353-6.

[23]   E.T. Igunnu, G.Z. Chen, Produced water treatment technologies, Int. J. Low-Carbon Technol. 9 (2014) 157–177. doi:10.1093/ijlct/cts049.

[24]   M. Nasiri, I. Jafari, B. Parniankhoy, Oil and Gas Produced Water Management: A Review of Treatment Technologies, Challenges, and Opportunities, Chem. Eng. Commun. 204 (2017) 990–1005. doi:10.1080/00986445.2017.1330747.

[25]   P.A. Sosa-Fernandez, J.W. Post, H. Bruning, F.A.M. Leermakers, H.H.M. Rijnaarts, Electrodialysis-based desalination and reuse of sea and brackish polymer-flooding produced water, Desalination. 447 (2018) 120–132. doi:10.1016/j.desal.2018.09.012.

[26]   G. Jing, X. Wang, H. Zhao, Study on TDS removal from polymer-flooding wastewater in crude oil: extraction by electrodialysis, Desalination. 244 (2009) 90–96. doi:10.1016/j.desal.2008.04.039.

[27]   P. Długołecki, B. Anet, S.J. Metz, K. Nijmeijer, M. Wessling, Transport limitations in ion exchange membranes at low salt concentrations, J. Memb. Sci. 346 (2010) 163–171. doi:10.1016/j.memsci.2009.09.033.

[28]   R. Abu-Rjal, V. Chinaryan, M.Z. Bazant, I. Rubinstein, B. Zaltzman, Effect of concentration polarization on permselectivity, Phys. Rev. E - Stat. Nonlinear, Soft Matter Phys. 89 (2014) 1–10. doi:10.1103/PhysRevE.89.012302.

[29]   Y. Kim, W.S. Walker, D.F. Lawler, Competitive separation of di- vs mono-valent cations in electrodialysis: Effects of the boundary layer properties, Water Res. 46 (2012) 2042–2056. doi:10.1016/j.watres.2012.01.004.

[30]   V.I. Zabolotsky, J.A. Manzanares, V. V. Nikonenko, K.A. Lebedev, E.G. Lovtsov, Space charge effect on competitive ion transport through ion-exchange membranes, Desalination. 147 (2002) 387–392. doi:10.1016/S0011-9164(02)00614-8.

[31]   A. Kitamoto, Y. Takashima, Ionic mass transfer in turbulent flow by electrodialysis with ion exchange membranes, J. Chem. Eng. Japan. 3 (1970) 182–191.

[32]   S. Peng, C. Wu, Light Scattering Study of the Formation and Structure of Partially Hydrolyzed Poly(acrylamide)/Calcium(II) Complexes, Macromolecules. 32 (1999) 585–589.

[33]   R. Zhang, W. Shi, S. Yu, W. Wang, Z. Zhang, B. Zhang, L. Li, X. Bao, Influence of salts, anion polyacrylamide and crude oil on nanofiltration membrane fouling during desalination process of polymer flooding produced water, Desalination. 373 (2015) 27–37. doi:10.1016/j.desal.2015.07.006.

[34]   R. Yuan, Y. Li, C. Li, H. Fang, W. Wang, Study about how the metal cationic ions affect the properties of partially hydrolyzed hydrophobically modified polyacrylamide (HMHPAM) in aqueous solution, Colloids Surfaces A Physicochem. Eng. Asp. 434 (2013) 16–24. doi:10.1016/j.colsurfa.2013.05.036.

[35]   T. Wang, S. Yu, L. an Hou, Impacts of HPAM molecular weights on desalination performance of ion exchange membranes and fouling mechanism, Desalination. 404 (2017) 50–58. doi:10.1016/j.desal.2016.10.007.

[36]   H. Guo, L. Xiao, S. Yu, H. Yang, J. Hu, G. Liu, Y. Tang, Analysis of anion exchange membrane fouling mechanism caused by anion polyacrylamide in electrodialysis, Desalination. 346 (2014) 46–53. doi:10.1016/j.desal.2014.05.010.

[37]   T. Sata, Studies on anion exchange membranes having permselectivity for specific anions in electrodialysis - Effect of hydrophilicity of anion exchange membranes on permselectivity of anions, J. Memb. Sci. 167 (2000) 1–31. doi:10.1016/S0376-7388(99)00277-X.

[38]   Z. Gu, J. Qiu, Y. Li, G. Cai, Heat pump system utilizing produced water in oil fields, 23 (2003) 1959–1970. doi:10.1016/S1359-4311(03)00143-1.

[39]   F. Guesmi, C. Hannachi, B. Hamrouni, Effect of temperature on ion exchange equilibrium between AMX membrane and binary systems of Cl − , NO−3 and SO2−4 ions, Desalin. Water Treat. 23 (2010) 32–38. doi:10.5004/dwt.2010.1837.

[40]   A. Chaabouni, F. Guesmi, I. Louati, C. Hannachi, B. Hamrouni, Temperature effect on ion exchange equilibrium between CMX membrane and electrolytes solutions, J. Water Reuse Desalin. 5 (2015) 535–541. doi:10.2166/wrd.2015.008.

[41]   P. Długołecki, P. Ogonowski, S.J. Metz, M. Saakes, K. Nijmeijer, M. Wessling, On the resistances of membrane, diffusion boundary layer and double layer in ion exchange membrane transport, J. Memb. Sci. 349 (2010) 369–379. doi:10.1016/j.memsci.2009.11.069.

[42]   J. Zheng, B. Chen, W. Thanyamanta, K. Hawboldt, B. Zhang, B. Liu, Offshore produced water management: A review of current practice and challenges in harsh/Arctic environments, Mar. Pollut. Bull. 104 (2016) 7–19. doi:10.1016/j.marpolbul.2016.01.004.

[43]   V. Ajao, H. Bruning, H. Rijnaarts, H. Temmink, Natural flocculants from fresh and saline wastewater : Comparative properties and flocculation performances, 349 (2018) 622–632. doi:10.1016/j.cej.2018.05.123.

3

[44] S. Mulyati, R. Takagi, A. Fujii, Y. Ohmukai, H. Matsuyama, Simultaneous improvement of the monovalent anion selectivity and antifouling properties of an anion exchange membrane in an electrodialysis process, using polyelectrolyte multilayer deposition, J. Memb. Sci. 431 (2013) 113–120. doi:10.1016/j.memsci.2012.12.022.

[45] S. Abdu, M.C. Martí-Calatayud, J.E. Wong, M. García-Gabaldón, M. Wessling, Layer-by-layer modification of cation exchange membranes controls ion selectivity and water splitting, ACS Appl. Mater. Interfaces. 6 (2014) 1843–1854. doi:10.1021/am4048317.

[46] A. Chapotot, G. Pourcelly, C. Gavach, Transport competition between monovalent and divalent cations through cation-exchange membranes - Exchange isotherms and kinetic concepts, J. Memb. Sci. 96 (1994) 167–181. doi:10.1016/0376-7388(94)00107-3.

[47] P. Sistat, G. Pourcelly, Chronopotentiometric response of an ion-exchange membrane in the underlimiting current-range. Transport phenomena within the diffusion layers, J. Memb. Sci. 123 (1997) 121–131. doi:10.1016/S0376-7388(96)00210-4.

[48] N. Kabay, Ö. Ipek, H. Kahveci, M. Yüksel, Effect of salt combination on separation of monovalent and divalent salts by electrodialysis, Desalination. 198 (2006) 84–91. doi:10.1016/j.desal.2006.09.013.

[49] K. Loganathan, P. Chelme-Ayala, M. Gamal El-Din, Treatment of basal water using a hybrid electrodialysis reversal-reverse osmosis system combined with a low-temperature crystallizer for near-zero liquid discharge, Desalination. 363 (2015) 92–98. doi:10.1016/j.desal.2015.01.020.

[50] V.P. Greben, I.G. Rodzik, Selectivity of transport of sodium, magnesium, and calcium ions through a sulfo-cationite membrane in mixtures of solutions of their chlorides, Russ. J. Electrochem. 41 (2005) 888–891. doi:10.1007/s11175-005-0150-8.

[51] R.W. Impey, P.A. Madden, I.R. McDonald, Hydration and mobility of ions in solution, J. Phys. Chem. 87 (1983) 5071–5083. doi:10.1021/j150643a008.

[52] K. Aoki, B. Wang, J. Chen, T. Nishiumi, Diffusion coefficients in viscous sodium alginate solutions, Electrochim. Acta. 83 (2012) 348–353. doi:10.1016/j.electacta.2012.08.004.

[53] G.C. Benson, A.R. Gordon, The conductance of aqueous solutions of potassium bromide at temperatures from 15° to 45°C, and the limiting mobility of bromide ion, J. Chem. Phys. 13 (1945) 18–20. doi:10.1063/1.1723981.

[54] Y.-H. Li, S. Gregory, Diffusion of ions in sea water and in deep sea sediments, Geochim. Cosmochim. Acta. 38 (1974) 703–714. doi:10.1016/0016-7037(74)90145-8.

[55] L.S. Boak, E.J. Mackay, H. Al-Mahrouqi, C.E. Inches, K.S. Sorbie, M.C.M. Bezerra, R.O. Mota, What level of sulphate reduction is required to eliminate the need for scale inhibitor squeezing?, Int. Symp. Oilf. Scale. (2005). doi:10.2118/95089-MS.

Appendix 3A. Effect of individual salts on the viscosity of flooding solution

Several studies have reported the influence of multivalent cations on the viscosity of HPAM solutions [8,15,34], but for compositions considerably different to the one used in this study. Thus, Figure A3.1 presents an evaluation of the effect of each individual salt on the apparent viscosity of the polymer fluid. The presence of just 4.2 mM of sodium bicarbonate is enough to significantly decrease the viscosity of the polymer solution with 40% compared to absence of salt. This large drop of viscosity occurs because the polymers cannot swell as much as in demi water, i.e. polymer coils overlap in demi water (semi-dilute regime) and are separated when salt is present (dilute regime).

3
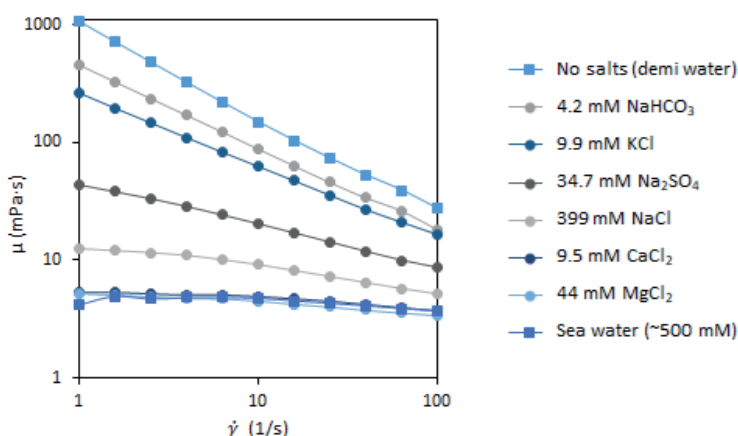
Figure A3.1. *Viscosity (μ) of solutions prepared with 1000 ppm of high MW HPAM and individual salts, measured at 40°C and shear rates (γ̇) between 1 and 100 s^{-1}*

Regarding the effect of divalent cations, it can be noticed that for similar molar concentrations of potassium and calcium chloride, the solution with calcium has a viscosity ten times lower than the solution prepared with potassium chloride. Other authors have also reported that, depending on the salt concentration and shear rate, the viscosity of HPAM solutions with added multivalent salts can decrease even one order of magnitude compared to solutions with only monovalent salts present [15–19]. It was also observed that solutions containing calcium and magnesium presented viscosity values that are half of the values obtained for the sodium chloride solution, despite their molar concentrations are 40 and 10 times smaller, respectively. This is due to multivalent ions not only causing the charge shielding effect, but also acting as a dynamic cross-linking agent to interconnect two different polymer molecules or two regions of the same one, further influencing the polyelectrolyte conformation and hence the rheological behavior of HPAM solutions [16].

These observations emphasize the urgency of primarily removing the multivalent cations from the PFPW to make it suitable for reuse. Otherwise, large amounts of polymer need to be added to obtain the desired viscosity and/or it is needed to employ more specialized (and expensive) polymer formulations that remain stable in brines with high hardness content [18].

Appendix 3B. Supplementary material

Table A3.1. *Average duration of experiments and switching points to constant voltage mode.*

| Tempe-rature	Current density	Experiment duration		Time for switching to constant voltage		Conductivity of diluate when switching		Charge passed before switching mode	
°C	A/m²	Min		min		mS/cm		10³ C	
		No HPAM	*HPAM*	*No HPAM*	*HPAM*	*No HPAM*	*HPAM*	*No HPAM*	*HPAM*
40	24	387	396	386	389	1.89	1.30	5.79	5.84
	48	222	202	201	184	4.68	4.20	6.04	5.53
	72	160	148	112	112	9.75	9.33	5.04	5.02
	96	120	118	79	78	12.06	12.15	4.75	4.67
20	24	398	406	379	381	2.83	2.57	5.69	5.71
	48	228	222	172	173	8.09	8.19	5.15	5.19
	72	168	171	105	100	12.86	14.56	4.70	4.50
	96	131	144	78	67	14.14	18.84	4.69	3.97
10	24	386	386	377	364	2.11	3.25	5.65	5.45
	48	199	212	176	168	4.43	7.75	5.28	5.04
	72	151	210	104	62	11.07	28.95	4.67	2.79
	96	158	203	54	28	25.18	37.46	3.19	1.68

3
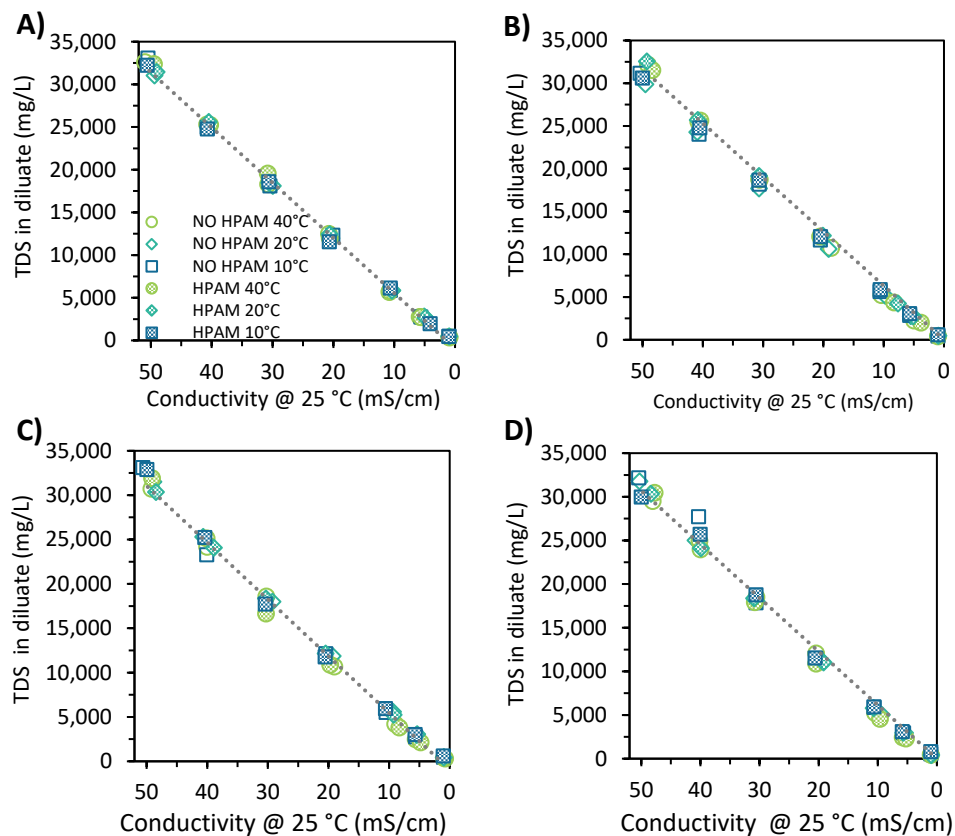
Figure A3.2. *Decrease of diluate's TDS as function of its conductivity in ED experiments at different current intensities:* **A)** *24 A/m², **B)** 48 A/m², **C)** 72 A/m², **D)** 96 A/m². The lines are only included as a visual reference and have no further meaning*
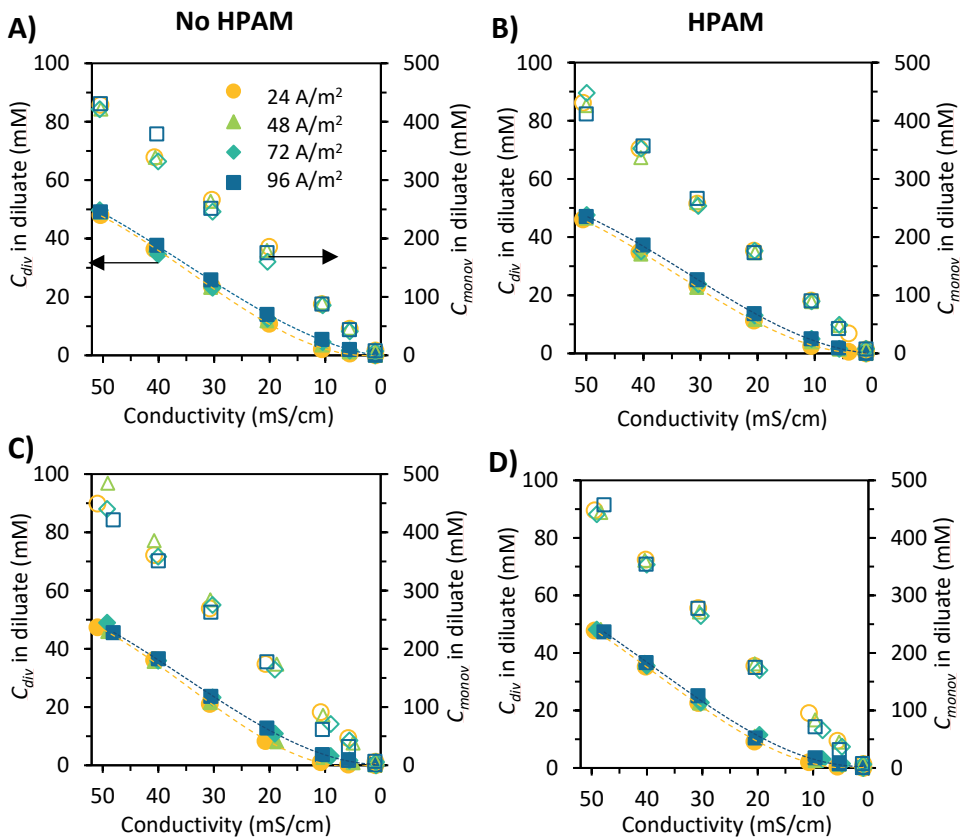
Figure A3.3. *Concentration of Ca²⁺ + Mg²⁺ (C_{div}, mM) (filled symbols) and Na⁺ + K⁺ (C_{monov}, mM) (open symbols) vs conductivity in the diluate during the electrodialysis at different current densities and temperatures. **A)** 10°C without HPAM, **B)** 10°C with HPAM, **C)** 40°C without HPAM, **D)** 4 °C with HPAM. Continuous lines are presented to guide the eye.*
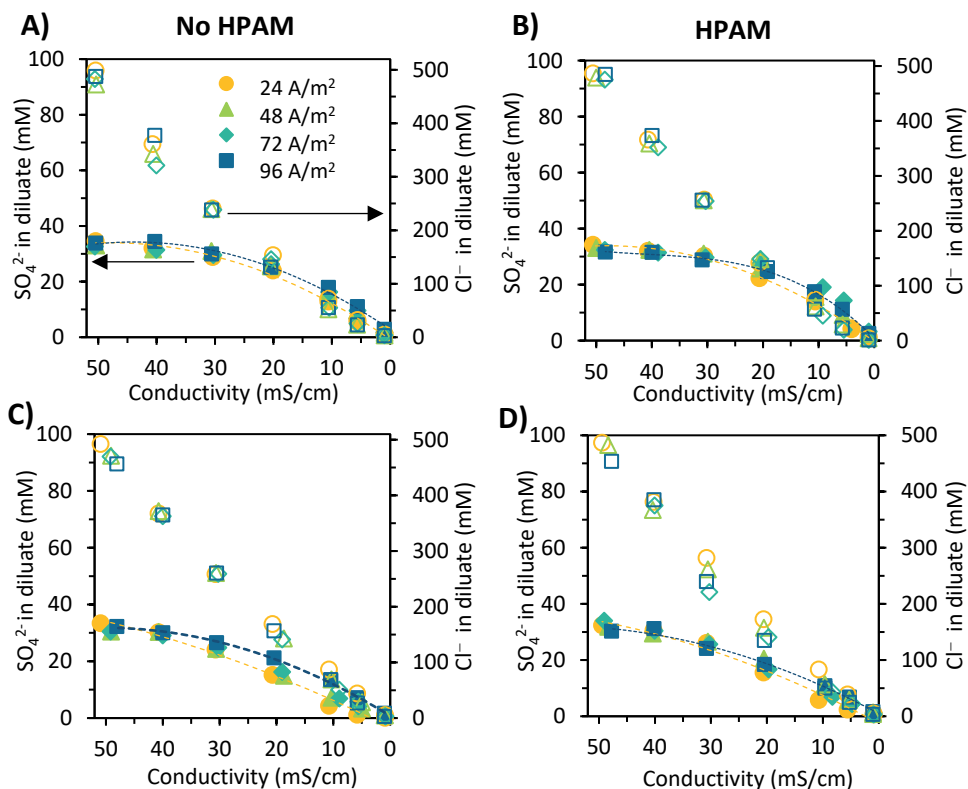
Figure A3.4. Concentration of SO_4^{2-} (mM) (filled symbols) and Cl^- (mM) (open symbols) vs conductivity in the diluate during the electrodialysis at different current densities and temperatures. *A)* 10°C without HPAM, *B)* 10°C with HPAM, *C)* 40°C without HPAM, *D)* 40°C with HPAM. Continuous lines are presented to guide the eye.
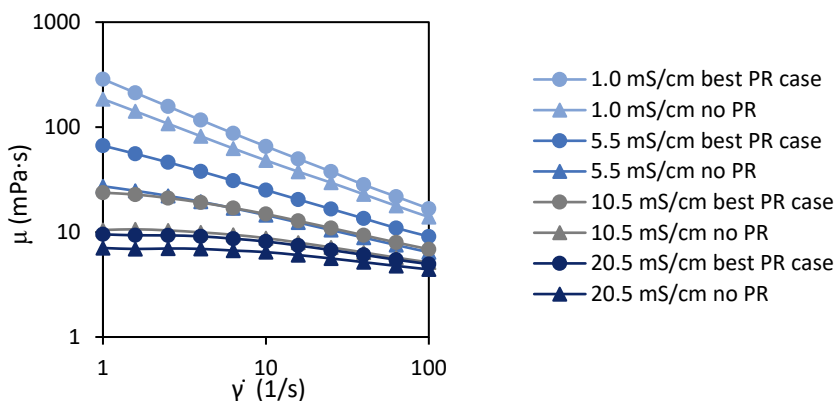
Figure A3.5. Viscosity of HPAM solutions prepared with desalted water. For the No preferential removal case ("no PR"), the seawater solution was diluted with demi water until reaching the desired conductivity. The best preferential removal case ("best PR case"), was prepared reproducing the ionic compositions attained during the runs at 40°C, 24 A/m² without polymer. All solutions contained 1.0 g/L of high MW HPAM, and their viscosities were measured at 40°C.
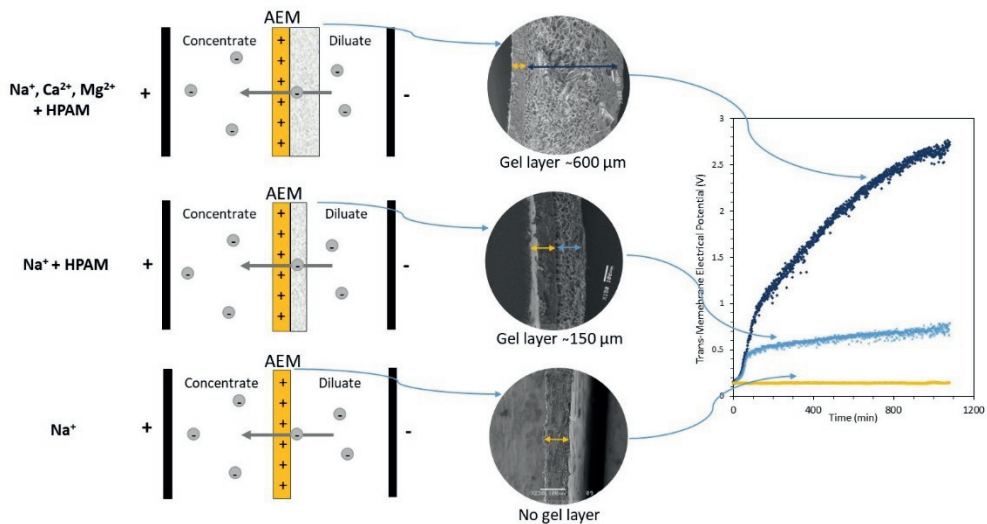
Chapter 4

Influence of feed composition on the fouling of anion exchange membranes desalinating polymer-flooding produced water

Abstract

Anion exchange membranes (AEMS) are known for being particularly prone to fouling when employed to desalinate polymer flooding produced water (PFPW), an abundant sub-product from the oil and gas industry. The formation of fouling on an AEM is thought to be affected by the composition of the solution, which includes various dissolved salts, partially hydrolyzed polyacrylamide (HPAM), crude oil, and surfactants. To test the influence of the feed, electrodialysis experiments were performed to desalinate feed solutions with different compositions, aiming to distinguish between their individual and combined effects. The solutions contained diverse mono- and divalent ions. The analysis included data collected during the desalination and characterization of the fouled AEMs by diverse analytical techniques. The results showed that HPAM produced the most severe effects in terms of visible fouling and increase of resistance. This polyelectrolyte fouls the AEM by adsorbing on its surface and by forming a viscous gel layer that hampers the replenishment of ions from the bulk solution. Ca and Mg have a large influence on the formation of thick HPAM gel layers, while the oily compounds have only a minimal influence acting mainly as a destabilizing agent. The membranes also presented scaling consisting of calcium precipitates. The effects of the gel layer were minimized by applying current reversal and foulant-free solution.

4.1 Introduction

Polymer-flooding produced water (PFPW) is an abundant stream from the oil and gas industry whose reuse can be beneficial, if adequately treated [1,2]. The stream is co-generated when polymer flooding technology is applied, which consists in injecting water viscosified with polymers into the oil reservoir, increasing the oil recovery by 5 to 30% [3]. The technology has been applied in more than 700 projects in 24 countries [4], and will likely continue to be implemented given the still increasing demand for oil [5]. This forecast also implies that large amounts of water will still be produced, provided that a single field can generate up to 75 million tons of PFPW every year [6]. Most of this water could be reused in the preparation of new polymer solutions for injection after receiving a primary treatment. However, if an additional desalination step is included after this basic treatment and the water is reused to prepare a viscous solution, the latter shows better rheological properties than solutions prepared with primary-treated PFPW or even with freshwater [1,7]. Furthermore, the desalination step is economically appealing since, in many scenarios, the savings in polymer can offset the desalination costs [8,9]. The desalination can be done via electrodialysis, a process that relies on the use of ion-exchange membranes (IEMs) and electric potential to transfer ions from a feed stream to a salty-concentrate. This technology, already operating on a pilot plant scale [1], has advantages over others because it allows the recovery of the desalted water and residual polymer in one stream [10], while the salt-containing stream still meets the requirements to be reinjected [11]. However, as for many membrane-based processes, the application of electrodialysis on a large scale is restricted by the occurrence of fouling on the IEMs [10].

Fouling is the undesirable attachment of particular substances or microorganisms to the outer or inner surface of a material [12]. The fouling occurring on IEMs when desalting PFPW causes a reduction in the desalination rates, an increase in the membrane's resistance, and a deterioration of the ion-exchange capacity [13,14]. Even after treating the PFPW with ultrafiltration [1,15], the stream still contains a variety of dissolved salts, surfactants, partially hydrolyzed polyacrylamide (HPAM), small amounts of solids in suspension and crude oil [1,11,15–17], which cause organic and inorganic fouling on the IEMs [13,14,17]. However, not all IEMs are fouled the same. The positively charged anion-exchange membranes (AEMs) are mainly fouled by the organic components, HPAM, and oil, while the negatively charged cation-exchange membranes (CEMs) are more susceptible to inorganic fouling [13]. When their individual resistance is measured, fouled AEMs presented a much higher increase compared to CEMs exposed to the same conditions [13,15]. Overall, the literature indicates that the impact of fouling by PFPW is more significant for AEMs than for CEMs, so it has been a priority of researchers to mechanistically understand and mitigate its formation.

The fouling caused by PFPW on AEMs has been studied in recent years. Guo et al. [18] carried out electrodialysis experiments of NaCl solutions with different HPAM concentrations at varying current densities, with the objective of finding the mechanism of AEM fouling by HPAM. The highest fouling phenomenon was observed with higher HPAM concentrations at higher current densities, and SEM analyses showed that a gel layer was formed on the diluate side of the AEM. Force-distance curves measured by AFM confirmed that electrostatic forces dominated the interactions between HPAM molecules and the AEMs. Thus, they suggested that the fouling was caused by negatively charged HPAM molecules moving to the positively charged AEM under electric field, forming a gel layer near the membrane surface, and fouling the AEM due to electrostatic interaction [18]. However, a previous study by Guolin et al. [10], had determined that crude oil caused the greatest increase in membrane resistance among AEMs fouled with either suspension solution, crude oil, or HPAM. They observed the formation of a compact oil film on the surface and inside the AEM, which would affect the permeation of the membrane. Later, Wang et al. [15] opposed this, concluding that HPAM affected the desalination performance and energy consumption more significantly than the oil-related effects, and that electrostatic interaction, interface thermodynamic interaction, and molecular weight of the polymer affected the membrane fouling [15].

Nevertheless, it is also known that the fouling effect can be enhanced by the interactions between inorganic and organic components [6,14]. This was recently described in the investigation of Xia et al. [13], who found through membrane resistance measurement and SEM analyses that the HPAM and the inorganic components (salts) have a synergistic effect on the fouling of IEMs. Although the study serves as a good precedent, it only evaluated the effect of a few components at fixed concentrations, and it was mainly focused on assessing the efficiency of chemical cleaning to remove the fouling from the membranes.

Accordingly, the objective of this work was to investigate how the formation of fouling on an anion exchange membrane is affected by the different components of PFPW, and to explain why this occurs. Contrary to most of the previous works, the solutions employed in this study do not only include sodium chloride, but also other mono- and divalent ions generally present in produced water, and which are known to affect the properties of HPAM [19,20]. Different concentrations of partially hydrolyzed polyacrylamide and of oily compounds were employed. The resistance of the fouling to the application of current reversal was also evaluated.

4.2 Materials and methods

4.2.1 Materials

4.2.1.1 *Six-compartment cell and setup*

Electrodialysis experiments were performed in a six-compartment cell with a four-electrode arrangement, previously described by Długołęcki et al. [21]. The cell consists of six blocks containing cylindrical compartments, with the cell electrodes located at the two extremities. The compartments, numbered 1 to 6 from left to right, are separated by five ion-exchange membranes (**Figure 4.1**). The potential difference over the middle membrane can be measured by employing two L-shaped Haber-Luggin capillaries, which are positioned on either side of the membrane pointing straight at each other. The capillaries, filled with 3M KCl solution, are connected through 30 cm tubes to the glass compartments in which two reference electrodes are positioned.

The membranes were alternated as in a conventional ED cell, with the AEM under study placed in the middle. Its effective area was reduced to 7.07 cm² by placing two plastic shields on either side. The other four auxiliary membranes had an effective area of 23.8 cm². The AEMs and CEMs employed in this study were FujiFilm type 10, kindly provided by FujiFilm Manufacturing Europe B.V. (The Netherlands), with properties summarized in **Table 4.1**.

**Table 4.1.** *Properties of the anion and cation exchange membranes employed in this study*

Membrane property	AEM type 10	CEM type 10
Backbone chemistry	Acrylamide [22]	Acrylamide
Thickness dry (μm)	125	135
Area resistance (Ω cm²)	1.7	2.0
Permselectivity (measured at 0.05-0.5M NaCl)	95	99
pH stability	1-13	1-13

As shown in the scheme of the setup (**Figure 4.1**), four different solutions were employed for each experiment. 1.0L of each solution was circulated in the following arrangement:

- Compartments 1 & 6. Electrode solution consisting of 0.05 M Na_2SO_4.
- Compartments 2 & 5. Buffer solution, with the same mineral composition as the feed solutions.
- Compartments 3 & 4. Concentrate and diluate solutions, respectively, with the same initial composition at each experiment.

During the experiments, the solutions were kept inside a 25 °C water bath (Julabo SW22). They were pumped through the cell at a rate of 170 mL/min by peristaltic

pumps (Cole-Parmer, Masterflex L/S Digital drive, USA), and 8.0 mm PTFE tubing from EmTechnik.
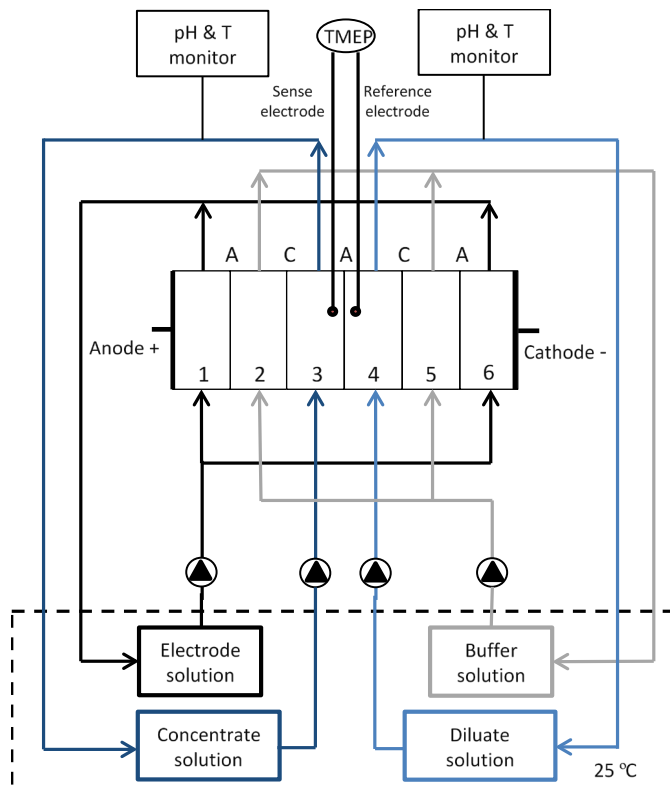
Figure 4.1. *Scheme of the six-compartment cell and setup employed to perform the electrodialysis experiments. The transmembrane electric potential (TMEP) is measured through Haber-Luggin capillaries placed at each side of the membrane.*

The current over the cell was applied with an Autolab PGSTAT12 (The Netherlands). This galvanostat also measured the potential over the middle (test) membrane through the two reference Ag/AgCl electrodes (QM711X, QIS, The Netherlands) and the capillaries. The pH and temperature of the diluate and concentrate solutions were monitored inline with Orbisint CPS11D-7BA21 probes connected to a Liquisys-M pH digital sensor, both from Endress+Hauser (Germany).

4.2.1.2 *Preparation of solutions*

Each electrodialysis experiment made use of feed solutions with different composition, which included varied mono- and multi-valent ions, viscosifying polymer, and oily compounds [10], as shown in **Table 4.2**. The mineral composition consisted of either sodium chloride or brackish water (BW). The latter composition was based on the Marmul field, in Oman [23], and is displayed in **Table 4.3** along

with one variant. All solutions were prepared by dissolving the specified salts in demineralized water to create stock solutions, which were later employed as a basis on which to add the HPAM and/or the oily components.

Table 4.2. *Composition of the diluate and concentrate solutions for the different fouling experiments.*

Experiment	Mineral composition	HPAM polymer	Oily compounds
E1	53.3 mM NaCl	-	-
E2	53.3 mM NaCl	1.0 g/L	-
E3	77.0 mM NaCl	1.0 g/L	-
E4a, E4b*	Brackish water (BW)	1.0 g/L	-
E5	BW with 3x[Ca + Mg]	1.0 g/L	-
E6	BW only Ca (x2)	1.0 g/L	-
E7	BW only Mg (x2)	1.0 g/L	-
E8	BW	-	2 mg/L crude oil
E9	BW	0.5 g/L	2 mg/L crude oil
E10	BW	1.0 g/L	2 mg/L crude oil
E11	77.0 mM NaCl	1.0 g/L	2 mg/L crude oil
E12	BW	1.0 g/L	20 mg/L crude oil
E13	BW	1.0 g/L	20 mg/L emulsion
E14	BW with 3x[Ca + Mg]	1.0 g/L	20 mg/L emulsion

*E4 was performed in duplicate.

Table 4.3. *Mineral composition of the solutions. Based on the composition reported in [23].*

Components	Brackish water (BW) (mM)	BW with 3x[Ca + Mg] (mM)
$NaHCO_3$	15.59	15.59
KCl	0.72	0.72
Na_2SO_4	2.51	2.51
NaCl	53.30	53.30
$CaCl_2*2H_2O$	0.65	1.96
$MgCl_2*6H_2O$	0.46	1.37

The solutions with HPAM were prepared by slowly adding the dry polymer to the vortex formed on the salt solution under fast stirring. Once all the polymer was added, the stirring speed was reduced and maintained for at least 24 hours to guarantee its hydration [2].

Regarding the oily compounds, two different compositions were studied: one with crude oil and one with a model emulsion. In both cases, stock solutions were prepared, characterized, and dosed to attain concentrations of 2 to 20 mg of oily compound per liter of test solution, as obtained after a secondary treatment [10,11].

The preparation of the model emulsion was based on the method described in [24]. In short, 346 mg of cationic cetyltrimethylammonium bromide (CTAB) surfactant

were dissolved in 998.0 g of brackish solution previously conditioned to 45 °C. Then, 2.0 g of hexadecane was added, and the solution was mixed at 14,000 rpm by an IKA T25 Ultra-Turrax emulsifying mixer (Germany) for 10 minutes. The emulsion had no visible phase separation, so its oil concentration was 2.0 g/L.

The stock solution with crude oil was prepared in a similar way. After heating 2.0L of brackish solution to 45°C, 2.0 g of crude oil was added, and the solution was mixed as described for the model emulsion. This mixture was rested for 24 hours, after which the water phase was recovered and stored as oil stock solution. Its oil concentration was estimated via TOC analysis (section 4.2.2.3).

All the feed solutions were prepared with analytical grade salts (NaCl, $CaCl_2 \cdot 2H_2O$, $MgCl_2 \cdot 6H_2O$, $NaHCO_3$, KCl, and Na_2SO_4), purchased from VWR and employed without further purification. The polymer employed was Flopaam 3230S (HPAM with MW= 5-8 million Da, 30% hydrolyzed), kindly provided by SNF (France). Model emulsions were prepared with analytical grade hexadecane (Merck, USA) and CTAB surfactant (Sigma-Aldrich, UK). The crude oil originated from the North Sea and was kindly provided by Shell.

4.2.2   Methods

4.2.2.1   *Electrodialysis experiments*

The electrodialysis experiments were run for 18 hours in constant current mode. The current density was fixed at 28.3 A/m^2, which is 36% of the limiting current density (LCD) when desalting a 53.3mM NaCl solution. The LCD was experimentally determined through the Cowan and Brown method [25], as described in the supplementary material.

For each experiment, a new membrane, previously conditioned in either NaCl or brackish solution, was placed in the middle compartment of the cell. Once the capillaries were aligned, the experiment was started. The potential over the membrane, pH, and temperature were logged every minute. As soon as the experiment finished, the fluids were removed from the cell and samples were taken. The AEM was removed, dried at room temperature, and stored. Next, the diluate and concentrate solutions were mixed in equal proportions, and the potential between the capillaries was tested for this solution at different currents. This measurement provided the average resistance of the solution, and by combining it with the solution conductivity, the distance δ between the capillaries could be calculated [26].

To explore the reversibility of the fouling, some experiments required switching of the direction of the electrical current. By doing so, the solutions in compartments 3

and 4 of the cell were desalted in an alternate form. Each experiment had a specific mineral composition and made use of solutions with and without HPAM.

4.2.2.2   *Membrane analysis*

Before being analyzed, the air-dried membranes were frozen in liquid nitrogen and cut using a scalpel. The pieces were stored at room temperature until analyzed. In addition, some membranes were examined by SEM after being freeze-dried. For these samples, a portion of the membrane was cut immediately after the experiment and stored in a freezer at -80°C. Then, the piece was freeze-dried in a Christ Alpha 2-4 LDplus freeze dryer for 48 hours and stored.

4.2.2.2.1   SEM/EDX measurements

The recovered membranes were analyzed with scanning electron microscopy (SEM) and energy-dispersive X-ray spectroscopy (EDX) by JEOL-6480LV (JEOL Ltd. Japan). The samples were gold-coated in a JEOL JFC-1200 fine coater. For SEM, each membrane was examined from three sides: the two faces and the cross-section. The EDX conditions were 15 kV accelerating voltage and 10 mm working distance.

4.2.2.2.2   Raman measurements

Full Raman spectra (up to 4,000 cm^{-1}) were obtained by employing a LabRAM HR Raman spectrometer from Horiba Jobin Yvon with an mpc3000 laser at 532.2nm and a 800mm focal length achromatic flat field monochromator. The laser was focused through an Olympus Bx41 microscope. The detector was a Synapse multichannel CCD. The spectra taken included both faces of the membranes (focusing on the ion exchange resin and avoiding the supporting fibers), salt precipitates, and a grain of polyacrylamide.

4.2.2.2.3   Contact angle measurements

Static contact angles were measured with a Dataphysics OCA 35 (Germany) contact angle meter by using the sessile drop method (2 μl) with MilliQ-water. The droplet was placed on the dry membrane after which a snapshot was taken, and from there the contact angle was determined. The reported values are the average of at least three measurements.

4.2.2.3   *Solution analysis*

1.5 mL samples of the solutions were taken before and after the experiments and later analyzed for their ionic and carbon species. Cations were measured by using inductive-coupled plasma optical emission spectroscopy (ICP-OES, Optima 5300DV, Perkin Elmer). Anions were analyzed with ion chromatography (IC, 761 Compact IC, Metrohm). The concentration of carbonate species was obtained from the inorganic carbon concentration measured with a TOC analyzer (Shimadzu TOC-

VCPH). The particle size distribution of selected HPAM solutions was determined with DIPA 2000 – Particle Analyzer (Prolyse).

4.3   Results and discussion

Section 4.3.1 combines the analyzes of data logged during the ED and that of the diluate side of the AEMs. Here we show that fouling was observed on both sides of the AEMs, but the effects on electrodialysis performance were mainly attributable to the development of a gel layer on the diluate side. Sections 4.3.2.-4.3.4 present the analyses of the concentrate side, process performance, and reversibility. Section 4.3.5 combines the presented information and literature findings to explain how solution composition affects the fouling by PFPW.

4.3.1   Formation of gel layer by HPAM (diluate side)

A common indication of the formation of a gel layer on a membrane is the increase in electric resistance [13,27]. The changes in resistance were measured as transmembrane electric potential (TMEP) between the two capillaries of our experimental setup. Although the TMEP would be affected by the increase of resistivity of the bulk diluate solution during the experiments, the decrease in conductivity was only 20%, so the impact was minimal. To account for variations among experiments in the distance δ between the capillaries, the recorded TMEP was divided by δ (section 4.2.2.1), and the obtained plots are included as **Figure 4.2**. The results in the figure are organized to highlight various effects, summarized in **Table 4.4.**

Table 4.4. Comparisons enabled by the experimental approach

Effect	Experiments involved
Addition of HPAM	E1, E2
Ionic strength	E2, E3
Mineral composition	E3, E4, E5, E6, E7
Mineral composition in presence of oil	E8, E10, E11
Increasing HPAM concentration	E8, E9, E10
Increasing crude oil concentration	E4, E10, E12
Addition of model emulsion with surfactant	E4, E12, E13, E14
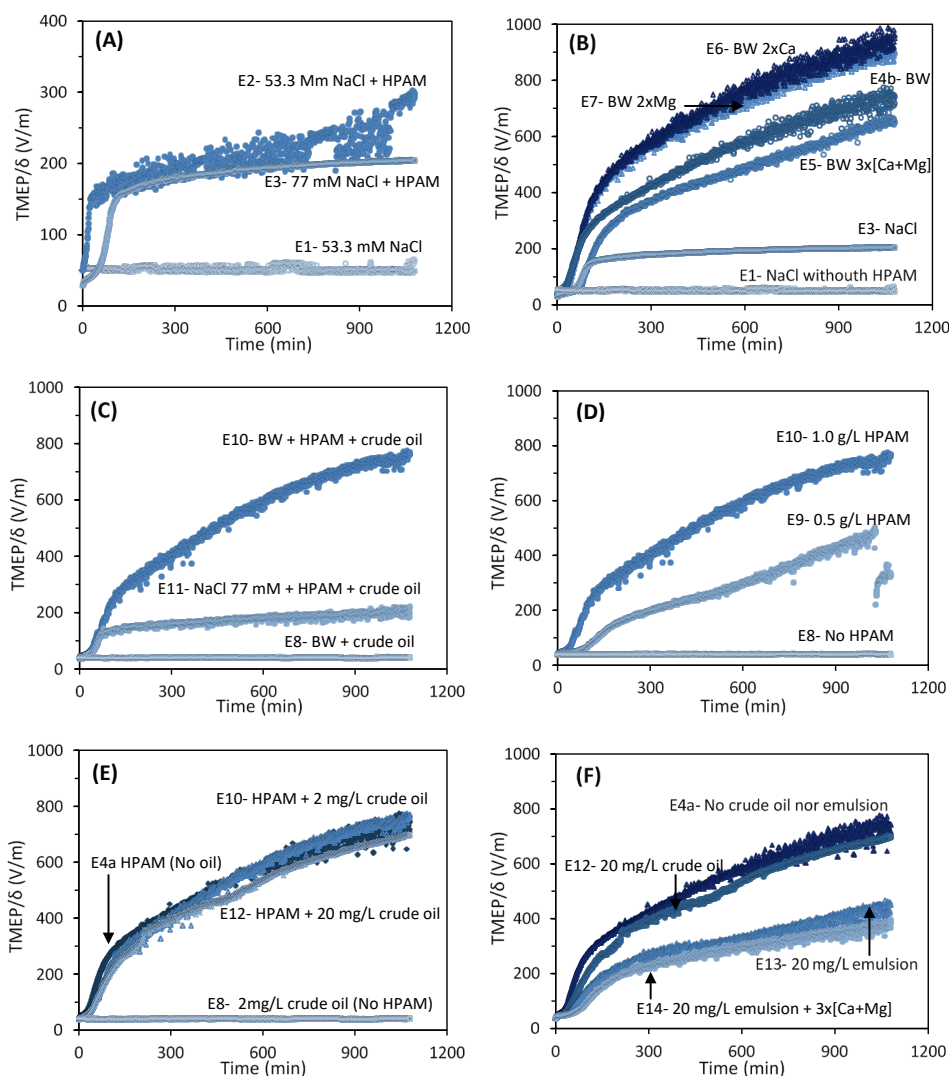
Figure 4.2. *TMEP/δ vs time of ED runs showing assorted effects. **(A)** Effect of ionic strength and HPAM on TMEP/δ. E1 and E2 had the same ionic strength, while E3 contained a higher concentration of NaCl. **(B)** Effect of the mineral composition in the absence of oil. **(C)** Effect of mineral composition in the presence of 2 mg/L of crude oil. **(D)** Effect of increasing the concentration of HPAM. **(E)** Effect of the addition of crude oil. **(F)** Effect of the addition of model emulsion.*

4.3.1.1   *Gel layer in the presence of NaCl and the effect of ionic strength*

Figure 4.2A shows the TMEP development for the experiments E1 to E3. As expected, the TMEP/δ of E1, the experiment without foulants, remained constant. In contrast, when HPAM was present in the same solution (E2), there was a clear increase in TMEP. The initial TMEP/δ of E2 was the same as for E1 because both experiments had the same ionic strength. However, in E2 the potential built up quickly in the first half-hour, after which the increase became more gradual. The

periods of instability in the E2 profile could be due to disturbances in the HPAM gel layer or the adhesion of bubbles to the capillaries.

The shape of the TMEP curve is like a typical chronopotentiogram profile [28], with a stabilization time in the order of minutes. The reason for this long stabilizing time is thought to be the slow build-up of the HPAM gel layer. The HPAM layer not only inhibits the replenishment of fresh solution near the membrane, thickening the diffusion boundary layer (DBL), but also causes the ionic transport pathway to become more tortuous [29], all of which increases the electrical resistance, as indicated by the TMEP profiles. Then, the stabilization period would be reached either when the gel layer stopped growing due to flow conditions in the cell, or when the DBL grew past the capillary tip (so the changes could not be measured anymore). However, the last option is highly unlikely because the reported thicknesses of DBLs are quite below 2.5 mm, which was the approximate distance from the membrane surface to the tip of the capillary. For example, for a 50 mM NaCl solution desalted in a cell without flow, Tanaka reported a DBL of 0.362 mm [30].

The profile of E3 shows two main differences when compared to E2: i) it originates and stabilizes at a lower TMEP/δ value, and ii) the voltage increase is less pronounced as it happens during a longer time. Both effects can be attributed to the higher ionic strength of E3. Solutions with higher ionic strength have less resistivity, which explains the lower initial and stabilization values. Additionally, at higher ionic strength the charges of HPAM are more shielded, so the polyelectrolyte becomes effectively less charged. Consequently, the driving force (electrical potential) working on the HPAM has a lower influence, so there is a decrease in polymer migration. This theory contrasts with the one proposed in [17], that suggested that at higher ionic strength, the lower hydrodynamic radius and viscosifying ability would lead to more migration of HPAM towards the anode.

The membranes and their gel layers were further studied with SEM. The FujiFilm type 10 AEM is made of an ion-exchange resin and reinforcement fibers, which are visible on both surfaces and in the cross-section (**Figure 4.3A**). Since the E1 solutions only contained NaCl, no precipitation occurred on the membrane (top row of the figure). The photographs from E2, in the same figure, show a gel layer on the diluate side of the membrane, as expected from the direction of the current in the cell and from the literature [18]. In solution, the polyelectrolyte is negatively charged, so it migrates towards the positively charged electrode (anode) under the influence of the applied voltage, accumulating on the diluate side of the membrane. The gel layer is thin enough to allow to still distinguish the fibers underneath.

The diluate sides of membranes E1 and E2 were also analyzed with Raman. As shown in **Figure 4.3B**, the profile obtained from E2 is closer to that of the dry HPAM

granule than to the clean membrane (E1), confirming that the layer on top of the membrane was HPAM.
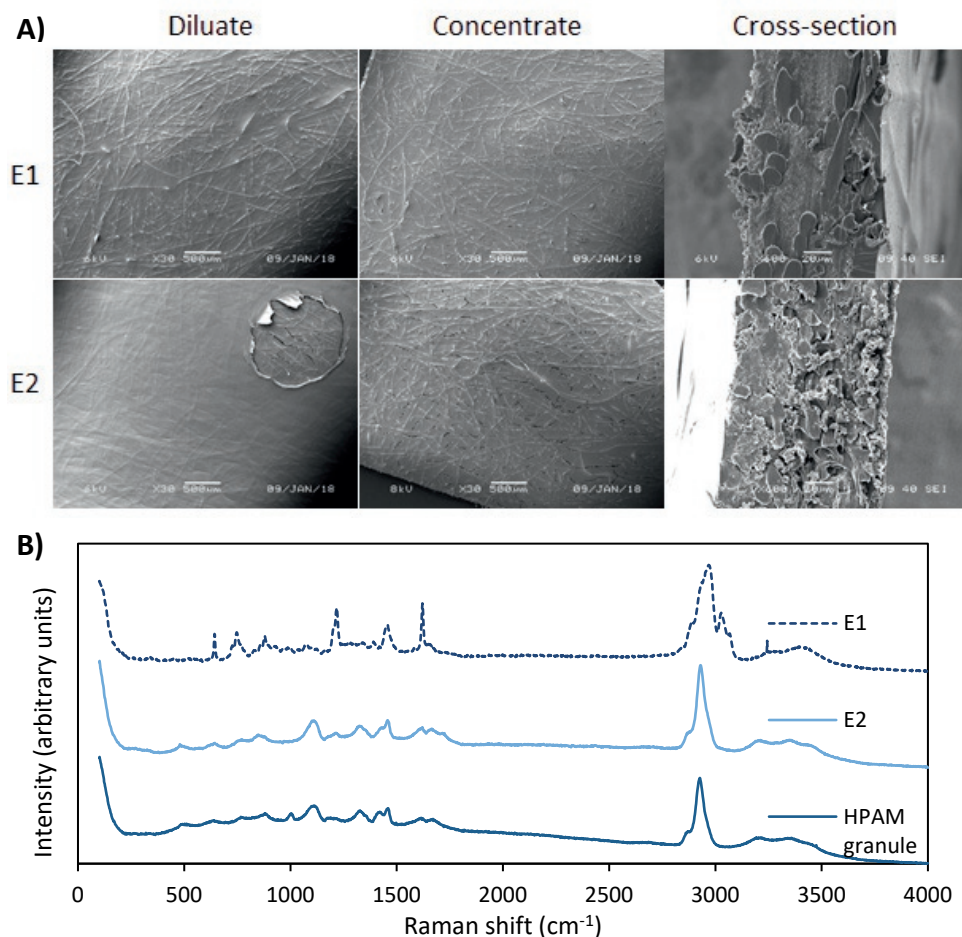
Figure 4.3. A) *SEM images from membranes E1 (no foulant) and E2 (NaCl + HPAM). The gel layer is visible on the diluate side of E2, but not in the image of the cross-section.* **B)** *Raman profiles from the diluate side of membranes E1 (clean), E2, and a dry HPAM granule.*

4.3.1.2 *Effect of mineral composition*

The effect of mineral composition on the formation of a gel layer can be first examined in **Figure 4.2B**, which shows the TMEP/δ for experiments E3 to E7. The most important feature to notice is the continued increase of TMEP/δ for the solution with brackish salts (E4b). The slope decreases after the inflection point around minute 100 but does not level off, and the final value is almost four times larger than that of E3 (NaCl + HPAM). The curve for E5 (3x[Ca+Mg]) has the same shape, and

although it remains slightly below that of E4b, still reaches a final value three times higher than that of E3. The experiments E6 and E7, with ionic strengths like E4 but containing only either calcium or magnesium, presented equally high TMEP/δ profiles.

Thereby, two kinds of TMEP/δ curves can be distinguished: the ones that tend to flatten relatively early, displayed during the experiments with only NaCl (E2 and E3), and the ones with a continuous increase, which belong to experiments containing a mixed mineral composition (E4 to E7). Indeed, a previous study also reported curves with different slope levels depending on the addition of HPAM of different MW in the solution [15]. In our case, considering that all solutions had approximately the same ionic strength, the observed differences can solely be attributed to the nature of the ions present, and specifically to the presence of divalent cations, as will be further explained in section 4.3.5.

The membranes recovered from these experiments were dried in two different ways and analyzed by SEM (section 4.2.2.2). As visible in **Figure 4.4A**, the air-dried gel layers compacted on the surface of the membranes, whereas the freeze-dried membranes maintained some structures, which might still be representative of the morphology of the gel layer as it was during the experiment. Based on the cross-section pictures and EDX analysis (**Figure 4.4B**), the thicknesses of the air-dried gel layers were estimated to be between 5 and 50 μm. In contrast, the freeze-dried layers were significantly thicker, between 50 and 550 μm. The combination of observations, summarized in **Table 4.5**, is indicatory for the differences in the in situ formation of the gel layer (photographs available in **Figure A4.2** and Figure A4.3**)**. For example, the freeze-dried layers of the experiments with NaCl solution (E3 and E11) were at least three times smaller than the gel layers from experiments with BW composition. This ratio is very similar to that shown in **Figure 4.2B**, where the final TMEP/δ of E4b was approximately 3.5 times larger than that of E3. Thus, our measurements suggest that the differences in the TMEP profiles could have been related to gel layers of different thicknesses, which could be linked to the different mineral compositions in the solutions. This is further discussed in section 4.3.5.
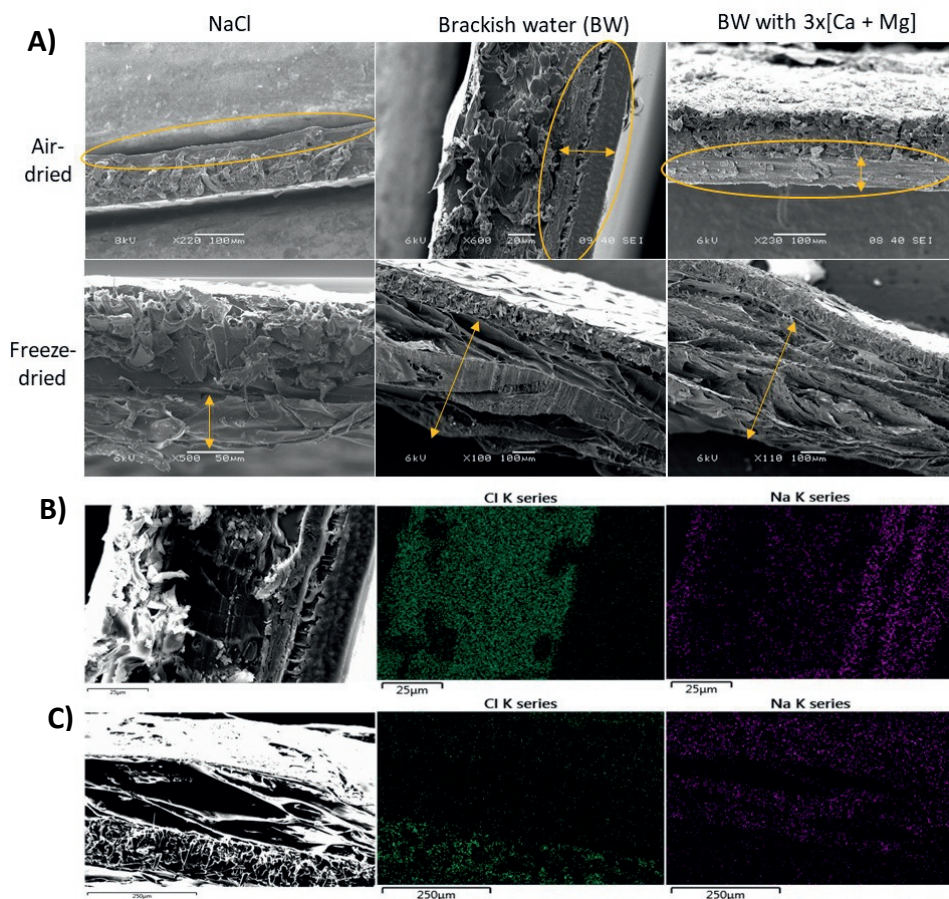
Figure 4.4. A) Examples of SEM images of the cross-sections of air-dried and freeze-dried membranes. The arrows and circles indicate the gel layers. *B)* EDX analysis of air-dried membrane from E4a. It shows a higher concentration of Cl the ion exchange resin, and Na presence mainly in the HPAM gel layer. *C)* EDX images of the freeze-dried membrane of E4b.

The elemental analysis of the diluate side showed differences between the fouled and the clean membranes (**Table 4.6**). The AEMs in which a gel layer was visible (E3 to E7) presented a decrease in the percentage of C and an increase in the percentage of N and O, which corresponds with the composition of the HPAM molecule. Furthermore, the amount of Cl detected diminished when there were thicker gel layers present. As shown in **Figure 4.4**, the ion-exchange resin on the AEM is rich in Cl, so it is logical that when thicker/denser gel layers were formed on top, less Cl from the bottom could be detected.

Table 4.5 . Summary of the SEM and EDX results

Membrane	Gel layer thickness (diluate side)			Precipitates (concentrate side)[2]		
	Observed	Air-dried (μm)	Freeze-dried[1] (μm)	Type	Common Elements	Traces
1	No	-	-	x	x	Fe O Si Mg
2	✓	10	N/A	x	x	Si O
3	✓	5	50	Scarce crystals	C, O	SO
4a	✓	34	N/A	Crystals	Ca, O	Mg O, Si
4b	✓	-	500	Crystals	Ca, O	Mg O
5	✓	6	504	Crystals & plaques	Ca, O	Mg O
6	✓	9	355	Crystals & scales	Ca, O	Mg O
7	✓	7	428	Small crystals	Mg, O	-
8	No	-	-	Scarce crystals	Ca, O	Mg O
9	✓	37	N/A	Scarce crystals	Ca, O	Na O
10	✓	37	N/A	Crystals	Ca, O	Mg O
11	✓	5	120	x	x	Na Cl Si Fe O
12	✓	25	N/A	Crystals & plaques	Ca, O	MgO
13	✓	16	530	x	x	Mg Si O Al
14	✓	52	350	Scales	Ca, O	Mg O

[1] N/A indicates that the freeze-drying procedure was not performed for that sample
[2] The SEM and EDX analysis of the concentrate side was performed on the air-dried membranes

Table 4.6. *Percentages of the main elements found on the diluate side of membranes E3 to E7.*

Element	M1 (Clean)	M3	M4b	M5	M6	M7
C	82.16	52.74	55.78	52.01	56.12	55.60
N	7.27	12.71	17.48	16.59	17.04	16.92
O	4.58	19.90	24.00	24.46	24.44	25.42
Cl	5.82	6.67	0.51	2.18	0.25	0.14
Na	0.02	7.47	1.48	4.14	1.82	1.78

Raman analyses were also performed on the diluate side of the membranes (data not shown). In all cases, the profiles were very similar to the one of the HPAM granule

(**Figure 4.3B**), so this characterization corroborates the gel layer to be formed mainly by HPAM.

4.3.1.3   *Effect of mineral composition in the presence of oil*

The influence of mineral composition on fouling in the presence of crude oil can be pondered by comparing experiments E8, E10, and E11, which had the same ionic strength and oil content but different mineral composition. **Figure 4.2**C shows that the TMEP/δ - time profile of the solution containing only BW plus 2 mg/L of crude oil but without HPAM (E8) remained flat during the whole experiment. The runs with NaCl+ HPAM+ oil (E11) and with BW+ HPAM+ oil (E10) showed profiles almost identical to their analogs without oil (E3 and E4a, respectively). As noticed for **Figure 4.2B**, the final TMEP/δ value for the experiment containing BW is roughly four times larger than the one containing only NaCl (770 vs 210 V/m). This indicates that the presence of 2 mg/L of crude oil did not have a significant effect on the increase of resistance, which was mostly determined by the mineral composition of the solution and the presence of HPAM.

The membranes recovered from these experiments were also analyzed with SEM and EDX. E8 did not show any significant gel layer nor precipitation. The air-dried membrane from E11 (NaCl), presented a gel layer of approximately 5.0 μm, while the gel layer in E10 (BW) was much thicker (37 μm) (**Table 4.5**). The membrane from E11 was also freeze-dried, and displayed gel layer thickness of 120 μm and a high porosity (**Figure A4.3**). These observations matched with the TMEP profiles, and again showed a correlation between the presence of multivalent ions and the thickness of the HPAM layer.

4.3.1.4   *Effect of HPAM concentration*

The effect of HPAM concentration in crude oil containing solutions can be evaluated from **Figure 4.2D**. At higher HPAM concentration, there was a higher increase rate of TMEP, as previously reported [18]. However, the membrane analysis indicated gel layers of similar thicknesses for E9 (0.5 g/L HPAM) and E10 (1.0 g/L HPAM). This suggests that the gel layer on E10 was more compact than the one on E9 when assuming no layer materials were lost during recovery. Regarding E8, which did not contain HPAM, no gel layer was observed.

4.3.1.5   *Effect of oil addition (crude oil and model emulsion with surfactant)*

The effect of increasing the concentration of crude oil can be inferred by comparing experiments E4, E10 and E12. **Figure 4.2E** shows that their TMEP/δ - time profiles were alike during most of the experiment, although at the end a slightly lower TMEP/δ was recorded for the higher oil concentration (E12). This suggests a destabilization of the gel layer by the oily compounds, limiting its thickness and/or

density. This theory is supported by the SEM observations of the dried gel layer, since membrane E12 had the thinnest of the three experiments (**Table 4.5**). Zhang et al. also concluded that the fouling layer formed by HPAM and oil was not as dense as the fouling formed by a single component [6].

Experiments E13 and E14 assessed the effect of an emulsion of hexadecane and CTAB surfactant in the fouling. Comparing these TMEP/δ -time profiles with E12 in **Figure 4.2F**, shows that in the presence of 20 mg/L of the hexadecane emulsion the TMEP/δ reaches much lower values than when the same concentration of crude oil is added. The destabilizing effect of the emulsion on the HPAM gel layer was larger probably because the positively charged cationic surfactant is attracted towards the (negatively charged) HPAM. Still, the profile of E14 (3x[Ca + Mg]), confirmed that the presence of higher concentrations of divalent cations does not further increase the formation of the gel layer, and it even slows down the increase of TMEP with time, just as observed for E5.

The membranes recovered from E13 and E14 were freeze-dried, and their SEM images revealed well preserved foam-like HPAM layers, thicker than 350 μm (**Table 4.5**). The SEM photographs from the diluate side (**Figure A4.3**, 300X) suggest that the gel layer on E14 was denser than in E13. This observation was reinforced by the EDX analyses of the membranes, which showed that the gel layer in E14 had a higher concentration of C, O, N, and Ca in the upper part (**Figure A4.4B**), indicating a higher concentration of HPAM and possible calcium precipitation. For the rest of the cross-section, the EDX showed that the cations were equally distributed across the gel layer for both E13 and E14.

The most significant difference found between experiments with and without crude oil was the hydrophilicity of the membranes, which was investigated through water contact angle measurements (section 4.2.2.2.3). It was found that when a HPAM dried gel layer was present on the diluate side, the contact angle was lower than for the clean membrane, meaning that it made the surfaces more hydrophilic (Figure A4.6). On the contrary, when crude oil was present, the hydrophobicity increased, independently of HPAM being present (E12) or not (E8). These observations coincide with the available literature [13,17], and indicate that hydrophobic oil components interact with both the AEM and the gel layer. Furthermore, Zuo et al. explained that the oil in solution can form negatively charged colloidal structures that migrate towards the diluate side of the AEM [17].

4.3.2   Salt precipitation (concentrate side)

Salt precipitation was found on the concentrate side of most membranes, which is common due to the higher concentration of ions in this compartment. The

precipitates were first spotted with SEM, and later analyzed with EDX and Raman. The SEM and EDX results are summarized in **Table 4.5**, and Figure A4.5. includes the SEM pictures.

SEM allowed to identify three recurrent morphologies for the precipitates, arbitrarily called "crystals", "scales" and "plaques" (**Figure 4.5**). The precipitation in the form of "crystals" occurred when the solutions had a varied mineral composition, that is, no precipitation was observed for experiments containing only NaCl. The "scales" were large and amorphous precipitates, only observed on the concentrate side of E6 (BW with only Ca) and E14 (BW with 3x[Ca+Mg]). The "plaques", which were flat precipitates, appeared when oil was added to the solution. When 2 mg/L of oil was added, the crystals became already more amorphous (E10 in **Figure A4.5**) than when no oil was present. However, the effect amplified significantly with an oil concentration of 20 mg/L (E12), and this membrane presented the highest amount of plaques (**Figure 4.5C**). EDX confirmed that all precipitates had similar compositions (**Figure 4.5D** & **E**), so the observed differences may be due to the presence of more nucleation sites in which the crystals could start to develop.

In general, more precipitation was observed for experiments that reached higher TMEP/δ values due to the presence of HPAM gel layers. For example, the amount of precipitation on membranes E8 (No HPAM), E9 (0.5 g/L HPAM) and E10 (1.0 g/L HPAM) increased in this order (**Figure A4.5**). The only exception was E7, which presented very few precipitates on the concentrate side. Thus, although the BW experiments with only calcium (E6) and only magnesium (E7) had similar TMEP/δ curves and gel layers, they showed contrasting amounts of mineral precipitation (**Figure A4.5**). The differences can be attributed to the slower migration of magnesium and to its higher affinity to the CEM, which reduces its availability on the concentrate stream [31], and to the higher solubility of the magnesium salts compared to the calcium ones.
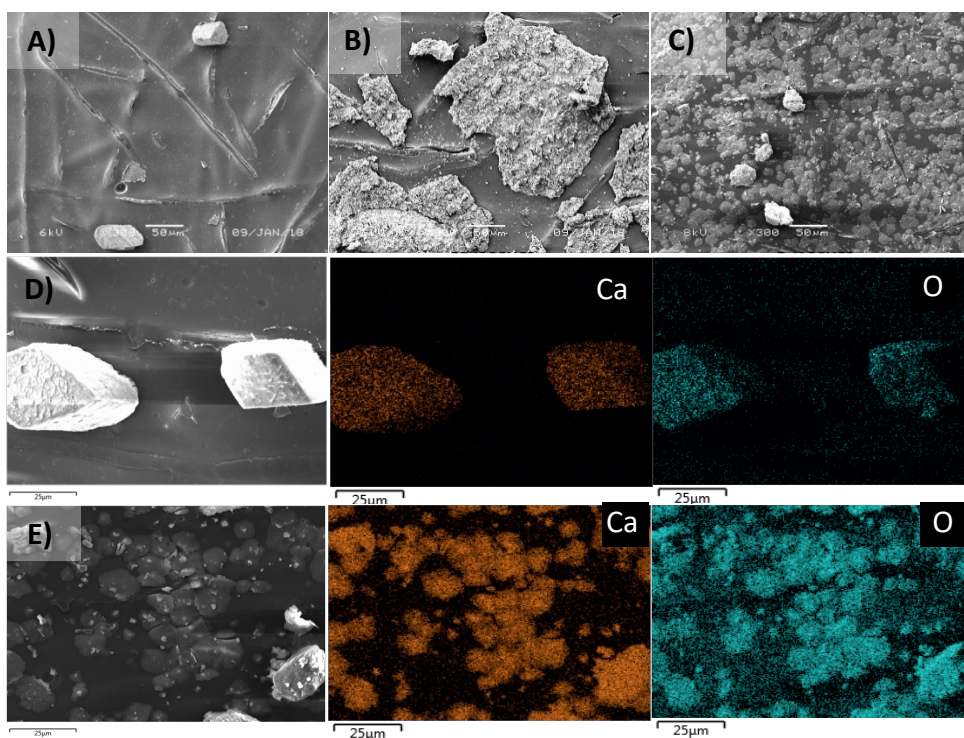
Figure 4.5. *SEM and EDX analysis of precipitates observed on the concentrate side of the AEMs.* ***A)*** *An example of "crystals", taken from E4A.* ***B)*** *Example of "scales" found on E14.* ***C)*** *Example of "plaques" taken from E12.* ***D)*** *EDX analysis of precipitates on membrane E4a, including SEM photograph, Ca and O distribution.* ***E)*** *EDX analysis of precipitates on membrane E12, also showing Ca and O presence.*

The EDX analysis indicated that most of the precipitates were composed by Ca and O (**Figure 4.5.** D & E), suggesting that they were in the form of calcium carbonate [31–33]. However, this could not be proven via EDX given that the background —the AEM— already had a high carbon content, so any other high concentration of carbon would not stand out. Magnesium was frequently found within the Ca-O precipitates, but in lower concentrations. Other elements detected were K, Na, and Cl, originating from the feed solutions, and others like Si and Fe, which probably originated from impurities in the dissolved salts, polymer, and crude oil.

Raman analysis was also performed on most of the membranes, but it only allowed to identify calcite as one of the precipitates on E14 (**Figure A4.7**). However, considering the EDX results and mentioned literature, it is likely that the precipitates were mainly composed of calcium carbonate.

4.3.3   Performance in terms of the transport of ions

Besides affecting the TMEP and in the membrane morphology, fouling is also likely to influence the ion-transport through the membranes and, therefore, the process performance. The transport of anions through the AEM was calculated from the average change in the concentration of anions in the diluate and concentrate compartments. The analysis distinguished between the monovalent ions, Cl^- and HCO_3^- (considering no pH above 10), and SO_4^{2-}, the only divalent anion. The theoretical number of charge equivalents transported (efficiency 100%) was estimated as 13.4 meq (1300 C), calculated from the applied current and the duration of the experiment [2].

Figure 4.6 presents the average changes in charge equivalents. In general, the experiments performed reasonably, transporting at least 70% of the theoretical number of equivalents. In most cases, the higher transport of equivalents corresponded to membranes with thinner gel layers. For example, the highest transport of charge equivalents was measured for experiments E11 and E2, which coincide in only having NaCl as mineral composition. On the other hand, the lowest transport was measured for E5 and E14, which presented a thick gel layer and precipitation on the concentrate side due to the additional divalent cations. The comparison of E8, E9, and E10 also shows a better performance when no HPAM was present.
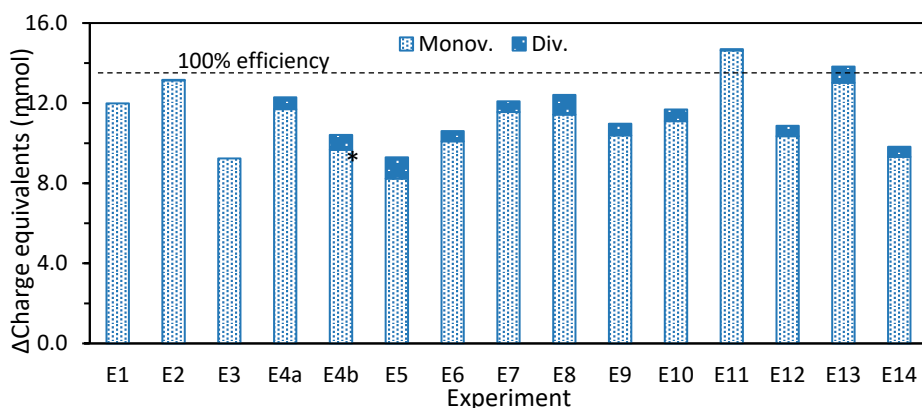
Figure 4.6. Average change of monovalent and divalent anions, presented as charge equivalents, in the diluate and concentrate solutions. The theoretical change in equivalents given the applied current and operative time was 13.4 meq, indicated by the discontinuous line (100% efficiency). The low performance measured in E3 can be attributed to a leaking capillary, detected after running the experiment. The traces of sulfate detected in E2 and E11 probably came from the electrode compartments.

As presented, the decrease in process performance in terms of transport of ions can be related to the incidence of fouling and scaling. The mechanisms behind are the reduction of the permselectivity of the membrane due to the shielding effect of the

gel layer, the increase in back-diffusion of ions, and the occurrence of water splitting [29]. The latter phenomenon was further analyzed through pH measurements, which demonstrated significant quantities of water splitting, as further explained in Appendix 4D.

4.3.4   Reversibility of fouling

The reversibility of the fouling was assessed through electrodialysis reversal experiments, each performed either with NaCl or BW composition. We present first the analysis for the NaCl experiment (**Figure 4.7A**). Before applying the electric current in a certain direction, the open-circuit voltage (OCV) of the cell was recorded. Since the cell might have some asymmetry, comparisons are made among periods with the same current direction. For the first two periods of 30 minutes, compartments 3 and 4 contained NaCl solutions without HPAM. As expected from the absence of foulants, the TMEP/δ values were constant, independently of the direction of the current. Then, after adding the solution with 1.0 g/L of HPAM (1 in the plot), the TMEP/δ curve increased in a sinusoidal shape, as observed in previous experiments, indicating the build-up of the gel layer. The current direction was maintained for 60 minutes, allowing the formation of a HPAM layer, and then reversed at minute 125. After the reversal, the TMEP/δ stabilized at the original value of -55 V/m, but when the current was reversed again to the positive direction (minute 160), the TMEP/δ increased again. Then, at point 2, the solution with HPAM is substituted by a solution without foulant, which causes a decrease in the TMEP, although it does not reach the base value. Finally, the TMEP/δ values during the last 30 minutes of the experiment were closer to the initial ones. A similar behavior was observed for the experiment with BW (**Figure 4.7B**), with the main difference that when the foulant was added, the increase in TMEP was much faster, as in previous experiments.

There are some details to highlight. The fact that after reversing the current at minute 125 the TMEP goes back to its original value, indicates that the fouling only has a tangible effect when it coincides with the diluate side of the membrane. This confirms that the increase in TMEP is caused by the depletion of ions at the diluate side of the AEM due to concentration polarization [34]. The HPAM layer is still present when the current stopped at minute 125, as indicated by the higher OCV value. Thus, when the current is reversed, the HPAM layer is probably still interacting with the membrane, but its effect is minimal since now it is placed on the concentrate side.
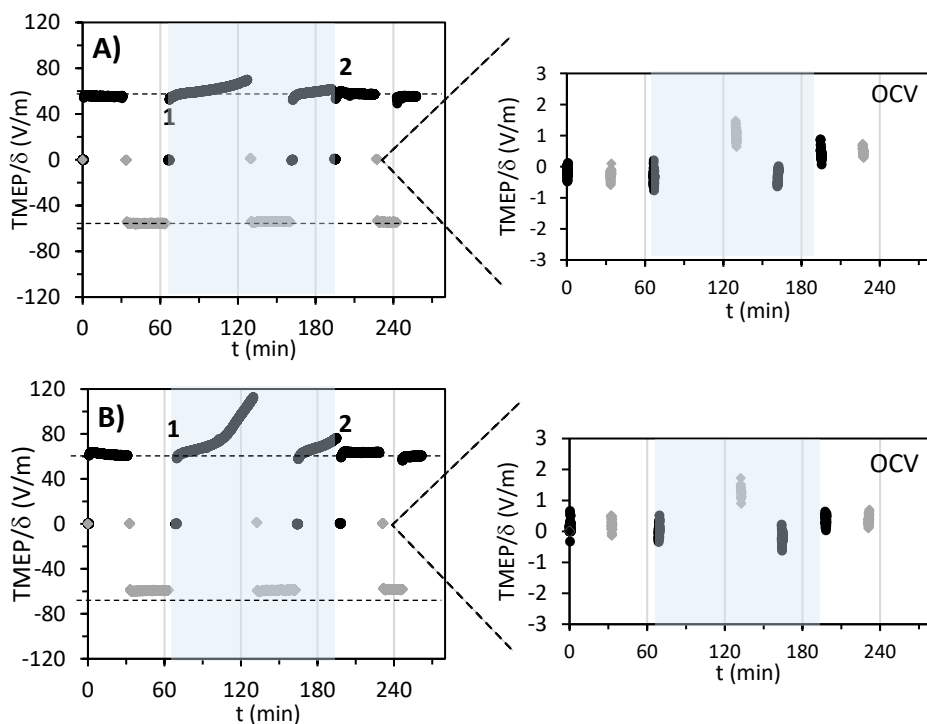
Figure 4.7. *TMEP/δ profile for the current reversal experiment with **A)** NaCl solution and, **B)** BW solution. Initially, compartments 3 and 4 contained solutions without foulants. At point 1, the solution on the diluate side was switched for a solution with the same mineral composition but containing 1 g/L of HPAM. At point 2, the solution with HPAM is substituted by the solution without it. Thus, the shaded area indicates when the solution with HPAM was present in the setup. The plots at the right are included to highlight the OCV measurements, which tended towards zero.*

It is also noteworthy that the formation of the second HPAM layer (minute 160), goes slightly faster than the first time that a layer was formed. This can be interpreted as a partial removal of the gel layer by the current reversal. However, when the solution without foulant is added and the current is reversed once more, the initial TMEP values are recovered. Two reasons could explain that the solution without HPAM has better results in removing the gel layer: i) the concentration gradient between the gel layer and the fresh solution, and ii) turbulence. The latter arises from the lower viscosity of the solution without HPAM [2], which causes more turbulence in the cell and therefore higher shear forces that overcome the remaining attraction of the fouling layer towards the membrane.

Thus, our experiments indicate that the HPAM gel layer, or at least most part of it, can be removed by a combination of current reversal and use of clean solutions. However, this is not a definite conclusion, as will be further explained in the following section.

4.3.5   General fouling mechanism

Once the results from the membrane analyses have been presented, this section combines the observations from the experiments into a fouling model.

4.3.5.1   *Distinction between adsorption of polyelectrolyte and formation of a gel-layer*

First of all, we would like to distinguish between two mechanisms involved in the fouling of AEMs by HPAM: i) the adsorption of the polyelectrolyte on the surface of the AEM, and ii) the development of a gel layer due to transport of HPAM towards the membrane and the entanglement of the polymer chains [18]. Indeed, when studying organic fouling on other types of polymeric membranes, authors have used a similar approach, differentiating between membrane-foulant and foulant-foulant interactions [35,36].

Regarding the adsorption stage, it has been thoroughly described how polyelectrolytes, including hydrolyzed polyacrylamide, adsorb on (oppositely charged) surfaces [37–40]. The adsorption occurs even when the concentration of polyelectrolyte in solution is as low as 1.0 mg/L, and is usually considered irreversible [39]. In contrast, a gel layer needs higher concentrations to develop, and since it would be physically attached, it should be reversible. This distinction between two mechanisms also helps to explain the results from section 4.3.4, which confirmed that most part of the gel layer was dispersed, but gave no evidence of the adsorbed layer. Actually, the literature suggests that the increase in resistance of a membrane with an adsorbed layer of polyelectrolyte would be minimal [41], and non-detectable with the current method, as observed in preliminary experiments (Figure A4.9). Thus, to confirm if adsorbed HPAM remains on the AEM after applying current reversal, other techniques would need to be employed.

However, for the relatively high concentration of HPAM in the PFPW of this study, the main fouling process is thought to be agglomeration near the membrane surface. During the electrodialysis, this anionic polyelectrolyte migrates towards the anode and accumulates on the diluate side of the AEM. The HPAM tends to accumulate predominantly due to the electrostatic attraction that exists between the charged polymer and AEM [17], and the van der Waals attraction that exists between polymer and membrane materials. Due to the increasing concentration of polyelectrolyte, the local viscosity of the solution also increases [17], creating a gel layer that can stay in place under moderate shear rates. Even when the surrounding solution is removed, the high viscosity of the gel layer retards the water depletion out of the gel layer, keeping the polymer-polymer and polymer-surface interactions intact and the gel layer due to that at its place, close to the AEM, so when the membrane is recovered the gel layer comes together with it.

4.3.5.2 *Ionic strength of solution and divalent cations influence the fouling by HPAM*

There are at least two aspects of the solution composition that directly affect the fouling by HPAM: the ionic strength and the presence of divalent cations. The ionic strength impacts the migration of HPAM towards the membrane, as suggested by the delayed and lower TMEP/δ profiles of the experiments with higher ionic strength. Regarding the divalent cations (calcium and magnesium), it was found that they affect the formation and morphology of the HPAM gel layer. Experiments with brackish composition reached TMEP values 3 to 5 times higher than for experiments in which only NaCl was present. These observations can be explained in that the divalent cations complexate HPAM molecules by forming inter and intra molecular bridges between them [6,20]. The complexation starts when HPAM and divalent cations are put in contact in the solution, but can continue for hours [20], thus it keeps occurring while the gel layer is forming. In specific, we found in the literature four phenomena related to the complexating effect of divalent cations that could influence the formation of the gel layer; one related to the membrane-foulant interaction and three to the foulant-foulant interaction.

Concerning the membrane-foulant interaction, it has been documented that when divalent cations are in solution, more mass of polyelectrolyte can be adsorbed than when only monovalents are present [40,42]. Depending on the concentration of divalent cations, polyelectrolyte chains can form micelles and thus would adsorb as aggregated molecules [40], which increases the amount of matter per area unit. The formation of aggregates and the coiling up of HPAM molecules also explains the first phenomenon related to the foulant-foulant interaction, which is that the gel layer formed in the presence of divalent cations can be more compact and denser [6]. We performed particle size analyses on HPAM solutions in NaCl, BW, and BW with 3x[Ca + Mg] and found, respectively, average sizes of 7.89, 7.37 and 5.33 μm. This means that the size of the particles decreased as the concentration of divalent cations increased, in agreement with previous measurements done for polyacrylamide solutions [43]. The second effect of divalent cations regarding the foulant-foulant interaction is that they could cause stronger adhesion forces between carboxylate-containing molecules (like HPAM), as reported in [35] for a fouled membrane and a probe with carboxylate groups on its surface. The third factor is that gels formed by polyacrylamide and divalent cations are reported to shrink with time [44]. A fourth factor, not particularly related to the presence of divalent cations but to the high voltages reached in the cell when they were present, is that HPAM gels can also diminish their volume under the influence of electric fields [45].

The aforementioned factors suggest that the gel layers formed in the presence of divalent cations are more compact and resistant to shear forces than the gels containing only monovalent cations. Indeed, the SEM images of some freeze-dried

membranes support this theory (**Figure 4.8**). For solutions with BW composition, the continuous increase of the TMEP profiles even past the inflection point could mean that the gel layer was increasing in thickness and/or density thanks to the morphology given by the divalent cations.
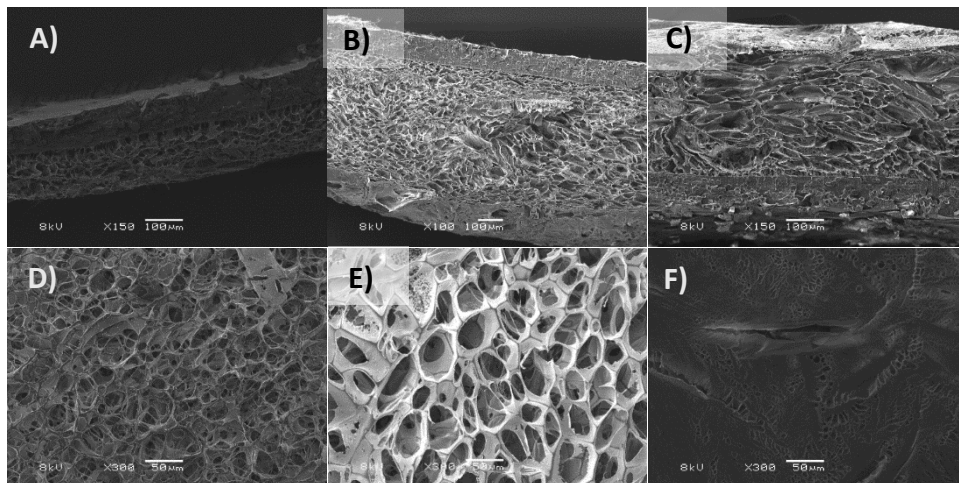

*Figure 4.8. Selected SEM images that illustrate the influence of divalent cations on HPAM layer thickness and density. Images **A), B)** and **C)** show, respectively, the cross-sections of E11 (NaCl 77 mM), E13 (BW) and E14 (BW with triple divalent cations). Images **D), E)** and **F)** show the top view of the same membranes in the mentioned order.*

Regarding the effect of the crude oil, it is suggested that it acts as a destabilizer of the HPAM-gel layers, as indicated by the slightly lower TMEP profiles and thinner gel layer thicknesses obtained when present in the feed solution. It can be that some charged oil components migrate towards the anode [17] and get embedded in the gel-layer, becoming impurities that make the layer less resistant to shear forces. Nevertheless, the employed oil concentrations were small compared to that of HPAM, so the observed effects were minimal.

4.3.5.3   *Effects of the HPAM gel layer*

The formation of the gel layer would have limited the replenishment of ions from the bulk solution to the surface of the AEM (concentration polarization), increasing the thickness of the diffusion boundary layer and causing the decrease of anions' concentration on the diluate side of the AEM. Due to the low concentration of anions, water eventually started to dissociate on the diluate side of the AEM, producing protons and hydroxyl groups [34]. This is exemplified in **Figure 4.9**, which shows that the pH changes started to occur soon after the TMEP started to increase, and they continue during the rest of the experiment. The protons tend to go towards the cathode, but first must go through the HPAM gel layer, where some of them might get adsorbed. This could have two consequences: a slight reduction of the coil size

(the HPAM in the gel layer is in the overlap regime, so the coils have already their random coil size), and the neutralization of the HPAM gel layer on the AEM [29]. Still, the pH on the diluate stream decreases, which can enhance HPAM precipitation [46] and, consequently, the constraints for the transport of ions, which translates in an autocatalytic or self-amplifying process [34].
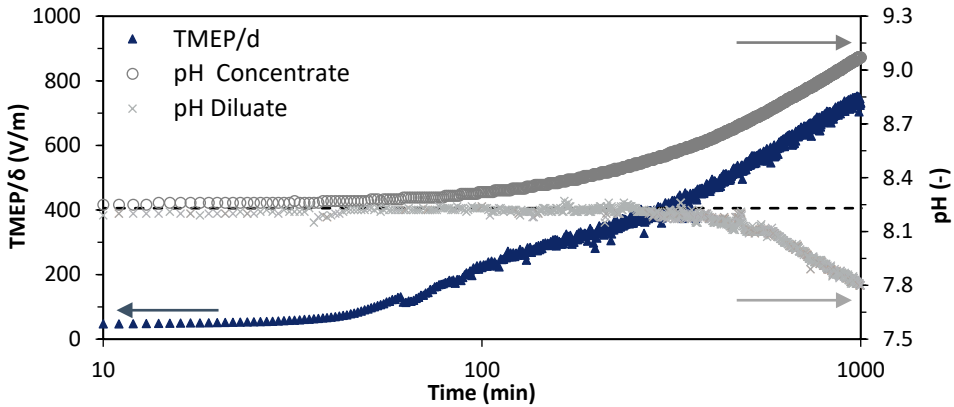
Figure 4.9. *TMEP/δ, pH of the diluate and pH of the concentrate during E10. The discontinuous line is plotted as a reference for the pH.*

Salt precipitation on the concentrate side of the AEM is also linked to the presence of the gel layer. While the HPAM layer is forming, water dissociation occurs at the interface of the layer and the AEM. The hydroxide ions migrate towards the concentrate side of the AEM, where two events can take place: i) divalent cations can precipitate directly with the hydroxide, and ii) the pH increases, allowing bicarbonate to be converted to carbonate, which can also increase precipitation [31]. The gel layer-precipitation relationship was demonstrated in E8 (no gel layer and minimal precipitation) and E9 (less HPAM in solution leading to slight precipitation).

4.4 Conclusions

In the applied concentration range, HPAM is the dominant foulant in terms of resistance increase and coverage of the AEM. Its anionic charge causes it to migrate towards the surface of the membrane at the diluate side when the electrical current is applied. There are two fouling mechanisms for the HPAM on the AEM: i) it adsorbs to the oppositely charged membrane due to electrostatic and hydrophobic interactions [18], and ii) it concentrates near the membrane surface and forms a gel layer of polyelectrolyte. However, most of the effects analyzed in this study are attributable to the formation of the gel layer on the diluate side of the membrane.

The mineral composition of polymer-flooding produced water influences the thickness and structure of the HPAM gel layer. Increased ionic strength decreases the migration of HPAM by coverage of negative charges. The presence of divalent cations in the solution likely causes the formation of thicker and denser HPAM gel layers. The presence of these gel layers hampers the replenishment of ions from the bulk solution to the surface of the membrane, lowering the limiting current density of the system. This condition triggers local pH changes and the precipitation of salts on the concentrate side of the AEM.

Despite its mineral composition, the gel layer shows a reversible nature when a combination of current reversal and foulant-free solution is employed, but most likely the small HPAM amount that is adsorbed on the surface of the AEM remains there, but barely affects the membrane performance.

Salt precipitation occurred frequently on the concentrate side of the membranes, mostly in the form of calcium carbonate. The presence of crude oil changed the morphology of the calcium carbonate precipitation and was found to destabilize the HPAM gel layer.

Our results agree with Xia et al. [13] regarding the joint effect of HPAM plus mineral foulants, but differ from theirs concerning the impact of the crude oil and oily compounds. For the present study, the effect of crude oil, either alone or in combination with the rest of the foulants, was minimal. The difference might be due to i) the lower oil concentration used in the present study, ii) the variable properties of crude oil depending on its origin [47], and iii) the use of membranes based on different chemistries. While the FujiFilm AEMs employed in the present study are based in an aliphatic compound (acrylamide), the membranes used by Xia et al. were based on an aromatic one (polyphenylene) [13]. Previous studies have indicated that membranes based on aliphatic compounds are less prone to suffer from organic fouling [48–50]. It is understood that the aromatic fractions of crude oil have a higher affinity for aromatic composed membranes, and thus have a high tendency to adsorb on them (i.e. through π-π interactions). Alternatively, aliphatic oil fractions predominantly adsorb on membranes through hydrophobic interactions, and the ab- and adsorbed layers appear to have only a minor effect on the functioning of the membranes used in our study. Thus, it appears that aliphatic membranes are also more suitable to treat streams containing crude oil, despite it naturally consists of a mixture of aliphatic and aromatic compounds.

If the TMEP recorded during the experiments are converted to resistances (using Ohm's law), the values are above 900 Ω*cm², which are notoriously high for a membrane and the liquid adjacent to it. Indeed, in our previous research employing a membrane stack [2], such high resistances were never reached. The thick gel layers

and consequent high resistances might have been propitiated by the hydrodynamic conditions in the six-compartment cell, which has thick compartments and lacks spacers to increase the turbulence. In order to better quantify the effect of fouling, it would be ideal to have flow conditions which are closer to the ones in an ED stack.

References

[1]   S. Liu, D.O. Company, X. Dong, H. Ban, T. Wang, W. Pan, Technology for Confecting Polymer Solution with Desalinated Produced Water. Paper SPE 110237, in: SPE (Ed.), 2007 SPE Annu. Tech. Conf. Exhib. Anaheim, California, USA, SPE, Richardson, TX, 2007: pp. 1–5.

[2]   P.A. Sosa-Fernandez, J.W. Post, H. Bruning, F.A.M. Leermakers, H.H.M. Rijnaarts, Electrodialysis-based desalination and reuse of sea and brackish polymer-flooding produced water, Desalination. 447 (2018) 120–132. doi:10.1016/j.desal.2018.09.012.

[3]   D.C. Standnes, I. Skjevrak, Literature review of implemented polymer field projects, J. Pet. Sci. Eng. 122 (2014) 761–775. doi:10.1016/j.petrol.2014.08.024.

[4]   J.J. Sheng, B. Leonhardt, N. Azri, Status of Polymer-Flooding Technology, J. Can. Pet. Technol. 54 (2015) 116–126. doi:10.2118/174541-PA.

[5]   J.A. Herschell, Water and Wastewater Treatment for Enhanced Oil Recovery, Mahon, Cork, Ireland, 2016.

[6]   R. Zhang, W. Shi, S. Yu, W. Wang, Z. Zhang, B. Zhang, L. Li, X. Bao, Influence of salts, anion polyacrylamide and crude oil on nanofiltration membrane fouling during desalination process of polymer flooding produced water, Desalination. 373 (2015) 27–37. doi:10.1016/j.desal.2015.07.006.

[7]   G. Jing, L. Xing, S. Li, C. Han, Reclaiming polymer-flooding produced water for beneficial use: Salt removal via electrodialysis, Desalin. Water Treat. 25 (2011) 71–77. doi:10.5004/dwt.2011.1766.

[8]   L. Henthorne, G.A. Pope, U. Weerasooriya, V. Llano, Impact of Water Softening on Chemical Enhanced Oil Recovery, in: Proc. - SPE Symp. Improv. Oil Recover. 2014, SPE, Tulsa, Oklahoma, 2014.

[9]   B. Sparrow, A. Ebsary, D. Mandel, M. Man, An advanced electrochemical system for EOR produced water desalination and reduced polymer consumption, in: Proc. - SPE Symp. Improv. Oil Recover. 2018, SPE, Tulsa, Oklahoma, 2018.

[10]   J. Guolin, W. Xiaoyu, H. Chunjie, The effect of oilfield polymer-flooding wastewater on anion-exchange membrane performance, Desalination. 220 (2008) 386–393. doi:10.1016/j.desal.2007.03.010.

[11]   J. Guolin, X. Lijie, L. Yang, D. Wenting, H. Chunjie, Development of a four-grade and four-segment electrodialysis setup for desalination of polymer-flooding produced water, Desalination. 264 (2010) 214–219. doi:10.1016/j.desal.2010.06.042.

[12]   S. Mikhaylin, L. Bazinet, Fouling on ion-exchange membranes: Classification, characterization and strategies of prevention and control, Adv. Colloid Interface Sci. 229 (2016) 34–56. doi:10.1016/j.cis.2015.12.006.

[13]   Q. Xia, H. Guo, Y. Ye, S. Yu, L. Li, Q. Li, R. Zhang, Study on the fouling mechanism and cleaning method in the treatment of polymer flooding produced water with ion exchange membranes, RSC Adv. 8 (2018) 29947–29957. doi:10.1039/c8ra05575k.

[14]   H. Guo, F. You, S. Yu, L. Li, D. Zhao, Mechanisms of chemical cleaning of ion exchange membranes: A case study of plant-scale electrodialysis for oily wastewater treatment, J. Memb. Sci. 496 (2015) 310–317. doi:10.1016/j.memsci.2015.09.005.

[15]   T. Wang, S. Yu, L. an Hou, Impacts of HPAM molecular weights on desalination performance of ion exchange membranes and fouling mechanism, Desalination. 404 (2017) 50–58. doi:10.1016/j.desal.2016.10.007.

[16]   J.I.S. Aguiar, C.R.E. Mansur, the Influence of Polymer Flooding on Produced Oily Water: a Review, Brazilian J. Pet. Gas. 10 (2016) 49–61. doi:10.5419/bjpg2016-0005.

[17]   X. Zuo, L. Wang, J. He, Z. Li, S. Yu, SEM-EDX studies of SiO2/PVDF membranes fouling in electrodialysis of polymer-flooding produced wastewater: Diatomite, APAM, and crude oil, Desalination. 347 (2014) 43–51. doi:10.1016/j.desal.2014.05.020.

[18]   H. Guo, L. Xiao, S. Yu, H. Yang, J. Hu, G. Liu, Y. Tang, Analysis of anion exchange membrane fouling mechanism caused by anion polyacrylamide in electrodialysis, Desalination. 346 (2014) 46–53. doi:10.1016/j.desal.2014.05.010.

[19]   P.A. Sosa-Fernandez, J.W. Post, F.A.M. Leermakers, H.H.M. Rijnaarts, H. Bruning, Removal of divalent ions from viscous polymer-flooding produced water and seawater via electrodialysis, J. Memb. Sci. 589 (2019) 117251. doi:10.1016/j.memsci.2019.117251.

[20]   S. Peng, C. Wu, Light Scattering Study of the Formation and Structure of Partially Hydrolyzed Poly(acrylamide)/Calcium(II) Complexes, Macromolecules. 32 (1999) 585–589.

[21]   P. Długołecki, K. Nymeijer, S. Metz, M. Wessling, Current status of ion exchange membranes for power generation from salinity gradients, J. Memb. Sci. 319 (2008) 214–222. doi:10.1016/j.memsci.2008.03.037.

[22]   B. Van Berchum, W.J. Van Baak, J. Hessing, Curable compositions and membranes, US 9,309,343 B2, 2016.

[23]   A.R. Al-Hashmi, T. Divers, R.S. Al-Maamari, C. Favero, A. Thomas, Improving polymer flooding efficiency in Oman oil fields. Paper SPE-179834-MS, in: SPE EOR Conf. Oil Gas West Asia Held Muscat, Oman, 21–23 March 2016., SPE, Muscat, 2016: p. 18.

[24]   J.M. Dickhout, J.M. Kleijn, R.G.H. Lammertink, W.M. de Vos, Adhesion of emulsified oil droplets to hydrophilic and hydrophobic surfaces – effect of surfactant charge, surfactant concentration and ionic strength, Soft Matter. 14 (2018) 5452–5460. doi:10.1039/C8SM00476E.

[25]   D.A. Cowan, J.H. Brown, Effect of turbulence on limiting current in electrodialysis cells, Ind. Eng. Chem. 51 (1959) 1445–1448. doi:10.1021/ie50600a026.

[26]   P. Sistat, A. Kozmai, N. Pismenskaya, C. Larchet, G. Pourcelly, V. Nikonenko, Low-frequency impedance of an ion-exchange membrane system, Electrochim. Acta. 53 (2008) 6380–6390. doi:10.1016/j.electacta.2008.04.041.

[27]   H.J. Lee, S.H. Moon, S.P. Tsai, Effects of pulsed electric fields on membrane fouling in electrodialysis of NaCl solution containing humate, Sep. Purif. Technol. 27 (2002) 89–95. doi:10.1016/S1383-5866(01)00167-8.

[28]   N. Pismenskaia, P. Sistat, P. Huguet, V. Nikonenko, G. Pourcelly, Chronopotentiometry applied to the study of ion transfer through anion exchange membranes, J. Memb. Sci. 228 (2004) 65–76. doi:10.1016/j.memsci.2003.09.012.

[29]   J.S. Park, J.H. Choi, K.H. Yeon, S.H. Moon, An approach to fouling characterization of an ion-exchange membrane using current-voltage relation and electrical impedance spectroscopy,

J. Colloid Interface Sci. 294 (2006) 129–138. doi:10.1016/j.jcis.2005.07.016.

[30] Y. Tanaka, Concentration polarization in ion-exchange membrane electrodialysis: The events arising in an unforced flowing solution in a desalting cell, J. Memb. Sci. 244 (2004) 1–16. doi:10.1016/j.memsci.2004.02.041.

[31] N. Cifuentes-Araya, C. Astudillo-Castro, L. Bazinet, Mechanisms of mineral membrane fouling growth modulated by pulsed modes of current during electrodialysis: Evidences of water splitting implications in the appearance of the amorphous phases of magnesium hydroxide and calcium carbonate, J. Colloid Interface Sci. 426 (2014) 221–234. doi:10.1016/j.jcis.2014.03.054.

[32] N. Cifuentes-Araya, G. Pourcelly, L. Bazinet, Water splitting proton-barriers for mineral membrane fouling control and their optimization by accurate pulsed modes of electrodialysis, J. Memb. Sci. 447 (2013) 433–441. doi:10.1016/j.memsci.2013.06.055.

[33] C. Casademont, G. Pourcelly, L. Bazinet, Effect of magnesium/calcium ratios in solutions treated by electrodialysis: Morphological characterization and identification of anion-exchange membrane fouling, J. Colloid Interface Sci. 322 (2008) 215–223. doi:10.1016/j.jcis.2008.02.068.

[34] E. Korngold, F. de Korosy, R. Rahav, M.F. Taboch, Fouling of anionselective membranes in electrodialysis, Desalination. 8 (1970) 195–220. doi:10.1016/S0011-9164(00)80230-1.

[35] Q. Li, M. Elimelech, Organic fouling and chemical cleaning of nanofiltration membranes: Measurements and mechanisms, Environ. Sci. Technol. 38 (2004) 4683–4693. doi:10.1021/es0354162.

[36] X. Jin, X. Huang, E.M. V Hoek, Role of specific ion interactions in seawater RO membrane fouling by alginic acid, Environ. Sci. Technol. 43 (2009) 3580–3587. doi:10.1021/es8036498.

[37] I. Szilagyi, G. Trefalt, A. Tiraferri, P. Maroni, M. Borkovec, Polyelectrolyte adsorption, interparticle forces, and colloidal aggregation, Soft Matter. 10 (2014) 2479–2502. doi:10.1039/c3sm52132j.

[38] E. Pefferkorn, Polyacrylamide at solid/liquid interfaces, J. Colloid Interface Sci. 216 (1999) 197–220.

[39] M. Porus, P. Maroni, M. Borkovec, Structure of adsorbed polyelectrolyte monolayers investigated by combining optical reflectometry and piezoelectric techniques, Langmuir. 28 (2012) 5642–5651. doi:10.1021/la204855j.

[40] T. Abraham, Effects of divalent salt on adsorption kinetics of a hydrophobically modified polyelectrolyte at the neutral surface - aqueous solution interface, Polymer (Guildf). 43 (2002) 849–855.

[41] S. Mulyati, R. Takagi, A. Fujii, Y. Ohmukai, T. Maruyama, H. Matsuyama, Improvement of the antifouling potential of an anion exchange membrane by surface modification with a polyelectrolyte for an electrodialysis process, J. Memb. Sci. 417–418 (2012) 137–143. doi:10.1016/j.memsci.2012.06.024.

[42] Y. Zhang, M. Tirrell, J.W. Mays, Effects of ionic strength and counterion valency on adsorption of hydrophobically modified polyelectrolytes, Macromolecules. 29 (1996) 7299–7301. doi:10.1021/ma960214u.

[43] M. Bjørsvik, H. Høiland, A. Skauge, Formation of colloidal dispersion gels from aqueous polyacrylamide solutions, Colloids Surfaces A Physicochem. Eng. Asp. 317 (2008) 504–511. doi:10.1016/j.colsurfa.2007.11.025.

4

[44]   P.-Y. Ben Jar, Y.S. Wu, Effect of counter-ions on swelling and shrinkage of polyacrylamide-based ionic gels, Polymer (Guildf). 38 (1997) 2557–2560.

[45]   T. Tanaka, N. Izumi, S.-T. Sun, S. Ueno-Nishio, Collapse of gels in an electric field, Science (80-.). 218 (1982) 467–469.

[46]   S. Choi, pH Sensitive polymers for novel conformance control and polymer flooding applications, The University of Texas at Austin, 2008.

[47]   M. Dudek, E. Kancir, G. Øye, Influence of the Crude Oil and Water Compositions on the Quality of Synthetic Produced Water, Energy and Fuels. 31 (2017) 3708–3716. doi:10.1021/acs.energyfuels.6b03297.

[48]   N. Tanaka, M. Nagase, M. Higa, Preparation of aliphatic-hydrocarbon-based anion-exchange membranes and their anti-organic-fouling properties, J. Memb. Sci. 384 (2011) 27–36. doi:10.1016/j.memsci.2011.08.064.

[49]   N. Tanaka, M. Nagase, M. Higa, Organic fouling behavior of commercially available hydrocarbon-based anion-exchange membranes by various organic-fouling substances, Desalination. 296 (2012) 81–86. doi:10.1016/j.desal.2012.04.010.

[50]   M. Higa, N. Tanaka, M. Nagase, K. Yutani, T. Kameyama, K. Takamura, Y. Kakihana, Electrodialytic properties of aromatic and aliphatic type hydrocarbon-based anion-exchange membranes with various anion-exchange groups, Polymer (Guildf). 55 (2014) 3951–3960. doi:10.1016/j.polymer.2014.06.072.

Appendix 4A. Supplementary material for Materials and methods

The limiting current density was determined using the method described by Cowan and Brown [25]. The diluate and concentrate consisted of 53.3 mM NaCl solutions, which was the lowest salt concentration among the ED experiments. Then, Figure A4.1. was obtained after calculating the average of each current series and correcting it for the membrane surface area. The graph shows that the last value within the linear relation of the sub-limiting current density region is 78 A/m^2, which corresponds to an applied current of 55 mA. Thus, the electrodialysis experiments were performed at a current density below this value (28.2 A/m^2). It should be noted that the surface area of the test membrane is three times smaller than the other membranes, so the LCD cannot be exceeded in the auxiliary membranes before it is exceeded at the test membrane.
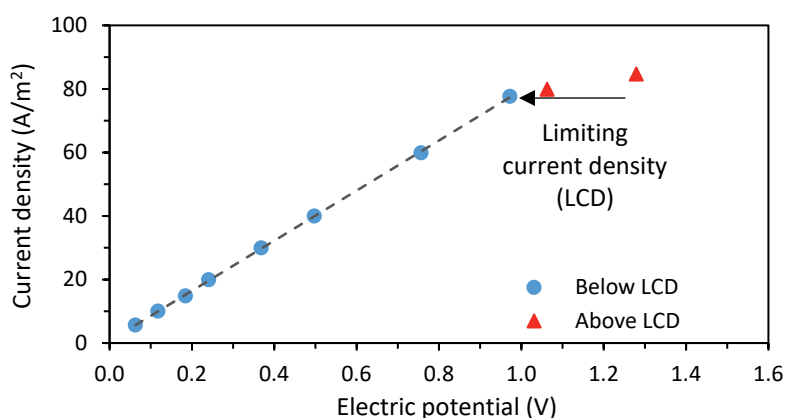
Figure A4.1. *Determination of limiting current density for AEM FujiFilm type 10 in 53.3 mM NaCl solution.*

Appendix 4B. SEM and EDX measurements

Although SEM/EDX data is summarized in **Table 4.5**, this appendix contains images that could not be included within the text. It should be noted that measuring the thicknesses of the gel layer may involve some inaccuracies, namely either the gel layer may have only remained partly attached during the recovery of the membrane, or the gel layer may have expanded during the freezing procedure.
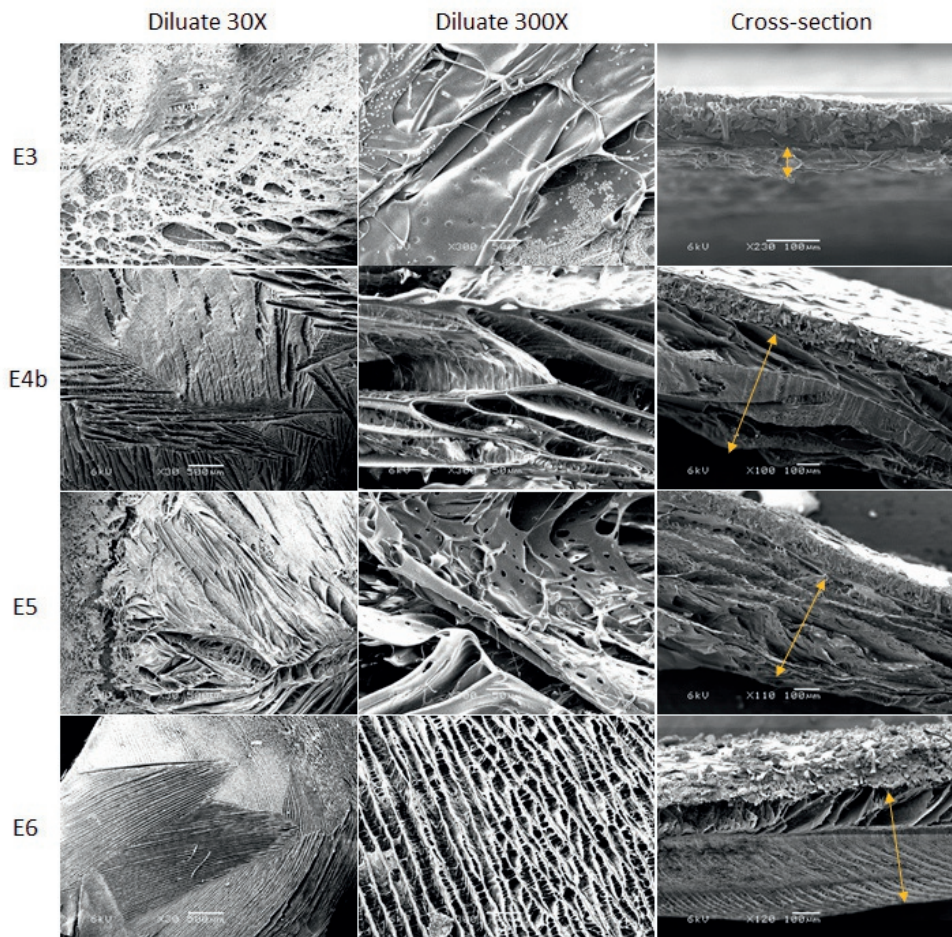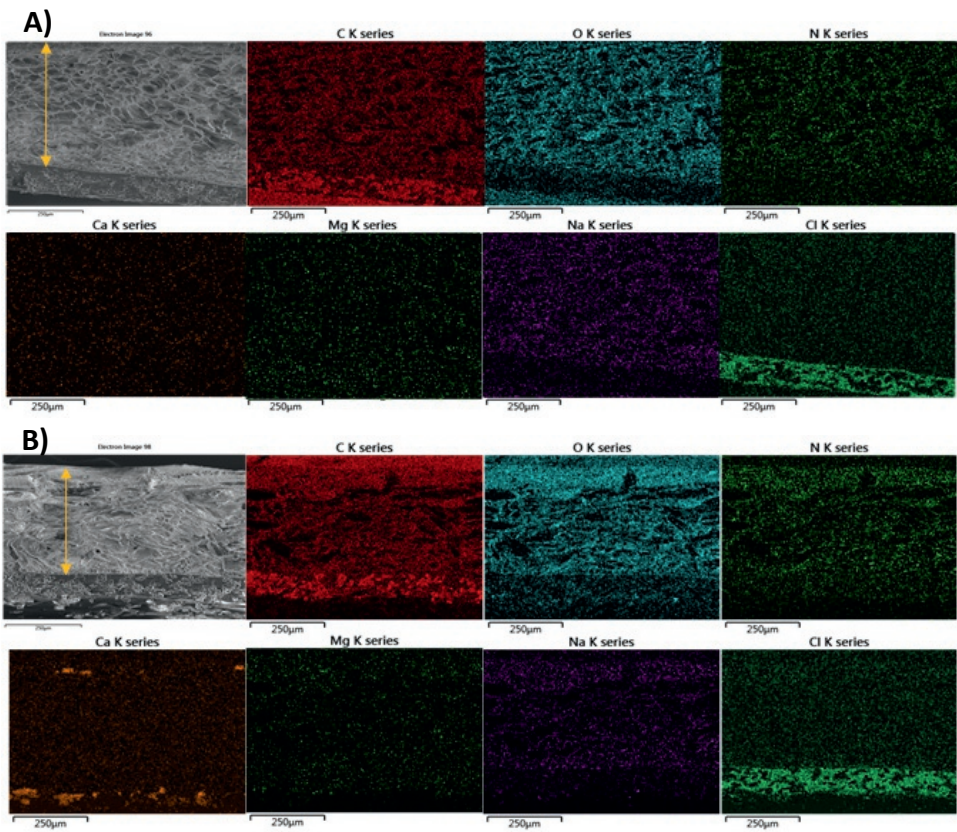
Figure A4.2. *SEM images of the gel layer for experiments E3 to E6 for the freeze-dried membranes. The arrows indicate the gel layer.*
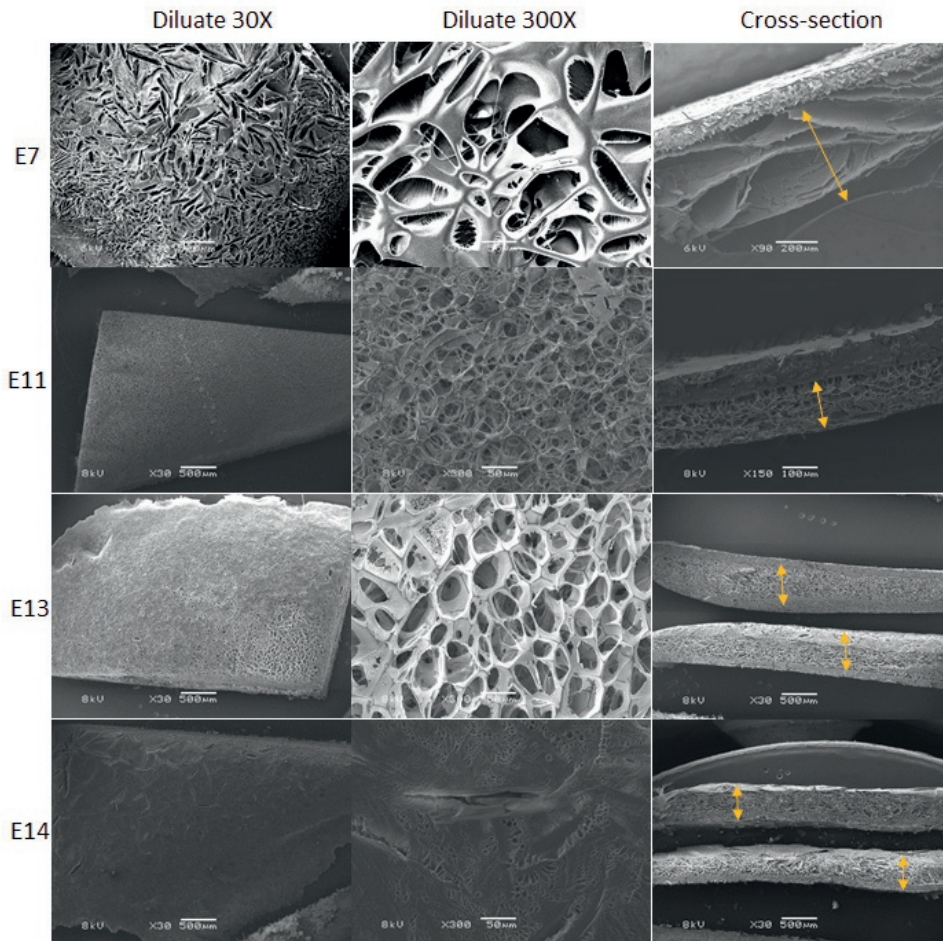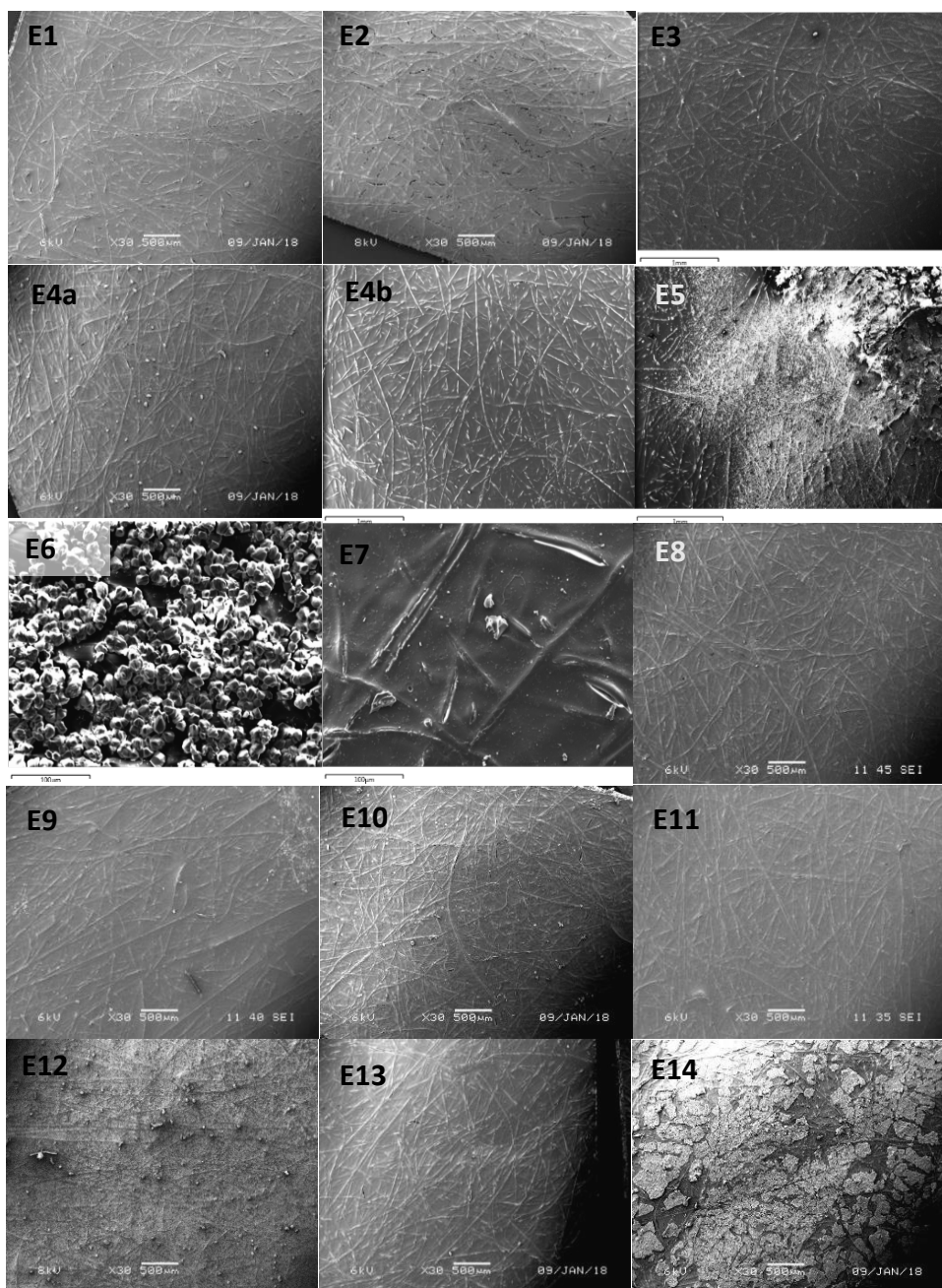
Figure A4.3. *SEM photographs of freeze-dried membranes recovered from E7, E11, E13, and E14. The arrows indicate the gel layer.*

Figure A4.4. Elemental composition of the freeze-dried cross-section of membranes *A)* E13 and *B)* E14. The membranes appear horizontally on the bottom of the images with the gel layers (signaled by arrows) on top of them.

Figure A4.5. *SEM images of the concentrate side of the AEMs. Notice that the magnifications for E6 and E7 are different from the rest.*

Appendix 4C. Contact angle and Raman measurements

Contact angle measurements were performed with MiliQ water in-air, as described in section 4.2.2.2.3. The conditions were chosen to minimize disturbances to the

fouling and to facilitate comparisons with the literature. However, by prioritizing these factors, others were left aside, like the membranes being underwater when they are under operation, which is not reflected when doing in-air measurements.
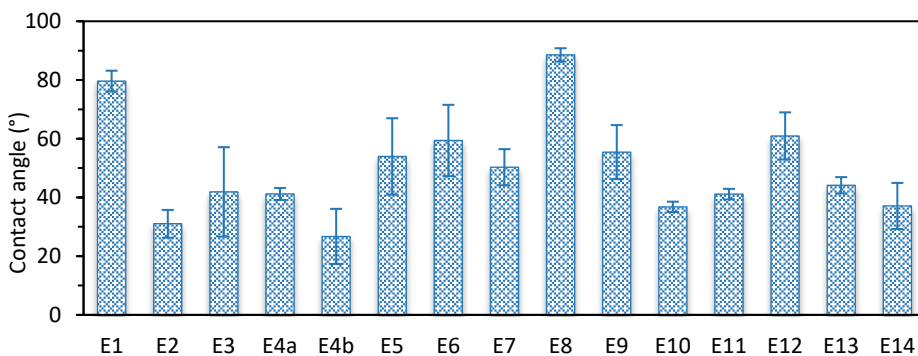
Figure A4.6. *Static contact angle measurements on the diluate side of the membranes.*

The Raman measurements confirmed the presence of HPAM on the diluate side of the membranes where it has already been identified via SEM (Figure 4.3). For the concentrate side, Raman allowed the clear identification of calcite ($CaCO_3$) on membrane E14, as shown in **Figure A4.7**. The presence of oil was indirectly observed on both sides of the AEM given the high luminescence that affected the Raman measurements when higher concentrations of oil were employed (E12).
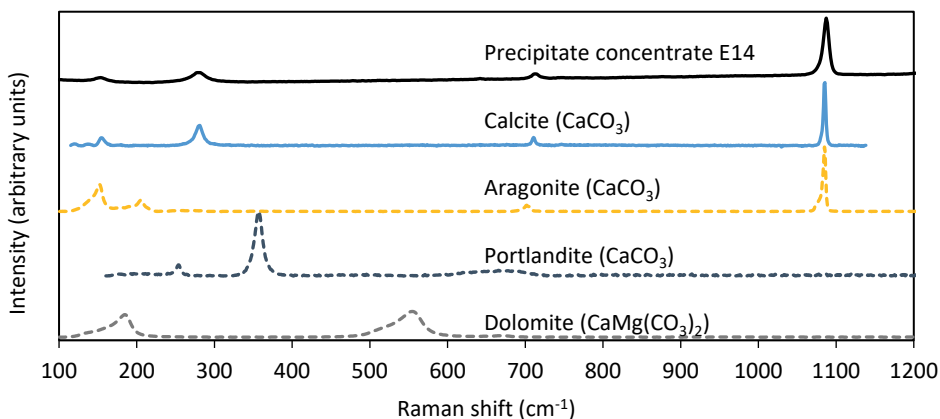

Figure A4.7. *Identification via Raman of a precipitate obtained from the concentrate side of membrane E14.*

Appendix 4D. Water splitting quantification

The NaCl-based solutions (E1-E3 and E11) had an initial pH around 7, while the BW-based solutions (E4-E10, E12-E14) were more alkaline, with an initial pH of 8.2, due to their content of carbonate. However, these values changed during the experiments. Even though the working current density was chosen below the LCD

of the least conductive solutions, the formation of the HPAM gel layer and concentration polarization could have caused some water to split [34]. As shown for experiment E10 in **Figure 4.9**, the pH of the concentrate solution started to increase around minute 40 of the desalination, coinciding with the increase in TMEP/δ. This happens because when limiting current density conditions are reached, the water will usually split on the diluate side of the membrane, where concentration polarization reduces the concentration of ions. Then, protons migrate to the cathode and hydroxide ions to the anode, causing an increase in the pH of the concentrate and a decrease in the pH of the diluate, as shown in the figure. Indeed, pH changes were recorded during most of the experiments, as shown in **Figure A4.8**, indicating an important degree of water splitting.
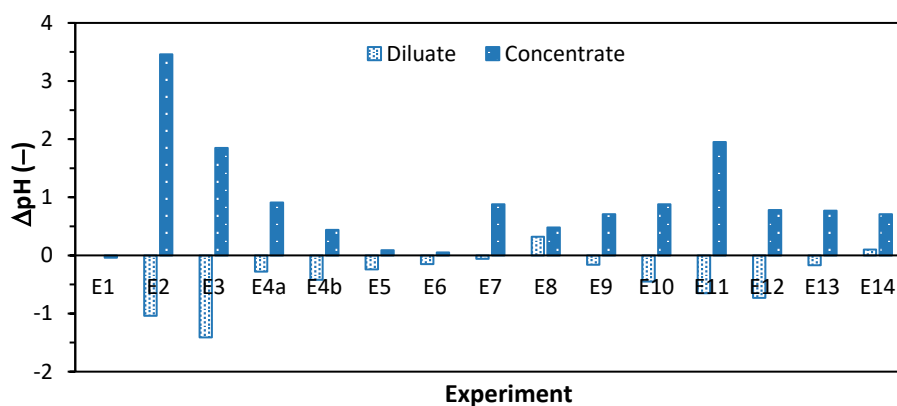

Figure A4.8. Absolute pH change of the concentrate and diluate solutions during the electrodialysis experiments.

From **Figure A4.8**, three main observations can be made. The first is that the largest changes in pH occurred in solutions E2, E3 and E11, even though the measured TMEP was lower. This is due to their lack of bicarbonate, which has a significant buffering capacity. Although HPAM and crude oil might also have some buffering effect, their influence was found to be minimal. The second observation is related to the larger increase of pH in the concentrate compared to the decrease in the diluate. This can be explained by: 1) the bicarbonate having a larger buffering capacity towards a lower pH (which can be calculated from its pK_z values); 2) the high mobility of the protons (which can pass among compartments even through the AEMs); and 3) the likely adsorption of protons on the fouling gel layer [29]. The final remark comes from the experiment without HPAM (E8), which was the only one to present a net increase of pH on both streams. This indicates that water splitting was also occurring, but since there was no gel layer there was more replenishment of fresh solution, and some of the hydroxyls were transferred to the bulk of the diluate stream causing the pH to increase.

Appendix 4E. Reverse fouling experiments with low HPAM concentrations

Additional fouling experiments were performed to determine the effect of the adsorption of HPAM on the electric resistance of the AEM. Therefore, these experiments made use of solutions with low concentrations of HPAM (1 mg/L). Figure A4.9 shows the TMEP/δ obtained when using the solution with brackish composition. The first two periods of 30 minutes were conducted with only salts solution. Then, the solutions containing 1 mg/L of HPAM were added in the minutes 65 and 180 in the diluate compartment. Both times, the current was in the right direction for the HPAM to displace towards the membrane, but still the changes in the TMEP were minimal. After 60 minutes of maintaining the current direction, it was reversed, but no change was detected. Similar results were obtained when using other mineral compositions (only NaCl and brackish with 3x[Ca + Mg]). Thus, the experiments indicated that the adsorption of HPAM does not contribute to the significant increase of resistance, as previously reported for polyelectrolytes adsorbed on IEMs [41].
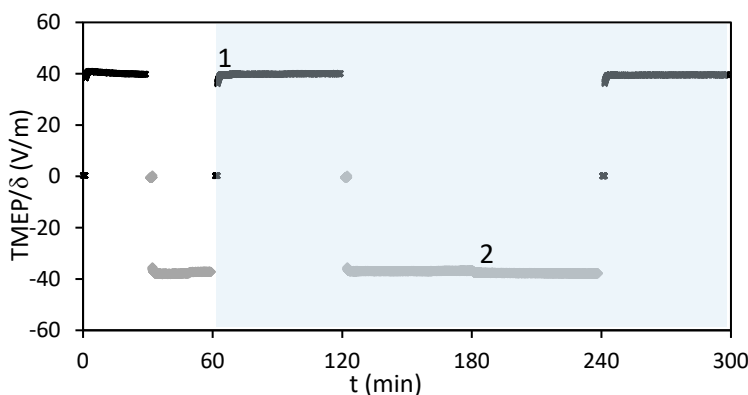
Figure A4.9. *Resistance profile for the current reversal experiment with brackish solution. At point 1, the current diluate solution is changed from brackish water (BW) to brackish water with 1 mg/L of HPAM. At point 2, the other solution is changed from BW to BW with 1 mg/L of HPAM. The shaded area indicates when HPAM-containing solutions were present in the cell.*
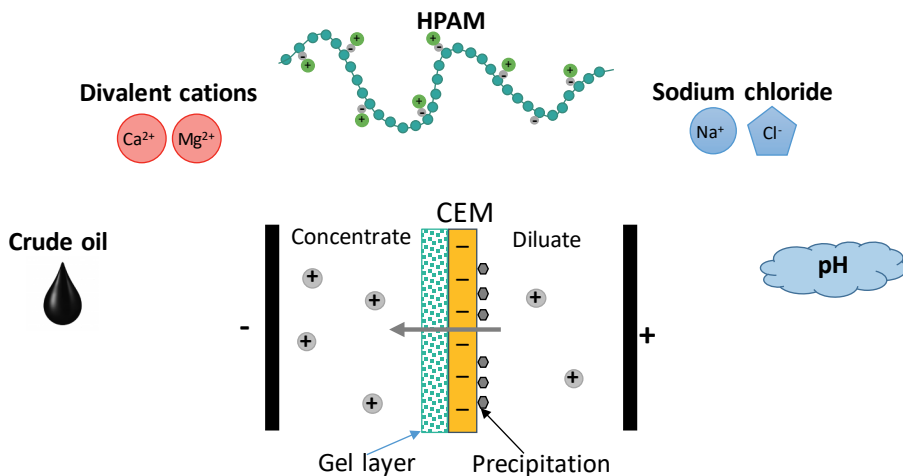
4

Chapter 5

Influence of feed composition on the fouling of cation exchange membranes desalinating polymer-flooding produced water

Abstract

Cation exchange membranes (CEMs) are subject to fouling when utilized to desalinate wastewater from the oil and gas industry, hampering their performance. The kind and extent of the fouling are most likely dependent on the composition of the stream, which in practical applications can vary significantly. To test the influence of the feed solution, fouling experiments were performed on commercial cation exchange membranes, which were used in electrodialysis runs to desalinate solutions of varying composition. The variations included ionic strength, type of ions, amount of viscosifying polyelectrolyte (partially hydrolyzed polyacrylamide), presence of crude oil, and surfactants. Performance parameters, like electric potential and pH, were monitored during the runs, after which the membranes were recovered and analyzed. Fouling was detected on most CEMs and occurred mainly in the presence of the viscosifying polyelectrolyte. Under normal pH conditions (pH~8), the polyelectrolyte fouled the concentrate side of the CEMs, as expected due to electrophoresis. Precipitation occurred mostly on the opposite side of the membrane, with different morphology depending on the feed composition.

5.1 Introduction

Polymer-flooding produced water (PFPW) is a by-product of industrial oil and gas production, especially when viscous polymeric solutions are pumped in the subsoil to increase the oil or gas recovery. The reuse of PFPW within the same process may be technically, economically, and sustainably beneficial. For this, the produced water stream should be at least partially desalinated, and electrodialysis is a sound technology to achieve this objective [1]. However, electrodialysis, as all membrane-based processes, is susceptible to suffer from fouling, a problem that hampers its industrial application, especially in the case of treating produced water with polymer compounds [2].

Among the two types (cationic and anionic) of ion exchange membranes (IEMs) used in an electrodialyzer, research has suggested that the anion exchange membrane (AEM) suffers most severe from fouling when desalinating PFPW [3,4] because many organic compounds in PFPW, including the partially hydrolyzed polyacrylamide (HPAM) used as a viscosifier, are negatively charged at neutral pH. These compounds move towards the anode under the electric field (electrophoresis) and deposit mainly on the positively charged AEM surface due to attractive electrical interactions [5]. Consequently, the majority of studies have been dedicated to (prevent) fouling on this kind of membranes [6–8].

In this line, one of our previous studies focused on the AEMs [9], specifically on understanding the influence of the composition of PFPW on fouling. It was found that the electrophoretically driven HPAM fouled the membrane and formed a gel layer, leading to increases in trans-membrane electric potential (TMEP). HPAM appears to foul the AEM due to two phenomena: adsorption on the AEM surface and formation of a viscous gel layer at the AEM-solution interface that hampers the replenishment of ions from the bulk solution. It was also observed that the presence of Ca^{2+} and Mg^{2+} lead to the formation of thick HPAM gel layers, while the presence of oily compounds had only a minimal effect.

In contrast to AEMs, the fouling by PFPW on cation exchange membranes (CEMs) has been less studied. Some publications have reported HPAM gel layers on the surface of the CEMs [3,4,10], despite there is a net electrostatic repulsion between the HPAM molecule and the CEM [6]. Fouling by oil and by inorganic precipitants has also been reported [4,10]. However, it is still not known how the different components of PFPW interact with the CEM surface and affect its fouling. Furthermore, the PFPW used in most studies contained only HPAM, salts, and oil, and have overlooked the fact that (generally cationic) surfactants are commonly employed together with the viscous polymer solutions for increasing oil recovery [11].

Accordingly, the objective of the investigation presented here was to reveal 1) the fouling mechanisms for cation exchange membranes employed to desalinate polymer-flooding produced water, and 2) how the variations in the water composition would affect this fouling. Synthetic feed solutions tested in ED setups were varied in concentrations of mono- and divalent ions (representative for being present in PFPW), HPAM, a synthetic emulsion of a cationic surfactant, and crude oil. Furthermore, the pH of the solution directly influences the electrochemical properties of ion-exchange membranes and the polyelectrolyte HPAM (including its electrophoretic mobility) [6,12]; therefore, the pH effects on fouling were also studied.

5.2 Materials and methods

5.2.1 Materials

5.2.1.1 *Preparation of solutions*

Synthetic solutions resembling PFPW with diverse compositions were employed for each electrodialysis experiment, as summarized in **Table 5.1**. The solution composition consisted of either dissolved sodium chloride (as the only salt) or a brackish water (BW) matrix (with a more diverse ionic composition), the latter resembling water from the Marmul field in Oman [13]. BW contained 53.3 mM NaCl, 15.6 mM $NaHCO_3$, 2.51 mM Na_2SO_4, 0.72 mM KCl, 0.65 mM $CaCl_2$, and 0.46 mM $MgCl_2$ [13]. In some experiments, the ionic composition was further adjusted to study the effects of concentrations of specific (cationic) ionic species and pH (**Table 5.1**).

The solutions with HPAM (MW= 5-8 million Da, 30% hydrolyzed) were prepared by slowly adding the polymer to the salt solution under fast stirring. The obtained mixture was left overnight under slow stirring and employed within three days of its preparation.

The concentration of HPAM in the prepared solutions is presumed to be above the overlap concentration c^*, defined as the concentration at which individual polymer molecules begin to interact, and inter-molecular crosslinking between two or more polymers can occur [14,15]. This conclusion was reached by comparing the results of Bjørsvik et al. [14] with our solutions. These authors determined c^* equal to 4.7 and 132 ppm for HPAM (MW= 11 million Da, 30% hydrolyzed) solutions prepared, respectively, in distilled water and 85.6mM NaCl solution. Therefore, for the highest salinity employed in the present study (77 Mm), c^* of HPAM has been calculated around 130 ppm, which is much lower than the concentrations of 0.5 to 1.0 g/L HPAM used (**Table 5.1**).

Table 5.1. Composition of the feed solutions for the electrodialysis experiments

Experiment	Solution composition	HPAM polymer	Oily compounds
E1	53.3 mM NaCl	-	-
E2	53.3 mM NaCl	1.0 g/L	-
E3	68.0 mM NaCl	1.0 g/L	-
E4*	Brackish water (BW)	1.0 g/L	-
E5	BW with 3x[Ca + Mg]	1.0 g/L	-
E6	BW	-	2 mg/L crude oil
E7	BW	0.5 g/L	2 mg/L crude oil
E8	BW	1.0 g/L	2 mg/L crude oil
E9	77.0 mM NaCl	1.0 g/L	2 mg/L crude oil
E10	BW	1.0 g/L	20 mg/L crude oil
E11	BW	1.0 g/L	20 mg/L model emulsion
E12	BW with 3x[Ca + Mg]	1.0 g/L	20 mg/L model emulsion
E13	BW (pH= 4.5)	1.0 g/L	2 mg/L crude oil
E14	BW (pH= 2.0)	1.0 g/L	2 mg/L crude oil

*Experiment E4 was performed in duplicate, a and b.

Regarding the oily compounds, two different compositions were studied: one with crude oil and one with a model emulsion prepared with a cationic surfactant. This kind of surfactant, mostly employed for flooding in carbonate reservoirs [16], was chosen due to its positive charge, opposite to that of the CEM. The preparation of the stock solutions was based on the method described in [17]. In the case of the synthetic emulsion, it was prepared by dissolving 346 mg (~1 mmol) of cationic cetyltrimethylammonium bromide (CTAB) surfactant in 998g of brackish solution previously conditioned to 45 °C. Then, 2.0 g of hexadecane was added, and the solution was mixed at 14,000 rpm by an IKA T25 Ultra-Turrax emulsifying mixer (Germany) for 10 minutes. The oil concentration of this emulsion was 2.0 g/L, so 10.0 mL was needed to obtain 20 mg/L in the feed solution.

For preparing the emulsion with crude oil, 2.0g of oil was added to 2.0L of BW previously heated to 45°C, and the mixture was emulsified with CTAB as described above. This mixture was let to rest for 24 hours, after which the water phase was recovered, analyzed, and stored as an oil stock solution. Its oil concentration was determined as 6.5 mg/L via gas chromatography after extracting the oil components with hexane [18].

The pH of solutions E13 and E14 was adjusted by adding 1.0M HCl. The pH for E13 was set at 4.5 because this is approximately the pKa for HPAM, which is mainly controlled by the carboxylic groups in the molecule [19]. The pH for E14 was chosen below the last known value at which HPAM has a negative zeta potential [6].

Analytical grade salts (NaCl, NaHCO$_3$, Na$_2$SO$_4$, KCl, CaCl$_2$·2H$_2$O, and MgCl$_2$·6H$_2$O) acquired from VWR were employed to prepare the feed solutions. The polymer used was Flopaam 3230S, kindly provided by SNF (France). Model emulsions were prepared with analytical grade hexadecane (Merck, USA) and CTAB surfactant (Sigma-Aldrich, UK). The crude oil originated from the North Sea and was kindly provided by Shell. The characteristics of this type of oil can be found in [20,21].
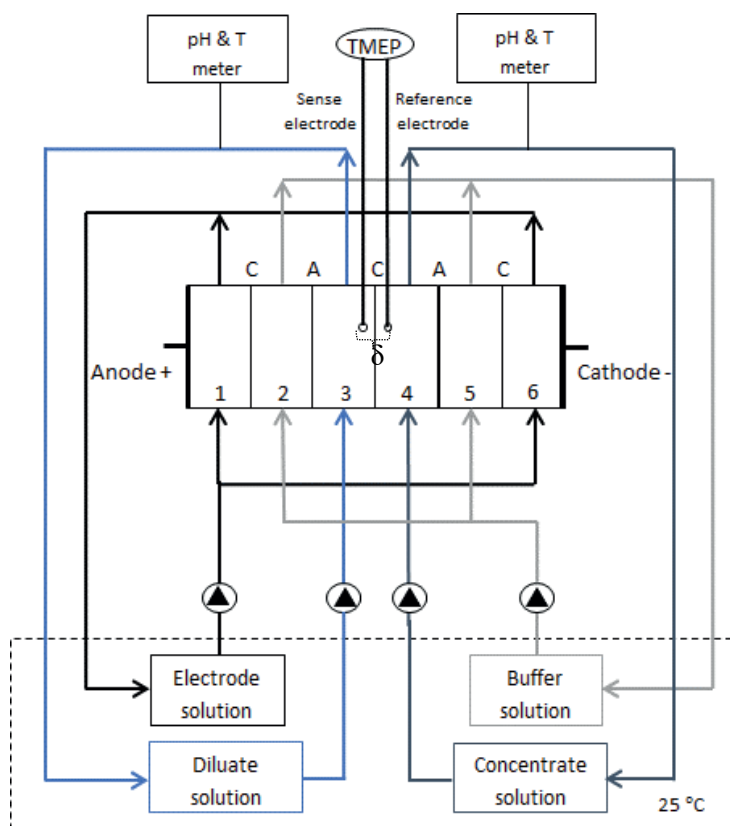
5.2.1.2 *Six-compartment cell and setup*

The experiments were performed in a six-compartment cell that has been previously described [22]. The cation-exchange membrane under study, with an effective area of 7.07 cm^2, was placed in the middle of the cell. Four auxiliary membranes, positioned alternately as in an electrodialysis stack, separated the rest of the compartments (see **Figure 5.1**). The membranes used in this study were FujiFilm type 10, provided by FujiFilm Manufacturing Europe B.V. (The Netherlands), with properties summarized in **Table 5.2**. Two L-shaped Haber-Luggin capillaries filled with a 3.0 M KCl solution were placed on each side of the test membrane. They were connected through 30 cm tubing, to two reference Ag/AgCl electrodes (QM711X, QIS, The Netherlands) that allowed to measure the transmembrane electric potential (TMEP) across the test CEM. The TMEP was recorded with an Autolab PGSTAT12 (The Netherlands), which also controlled the electric current passing through the cell.

As indicated in **Figure 5.1**, four solutions were circulated through the cell:

- Compartments 1 and 6. 1.0 L of 0.05 M Na$_2$SO$_4$ as the electrolyte solution.
- Compartments 2 and 5. 1.0 L of a solution with the same mineral composition as the feed, as a buffer.
- Compartments 3 and 4. For each, 1.0 L of the solutions listed in **Table 5.1**, becoming diluate and concentrate.

The temperature of the solutions was kept at 25 °C utilizing a water bath (Julabo SW22). The solutions were pumped through the cell at a rate of 170 mL/min by peristaltic pumps (Cole-Parmer, Masterflex L/S Digital drive, USA). Their pH and temperature were continuously monitored with Orbisint CPS11D-7BA21 probes connected to a Liquisys-M pH digital sensor, both from Endress+Hauser (Germany).

Figure 5.1. *Scheme of the six-compartment cell and setup. The cell uses three cation-exchange membranes (C) and two anion-exchange ones (A) to separate the six compartments. The cation exchange membrane under analysis is placed in the middle of the cell, sided by two Haber-Luggin capillaries, which allow measuring the TMEP across the distance δ. Adapted from [9].*

Table 5.2. *Properties of the cation and anion exchange membranes employed in this study [23]*

Membrane property	CEM type 10	AEM type 10
Backbone material	Acrylamide	Acrylamide
Reinforcement	Polyolefin	Polyolefin
Functional group [24]	$-SO_3-$	$-(CH_3)_3N^+$
Thickness dry (μm)	135	125
Area resistance (Ω cm^2, measured in 0.5M NaCl)	2.0	1.7
Permselectivity (measured at 0.05-0.5M NaCl)	99	95
pH stability	1-13	1-13

5.2.2 Methods

5.2.2.1 *Electrodialysis experiments*

The electrodialysis experiments were run for 18 hours at a fixed current density of 28.3 A/m². The current density represents 45% of the limiting current density (LCD) for a 53.0 mM NaCl solution, determined by the Cowan & Brown method [25] (**Figure A5.1**). The duration of the experiment was chosen to allow a partial demineralization of the bulk diluate solution (~20%).

Once the ED run was finished, the cell was emptied, and the test membrane was carefully recovered and stored (see section 5.2.2.2). The diluate and concentrate solutions were combined, and the new solution used in the compartments 3 and 4 to test the potential between the capillaries at different currents. This measurement provided the average resistance of the solution, which, combined with its conductivity, allowed to calculate the distance δ between the capillaries [26].

The reversibility of the fouling by HPAM was studied through electrodialysis reversal experiments. They consisted of alternatively desalting solutions with and without HPAM in the compartments 3 and 4 of the cell by switching the direction of the electrical current.

5.2.2.2 *Membrane analysis*

After the ED experiments, the inner compartments of the cell were emptied, the cell opened, and the membranes were slowly withdrawn. They were carefully placed inside glass recipients, tilted approximately 45° to avoid any perturbation to the materials recovered. The membranes were left drying at ambient temperature (23°C) for one day, after which they were cut in smaller pieces and stored until analyzed by the following techniques.

5.2.2.2.1 SEM/EDX measurements

The scanning electron microscopy (SEM) and energy-dispersive X-ray spectroscopy (EDX) were performed in JEOL-6480LV (JEOL Ltd. Japan). The samples were further dried in a desiccator and gold-coated with a JEOL JFC-1200 fine coater. Each membrane was analyzed from the two faces and the cross-section. The samples used for the cross-section images were prepared by first freezing them in nitrogen [6] and then cutting them with a scalpel. The EDX conditions were 15 kV accelerating voltage and 10 mm working distance.

5.2.2.2.2 Raman measurements

Raman spectra were obtained using a LabRAM HR Raman spectrometer from Horiba Jobin Yvon with an mpc3000 laser at 532.2 nm and an 800 mm focal length achromatic flat field monochromator. The laser was focused through an Olympus

Bx41 microscope. The detector was a Synapse multichannel CCD. The analysis was performed on both faces of the membranes (focusing on the ion exchange resin and avoiding the supporting fibers), plus some salt precipitates and one grain of HPAM. The foulants were identified by comparing the Raman spectra of the fouled membranes with that of the clean one (E1), as well as with the spectra of an HPAM granule, a CEM fiber, calcite, and of other salts possibly present (brucite, aragonite, portlandite, etc.).

5.2.2.2.3   Contact angle

Static contact angles were measured with a Dataphysics OCA 35 (Germany) contact angle meter by using the sessile drop method with 2 µl of MilliQ-water [5,27]. While the droplet was still hanging from the syringe, the holder with the dry membrane was lifted until the membrane contacted the liquid. Once the droplet was placed on the membrane and the syringe withdrawn, a snapshot was taken. The contact angle was determined from the snapshot, and the procedure repeated at least three times on different spots of the sample.

5.2.2.3   *Solution analysis*

The composition of the solutions was measured before and after the experiments. Cations were determined by using inductive-coupled plasma optical emission spectroscopy (ICP-OES, Optima 5300DV, Perkin Elmer). Anions were analyzed with ion chromatography (IC, 761 Compact IC, Metrohm). The concentration of carbonate species was calculated from the inorganic carbon concentration measured with a total organic carbon (TOC) analyzer (Shimadzu TOC-VCPH).

5.3   Results and discussion

5.3.1   Analysis of TMEP during ED

The transmembrane electrical potential (TMEP) was monitored during the electrodialysis experiments. This measurement reflects the voltage loss due to the multiple resistances: the membrane, the boundary layers, and a fraction of the two bulk solutions. Since the distance δ between the capillaries varied for some experiments, the reported values are TMEP/δ. The plots thereby obtained were grouped to identify specific effects, as presented in **Figure 5.2**.
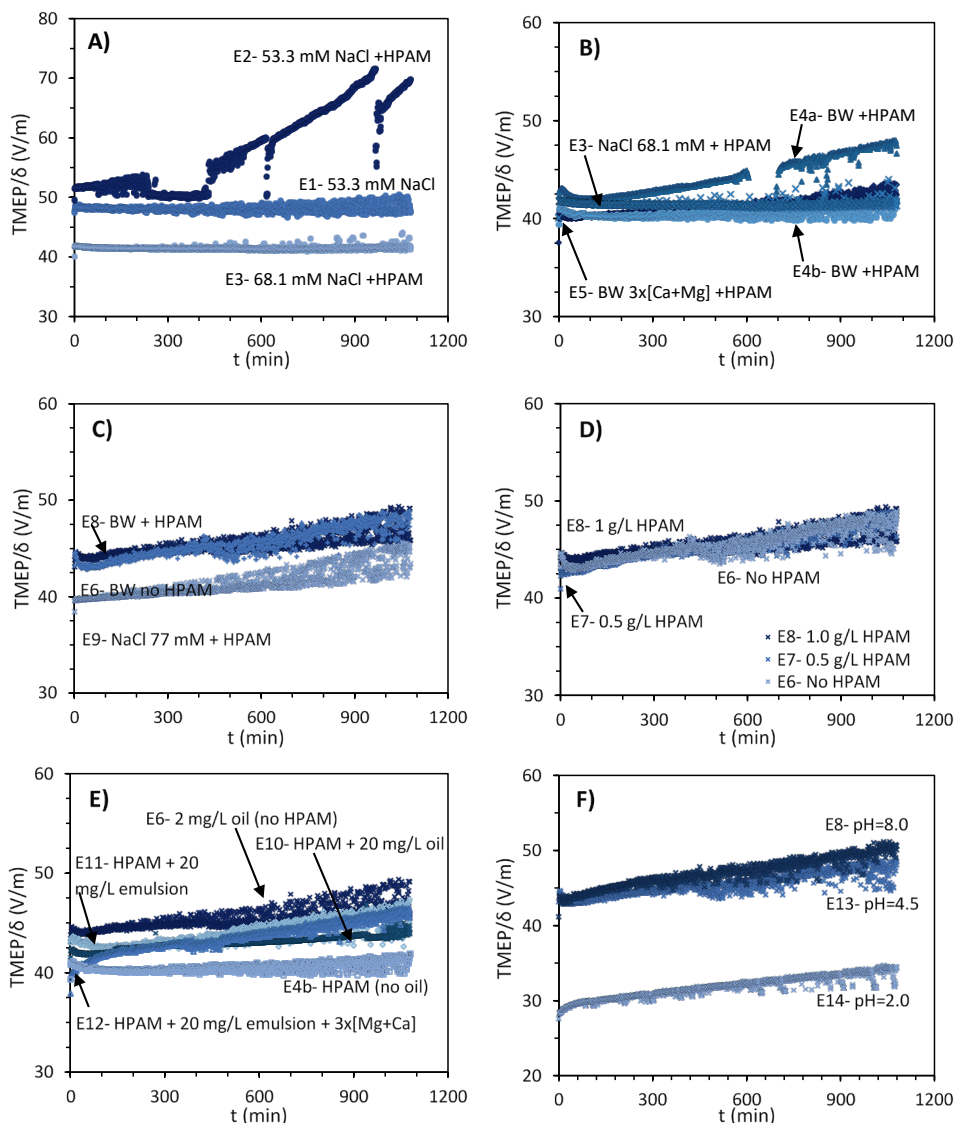
Figure 5.2. *TMEP/δ vs. time t of ED runs grouped to show diverse effects. **(A)** Effect of ionic strength and HPAM. **(B)** Effect of the mineral composition in the absence of oil. **(C)** Effect of mineral composition in the presence of 2 mg/L of crude oil. **(D)** Effect of increasing the concentration of HPAM. **(E)** Effect of the addition of crude oil and model emulsion. **(F)** Effect of solution pH.*

5.3.1.1   *Gel layer in the presence of NaCl and the effect of ionic strength*

Figure 5.2A shows the TMEP/δ development for E1, E2, and E3. Since E1 contained only sodium chloride and no foulants, there is no increase in TMEP. In contrast, for the solution containing sodium chloride plus 1.0 g/L of HPAM (E2), the TMEP steadily increases throughout the experiment, probably an indication of the concentration polarization building up. The TMEP dropped on three occasions, but

it eventually recovered and continued with its original trend. The drops are thought to be caused by disturbances in the signal due to polymer conglomerates sticking together between the capillary and the membrane. Then, once the conglomerate is removed due to mixing in the cell, the restoration of TMEP occurs within the same trendline.

The comparison of E2 and E3 in the same figure shows that the higher the ionic strength, the lower the TMEP. This was expected since solutions with higher ionic strength have higher conductivity, which facilitates the transport of electrical current. This observation indicates that the resistance of the solution contributes significantly to the TMEP measurement. Previously, Galama et al. [28] concluded that the membrane conductivity is limited by the conductivity of the ionic solution when the external concentration was lower than 0.3M. A second reason for the lower TMEP could also be a reduction in the formation of fouling due to the diminished transport of HPAM. This can be explained by the decrease of the electrophoretic mobility of charged macromolecules when placed in a solution of higher ionic strength, as in the case of solution E3 compared to E2.

5.3.1.2 *Effect of mineral composition (with and without oil)*

The effect of the different mineral compositions is shown in **Figure 5.2B**. Although the theoretical ionic strength of E3 was lower than for E4, their initial conductivities were the same (**Table A5.1**), which explains that the initial TMEP/δ was also identical. During the experiment, the TMEP of the run E4a presented a slight increase, while that of E4b and E3 remained constant. This was probably due to a smaller δ for E4a (δ= 38 and 77 mm for E4b and E3, respectively), which affected the hydrodynamics in the cell (a numerical estimation would be only possible by fluid dynamics simulations, outside the scope of this article). Still, when more divalent cations were added to the solution (E5), the TMEP/δ also remained flat during the experiment. This indicates that the mineral composition did not influence the concentration polarization of ions in the diluate side of the membrane, contrary to what was previously observed for the AEM [9]. It is worth to point out that during the referred study, the TMEP/δ values were above 800 V/m, 20 times higher than was reached for the CEMs.

The analysis of the experiments with different mineral composition in the presence of crude oil (**Figure 5.2C**), leads to the same conclusions. In this case, E9 had the same ionic strength as E8, but its measured conductivity was higher, which caused the lower TMEP/δ at the start and during the experiment.

5.3.1.3   *Effect of HPAM concentration*

Figure 5.2D shows that increasing the concentration of HPAM does not have a significant effect on the TMEP. The TMEP recorded for the experiments without HPAM (E6) is practically the same as for the experiments with 0.5 g/L (E7) or 1.0 g/L (E8) of it. This demonstrates that, for the CEM, the increase in TMEP is caused only by the concentration polarization on the diluate side and is not related to the HPAM accumulation on the concentrate side of the CEM.

5.3.1.4   *Effect of oil addition (crude oil and model emulsion)*

Figure 5.2E shows the influence of crude oil and emulsion presence in the feed solutions. Instead of increasing the TMEP as could have been expected from having an increased variety of organic compounds in solution, the tenfold increase of crude oil (E10) slightly lowers the measured TMEP. Despite the variations in the final part of the measurements during E10, the curves suggest that oil presence mitigates the TMEP development, probably because it disrupts the formation of thick HPAM gel layers.

The comparison between having 20 mg/L of crude oil (E10) versus having 20 mg/L of hexadecane emulsion (E11) shows minimal differences. The run with emulsion had a slightly larger TMEP/δ, but besides that, the development during the experiment was the same. Similar remarks can be obtained from comparing the experiments containing the synthetic emulsion (E11 and E12). Although the curves showed marginally different tendencies during the first 100 minutes of the experiment, they leveled and remained equal all the subsequent time. This indicates that the presence of oily compounds related to crude oil (> C16 and predominantly non-soluble compounds) and surfactants, did not affect the TMEP developments.

5.3.1.5   *Effect of pH decrease*

Figure 5.2F shows the effect of pH variation in the TMEP/δ development. Due to the addition of HCl, the conductivity of the feed solution for E14 solution increased to 11.7 mS/cm (~4 mS/cm above that of E8), causing a lower TMEP for E14. Still, the development of the three TMEP curves (E8, E13, and E14) was the same, which confirms that TMEP measurements were mainly determined by the conductivity of the solutions. Nevertheless, the pH variation was expected to cause the partial protonation of HPAM, affecting its migration and, consequently, the fouling on the CEMs, as will be presented in the following section.

5.3.2   Membrane analyses

In general, when HPAM was present in solution, the membranes recovered from the cell presented a visible viscous layer covering one side of the CEM, from now on referred as a gel layer [6,29], or as "dried gel layer" since the analyses were

performed on dried membranes. Their analyses are presented by analytical techniques.

5.3.2.1 *Surface analysis by SEM and EDX*

5.3.2.1.1 Concentrate side

The SEM analysis of the E1 membrane (exposed only to NaCl) did not show any form of fouling, as shown in **Figure 5.3**. The same figure shows that, when HPAM was present in the feed solutions (E2), a dried gel layer was found on the concentrate side, covering the entire surface of the membrane. The side where HPAM appeared is consistent with the current direction applied in the cell because the negatively charged polyelectrolyte migrates towards the anode under the influence of the electric field [6]. Indeed, HPAM gel layers were found on the concentrate side of all the membranes exposed to HPAM containing solutions. The EDX of the cross-sections of the membranes did not show salt precipitates being covered under the HPAM gel layers.
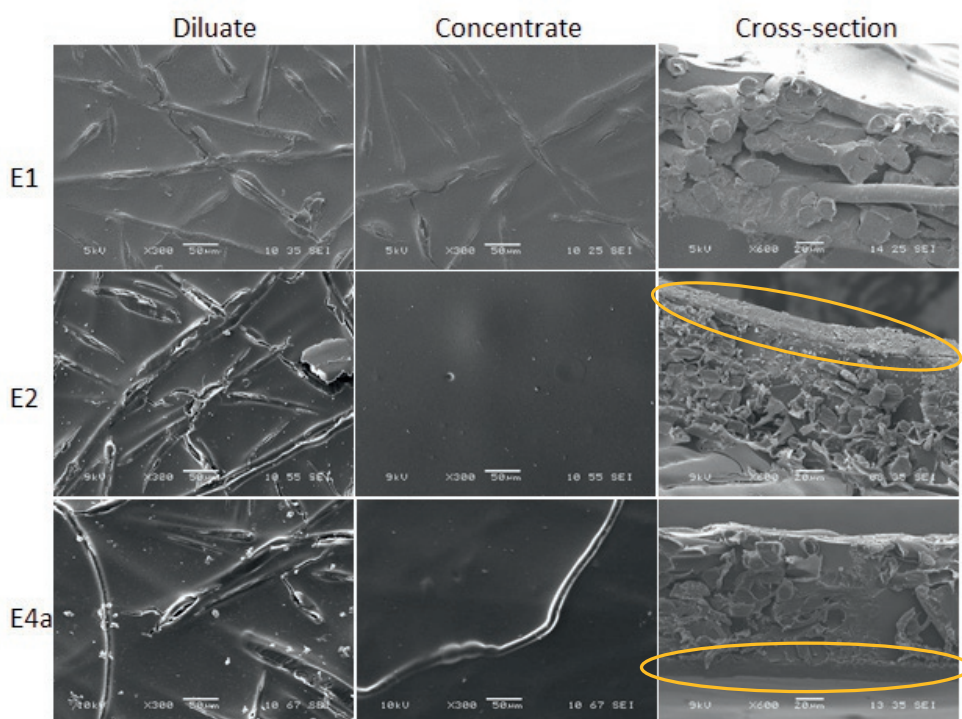
Figure 5.3. *SEM images from the diluate, concentrate, and cross-section of membranes E1, E2, and E4. The magnifications for the diluate and concentrate asides are 300x, while for the cross-sections are 600x.*

Although SEM is mainly considered a qualitative technique, it can be used to estimate the thickness of polyelectrolyte layers placed on top of membranes [30,31]. Therefore, the SEM cross-section pictures of the CEMs were used to quantify the approximated thickness of the dried gel layers, as reported in **Table 5.3**. However, it must be emphasized that the overall thickness of the gel layer on top of the membrane is highly dependent on the way it was extracted from the cell, on how it was dried, and on the viscosity of the surrounding solution. The last item becomes especially significant when the polymer concentration is above overlap, as in this case, since the HPAM molecules are interacting and increase the amount of solution withdrawn with the membrane. Still, we report the dried-gel layer thicknesses because they can be compared against those reported in our previous study for AEMs [9]. Furthermore, since the experimental work was carried out by the same team, the methodology differences are minimal.

As presented in **Table 5.3**, the maximum measured thicknesses ranged between 5 and 14 µm. Their variation was small, corresponding well with the similar TMEP profiles described in section 5.3.1. The reproducibility of the experiments becomes apparent when correlating the gel layer very well to the properties of the liquid. When comparing the dried gel layers observed on the CEMs to those previously observed on the AEMs [9], two main differences were noticed. The first is that 4 to 10 times thicker gel layers were found on the AEMs (up to 52 µm). The second difference is that in the case of CEMs, the presence of divalent cations (Ca and Mg), did not seem to affect the thickness of the gel layers, as observed for the AEMs. These results are only indicatory, and further research is needed to demonstrate the significance and reproducibility of these observations conclusively.

It was observed that the addition of synthetic emulsion (E11) and crude oil (E8, E10) produced thinner gel layers than for the experiment without oily compounds (E4). This observation suggests that the oily compounds make the HPAM gel layer less stable, as was previously proposed for the AEMs [9]. The influence of the cationic surfactant is thought to be minimal since its molar concentration (<0.01 mmol/L) is much lower than the charge of HPAM in solution (5.62 meq/L) [32]. Moreover, the variations in HPAM concentration (E7 vs. E8), both above the overlap concentration (section 5.2.1.1), did not cause significant changes in the observed thickness of the gel layer.

For the experiments at low pH (E13 and E14), no HPAM dried layer was observed. This lack of layer is likely related to the protonation of HPAM, whose charges become shielded at lower pH, preventing the molecule from migrating under the influence of the electric field. Furthermore, the low pH also reduces the viscosity of HPAM solutions, so less solution is recovered together with the membrane due to the no-slip effect.

Table 5.3. *Summary of the SEM/EDX and Raman results*

Exp.	Concentrate side			Diluate side		
	Gel layer observed	Max. thickness (µm)	Raman identification	Type of precipitates	Common elements	Traces
E1	No	BDL[a]	Clean CEM	None	-	-
E2	✓	14	HPAM	Scarce	-	Na, Cl
E3	✓	BDL	NM[b]	Scarce	C, O	Mg, Cl
E4a	✓	13	HPAM	Plaques	CaCO$_3$[c]	Mg, O
E4b	✓	4	NM[b]	Scarce	Na, O	Ca
E5	✓	13	HPAM	Amorphous	Ca, O	Mg
E6	No	BDL	Clean CEM	None	-	K, Cl
E7	✓	6	HPAM	+Plaques	Ca, O	Fe
E8	✓	8	HPAM	+Plaques	Ca, O	K, Cl
E9	✓	12	HPAM	None	-	Na, Cl, O
E10	✓	6	HPAM	+Plaques	Ca, O	Mg
E11	✓	11	HPAM	Plaques	Ca, O	Si
E12	✓	6	HPAM, CaCO$_3$	None	-	-
E13	No	BDL	Clean CEM	Particulates	C, O	Na, Cl
E14	No	BDL	Clean CEM	Particulates	C, O	Si, O

a Below detection limit

b Not measured

c Compound identified by Raman. EDX identified Ca and O.

5.3.2.1.2   Diluate side

Salt precipitation is frequently formed on the concentrate side of the IEMs since it is at this side that the higher concentrations of ions are reached [2]. However, as presented in **Table 5.3**, most of the membranes displayed precipitates on their diluate side, and only when an HPAM gel layer was present on the opposite side. One might suggest that the precipitates formed by adhered liquid drying on this side of the membrane, but this option can be discarded considering previous analyses on CEMs [33]. The precipitates were more abundant and had different morphologies than those observed on CEMs recovered after performing electrodialysis in a stack [33]. Furthermore, it was found that the precipitates presented different morphologies, so they were arbitrarily classified as plaques, amorphous, or particulates, all exemplified in **Figure 5.4**. They were also related to specific feed conditions, as will be further explained.
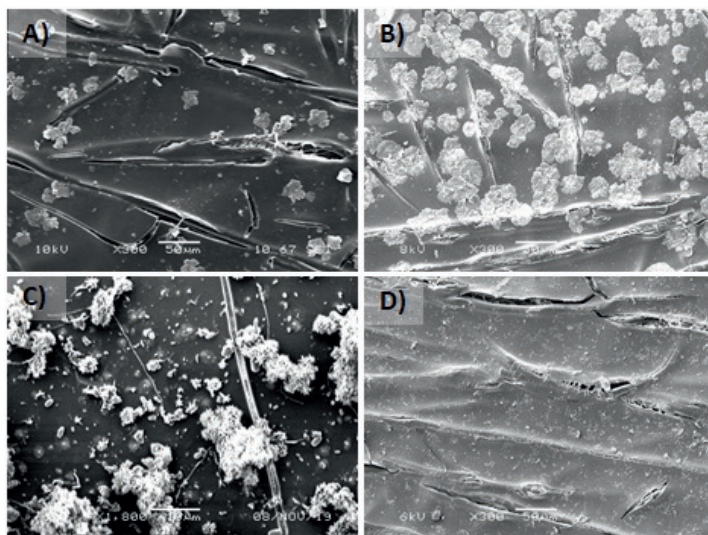
Figure 5.4. Different fouling precipitates observed for the CEM. A) Deposits in the form of "plaques" from the diluate side of E4. B) Larger "plaques" on the diluate side of E10. C) Amorphous precipitation from E5. D) "Particulates" on the diluate side of E13.

The precipitation in the form of "plaques" (**Figure 5.4A**) appeared when the solution had a BW composition and HPAM, but no oil (E4 and E11). Larger "plaques" (**Figure 5.4B**) were observed for membranes exposed to BW solution plus crude oil (E7, E8, and E10). The most substantial amount of them was found on the diluate side of membrane E10, coinciding with the higher concentration of crude oil. The composition of the plaques consisted mainly of Ca and O, with some traces of Mg. This particular precipitation shape was also found on AEMs exposed to crude oil [9], and therefore seems to be independent of the electrical surface and field characteristics, but related to the membrane (pure phase), oil and aqueous liquid interfacial interactions of which the exact mechanisms and results thereof in ionic precipitation and crystallization are somewhat difficult to be interpreted.

The "particulates" (**Figure 5.4D**) were only spotted on membranes exposed to solutions with low pH (E13, E14). The EDX analysis showed that, unlike all the other precipitates, these did not contain calcium, and only consisted of oxygen and carbon. Since the particulates only showed up at low pH values (4.5 and 2.0), it could be that HPAM or other components of the crude oil became protonated due to the acidic conditions, so their overall molecular charge became less negative (pH 4.5, close to the pKa of HPAM) [19], or even positive (pH 2.0). This would mean that, under an electric field, they would not migrate to the anode but even, when positively charged, towards the cathode, precipitating now on the diluate side of the CEM. Park et al. also reported fouling on the diluate side of a CEM caused by a positively charged polymer (poly(ethylene imine)) [34].

By comparing the TMEP curves with the SEM images and the degree of salt precipitation, it was determined that the salt precipitation did not influence the measured TMEP, meaning that the transport of ions through the membrane was not affected by their presence.

5.3.2.2 *Raman measurements*

Raman spectra were taken on both sides of each membrane, and the results of the analysis are summarized in **Table 5.3**.

5.3.2.2.1 Concentrate side

Figure 5.5 shows the Raman profiled for selected CEMs, together with that of a clean membrane (E1), and a clean HPAM granule. The last two served as references for the rest of the membranes. The profile from the concentrate side of membrane E2 was much more similar to that of the HPAM granule than to the clean membrane, which corresponds well with the SEM observations of an HPAM gel layer covering the CEM (**Figure 5.3**). The profiles obtained from the membranes of E4a and E8 were also closer to that of pure HPAM than to that of the clean membrane. However, in these profiles, it is still possible to observe some of the distinctive peaks of the clean membrane, like the one at 1610 cm^{-1}. Either a thinner HPAM layer or discontinuities in the layers may be causing this. The spectrum of E12 was also a combination of the profiles of the clean membrane and an HPAM granule, plus some additional peaks. The ones between 2800 and 2900 cm^{-1} were identified as belonging to a CEM fiber, while the peak at 1088 cm^{-1} was identified as belonging to calcite (calcium carbonate), which indicates some precipitation also on this side of the CEM.
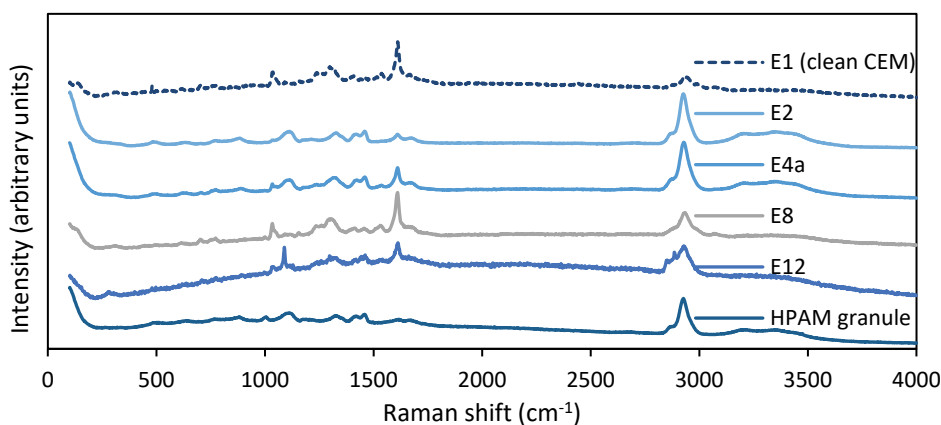
Figure 5.5. *Raman profiles from the concentrate side of membranes E1, E2, E4a, E8, E12, and from an HPAM granule*

The profiles obtained from the low pH experiments (E13 and E14) did not differ from the reference membrane, indicating that no significant amount of HPAM nor oil was present on their concentrate side.
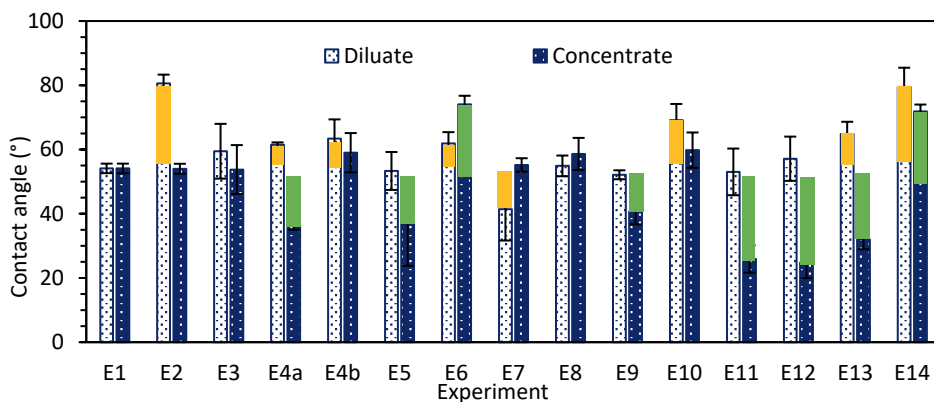
5.3.2.2.2 Diluate side

Raman profiles were also obtained for the diluate side of the CEMs. The only identifications for this side of the CEMs was a small presence of HPAM on the diluate side of E7, and the identification as calcite ($CaCO_3$) for one of the precipitates on membrane E11. This corresponds with the Ca and O composition identified via EDX. For the rest of the experiments, there were no deviations from the spectrum of the clean membrane, indicating small fouling tendency on this side of the CEM, and confirming that the amount of HPAM solution extracted with the membrane was too small to be detected by the analytical method.

5.3.2.3 *Contact angle measurements*

Figure 5.6 summarizes the contact angle measurements for both sides of the membranes. In general, the contact angles on the concentrate side were smaller than those of the reference (E1) and the diluate side, indicating higher hydrophilicity. For most cases (E3-E5, E11-12), this observation corresponds with the sides on which HPAM gel layers were observed and was expected since HPAM is hydrophilic. On the contrary, when moderated amounts of crude oil were also added to the solution (E6, E8, E10), the contact angle, and therefore the hydrophobicity, of the concentrate side increased. This surge in hydrophobicity may be related to oil fouling on the concentrate side: oil in solution can form negatively charged colloidal structures [8], which would migrate towards the anode, just like HPAM, and form a film also on the concentrate side of the CEM. Alternatively, the oil components could interact with the membrane by hydrophobic interactions, with some oil molecules even penetrating the membrane matrix and blocking the ion-exchange sites [2].

Concerning the diluate side, most CEMs presented higher contact angles than the reference: E2, E4 (HPAM-containing), E6 (only oil), and E10, E13, and E14 (HPAM + oil). The higher contact angle indicates lower hydrophilicity and coincides with the absence of HPAM gel layers (section 5.3.2). In most cases, the lower hydrophilicity also coincides with the presence of precipitation. Different forms of precipitated crystals can influence surface roughness, hydrophobicity, and interfacial water tension, which are reflected when conducting contact angle measurements. In the case of E6, since no HPAM was present in the feed solution, it might be that the conditions were favorable for oil components to penetrate the CEM matrix from the concentrate side. This suggests a complex interaction between HPAM, oil, and ionic composition.

Figure 5.6. *Water contact angles measured on the diluate and concentrate sides of the recovered CEMs. The colored parts (yellow and green) indicate significant differences (>10% between the measured contact angle and the reference E1.*

The contact angles measured for the low-pH experiments indicated different behaviors. For E13, performed at pH 4.5, the diluate side presented decreased contact angle con the concentrate side and higher contact angle in the diluate side, very similar to the general tendencies. This suggests that HPAM at pH close to its pKa still migrated towards the anode. On the contrary, the experiment at pH 2.0 (E14) presented high contact angles on both sides of the CEM. For the concentrate side, the effect can be related to the reduced activity of HPAM, while for the diluate side, the hypothesis presented for E6 might also be applicable.

5.3.3 pH of solutions

The pH of the diluate and concentrate solutions was monitored during the experiments, and the overall change is shown in **Figure 5.7**. For all the experiments, there was a measurable change of pH, which in most cases, was an increase in the diluate and concentrate solutions. This is an indication of water splitting. Although the current density was chosen below the limiting current density of the least conductive solutions, water splitting could occur due to concentration polarization on the diluate side of the membrane, where the concentration of ions is lower [35]. The generated protons will migrate to the cathode and hydroxide ions to the anode. Thus, for the CEMs, it is expected that the diluate increases in pH, and the concentrate decreases. However, the changes were much lower than the ones measured for AEMs under similar circumstances [9].
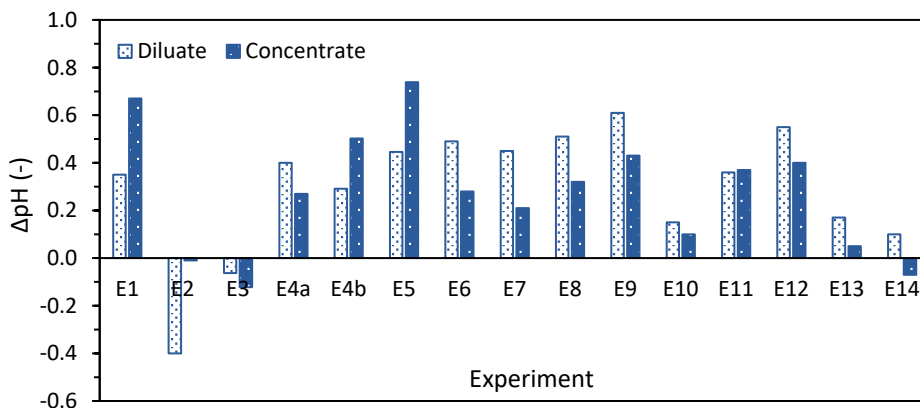
***Figure 5.7.** Absolute pH changes of the concentrate and diluate solutions during the ED experiments*

5.3.4   Performance evaluation by solution analysis

Considering the current density and the duration of the ED run, it was expected to remove a maximum of 13.4 meq (1,300 C) from the diluate solution. This is the theoretical number of charge equivalents transported if the desalination efficiency was 100%. However, the formation of fouling could have affected the coulombic efficiency. Thus, the CEM performances were analyzed from the measured changes in the concentration of cations. The average changes, calculated in charge equivalents for the diluate and the concentrate compartments, are presented in **Figure 5.8**.

Regarding the change of monovalent cations (sodium and potassium), the figure shows considerable variations in their transport. Several experiments presented changes greater than the calculation for 100% efficiency (discontinuous line), which is thought to be caused by the leakage of cations from the adjacent compartments of the cell. Although they were separated by two AEMs, the permselectivity of the latter is 95% (**Table 5.2**), meaning that they allow the passage of some cations. Then, although the measured values are affected by this systematic error, they can still be used to compare the effects of fouling on membrane performance.
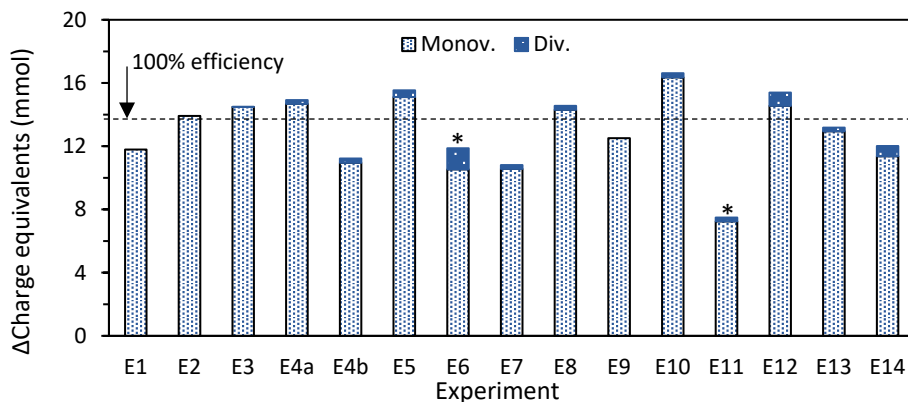
Figure 5.8. *Average change of monovalent and divalent anions, presented as charge equivalents, in the diluate and concentrate solutions. The theoretical change in equivalents (calculated from the applied current and operative time) was 13.4 meq, indicated by the discontinuous line (100% efficiency). The low performances measured for E6 and E11 can be attributed to a contaminated sample.*

Continuing with the evaluation of monovalent transport, **Figure 5.8** shows that the more extensive transport was measured for the experiment with a high concentration of oil (E10). Coincidently, this experiment also presented one of the smallest changes in pH (**Figure 5.7**). This suggests that since oil disrupts the formation of thick HPAM layers, there was less concentration polarization and water splitting, so the transport of Na and K could be higher.

The results for the divalent cations are also included in **Figure 5.8**. The transport of the divalent cations was, in most cases, proportional to their concentration in the original solution. However, E12 and E14 presented slightly more significant changes in divalent cations. For E12, the higher concentration of divalent cations in the feed solution helps to explain the higher transport. Still, both experiments coincide in not presenting an HPAM gel layer on the concentrate side. Thus, it is suspected that this lower gel layer formation allowed the divalent cations to migrate more. Another cause could be that, when the gel layer is formed, divalent cations tend to stay in the vicinity of the HPAM molecules.

The small change in equivalents for E11 and the high transport of divalent cations measured for E6 (**Figure 5.8**) can only be attributed to experimental errors. In both cases, it is likely that the samples were contaminated when taken out, so the measured equivalents are not related to the process performance. This can be confirmed from the measured conductivities of the solutions (**Table A5.1**).

5.3.5 Effect of current reversal

The reversibility of the fouling was evaluated through current reversal experiments. These consisted of desalinating the solutions inside compartments 3 and 4 in an alternate way. **Figure 5.9A** shows the TMEP/δ profiles obtained for the experiment ran with a feed solution of NaCl 68.1mM. Initially, compartments 3 and 4 contained NaCl solution without foulants, which explains the flat TMEP/δ profiles for both current directions (until minute 60).

At minute 60 (**1**), the solution acting as concentrate is switched by a solution with the same mineral composition plus 1.0 g/L HPAM. This would cause the formation of an HPAM gel layer on the concentrate side of the CEM. Still, the TMEP/δ did not show any significant alteration. However, when the current direction was switched at minute 120, the TMEP/δ initiated at a different value and gradually became more negative peaked at its lowest value and then stabilized. This indicates that, when the gel layer and the desalting solution are on opposite sides of the membrane, no significant TMEP changes occur. When the current direction was switched, the previously formed gel layer is not immediately removed by electrophoresis. The TMEP is first low (**a**) because concentration polarization caused an accumulation of ions on this side. After some minutes of transporting cations in the new direction, their concentration on the diluate side of the CEM decreases, so these need to be transported from the bulk solution through the gel layer that is still in place. The gel layer poses a resistance to the transport of cations, which causes a spike in measured TMEP (**b**). After a short period, the reversed current eventually pulls the HPAM gel layer away from the membrane due to a combination of electrophoresis and shear forces, which causes the TMEP to return to its original value.

At minute 150, when the current direction is switched again, there was no gel layer forming on the diluate side of the CEM, so the TMEP stabilizes in a short time. At time **2**, the concentrate solution (containing HPAM) is replaced by the initial NaCl solution without polymer, but this does not cause any change in TMEP because the cations are transported from the other side. When the current direction was switched two more times, the TMEP stabilized in a short period since there was no HPAM in solution forming gel layers.

The experiment running with the BW solution rendered similar results, as can be observed in **Figure 5.9B**.
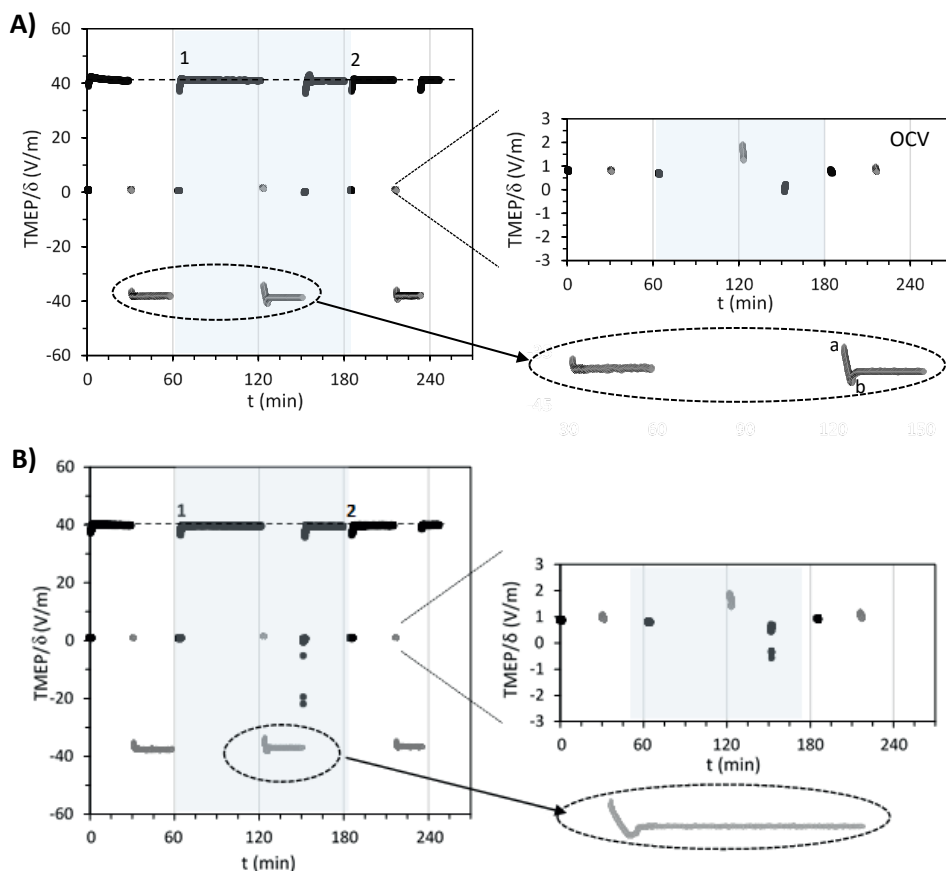
Figure 5.9. *TMEP/δ vs. time for the current reversal experiments with. At the beginning of the experiment, the diluate and concentrate consisted of salts solutions without foulants. At point 1, the concentrate solution was switched for a solution with 1.0 g/L of HPAM. At point 2, this solution was substituted again by the one without HPAM. **A)** experiment with NaCl 68.1 mM, **B)** with BW.*

5.3.6 Fouling mechanism

From the above results, we hypothesize the following processes. When an electrical potential is applied, HPAM in solution at moderate pH migrates towards the anode, accumulating on the concentrate side of the CEMs. The gel layer grows as the process continues to thicknesses about 10 to 20 fold lower values, as found for AEM [9]. This confirms that the electric charge of the membrane has a considerable influence on the degree of fouling of HPAM.

Precipitation occurred on the diluate side of the membranes, but only where a gel layer was present on the opposite side. In electrodialysis, precipitation occurs typically on the concentrate side of the membrane, where the number of ions increases due to concentration polarization. This happens because the flux in the

membrane is usually higher than the transport number of ions in the bulk solutions [36], so the ions emerge from the membrane faster than they can disperse into the concentrate solution. This results in a concentration increase at the concentrate-membrane interface.

However, in all the CEMs from this study, the precipitation occurred on the diluate side of the membrane, and only when a gel layer was formed on the opposite side. HPAM migrates and starts accumulating on the concentrate side of the CEMs as soon as the electric potential is applied to the cell. With the gel layer forming on its surface, the Donnan exclusion of the CEM decreased due to the fouling growth, causing decay in membrane permselectivity [37]. This allowed OH^- ions to leak towards the anode, from the concentrate to the diluate compartment [35,38,39]. On the diluate side of the CEM, there might be an abundance of calcium ions diffusing through the boundary layer, which could precipitate with the OH^- in the form of $Ca(OH)_2$. The generation of OH^- ions by CEM provides conditions for the formation of scaling [2]. Still, some of the generated OH^- ions reached the bulk of the diluate compartment, as evidenced by the slight increase of pH during most of the experiments (**Figure 5.7**).

The increase of pH in both compartments would have also ruled the carbonate species in solution from the first equilibrium pair H_2CO_3/HCO_3^- (pK_a= 6.38) to the second one HCO_3^-/CO_3^{2-} (pK_a= 10.3). The CO_3^{2-} generated is also likely to precipitate with calcium as $CaCO_3$ [40] on the diluate side of the CEM. Considering that EDX identified Ca and O as the components of most of the precipitates and that Raman was positive for calcite in very few cases, it is likely that the precipitation occurred first in the form of amorphous calcium carbonate [40,41]. With time, this compound can transform into crystalline calcium carbonate polymorphs [41], but the process is delayed by the presence of magnesium at the boundary layer.

5.4   Conclusions

Under the influence of the electric potential, an HPAM gel layer forms on the concentrate side of the CEM. Given its location, the gel layer does not interfere significantly with the transport of cations through the membrane, which is translated in a minimal increase in the measured trans-membrane electric potential (TMEP).

Precipitates in considerable quantities formed on the diluate side of the membrane, but only when an HPAM gel layer had formed on the other side. This was related to the decrease of selectivity of the CEM, which allows the leak of OH^- ions from the concentrate to the diluate compartment.

The presence of oily compounds, either synthetic emulsion or crude oil, makes the HPAM gel layer less stable, producing even minor increases in TMEP. There was more precipitation observed on membranes exposed to oil than on those exposed to the synthetic emulsion with hexadecane and surfactant.

References

[1]   P.A. Sosa-Fernandez, J.W. Post, H. Bruning, F.A.M. Leermakers, H.H.M. Rijnaarts, Electrodialysis-based desalination and reuse of sea and brackish polymer-flooding produced water, Desalination. 447 (2018) 120–132. doi:10.1016/j.desal.2018.09.012.

[2]   S. Mikhaylin, L. Bazinet, Fouling on ion-exchange membranes: Classification, characterization and strategies of prevention and control, Advances in Colloid and Interface Science. 229 (2016) 34–56. doi:10.1016/j.cis.2015.12.006.

[3]   T. Wang, S. Yu, L. an Hou, Impacts of HPAM molecular weights on desalination performance of ion exchange membranes and fouling mechanism, Desalination. 404 (2017) 50–58. doi:10.1016/j.desal.2016.10.007.

[4]   Q. Xia, H. Guo, Y. Ye, S. Yu, L. Li, Q. Li, R. Zhang, Study on the fouling mechanism and cleaning method in the treatment of polymer flooding produced water with ion exchange membranes, RSC Adv. 8 (2018) 29947–29957. doi:10.1039/c8ra05575k.

[5]   H.J. Lee, J.H. Choi, J. Cho, S.H. Moon, Characterization of anion exchange membranes fouled with humate during electrodialysis, Journal of Membrane Science. 203 (2002) 115–126. doi:10.1016/S0376-7388(01)00792-X.

[6]   H. Guo, L. Xiao, S. Yu, H. Yang, J. Hu, G. Liu, Y. Tang, analysis of anion exchange membrane fouling mechanism caused by anion polyacrylamide in electrodialysis, Desalination. 346 (2014) 46–53. doi:10.1016/j.desal.2014.05.010.

[7]   J. Guolin, W. Xiaoyu, H. Chunjie, The effect of oilfield polymer-flooding wastewater on anion-exchange membrane performance, Desalination. 220 (2008) 386–393. doi:10.1016/j.desal.2007.03.010.

[8]   X. Zuo, L. Wang, J. He, Z. Li, S. Yu, SEM-EDX studies of SiO2/PVDF membranes fouling in electrodialysis of polymer-flooding produced wastewater: Diatomite, APAM and crude oil, Desalination. 347 (2014) 43–51. doi:10.1016/j.desal.2014.05.020.

[9]   P.A. Sosa-Fernandez, S.J. Miedema, H. Bruning, F.A.M. Leermakers, H.H.M. Rijnaarts, J.W. Post, Influence of solution composition on fouling of anion exchange membranes desalinating polymer-flooding produced water, Journal of Colloid And Interface Science. 557 (2019) 381–394. doi:10.1016/j.jcis.2019.09.029.

[10]   H. Guo, F. You, S. Yu, L. Li, D. Zhao, Mechanisms of chemical cleaning of ion exchange membranes: A case study of plant-scale electrodialysis for oily wastewater treatment, Journal of Membrane Science. 496 (2015) 310–317. doi:10.1016/j.memsci.2015.09.005.

[11]   M.S. Kamal, A.S. Sultan, U.A. Al-Mubaiyedh, I.A. Hussein, Review on Polymer Flooding: Rheology, Adsorption, Stability, and Field Applications of Various Polymer Systems, Polymer Reviews. 55 (2015) 491–530. doi:10.1080/15583724.2014.982821.

[12]   H.J. Lee, S.H. Moon, Enhancement of electrodialysis performances using pulsing electric fields during extended period operation, Journal of Colloid and Interface Science. (2005). doi:10.1016/j.jcis.2005.02.027.

5

[13]   A.R. Al-Hashmi, T. Divers, R.S. Al-Maamari, C. Favero, A. Thomas, Improving polymer flooding efficiency in Oman oil fields. Paper SPE-179834-MS, in: SPE EOR Conference at Oil and Gas West Asia Held in Muscat, Oman, 21–23 March 2016., SPE, Muscat, 2016: p. 18.

[14]   M. Bjørsvik, H. Høiland, A. Skauge, Formation of colloidal dispersion gels from aqueous polyacrylamide solutions, Colloids and Surfaces A: Physicochemical and Engineering Aspects. 317 (2008) 504–511. doi:10.1016/j.colsurfa.2007.11.025.

[15]   M. Rashidi, A.M. Blokhus, A. Skauge, Viscosity Study of Salt Tolerant Polymers, Journal of Applied Polymer Science. 117 (2010) 1551–1557. doi:10.1002/app.

[16]   C. Negin, S. Ali, Q. Xie, Most common surfactants employed in chemical enhanced oil recovery, Petroleum. 3 (2017) 197–211. doi:10.1016/j.petlm.2016.11.007.

[17]   J.M. Dickhout, J.M. Kleijn, R.G.H. Lammertink, W.M. de Vos, Adhesion of emulsified oil droplets to hydrophilic and hydrophobic surfaces – effect of surfactant charge, surfactant concentration and ionic strength, Soft Matter. 14 (2018) 5452–5460. doi:10.1039/C8SM00476E.

[18]   M. de Graaff, M.F.M. Bijmans, B. Abbas, G.J.W. Euverink, G. Muyzer, A.J.H. Janssen, Biological treatment of refinery spent caustics under halo-alkaline conditions, Bioresource Technology. 102 (2011) 7257–7264. doi:10.1016/j.biortech.2011.04.095.

[19]   S. Choi, pH Sensitive polymers for novel conformance control and polymer flooding applications, The University of Texas at Austin, 2008.

[20]   M.J. Teräväinen, J.M.H. Pakarinen, K. Wickström, P. Vainiotalo, Comparison of the composition of Russian and North Sea crude oils and their eight distillation fractions studied by negative-ion electrospray ionization fourier transform ion cyclotron resonance mass spectrometry: The effect of suppression, Energy and Fuels. 21 (2007) 266–273. doi:10.1021/ef060294v.

[21]   T.I. Roe Utvik, Chemical Characterisation of produced water from four offshore oil production platforms in the North Sea, Chemosphere. 39 (1999) 2593–2606.

[22]   P. Długołecki, K. Nymeijer, S. Metz, M. Wessling, Current status of ion exchange membranes for power generation from salinity gradients, Journal of Membrane Science. 319 (2008) 214–222. doi:10.1016/j.memsci.2008.03.037.

[23]   Brochure of FujiFilm Membrane Technology, Ion Exchange Membranes for water purification, Version 1.0, 2018. (2018) 6. https://www.FujiFilmmembranes.com/images/FujiFilm_IEM_product_version_1.2_publish_website.pdf (accessed September 20, 2019).

[24]   B. Van Berchum, W.J. Van Baak, J. Hessing, Curable compositions and membranes, US 9,309,343 B2, 2016.

[25]   D.A. Cowan, J.H. Brown, Effect of turbulence on limiting current in electrodialysis cells, Industrial and Engineering Chemistry. 51 (1959) 1445–1448. doi:10.1021/ie50600a026.

[26]   P. Sistat, A. Kozmai, N. Pismenskaya, C. Larchet, G. Pourcelly, V. Nikonenko, Low-frequency impedance of an ion-exchange membrane system, Electrochimica Acta. 53 (2008) 6380–6390. doi:10.1016/j.electacta.2008.04.041.

[27]   A.E. Contreras, Z. Steiner, J. Miao, R. Kasher, Q. Li, Studying the role of common membrane surface functionalities on adsorption and cleaning of organic foulants using QCM-D, Environmental Science and Technology. 45 (2011) 6309–6315. doi:10.1021/es200570t.

[28]   A.H. Galama, D.A. Vermaas, J. Veerman, M. Saakes, H.H.M. Rijnaarts, J.W. Post, K. Nijmeijer,

Membrane resistance: The effect of salinity gradients over a cation exchange membrane, Journal of Membrane Science. 467 (2014) 279–291. doi:10.1016/j.memsci.2014.05.046.

[29] H. Zhang, Z. Zhong, W. Xing, Application of ceramic membranes in the treatment of oilfield-produced water: Effects of polyacrylamide and inorganic salts, Desalination. 309 (2013) 84–90. doi:10.1016/j.desal.2012.09.012.

[30] F. Caruso, D.N. Furlong, K. Ariga, I. Ichinose, T. Kunitake, Characterization of polyelectrolyte-protein multilayer films by atomic force microscopy, scanning electron microscopy, and fourier transform infrared reflection-absorption spectroscopy, Langmuir. 14 (1998) 4559–4565. doi:10.1021/la971288h.

[31] Y. Li, X. Wang, J. Sun, Layer-by-layer assembly for rapid fabrication of thick polymeric films, Chemical Society Reviews. 41 (2012) 5998–6009. doi:10.1039/c2cs35107b.

[32] P.A. Sosa-Fernandez, J.W. Post, F.A.M. Leermakers, H.H.M. Rijnaarts, H. Bruning, Removal of divalent ions from viscous polymer-flooding produced water and seawater via electrodialysis, Journal of Membrane Science. 589 (2019) 117251. doi:10.1016/j.memsci.2019.117251.

[33] P.A. Sosa-Fernandez, J.W. Post, M.S. Ramdlan, F.A.M. Leermakers, H. Bruning, H.H.M. Rijnaarts, Improving the performance of polymer-flooding produced water electrodialysis through the application of pulsed electric field, Desalination. 484 (2020). https://doi.org/10.1016/j.desal.2020.114424.

[34] J.-S. Park, H.-J. Lee, S.-J. Choi, K.E. Geckeler, J. Cho, S.-H. Moon, Fouling mitigation of anion exchange membrane by zeta potential control, Journal of Colloid and Interface Science. 259 (2003) 293–300. doi:10.1016/S0021-9797(02)00095-4.

[35] N. Cifuentes-Araya, G. Pourcelly, L. Bazinet, How pulse modes affect proton-barriers and anion-exchange membrane mineral fouling during consecutive electrodialysis treatments, Journal of Colloid and Interface Science. 392 (2013) 396–406. doi:10.1016/j.jcis.2012.09.067.

[36] V. V. Nikonenko, A. V. Kovalenko, M.K. Urtenov, N.D. Pismenskaya, J. Han, P. Sistat, G. Pourcelly, Desalination at overlimiting currents: State-of-the-art and perspectives, Desalination. 342 (2014) 85–106. doi:10.1016/j.desal.2014.01.008.

[37] C. Casademont, G. Pourcelly, L. Bazinet, Effect of magnesium/calcium ratios in solutions treated by electrodialysis: Morphological characterization and identification of anion-exchange membrane fouling, Journal of Colloid and Interface Science. 322 (2008) 215–223. doi:10.1016/j.jcis.2008.02.068.

[38] C. Casademont, M.A. Farias, G. Pourcelly, L. Bazinet, Impact of electrodialytic parameters on cation migration kinetics and fouling nature of ion-exchange membranes during treatment of solutions with different magnesium/calcium ratios, Journal of Membrane Science. 325 (2008) 570–579. doi:10.1016/j.memsci.2008.08.023.

[39] N. Cifuentes-Araya, G. Pourcelly, L. Bazinet, Impact of pulsed electric field on electrodialysis process performance and membrane fouling during consecutive demineralization of a model salt solution containing a high magnesium / calcium ratio, Journal of Colloid and Interface Science. 361 (2011) 79–89. doi:10.1016/j.jcis.2011.05.044.

[40] N. Cifuentes-Araya, G. Pourcelly, L. Bazinet, Multistep mineral fouling growth on a cation-exchange membrane ruled by gradual sieving effects of magnesium and carbonate ions and its delay by pulsed modes of electrodialysis, Journal of Colloid and Interface Science. 372 (2012) 217–230. doi:10.1016/j.jcis.2011.12.067.

[41] T. Ogino, T. Suzuki, K. Sawada, The formation and transformation mechanism of calcium carbonate in water, Geochimica et Cosmochimica Acta. 51 (1987) 2757–2767.

5

Appendix 5A. Supporting information
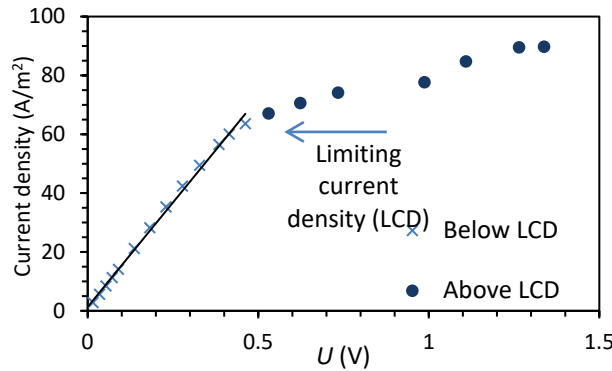
Figure A5.1. *Current density i versus measured voltage U measured in the 6-compartment cell for diluate and concentrate solutions consisting of 53.3 mM NaCl, which was the lowest salt concentration used during the experiments. The limiting current density corresponds to the last point falling within the linear trendline (64 A/m²).*

Table A5.1. *Conductivity (in mS/cm) of the bulk diluate and concentrate solutions before and after the electrodialysis experiments*

Experiment	Pre-experiment		Post-experiment	
	Diluate	Concentrate	Diluate	Concentrate
E1	n.a.	n.a.	n.a.	n.a.
E2	6.08	6.015	4.76	7.654
E3	7.83	7.72	6.41	9.12
E4a	7.53	7.61	6.66	9.24
E4b	8.15	8.07	6.90	9.22
E5	8.55	8.49	7.60	9.84
E6	7.62	7.62	6.39	8.93
E7	7.59	7.58	6.38	8.89
E8	7.69	7.65	6.51	8.86
E9	8.99	8.96	7.59	10.11
E10	7.73	7.69	6.43	8.91
E11	7.74	7.68	6.53	9.03
E12	8.05	8.17	6.93	9.31
E13	8.31	8.41	7.04	9.59
E14	11.72	11.72	9.46	12.01
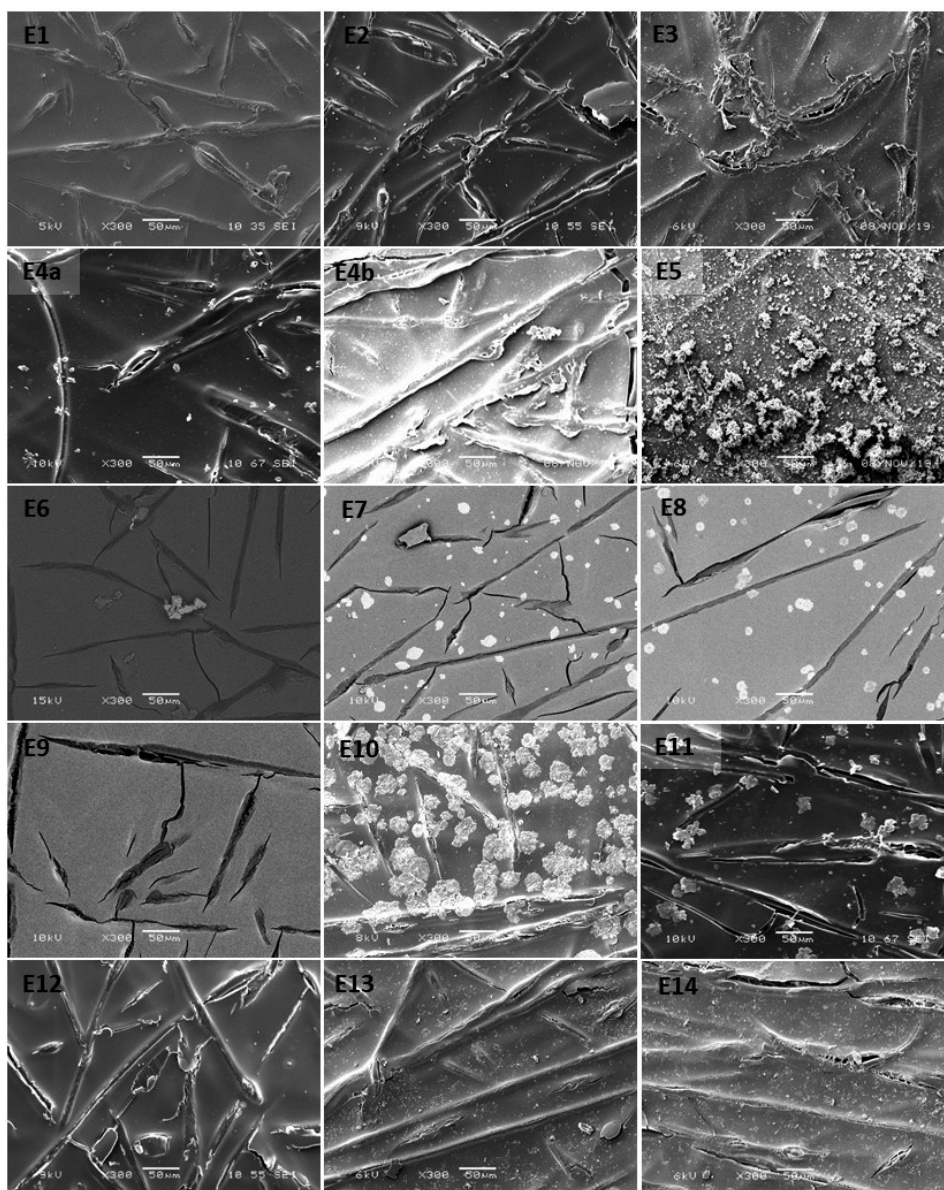
Figure A5.2. *SEM photographs taken from the diluate side of cation exchange membranes after ED experiments. All images are taken at a 300x magnification. Precipitation is clearly observed on membranes E4a, E4b, E5, E7, E8, E10 and E11, and in minor amounts in E3, E6, E13 and E14.*
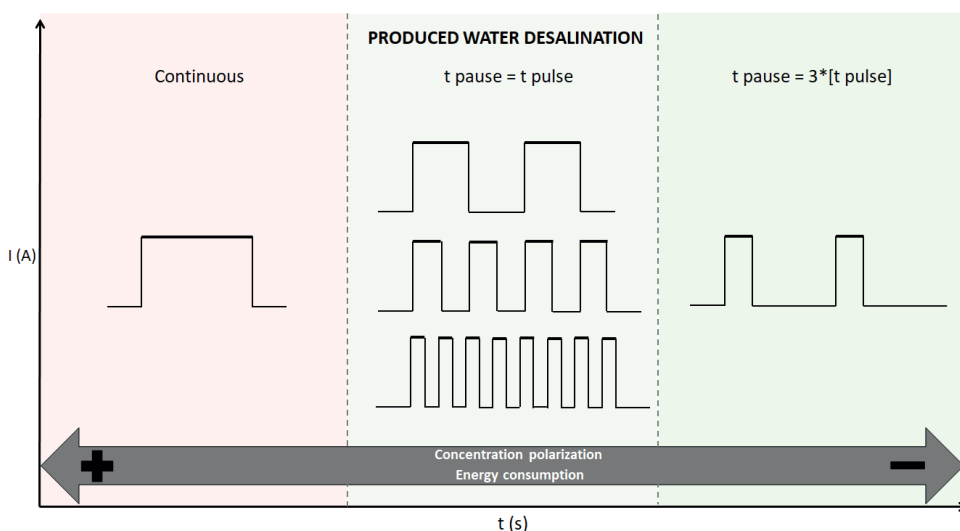
Chapter 6

Improving the performance of polymer-flooding produced water electrodialysis through the application of pulsed electric field

Abstract

Concentration polarization and fouling hamper the desalination of polymer-flooding produced water (PFPW) via electrodialysis (ED). This water is an abundant by-product from the oil and gas industry. A common technique to mitigate both problems is the application of pulsed electric field (PEF), which consists in supplying a constant current during a short time (pulse) followed by a time without current (pause). Accordingly, this work evaluated the application of PEF during the ED of PFPW to improve the process performance and to reduce fouling incidences. The experimental work consisted in performing ED batch runs in a laboratory-scale stack containing commercial ion exchange membranes. Synthetic PFPW was desalinated under different operating regimes until a fixed number of charges were passed. After each experiment, a membrane pair was recovered from the stack and analyzed through diverse techniques. The application of PEF improved the ED performance in terms of demineralization percentage and energy consumption, the latter having reductions of 36% compared to the continuous mode. In general, the shorter the pulses, the higher the demineralization rate and the lower the energy consumption. Regarding the application of different pause lengths, longer pauses yielded lower energy consumptions, but also lower demineralization. Amorphous precipitates composed of polymer and calcium fouled most on the anion and cation exchange membranes, independently of the applied current regime, but in a moderate amount. Finally, the present study relates the observed effects of PEF application to the electrophoresis and diffusion of HPAM and shows that PEF is a sound option to enhance the desalination of PFPW.

6.1 Introduction

Concentration polarization and fouling are probably the two most important issues to tackle to expedite the application of electrodialysis in the industrial scale [1,2]. Electrodialysis (ED) is an electro-membrane process that uses an electric potential as a driving force to selectively transfer charged particles from one solution to another through ion-exchange membranes (IEMs). In this context, concentration polarization denotes the depletion and the accumulation of ions on the surface of the membranes, and it is caused by differences between ion transport numbers in an electrolyte solution and those in an IEM [3] (see **Figure 6.1A**). On the other hand, fouling refers to the undesirable attachment of species on the surface or the inner part of a membrane, and has different causes depending on the type of species attaching [4]. Actually, fouling can appear as a consequence of concentration polarization; for example, due to the accumulation of salts beyond their maximum solubility on the concentrate side of the membranes (scaling), or propitiated by the local changes in pH when water dissociates on the surface of the IEMs [5]. Ultimately, fouling can cause alterations in the membrane structure [4], and both phenomena can cause a decrease of membrane permselectivity, water dissociation, and decreased process performance.

Both phenomena, concentration polarization and fouling, have been documented when desalting polymer-flooding produced water (PFPW), an abundant stream from the oil and gas industry with reuse potential after partially demineralized [6–13]. PFPW is obtained in different locations around the world after applying polymer flooding technology to increase the oil recovery [6,14]. PFPW has a complex composition that includes organic compounds, dissolved gases, solid impurities, and minerals [15]. The characteristic component of PFPW is a viscosifying polymer of high molecular weight, typically partially hydrolyzed polyacrylamide (HPAM) [16]. In solution, HPAM is negatively charged. Thus, when exposed to an electric field, HPAM is attracted and moves towards the positive side (anode), a phenomenon called electrophoresis. Electrophoresis also happens during the electrodialysis of PFPW, so the HPAM in solution moves towards the cathode and forms a gel layer on top of the IEMs [7,10] (see **Figure 6.1B**). The accumulation of HPAM causes concentration polarization and produces severe fouling, particularly on the positively charged anion-exchange membranes (AEMs) [10,11].

To minimize concentration polarization during ED, several strategies have been evaluated, including the use of ion-conductive spacers [17], membranes with undulated or profiled surface [18], air-sparging [19], modified cell configurations [20], etc. To prevent and control fouling on IEMs, strategies like membrane modification [21], use of cleaning agents [11], incorporation of pretreatments [22], and periodical reversal of the polarity [23], have been suggested. However, one strategy that has proved effective for reducing the negative effects of both

concentration polarization and fouling is the use of non-stationary electric fields [2,4,24].
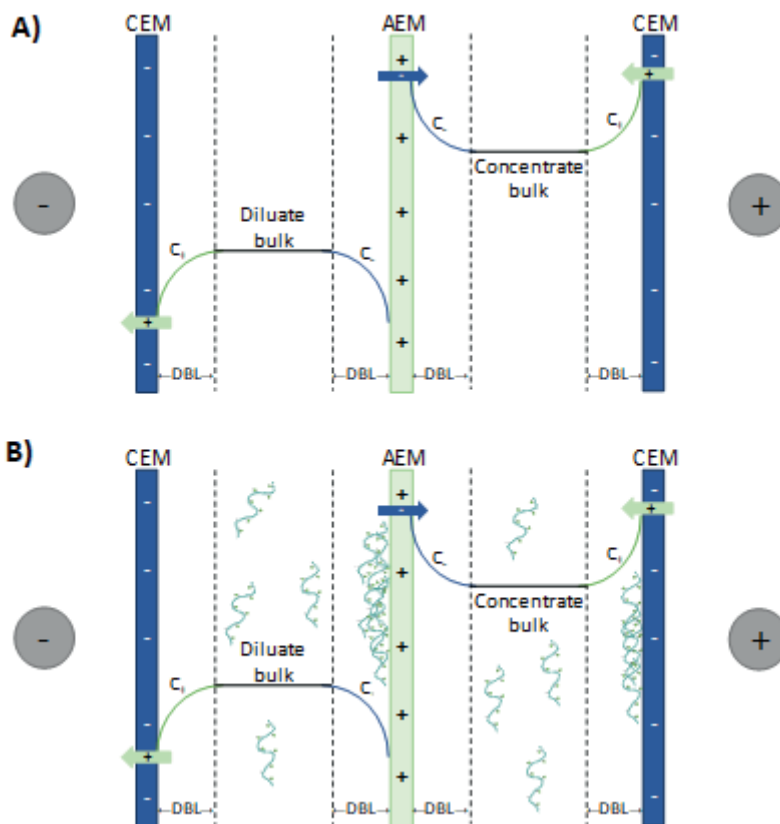
Figure 6.1. A) *Scheme representing concentration polarization in the diffusion boundary layers (DBLs) for the CEM and AEM during electrodialysis. The DBLs cover the areas between the IEMs and the discontinuous lines. On the diluate side of the IEMs, the concentration of counter-ions decreases, while in their concentrate side, it increases.* *B)* *Concentration polarization when desalting polymer-flooding produced water. The negatively charged HPAM (curly green molecules in the scheme) migrates towards the positive anode.*

A non-stationary regime can be created by applying pulses of voltage that alternate with pauses (t_{on}/t_{off}) of a certain duration [25]. The perturbations caused by the non-stationary electric fields may scale down the concentration polarization because, during the pause lapse, ion transport from the bulk solution to the membrane continues through diffusion and convection, so the concentration gradient decreases before the application of the pulse [2].

The use of non-stationary electric field, from now on referred as pulsed electric field (PEF), was first proposed to control the concentration polarization phenomenon and

separate Na^+ from Ca^{2+} [26]. Later, Mishchuk et al. determined that the application of PEF can lead to a weakening of concentration polarization and an intensification of electrodialysis [25]. They made a theoretical analysis and concluded that the intensification of the electrodialysis would be most evident if the duration of the current or the voltage pulses is considerably shorter than the calculated characteristic time to build up the polarization layer. Malek et al. [27] investigated the impact of applying pulsed voltage on ED performance when desalting NaCl solutions. They found that in the sub-limiting regime, concentration polarization had a negligible impact on ED performance, and thus, applying pulsed voltage led only to reduced water production. On the contrary, in the limiting current region, both water dissociation and desalination time decreased with increased frequency. Therefore, by selecting an optimal pulse regime, they were able to operate safely above the limiting current density (LCD), obtaining higher water production with negligible water splitting, and having only a minimal increase in the energetic cost. The use of PEF has also proved beneficial in terms of performance when using electrodialysis to desalinate model salt solution containing whey proteins [20], humate [28], and copper mine tailings [29].

Regarding fouling, the application of PEF has proven beneficial to mitigate fouling caused by humate [30,31], casein solution [32], and minerals (calcium and magnesium) [24,33] during electrodialysis. In the case of the casein solution [32], it was found that the use of long pauses during the application of PEF could remove protein fouling on the surface of AEM. Regarding the solution with high calcium and magnesium content [24], the application of pulse/pause regimes with ratio 1 proved beneficial for decreasing scaling formation. The working principle behind the effectiveness of PEF is also related to reducing concentration polarization, in this case, to avoid the accumulation and close packing of foulants on the surface of the membrane. It has been documented that, depending on the characteristics of the foulants, there is usually an optimum frequency or t_{on}/t_{off} regime that would effectively minimize the fouling [31,33]. However, given that this optimum operation mode depends on the foulant characteristics and the cell configuration, it must be experimentally determined. Some models have been recently developed, like the one proposed by Sistat et al. to describe the pulsed-electric field mode electrodialysis at sub-limiting currents [34], but when the feed solutions are more complex than NaCl solutions, the best approach is still to experimentally find the optimal conditions.

In this study, we evaluate the application of pulsed electric field (PEF) during the electrodialysis of polymer-flooding produced water (PFPW) to improve the process performance and to reduce fouling incidence. Since the benefits of applying PEF depend on the application of an adequate pulse and pause regime(s), several ratios of applied current and pause regime were employed during the batch electrodialysis

of synthetic PFPW containing salts, HPAM, and crude oil. The effects of applying different regimes were evaluated through different performance parameters and by recovering some IEMs from the stack and analyzing them. Finally, our observations are related to the electrophoresis and diffusion of HPAM molecules during the ED process.

6.2 Materials and methods

Experiments were designed to evaluate the performance of electrodialysis under the application of PEF. After the ED experiments, membranes were recovered from the stack and further analyzed.

6.2.1 Materials

6.2.1.1 *Preparation of solutions*

Three types of feed solutions were employed during the experiments, either consisting of brackish water ("BW"), brackish water + polymer ("BW+P"), and brackish water + polymer + oil ("BW+P+O"). All solutions were prepared with demineralized water and contained the same salt composition, based on that of the Marmul field [35], as presented in **Table 6.1.** The pH of the fresh solutions was 7.9.

Table 6.1. Composition of brackish solution

Component	Concentration (mM)
NaCl	53.30
$NaHCO_3$	15.59
KCl	0.72
Na_2SO_4	2.51
$CaCl_2 \cdot 2H_2O$	0.65
$MgCl_2 \cdot 6H_2O$	0.46

The "BW+P" solutions consisted of the brackish water plus 250 mg/L of partially hydrolyzed polyacrylamide (HPAM) with MW = 4.4 – 4.8 million Dalton. The solution was prepared by slowly pouring the polymer inside the BW solution under fast agitation, after which it was left stirring at low speed overnight.

The third feed solution, BW+P+O, included 250 mg/L of HPAM plus 2.0 mg/L of crude oil. To prepare the solution, 1.98 L of BW solution was heated up to 45^0C in a water bath. Then, 2.0 g of crude oil was added to the solution and emulsified with an emulsifying mixer for 15 minutes. The mixture was rested for 24 hours, after which the water phase was recovered and dosed to the feed solution.

All salts employed to prepare the solutions (NaCl, KCl, MgCl$_2$·6H$_2$O, CaCl$_2$·2H$_2$O, Na$_2$SO$_4$, and NaHCO$_3$) were analytical grade, purchased from VWR (Belgium), and employed without further purification. The HPAM employed was Flopaam 3130S (MW= 4.4 to 4.8 million Da and 30% hydrolyzed), kindly provided by SNF (France). The crude oil originated from the North Sea and was provided by Shell. NaOH and HCl solutions utilized for chemical cleaning were prepared from analytical grade reagents purchased from VWR.

6.2.1.2 *Electrodialysis setup*

Experiments were performed in an ED stack, similar to the one previously described [12], but containing seven cell pairs and different membranes. The stack consisted of seven AEM type 10, six CEM type 10 (both kindly provided by FujiFilm Manufacturing Europe B.V.), and two Neosepta CMX (purchased from Eurodia, France) (see **Table 6.2**). The Neosepta CMX membranes were placed at both ends of the stack to ensure minimal water transport. The working area of the membranes (104 cm^2), spacers, gaskets, and electrodes were the same as previously reported. A potentiostat/galvanostat Ivium-n-Stat (Ivium Technologies, The Netherlands) controlled the electrical current and measured the potential difference over the cell. The potential difference was measured using two reference Ag/AgCl gel electrodes (QM711X, QIS, The Netherlands) connected to the ED cell. **Figure 6.2** includes a scheme of the setup.

Table 6.2. *Properties of the anion and cation exchange membranes employed in this study. Data taken from their suppliers.*

Membrane property	AEM FujiFilm 10	CEM FujiFilm 10	Neosepta CMX
Backbone chemistry	Acrylamide	Acrylamide	Divinyl-benzene
Thickness dry (μm)	125	135	170
Area resistance (Ω cm^2, measured in 0.5M NaCl)	1.7	2.0	3.0
Permselectivity (measured at 0.05-0.5M NaCl)	95	99	92.5[a]
pH stability	1-13	1-13	0-10

[a]Measured @ 0.1M-0.5M NaCl [36].

The diluate, concentrate, and electrolyte solutions were pumped by three independent MasterFlex pumps. The conductivities of the diluate and concentrate were measured in line with two conductivity probes (Orion DuraProbe 4-electrode conductivity cell 013005MD) directly before the ED stack. The probes were connected to a transmitter box (Orion Versastar Pro), which corrected the measured values to the reference value at 25 °C. The pH of the solutions was also measured online with two pH probes (MemoSENS Endress+Hauser) connected to a

transmitter box (P862, QIS). Two back-pressure valves, set at 0.25 bar, were placed at the outlet of the electrolyte solution to guarantee the complete filling of the compartments.
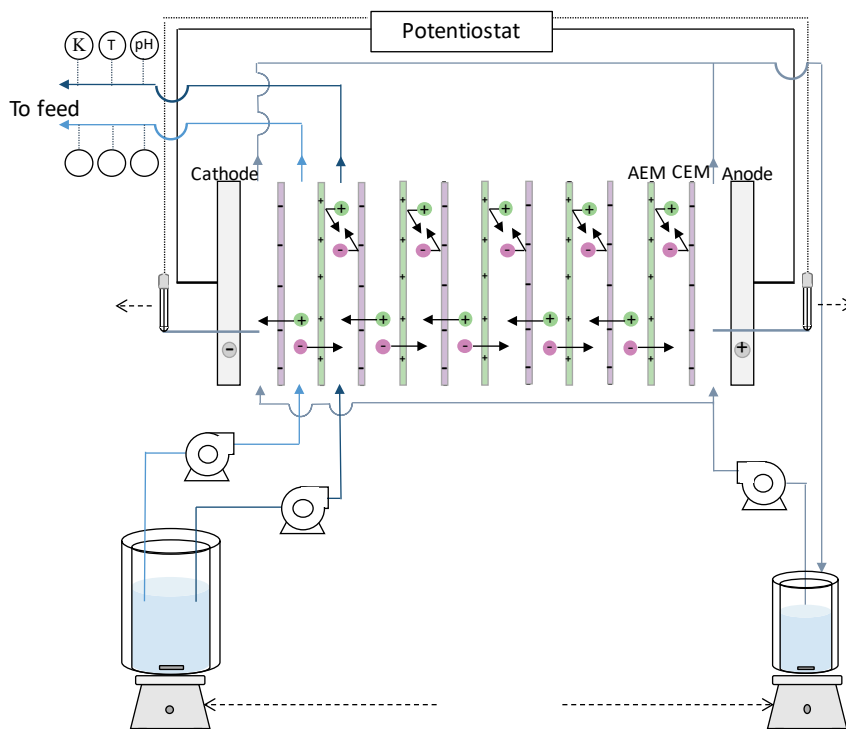
Figure 6.2. *Scheme of the experimental setup. Desalination experiments were performed in batch mode in an ED stack containing 7 cell pairs. Diluate, concentrate and electrolyte solution consisted each in 2.0 L. Conductivity (κ), pH, and temperature were continuously monitored. Adapted from [12].*

6.2.2 Methods

6.2.2.1 *Electrodialysis runs*

The electrodialysis experiments were run in batch mode under different current regimes, summarized in **Table 6.3**. Most of the experiments were run at intermittent regimes, that is, comprising a pulse of applied current (t_{on}) and pause period (t_{off}). The operational regimes were chosen to cover a wide range of pulse and pause sets, and to study the impact of the pulse and pause durations as well as the pulse/ pause ratios on the ED performance, since the literature reports improved performances employing regimes that go from dozens of cycles per day [29] to several cycles per second [34]. In addition, there were experiments run in continuous mode, and one including a back-pulse of 0.1s, during which the current streamed in the opposite direction.

Table 6.3. *Current regimes and feed solutions chosen for this study. Regimes selected in between those in the literature [4,29,34].*

Operating regimes	BW *	BW+P *	BW+P+O
Continuous	X	X	X
t_{on}/t_{off} = 100s/100s		X	X
t_{on}/t_{off} = 100s/300s		X	X
t_{on}/t_{off} = 10s/10s		X	X
t_{on}/t_{off} = 10s/30s		X	X
t_{on}/t_{off} = 1s/1s		X	X
t_{on}/t_{off} = 1s/3s		X	X
t_{on}/t_{off} = 3s/1s		X	X
t_{on}/t_{off} = 0.1s/0.1s		X	X
Back-pulse (t_{on} =100s, t_{off} = 50s, t_{back}= 0.1 s, t_{off} = 49.9s)		X	X

* For these feed solutions, experiments were performed in triplicate, but membranes were recovered only from one run.

The rest of the operational parameters, including volume and current density, were kept constant. The current density was set at 32 A/m², so 55% of the limiting current density measured for the BW+P solution (**Figure A6.1A**). All experiments were run until a theoretical charge of 2000 C (or 14 x 10³ C considering the 7 cell pairs) was transferred. This number of charges was set taking into account a desirable final composition of ~1.0g/L, which would make the desalted PFPW easy to reuse [12]. The diluate and concentrate consisted each on 2.0 L of solution with the same composition. Feed and electrolyte solutions were circulated in the ED cell at flow rates of 170 mL/min (average linear speed of 1.3 cm/s) and 150 mL/min, respectively. The experiments were performed in a laboratory with a controlled temperature of 23 ± 1°C.

The solutions were circulated in the ED cell for 10 minutes before the start of the experiment. During the experiment, the applied current, stack voltage, and transported charges were recorded using the software provided by Ivium (IviumSoft). Samples were periodically taken. The final volumes of the solutions were measured with a graduated cylinder.

6.2.2.2   *Membrane recovery and stack washing*

Immediately after each experiment, the ED stack was opened and the two middlemost membranes, one AEM and one CEM, were withdrawn for further analysis. After substituting them with new membranes, the stack was closed and cleaned-in-place. The cleaning procedure consisted in 15 minutes wash with HCl solution (pH = 2), 15 minutes rinse with NaCl solution (5.0 g/L), 15 minutes wash with NaOH solution (pH = 12), 15 minutes rinse with NaCl solution (5.0 g/L), and a final rinse of at least 15 minutes with BW solution [9,11].

The recovered membranes were cut in four equal pieces (~25 cm^2), as indicated in **Figure A6.2**. One of the lower parts, where the fluid inlet is located, was stored in a freezer at –80^{0}C, to be later freeze-dried and analyzed by SEM. The other lower piece was placed in a flask containing 200 mL of Milli-Q water and left under slow agitation for 48 hours. Samples of this solution were then taken for performing composition analyses (section 6.2.3.4).

6.2.3   Analysis

6.2.3.1   *Percentage of demineralization*

Measured conductivities were employed to calculate the percentage of demineralization, according to equation 1 [20].

$$\eta = \frac{\kappa_0 - \kappa_d}{\kappa_0} * 100\% \qquad\qquad /6.1/$$

Where η is the demineralization percentage of ED, κ_0 is the initial conductivity (mS/cm) of the feed solution, and κ_d is the conductivity of the diluate solution (mS/cm). The calculation is based on the assumption that conductivity and salinity are directly proportional, valid for the low salinities used in this study [12]. Statistical analysis for this data consisted in calculating the single sample Z score, to determine if the values of BW+P+O differed from the ones obtained for BW+P with a confidence of 95%.

6.2.3.2   *Transport number*

The transport number of each ionic species t_i (-) were calculated using the following equation [13,37]:

$$t_i = J_i / \sum [J_s] \qquad\qquad /6.2/$$

Where J_i denotes the ion flux (eq/m^{2}h) of ion or group ions i and $\Sigma[J_s]$ is the total ion flux.

6.2.3.3   *Energy consumption (EC)*

The energy consumption was calculated as [32]:

$$EC = \frac{\int I(t) \cdot U(t)\, dt}{V_{D,f}} \qquad\qquad /6.3/$$

Where $I(t)$ is the current (A), $U(t)$ the voltage (V), and $V_{D,f}$ is the final volume of diluate (m³). For this set of data, the statistical analysis consisted in the two-sample t-test for equal means, with a confidence interval of 95%.

6.2.3.4 *Solution analysis*

Solution samples taken during the experiments and from membrane rinsing were analyzed for their ionic and carbon composition. Cations were analyzed with inductive-coupled plasma optical emission spectroscopy (ICP-OES, Optima 5300DV, Perkin Elmer), and anions with ion chromatography (761 Compact IC, Metrohm). Total Carbon, inorganic carbon, and total organic carbon (TOC) were measured using a TOC analyzer (Shimadzu TOC-VCPH).

The change in TOC after the desalination (Δ_{TOC}) was calculated using the following equation:

$$\Delta_{TOC} = \frac{TOC_0 - TOC_f}{TOC_0} \times 100\% \qquad \text{/6.4/}$$

where TOC_0 and TOC_f represent, respectively, the measured TOC values (mg/L) before and after ED.

6.2.3.5 *SEM/EDX*

Membrane samples from selected experiments were analyzed with SEM/EDX. First, the membrane pieces stored at ─80⁰C were vacuumed in a freeze dryer (Christ Alpha 2-4 LDplus) for two days. Then, the dried membranes were twice gold coated by JEOL JFC-1200 fine coater for 15 s. The samples were analyzed using Scan Electron Microscopy (SEM) and Energy Dispersed X-ray spectroscopy (EDX) manufactured by JEOL JSM-6480LV (Europe). The EDX measurements were conducted at 300X magnification, applying 15kV accelerating voltage.

6.2.3.6 *Membrane resistance*

The electrical resistance of selected IEMs was measured in a six-compartment cell, as previously described by Galama et al. [38]. The four inner compartments contained 0.5M NaCl solution, while the two outermost ones were filled with 0.5M Na₂SO₄ as the electrolyte solution. The solutions were circulated in each compartment at 170 mL/min using peristaltic pumps. The membrane under evaluation, placed in the middle of the cell, had an effective area of 7.07 cm². It was sided by two Habber-Luggin capillaries, each filled with 3.0 M KCl solution and connected to an Ag/AgCl gel reference electrode, which allowed us to measure the potential drop across them. The temperature of the solutions was maintained at 25⁰C with a thermostatic bath.

Before the measurement, the recovered membranes were pre-conditioned in 0.5 M NaCl for at least three days. Once the membrane was placed in the cell, the solutions were circulated for 1 h before doing the measurements. The membrane resistance was determined using chronopotentiometry: increasing values of current density were applied for 2 min each, while the electric potential was recorded. The current over the cell was provided by Autolab PGSTAT12 (The Netherlands). The protocol was repeated three times for each membrane, plus another time without the membrane to obtain a blank measurement. The area resistances (Ω cm^2) were obtained from the inverse of the slope when plotting the applied current density (A/cm^2) on the x-axis and the potential (V) on the y-axis (see **Figure A6.3**). Then, the membrane resistance was calculated by subtracting the resistance of the blank from the resistance with the membrane.

6.2.3.7 *Polyelectrolyte displacement*

HPAM displacement during electrophoresis was calculated via equation 5, which relates the distance x_E (m) to the electrophoretic mobility of HPAM μ (m^2 V^{-1} s^{-1}), the electric field E (V/m) and the time t_{on} (s):

$$x_E = \mu E t_{on} \qquad /6.5/$$

The electrophoretic mobility of HPAM was estimated to be 1.2 x10^{-8} m^{2}V^{-1}s^{-1} by using the Smoluchowski equation and a zeta potential of -17 mV, which corresponds to HPAM in a pH 8 solution [7].

The electric field can be calculated from the current intensity I, the conductivity of the diluate solution κ_d, and the membrane area S (m^2) [39]:

$$E = \frac{I}{\kappa_d S} \qquad /6.6/$$

Eq. 6 can be substituted in eq. 5 to obtain x_E as a function of the conductivity of the diluate, obtaining the following equation:

$$x_E = \frac{\mu I t_{on}}{\kappa_d S} \qquad /6.7/$$

The linear distance x_D covered by the diffusing HPAM molecule during the pause (t_{off}) was calculated employing the HPAM diffusion coefficient D_{HPAM} (m^2/s) in the mean-square displacement equation:

$$x_D = \sqrt{6D_{HPAM}t_{off}}$$ /6.8/

The HPAM diffusion coefficient D_{HPAM} was calculated to be 2.17×10^{-13} m²/s. This value was obtained employing the Einstein-Stokes equation [40] and a particle radius of 100 nm [41].

6.3 Results and discussion

It is well-known that the pulse-pause duration ratio and the pulse frequency are important parameters for the optimization of the desalination [25,27] and the reduction of fouling [32,33,42]. The first sub-section presents the evaluation of the electrodialysis performance under the current regimes enlisted in **Table 6.3**, followed by the analysis of fouling in section 6.3.2.

6.3.1 Desalination performance in different operating regimes

Since the ED experiments were run under constant current density, the cell potential varied during the desalination. During the first cycles of each run, the cell potential remained practically constant, as shown in plots **A**, **C**, and **E** in **Figure 6.3**. On the contrary, during the last cycles of each experiment, the cell potential increased significantly, frequently reaching the 10 V limit of the potentiostat (**Figure 6.3B**, **D**, **F**). This is an indication of concentration polarization developing during the application of the pulse at low dilute concentrations, as previously described in the literature [25].
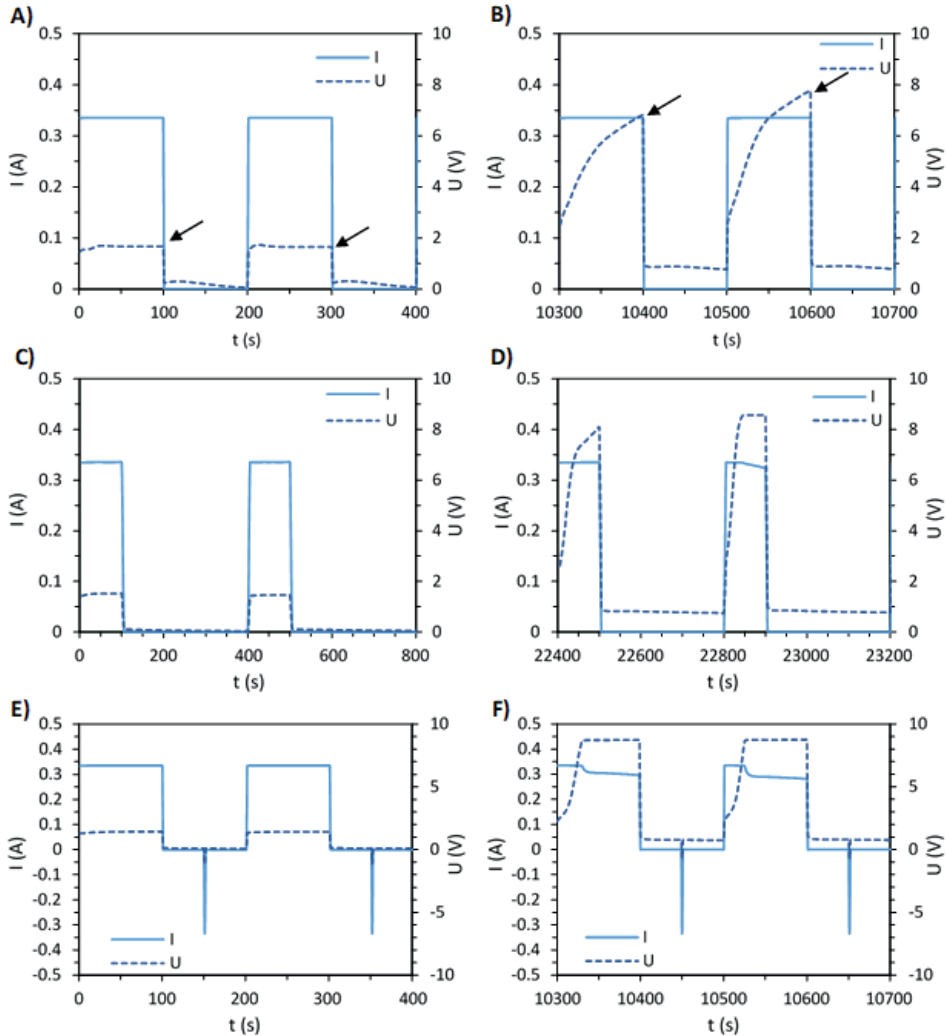
Figure 6.3. *Examples of data recorded during the experiments. The plots show the electric current I (left axis, continuous lines) and potential U (right axis, discontinuous lines) for three different regimes. **A** and **B** show, respectively, the first and a nearly final cycle of a 100s/100s run; **C** and **D** show the same plots for a 100s/300s run, and the ones for the back-pulse case are figures **E** and **F**. The arrows in plots A and B indicate the data points employed to create Figure 6.4.*

The complete desalination process is shown in **Figure 6.4A**, which displays the electric potential in the cell as a function of time for the different regimes applied. The figure also shows that the experiments had different durations, ranging between 100 and 400 minutes, due to the use of operation modes that involved diverse pulse/pause durations. Therefore, the experiments were mainly evaluated in function of the theoretical transported charge Q, as represented in **Figure 6.4B**. To maintain their readability, plots **Figure 6.4A** and **4B** include only the last value recorded after a cycle, as indicated with the black arrows in **Figure 6.3**.
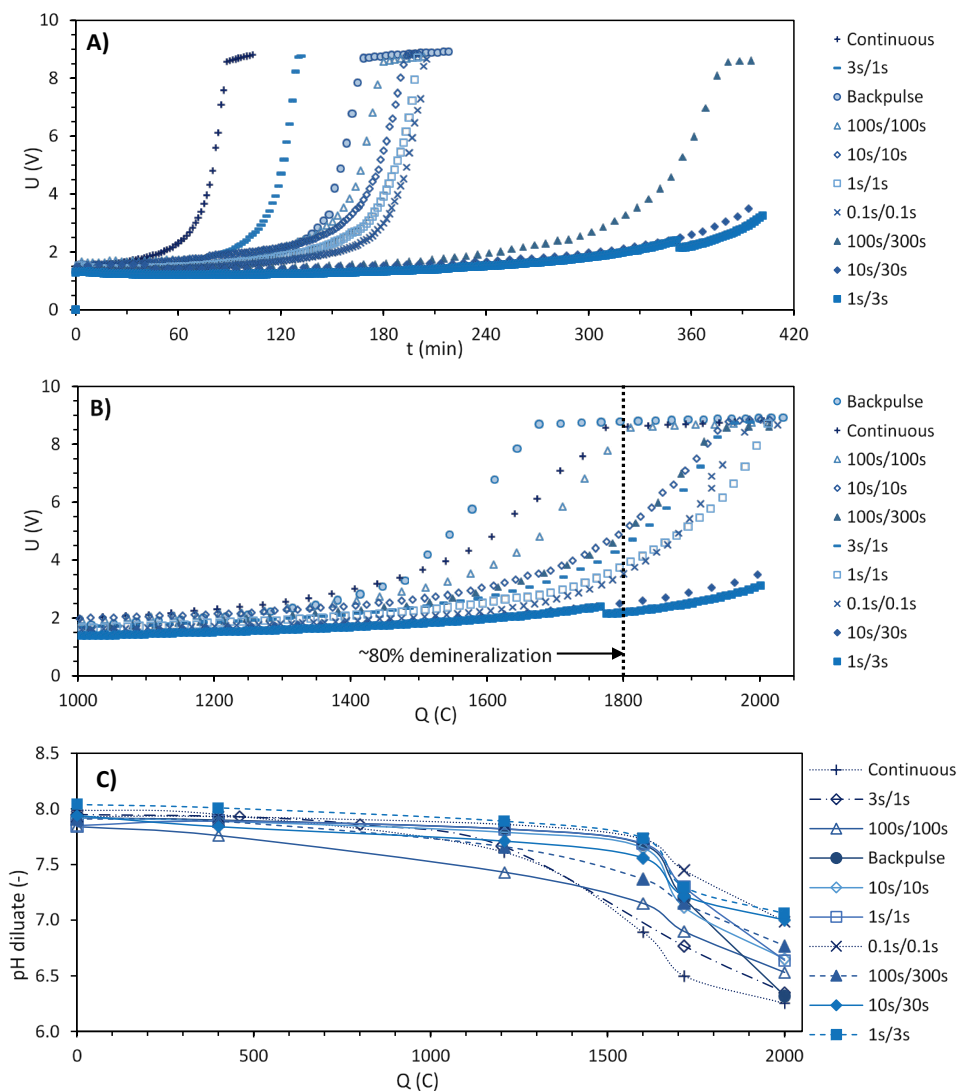
Figure 6.4. *Measured electric potential U vs time (A), U vs transported charges Q (B), and pH of the diluate vs Q (C) during the batch electrodialysis of BW+P solutions for the different current regimes applied. The plots present one series of data representative of the 3 series performed.*

The pH of the diluate solution exiting the ED-cell was also continuously monitored, and is included in **Figure 6.4C**. Changes occurred despite the solution contained a high percentage of bicarbonate, which acts as a buffer. The figure shows that the most severe changes occurred for the continuous operation, followed by the PEF regimes with longer pulse time, mainly after 1600 C had passed. On contrary, the regimes 10s/30s, 1s/3s, and 0.1s/0.1s presented the smallest changes of pH. The

changes in pH coincide with the voltages in **Figure 6.4B**, which indicates that when larger potentials were reached, more water was dissociated causing the observed pH changes.

6.3.1.1 *Percentage of demineralization*

The percentage of demineralization (η) was calculated from the conductivity readings of the diluate stream (6.2.3.1), which had an average initial value of 7.70 mS/cm. The demineralization achieved for all performed experiments is presented in **Figure 6.5**. For the solutions with HPAM (BW+P), the figure shows that the application of intermittent regimes increased the demineralization levels achieved compared to the continuous mode. Higher demineralization percentages were obtained for the shorter pulse intervals (excluding the 0.1s/0.1s regime), so the highest value (91.5%) was achieved for the 1s/1s regime. It is also clear that the runs with the longer pauses (100s/300s, 10s/30s, and 1s/3s) had slightly lower demineralization compared to their analog experiments with shorter pauses (100s/100s, 10s/10s and 1s/1s). This lower efficiency of the operating regimes with longer pauses is explained by the back-diffusion of the transferred salts due to osmosis. A higher demineralization was also reported by other authors during the use of PEF [24,43,44]. For Lemay et al., high-frequency PEFs in combination with short pulse/pause ratio improved the DR the most for the same number of charges transported [43]. This condition could enhance the ion transport because concentration polarization was diminished.

The demineralization percentages achieved when desalinating BW+P+O were, in most cases, higher than the averages for BW+P feed, suggesting that the addition of crude oil to the solutions did not affect, or even improved, the performance. This could be related to the oil reducing the stability of the gel layer formed by HPAM and thus also concentration polarization, as we suggested in our previous research [45]. For the BW+P+O set, the tendencies were like the ones observed for BW+P, except for the 0.1s/0.1s and the 1s/3s regimes, which presented the highest demineralization percentages. The regime 1s/3s also showed a good performance, contrary to the BW+P results, suggesting that the pause lapse was not enough to allow the ions to back diffuse.
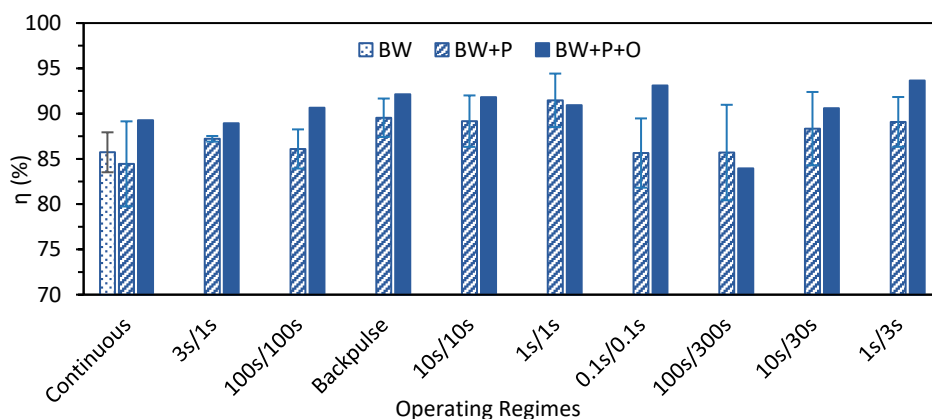
Figure 6.5. *Demineralization percentage η achieved after performing ED for BW, BW+P, and BW+P+O solutions.*

6.3.1.2 *Migration of cations*

Concentration polarization can also affect the performance of membranes regarding selectivity and specific ion removal [13,46]. Therefore, our analysis included the removal of the cationic species. It was observed that the concentration (c) of sodium and potassium in the diluate decreased linearly, while those of calcium and magnesium could be better described by a 2nd order polynomial (**Figure A6.4A**). The same tendencies had been already observed in our previous work [13]. Thus, for comparison purposes, the analysis focused on the initial part of the experiments, to be specific until the first 1050 C were transported, where the concentration decrease can be considered linear (**Figure A6.4B**). The transport numbers t_k of each cation were calculated using the concentrations obtained from the samples taken during the first part of the experiments (see section 6.2.3.2). In this way, 5 to 9 t_k values were obtained for each cation for each current regime, and their averages are shown in **Figure 6.6**.

Figure 6.6A includes the calculated t for Na^+. Given its relatively high concentration in the feed solution, an average of 94% of the current was transported by this ion, although slightly lower t values were measured for some regimes, especially 100s/300s and 10s/30s. The lower t of Na° in those regimes was compensated by larger transport numbers for Ca^{2+}, as shown in **Figure 6.6B**. This could be explained by considering that during the pause, the initial time is used to remove the polarization layer, and if the pause is long, back diffusion of ions starts to happen. Thus, the lower t numbers for Na could be due to the back diffusion of this ion during the long pause. When the pause was shorter, like in the 1s/3s regime, there were no large differences in the transport numbers, probably because the relaxation time was too short to allow significant back-diffusion. On the other hand, the

transport numbers of K^+ and Mg^{2+} remained constant despite the operation mode. When comparing the migration of cations using conventional and pulsed electrodialysis, Casademont et al. [20] also reported for the latter a larger increase in the migration of Ca^{2+} compared to the rest of the ions. The increase in Ca^{2+} transport can be related to the reduction of concentration polarization when pulsed electrodialysis is applied. Less concentration polarization of ions in the diluate side facilitates that those with slower diffusion coefficients, like Ca^{2+} and Mg^{2+}, to reach the surface of the CEM [13,46]. Once in contact with the membrane, the transport of Ca^{2+} is facilitated, while that of Mg^{2+} still has to overcome an energy barrier caused by the necessity of a partial dehydration of its ions [47].
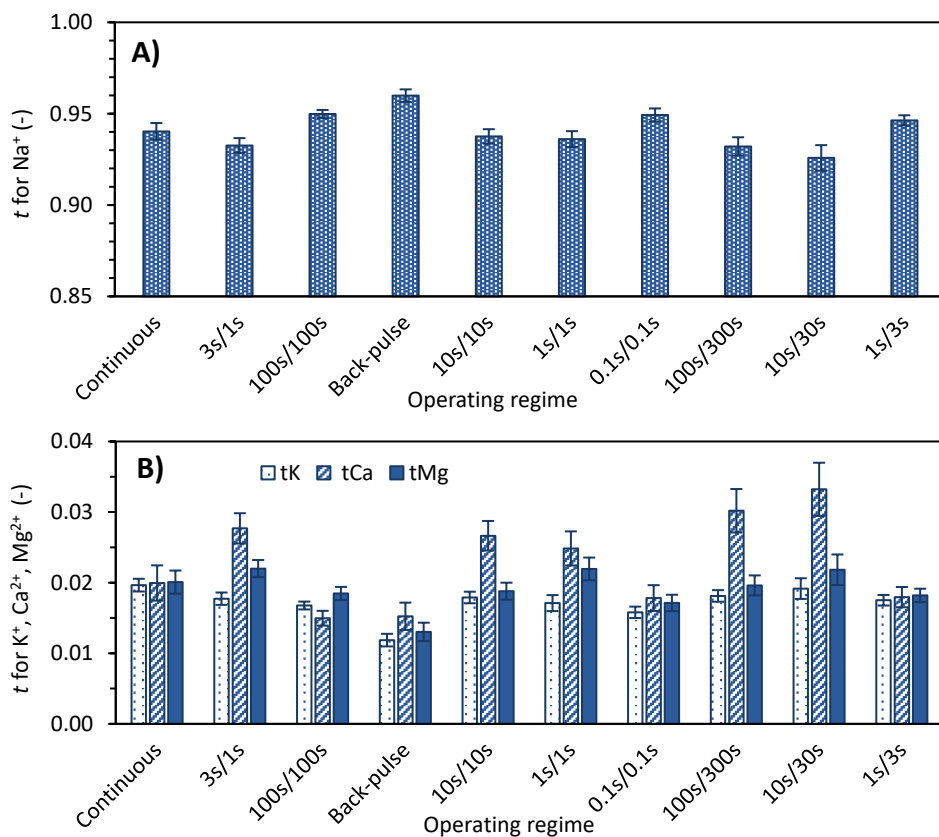
Figure 6.6. Transport number t for Na⁺ (A) and for of K⁺, Ca²⁺, and Mg²⁺ (B) calculated from the samples taken during the first 1000C of the experiments.

6.3.1.3 *Energy consumption*

The energy consumption (EC) for the different operation modes was calculated employing Eq. 3. Two values of energy consumption are reported: the energy required to obtain 80% of demineralization (conductivity of 1.5 mS/cm, see **Figure**

6.4B), and the energy required to transport 2000 C. The intermediate calculation for 1.5 mS/cm was set to compare the energy consumption when the same quality of diluate is achieved, since in cases when higher demineralization degrees were attained, the energy consumption would also increase due to the higher resistivity of the solution. A second reason to report two EC values is to assess if the advantages of the intermittent mode become more important in the over-limiting current regime, as reported in the literature [2,27,34]. In preliminary experiments, it was determined that the limiting current density when desalting a solution of 1.5 mS/cm is 10 A/m² (**Figure A6.1B**), much lower than the experimental current density of 32 A/m².

The EC's calculated for all the experimental conditions are included in **Figure 6.7**. The BW and BW+P results are presented with error bars since they were performed by triplicate, contrary to the BW+P+O runs, which were executed in singular since their performance was comparable that of the runs without oil. Indeed, all the EC measurements for BW+P+O fall within EC ± 1 standard deviation for the BW+P solutions, meaning that statistically they do not differ. The plot also shows that, in general, lower energy consumptions were obtained for the pulsed regimes compared to the continuous one. The only exceptions were the two 3s/1s cases and the 100s/100s regime for BW+P, which had an EC alike the continuous case. Furthermore, the other two regimes with 100s pulse (back-pulse and 100s/300s) also presented a minimal reduction in EC. Still, the statistical test for BW+P results indicates that none of the EC's obtained after applying a PEF mode differs from the EC achieved in continuous (p>0.05).

Regarding the effect of the pause length, slightly lower energy consumptions were obtained for the longer pauses, so the lowest energy demand was recorded for the 1s/3s regime. This coincides with the data shown in **Figure 6.4A**, which suggested that limiting conditions were reached for most regimes, except the 10s/30s and 1s/3s ones. Furthermore, while treating black Kraft liquor, Haddad et al. also measured the lowest energy consumption for pauses much longer than the pulses [48]. The EC calculated to achieve the intermediate (1.5 mS/cm) and the final product fall within the same tendency, indicating that the application of PEF has measurable effects even when used in the sub-limiting regime.

Although not particularly related to the application of PEF, it was unexpected to obtain the highest energy consumption for the brackish solution without polymer. Considering the inverse relationship between viscosity and Reynolds, a solution with lower viscosity (like the BW) would achieve higher turbulence and mixing. However, our results indicate the opposite. Thus, it is thought that the higher viscosity of the BW+P solutions stabilizes the laminar flow, which would reduce the

channeling and dead zones in the ED stack, so these runs make better use of the available membrane area.
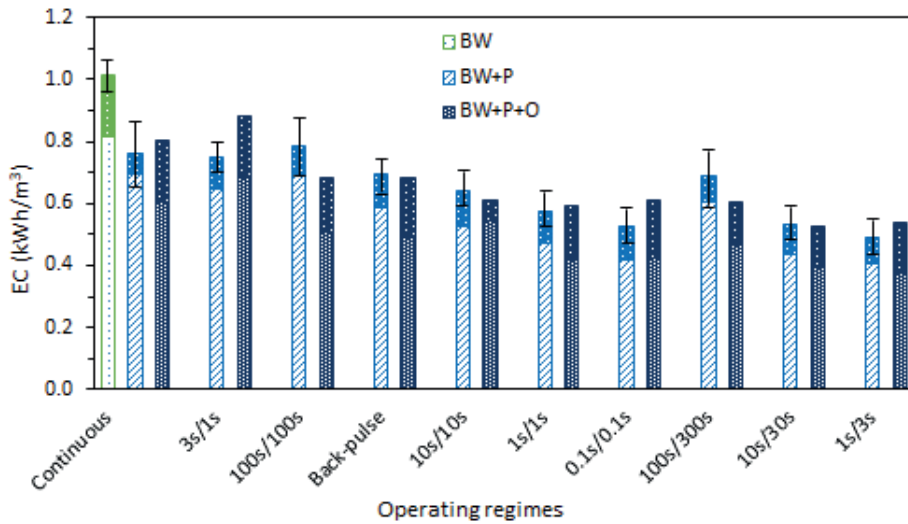
Figure 6.7. *Energy consumption (EC) per volume of product for the different regimes while desalinating BW, BW+P, and BW+P+O solutions. The lower (lighter) part of the bars indicate the EC for reaching 80% demineralization, while the entire bar shows the EC after passing 2000 C. The error bars indicate the standard error, calculated from at least three replicate runs.*

Figure 6.8 shows that if both, energy consumption and demineralization percentage, are considered, the most promising results were obtained for the regimes involving pulses of 1s. Previous studies have also found that shorter pulses result beneficial in terms of process performance [2,25,34,43,49], although in some cases operating with very small pulses does not lead to further improvement due to the nature of the foulants [30], which was probably the case for the 0.1s/0.1s regime In contrast, during whey demineralization, Lemay et al. reported their best results using the referred regime (0.1s/01s), which they attributed to the occurrence of voltage peaks and electro-convective vortices [43]. It must be noticed that while the demineralization results varied 8% at most, the effects of the intermittent regimes in energy consumption were much larger, reducing it 36% for the same feed solution. This observation also applies to the best performers, since the 1s/1s is only 2% better than 1s/3s in terms of demineralization percentage but spends 14% more energy. Yet, before ranking the current regimes, it is necessary to consider if they also provide good results in terms of minimizing fouling formation.
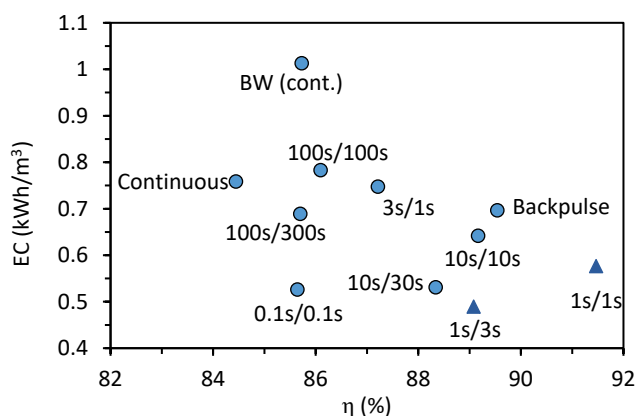
Figure 6.8. *Energy consumption (EC) vs. demineralization percentage (η) for BW and BW+P solutions desalinated until 2000 C had been transported.*

6.3.2 Fouling analysis

6.3.2.1 *TOC*

The concentration of HPAM in solution was monitored through Total Organic Carbon (TOC) analyses (section 6.2.3.4) of the diluate and the concentrate. As an example, **Figure 6.9A** and **B** show, respectively, the TOC concentrations for the continuous and the 1s/1s regimes while desalting BW+P solutions. The HPAM concentration remained stable during most of the process, but still slight variations occurred at the end of the experiment. Given the relatively big MW of the HPAM (4.4 - 4.8 million Da), it is very unlikely that it could be transported through the IEMs. Another potential explanation for the TOC changes would be water transport affecting the measured concentration of the solutes [12]. However, the solutions presented a maximum change of volume of 5% after the experiments, which is not enough to explain the larger variations of TOC. Thus, the most feasible explanation is that TOC values varied because part of the dissolved HPAM remained in the stack. Besides migrating towards the IEMs, some HPAM remained in the corners of the spacers, as has been previously reported for other types of fouling [50].

Considering the previous observations, the overall TOC changes in an experiment were analyzed employing Eq. 4, and the results are summarized in **Figure 6.9C**. From the equation, positive Δ_{TOC} values indicate a decrease of TOC, while negative values indicate the opposite. However, most of the measured TOC changes were within the normal error range (less than 10%), so for these cases, the conclusion is that there wasn't a significant amount of HPAM remaining in the ED stack. Larger changes were measured for the 100s/100s, 10s/30s, and the back-pulse runs, but they do not follow any clear tendency, so it is not possible to conclude if there is some relationship between the operating regime and the TOC concentration in solution.

The same can be said from other large Δ$_{TOC}$ values measured for the experiments with BW+P+O feed solutions (**Figure A6.6**).
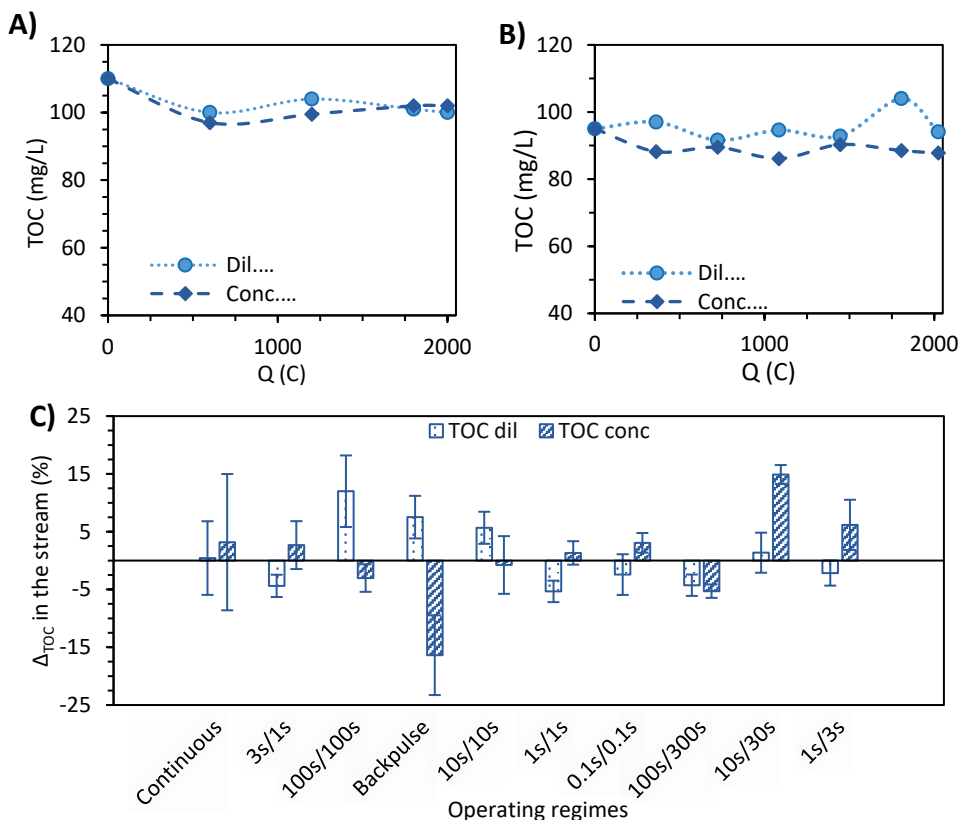

Figure 6.9. *TOC concentration vs transported charges Q in the diluate and concentrate of **A)** a run in the continuous mode and **B)** a 1s/1s run. **C)** Δ$_{TOC}$ analysis for experiments with feed BW+P.*

6.3.2.2 *Membrane rinsing*

After the ED runs, recovered membrane pieces of approximately 25 cm² were soaked in 200 mL of Milli-Q water (section 6.2.2.2). The rinsing water was later analyzed to determine the ionic and carbon content, and the results of these measurements are shown in **Figure 6.10**. The analyses from the CEMs after desalting BW+P (**Figure 6.10A**) revealed that the ions released by the membrane were mainly Na^+ and Cl^-, with some traces of SO_4^{2-}. Remarkably, most CEMs released organic carbon, indicating that the HPAM recovered with them was loosely attached. On the contrary, for the AEM rinse solution (**Figure 6.10B**), no organic carbon was detected, except for the back-pulsed regime. This suggests that any HPAM recovered with the membrane was strongly attached. In addition, the AEM analysis also showed that Na^+ and Cl^- were the most abundant ions. Instead of sulfate, traces of the other cations (Ca^{2+}, Mg^{2+}, and K^+) were released.
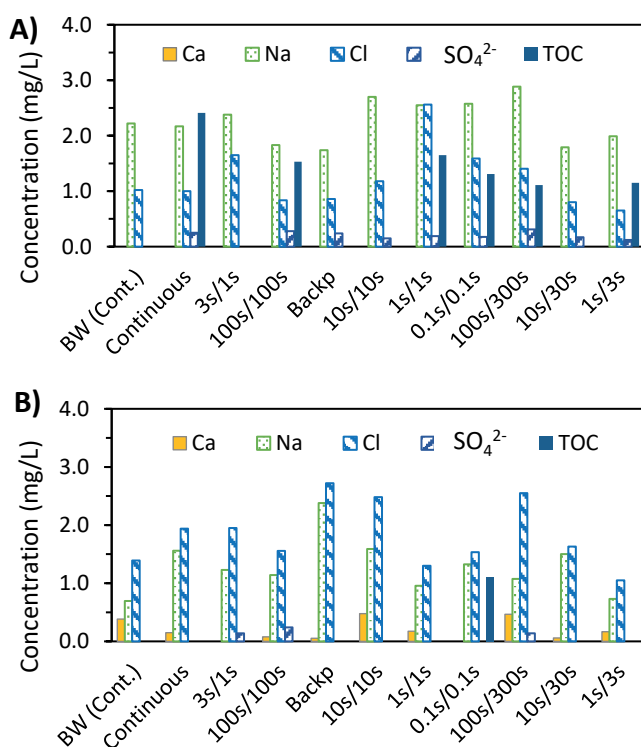
*Figure 6.10. Concentration of species in rinsing solution of membranes recovered after the ED of feed solutions BW and BW+P. **A)** and **B)** show, respectively, the results from the CEMs and AEMs.*

The analysis for the BW+P+O solutions (**Figure A6.7**) rendered similar results. Organic carbon was only released from the CEMs. Sodium and chloride were present in the rinse solution of both membranes, although the amounts released from the AEMs were higher than for the rest of the analyses.

6.3.2.3   *SEM/EDX for selected experiments*

Membranes taken from the continuous and from the intermittent runs 100s/100s, 1s/1s, 1s/3s, and 0.1s/0.1s were further analyzed with SEM and EDX. **Figure 6.11** shows the SEM photographs of the AEMs and CEMs after desalting "BW+P" feed solutions in the continuous and the 1s/1s and 1s/3s modes. They show that, regardless of the operation mode, small amounts of fouling were present on both sides of the AEMs and on the diluate side of the CEM. The fouling appears to be an amorphous precipitation, and given the relatively large sizes of the particles, it is likely that their composition included HPAM and salts. Considering the configuration of the ED stack, HPAM was expected to accumulate on the diluate side of the AEM and on the concentrate side of the CEM. This is because, under the influence of the electric field, electrophoresis drives the negatively charged

187

molecules towards the anode, but since they are too large to pass through the IEMs, they accumulate on their surface [7,10]. AEMs are especially affected by organic fouling, which is more severe and stable on them due to the electrostatic and hydrophobic interactions between the foulants and the membranes [51]. All SEM images, even those from the continuous run, show scarce precipitants that cover only a small fraction of the membrane surface, which contrasts with our previous observations of thick gel layers covering the entire surface of the membranes [45]. The differences can be attributed to the lower concentration of HPAM in solution, shorter desalination times, and the use of an ED stack with spacers, the last element enhancing turbulence and thus also acting against concentration polarization.

Regarding the CEMs, the images from the three current regimes also show some precipitation on their concentrate side, while the diluate side remained almost clean. This can be explained from the concentrate side being susceptible to two kinds of fouling: HPAM fouling driven by the electric field [10], and salt precipitation or scaling. Scaling usually happens on the concentrate side of the CEMs since it is here that the cations accumulate due to concentration polarization (see Figure 6.1. A), making them susceptible to precipitate either as carbonates or as hydroxides [24].

The SEM photographs of IEMs after desalting BW+P+O feed are included in **Figure 6.11B**. As for **Figure 6.11A**, they show scarce amorphous precipitation, which was not obviously affected by the different operation modes. Precipitation was observed on both sides on both kinds of membranes, including the diluate side of the CEM. This suggests that some components present in oil might have acted as linking agents between HPAM and the negatively charged membrane. Additionally, the concentrate side of the CEM obtained from the continuous run displayed a different kind of precipitate, consisting of a conglomerate of several spheres, which EDX identified as rich in calcium and oxygen. The spheres were likely a form of $CaCO_3$ precipitate, since the literature reports the formation of similar aggregates by using polymers as crystal-growth modifiers [52].
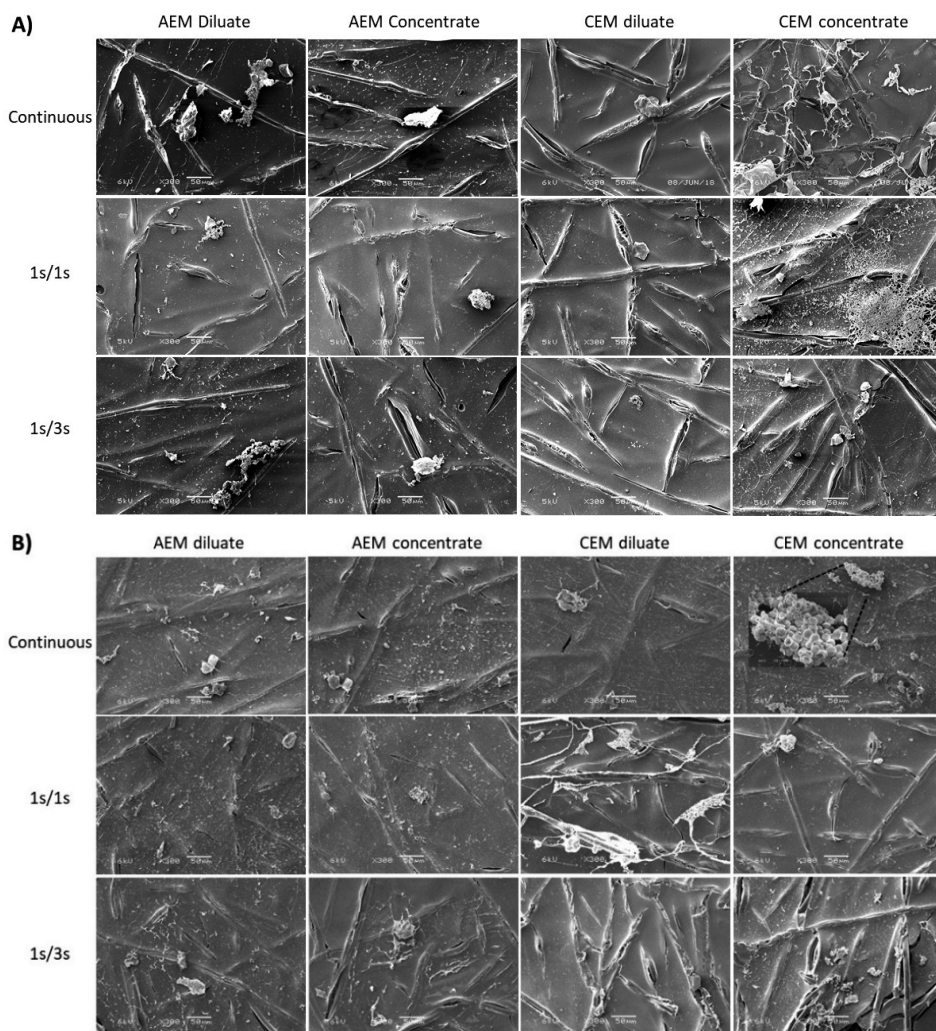
Figure 6.11. *SEM photographs of recovered membranes from the experiments with feed solutions BW+P (**A**) and BW+P+O (**B**). Pictures were taken at an accelerating voltage of 5 or 6 kV and are magnified 300x. The reference lines represent 50 μm. The precipitate found on the CEM concentrate side after continuous ED is magnified 2700x.*

The elemental composition of the surface of the IEMs was determined via EDX. The first two rows of Table 6.4 show the main components of the CEM exposed only to BW solution, which can be used as a base to compare the rest of the measurements. The main elements detected are C, N, O, and S, corresponding to the composition of the membrane, plus the divalent cations Ca^{2+} and Mg^{2+}, presumably because they remain as counter-ions inside the CEM. Still, some spots on the membranes presented higher concentrations of calcium and magnesium, which can easily precipitate after binding with either carbonate or hydroxide ions [53,54]. Then, when analyzing the membranes fouled with BW+P solution, the elemental compositions

remained almost identical to that of the clean membrane (**Table A6.1**). The only differences were a slight decrease in the N content and a minimal increase in the one of Ca, probably due to concentration polarization.

The CEMs analyzed after desalting BW+P+O feed (**Table 6.4**) presented more obvious differences. The membrane used to desalinate BW+P+O in continuous mode had a high content of C (72-76%) and a low content of O (~10%), which could be related to the adsorption of hydrocarbons from the oil emulsion. Still, the application of pulsed regimes seemed to have positive results in lowering organic fouling, since the CEMs recovered from experiments using intermittent regimes presented compositions closer to that of the clean membrane.

Table 6.4. EDX elemental analysis of CEMs recovered from selected ED experiments

Feed solution	Experiment	Side	Percentage (%)							
			C	N	O	Na	Mg	S	Cl	Ca
BW	Continuous	D	58.18	9.79	22.44	2.92	0.13	5.71	0.03	0.59
		C	60.74	9.77	20.49	2.63	0.20	5.20	0.15	0.66
BW+P+O	Continuous	D	76.12	10.10	9.48	0.08	0.01	0.16	4.05	-
		C	72.65	11.33	10.53	0.09	0.01	0.18	4.76	0.40
	100s/100s	D	64.54	7.06	20.10	2.54	0.16	4.95	0.01	0.52
		C	63.19	7.44	20.47	2.72	0.17	5.25	0.04	0.57
	1s/1s	D	60.64	7.80	22.06	2.99	0.17	5.62	0.07	0.54
		C	62.53	7.91	20.74	2.78	0.18	5.19	0.02	0.52
	1s/3s	D	65.22	7.16	19.23	2.71	0.14	4.95	0.03	0.44
		C	63.01	7.15	20.82	2.94	0.18	5.28	0.03	0.46
	0.1s/0.1s	D	60.49	8.29	22.00	2.88	0.18	5.42	0.05	0.53
		C	60.70	7.86	21.98	2.90	0.18	5.58	0.04	0.60

Table 6.5 summarizes the EDX analyses for the selected AEMs. The membrane recovered after desalting BW solution presented slightly higher carbon and nitrogen content than the CEM from the same experiment (62% and 24%, respectively), which is reasonable since the functional groups of the AEM are quaternary amines. The AEM exposed to BW+P solution under continuous mode presented a very similar composition to that of the clean membrane. From our previous research [45], HPAM presence is expected to cause an increase in O and a decrease in Cl, especially on the diluate side of the AEM, where the polyelectrolyte tends to form a gel layer. The same was observed on the diluate side of the membrane under the 0.1s/ 0.1s regime (**Table 6.5**), but not so much for the rest of the membranes exposed to BW+P solution.

The explanation would be the scarce presence of HPAM on the membranes, as previously noticed from the SEM images (**Figure 6.11**).

Regarding the analysis of AEMs fouled by BW+P+O solution (**Table A6.2**), the elemental compositions seemed consistent independently of the applied current regime. Compared to the BW case, the membranes showed slight increases of C and O on both faces, probably related to the adsorption of HPAM and oil, as observed for the CEM.

Table 6.5. EDX elemental analysis of AEMs recovered from selected ED experiments

Feed solution	Experiment	Side	Percentage (%)							
			C	N	O	Na	Mg	S	Cl	Ca
BW	Continuous	D	62.00	24.29	8.41	-	0.02	0.18	5.09	-
		C	61.58	24.33	8.78	-	0.03	0.17	4.95	0.17
BW+P	Continuous	D	60.22	24.90	9.89	0.13	0.02	0.18	4.64	0.02
		C	61.72	25.03	8.96	0.10	0.01	0.12	3.95	0.01
	100s/100s	D	74.01	11.33	10.21	0.10	-	0.10	4.14	-
		C	55.88	24.70	13.00	0.12	0.05	0.18	4.31	1.66
	1s/1s	D	76.05	10.70	8.69	0.01	-	0.14	4.27	0.11
		C	73.03	12.92	9.50	0.03	0.01	0.15	4.30	0.01
	1s/3s	D	72.74	11.88	10.37	0.08	0.01	0.16	4.73	-
		C	74.89	11.93	8.62	0.02	-	0.15	4.33	0.01
	0.1s/0.1s	D	60.22	7.46	23.02	2.84	0.21	5.43	0.03	0.61
		C	74.91	10.53	9.88	0.06	0.02	0.15	4.44	-

Overall, the AEMs presented higher increases of carbon content compared to the CEMs, which is sound given their affinity to HPAM. Less organic fouling occurred during the application of pulsed regimes of 1s/1s and 1s/3s. Longer pauses, like 1s/3s, were effective in reducing the organic fouling as nitrogen (N) concentration dropped to 7.4 %. However, during this regime, also more minerals (Na, Ca, O, and S) were spotted on the concentrate side of the AEM.

6.3.2.4   Membrane resistance

The last evaluation method for the fouled membranes was their electrical resistance. Comparing the membrane resistance before and after performing the electrodialysis can help to determine membrane damage due to irreversible fouling inside or on its surface [55]. The electrical resistance was measured by first obtaining the slopes of I-V curves performed with and without the membrane. Then, the membrane

resistance was calculated by subtracting the resistance without membrane from the resistance with the membrane (section 6.2.3.6).

Figure 6.12A shows the measured resistances of the CEMs recovered from selected experiments. The resistance measured for the CEM exposed to BW was 2.4 $\Omega \cdot cm^2$, slightly higher than the 2.0 $\Omega \cdot cm^2$ reported by the supplier, which can be explained by some multivalent ions remaining in the membrane despite the long conditioning time. Then, the Figure shows that the membranes exposed to BW+P and BW+P+O recorded small resistance increases, varying between 3 to 20%. The only membrane that, instead of increasing presented a decrease in electric resistance, was the one recovered after desalting BW+P in a 1s/3s mode. Probably this was due to the long pause, as further explained in section 6.3.3.
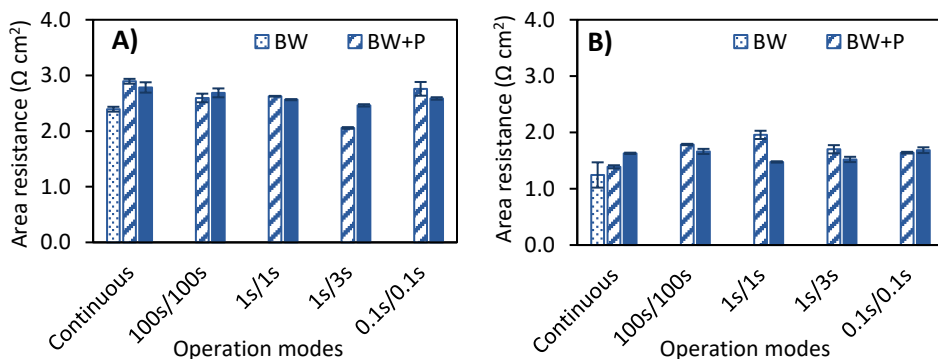
*Figure 6.12. Measured electric area resistances of selected CEMs **(A)** and AEMs **(B)** recovered after the ED runs.*

Regarding the AEMs, **Figure 6.12B** shows that their electric resistances were lower than for the CEM, many below the 1.7 $\Omega \cdot cm^2$ reported by the supplier. The membranes exposed to BW+P and BW+P+O solutions also suffered slight resistance increases compared to the AEM exposed to BW solution, but the differences were minimal.

6.3.3   Linking the performance with HPAM net displacement

It has been mentioned that due to the complexity of phenomena occurring during the application of the pulsed regimes, no mathematical model can yet fully describe such process. However, it is possible to understand why the shorter pulses deliver the best effects in terms of performance by considering the electrophoretic and diffusion properties of HPAM. During the pulse, HPAM would displace due to electrophoresis a distance x_E, which is proportional to its electrophoretic mobility and the electric field, as expressed in Eq. 7. Then, during the pause, HPAM would diffuse back and possibly nullify the electrophoretically induced concentration

polarization, according to Eq. 8. These equations were employed to calculate the displacement of HPAM molecules during the pulse (t_{on}) and pause (t_{off}) times studied in this investigation.

The calculated displacements are included in **Figure 6.13**, which shows them as a function of Q: the equation relating Q and the conductivity of the diluate κD was obtained by plotting the experimental data of various runs, and is included in **Figure A6.5**. The figure shows that the calculated displacements during t_{off} result in horizontal lines, which only depend on the pause time. On the other hand, the displacements calculated due to electrophoresis increase along the desalination process, since they are an inverse function of the conductivity of the diluate.

The lines' intersections in **Figure 6.13** mark the moment at which the back-diffusion does not compensate anymore the HPAM displacement due to electrophoresis. For example, for the 0.1s/0.1s regime, this moment is calculated to occur almost after 2000C have been transported, meaning that, during most part of the ED, the HPAM would have remained in the bulk solution. When having pulses of 1s, the electrophoretic displacement overtakes the one by diffusion sooner during the process, around 1700C for t_{off}= 3s and around 1250C for t_{off}= 1s. According to these calculations, the best performance should have been obtained for the experiments under the 0.1s/0.1s regime, followed by 1s/3s, 1s/1s, and 10s/30s. Although not in that particular order, the results shown in **Figure 6.4B** and **Figure 6.8** coincide with those predictions. For the rest of the regimes, the calculated diffusion is too small to compensate the electrophoretic displacement, so it is likely that several HPAM molecules would reach the membrane surface and start forming a gel layer. Once the HPAM starts forming a gel layer, it would be very difficult to disassemble it by simple diffusion, especially if the overlap concentration is reached. Thus, it is desirable to avoid HPAM reaching and accumulating at the membrane surface; or at least, to delay this moment as much as possible by keeping a short pulse duration. A balance of the electrophoretic mobility with back diffusion was performed to determine how long would the periods need to be to compensate the electrophoresis-based displacement by the diffusion-based one (for t_{on}= t_{off}). For the initial conditions (κD= 7.8 mS/cm), it was calculated that a regime of 5s/5s would equalize the HPAM displacement, while for the final conditions (κD= 1.0 mS/cm), the optimal t_{on}/t_{off} decreases to 0.1s/0.1s. Thus, the experimentally found optimal regime (1s/1s) falls within these values.

6
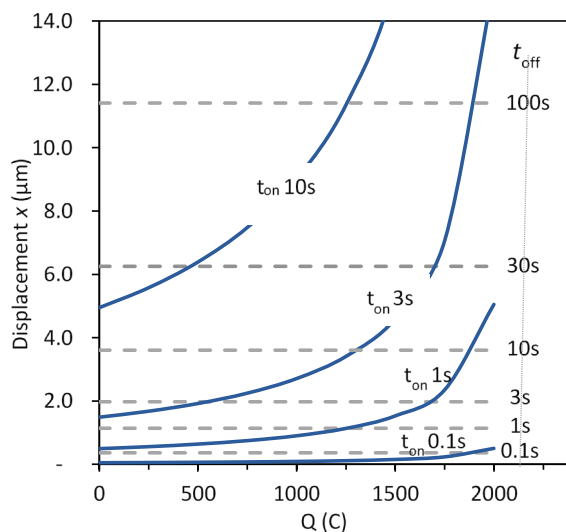
Figure 6.13. *Calculated displacement x of the HPAM molecule vs. transported charges Q. The displacement during the pulse (t_on) was calculated employing Eq. 7, while that during the pause (t_off) was calculated with Eq. 8.*

Finally, since the application of this methodology involved the highly time-consuming method of disassembling the ED stack, the need of a reliable evaluation parameter that would allow a fast screening of the different regimes became evident. Three parameters were chosen: stack resistance, the electrodialysis membrane fouling index (EDMFI) proposed by Lee et al. [30], and a normalized version of the EDMFI. The parameters were calculated for the results involving BW+P, and are presented in **Figure A6.8**-**Figure A6.10**. Overall, the three parameters lead to the same conclusions: the operating regimes with the highest concentration polarization + fouling tendency were the continuous and the backpulse mode. In a similar way, the evaluation parameters pointed out that the 10s/30s and 1s/3s regimes were the best for mitigating the negative effects of concentration polarization and fouling. This ranking coincided with the one obtained from the electric potential measurements (**Figure 6.4B**) on both the best and worst regimes to use, corroborating that the latter is a reliable reference for performance.

6.4 Conclusions

The use of pulsed electric field to desalinate polymer-flooding produced water improved the performance in terms of demineralization percentage and energy consumption. In general, the shorter the pulse periods, the higher the demineralization rate and the lower the energy consumption. The only exception was for the runs with 0.1s pulses, which rendered low energy consumption but also lower demineralization percentages, possibly because the high frequency could cause a closest packing of the HPAM [30]. For regimes with the same pulse and

different pause period, longer pauses yielded lower energy consumptions, but also lower demineralization of the stream.

For a feed stream consisting of brackish water + HPAM, the best performances were obtained employing the regimes 1s/1s (in terms of achieved demineralization) and 1s/3s (regarding energy consumption). Both regimes provided similar results in terms of fouling development. Thus, choosing an optimal regime results a complicated task. When comparing the performance of the 1s/1s and the 1s/3s regimes, the gain in energy consumption for 1s/3s is higher than the gain in demineralization for 1s/1s. However, the regime 1s/3s also implies that the membrane stack is effectively in use only 25% of the time. Considering all these factors, the most promising of the regimes would be 1s/1s. Still, it is likely that other combinations of pulse and pause would also yield favorable results, especially if the pulse time is under 5s.

The addition of oil to the solutions did not influence significantly the performance results, and in many cases, they were slightly better in the presence of oil. This result supports the idea that the HPAM gel layer becomes less stable when oily compounds are present in the solution.

The membrane analysis showed that minor fouling developed on both kinds of membranes, anionic and cationic. The fouling was in the form of amorphous precipitates consisting mainly of HPAM and some calcium precipitates. The HPAM fouling was loosely adhered to the CEM, while that on the AEM was not easily removed. The presence of crude oil in the solution slightly increased the amount of membrane fouling.

Since the ED stack has good hydrodynamic properties, the formation of HPAM gel layers was minimized, especially when compared to our previous observations from experiments performed in a six-compartment cell [45]. Therefore, for future experiments, it would be desirable to evaluate the membranes after longer use periods. Finally, it is worth to mention that the application of PEF to desalinate streams in a larger scale, would depend on the availability of power sources designed to be continuously switched on and off.

References

[1]   H. Strathmann, Electromembrane Processes: Basic Aspects and Applications, in: Comprehensive Membrane Science and Engineering, Elsevier B.V., 2010: pp. 391–429. doi:DOI: 10.1016/B978-0-08-093250-7.00048-7.

[2]   S. Mikhaylin, V. Nikonenko, G. Pourcelly, L. Bazinet, Intensification of demineralization process and decrease in scaling by application of pulsed electric field with short pulse/pause

conditions, Journal of Membrane Science. 468 (2014) 389–399. doi:10.1016/j.memsci.2014.05.045.

[3]   J.H. Choi, J.S. Park, S.H. Moon, Direct measurement of concentration distribution within the boundary layer of an ion-exchange membrane, Journal of Colloid and Interface Science. 251 (2002) 311–317. doi:10.1006/jcis.2002.8407.

[4]   S. Mikhaylin, L. Bazinet, Fouling on ion-exchange membranes: Classification, characterization and strategies of prevention and control, Advances in Colloid and Interface Science. 229 (2016) 34–56. doi:10.1016/j.cis.2015.12.006.

[5]   E. Korngold, F. de Korosy, R. Rahav, M.F. Taboch, Fouling of anionselective membranes in electrodialysis, Desalination. 8 (1970) 195–220. doi:10.1016/S0011-9164(00)80230-1.

[6]   J. Guolin, W. Xiaoyu, H. Chunjie, The effect of oilfield polymer-flooding wastewater on anion-exchange membrane performance, Desalination. 220 (2008) 386–393. doi:10.1016/j.desal.2007.03.010.

[7]   H. Guo, L. Xiao, S. Yu, H. Yang, J. Hu, G. Liu, Y. Tang, Analysis of anion exchange membrane fouling mechanism caused by anion polyacrylamide in electrodialysis, Desalination. 346 (2014) 46–53. doi:10.1016/j.desal.2014.05.010.

[8]   X. Zuo, L. Wang, J. He, Z. Li, S. Yu, SEM-EDX studies of SiO2/PVDF membranes fouling in electrodialysis of polymer-flooding produced wastewater: Diatomite, APAM and crude oil, Desalination. 347 (2014) 43–51. doi:10.1016/j.desal.2014.05.020.

[9]   H. Guo, F. You, S. Yu, L. Li, D. Zhao, Mechanisms of chemical cleaning of ion exchange membranes: A case study of plant-scale electrodialysis for oily wastewater treatment, Journal of Membrane Science. 496 (2015) 310–317. doi:10.1016/j.memsci.2015.09.005.

[10]   T. Wang, S. Yu, L. an Hou, Impacts of HPAM molecular weights on desalination performance of ion exchange membranes and fouling mechanism, Desalination. 404 (2017) 50–58. doi:10.1016/j.desal.2016.10.007.

[11]   Q. Xia, H. Guo, Y. Ye, S. Yu, L. Li, Q. Li, R. Zhang, Study on the fouling mechanism and cleaning method in the treatment of polymer flooding produced water with ion exchange membranes, RSC Adv. 8 (2018) 29947–29957. doi:10.1039/c8ra05575k.

[12]   P.A. Sosa-Fernandez, J.W. Post, H. Bruning, F.A.M. Leermakers, H.H.M. Rijnaarts, Electrodialysis-based desalination and reuse of sea and brackish polymer-flooding produced water, Desalination. 447 (2018) 120–132. doi:10.1016/j.desal.2018.09.012.

[13]   P.A. Sosa-Fernandez, J.W. Post, F.A.M. Leermakers, H.H.M. Rijnaarts, H. Bruning, Removal of divalent ions from viscous polymer-flooding produced water and seawater via electrodialysis, Journal of Membrane Science. 589 (2019) 117251. doi:10.1016/j.memsci.2019.117251.

[14]   G. Riethmuller, A. Abri, N. Al Azri, G. Stapel, S. Nijman, W. Subhi, R. Mehdi, Opportunities and Challenges of Polymer Flooding in Heavy Oil Reservoir in South of Oman, SPE EOR Conference at Oil and Gas West Asia. (2014). doi:10.2118/169737-MS.

[15]   J. Guolin, X. Lijie, L. Yang, D. Wenting, H. Chunjie, Development of a four-grade and four-segment electrodialysis setup for desalination of polymer-flooding produced water, Desalination. 264 (2010) 214–219. doi:10.1016/j.desal.2010.06.042.

[16]   D.A.Z. Wever, F. Picchioni, A.A. Broekhuis, Polymers for enhanced oil recovery: A paradigm for structure-property relationship in aqueous solution, Progress in Polymer Science (Oxford). 36 (2011) 1558–1628. doi:10.1016/j.progpolymsci.2011.05.006.

[17]   P. Długołecki, J. Dabrowska, K. Nijmeijer, M. Wessling, Ion conductive spacers for increased

power generation in reverse electrodialysis, Journal of Membrane Science. 347 (2010) 101–107. doi:10.1016/j.memsci.2009.10.011.

[18]   D.A. Vermaas, M. Saakes, K. Nijmeijer, Power generation using profiled membranes in reverse electrodialysis, Journal of Membrane Science. 385–386 (2011) 234–242. doi:10.1016/j.memsci.2011.09.043.

[19]   D. Vermaas, David A. Kunteng, J. Veerman, M. Saakes, K. Nijmeijer, Periodic Feedwater Reversal and Air Sparging As Antifouling Strategies in Reverse Electrodialysis, Environmental Science and Technology. 48 (2014) 3065–3073. doi:org/10.1021/es4045456.

[20]   C. Casademont, P. Sistat, B. Ruiz, G. Pourcelly, L. Bazinet, Electrodialysis of model salt solution containing whey proteins : Enhancement by pulsed electric field and modified cell configuration, Journal of Membrane Science. 328 (2009) 238–245. doi:10.1016/j.memsci.2008.12.013.

[21]   S. Mulyati, R. Takagi, A. Fujii, Y. Ohmukai, T. Maruyama, H. Matsuyama, Improvement of the antifouling potential of an anion exchange membrane by surface modification with a polyelectrolyte for an electrodialysis process, Journal of Membrane Science. 417–418 (2012) 137–143. doi:10.1016/j.memsci.2012.06.024.

[22]   X.H. Zhen, S.L. Yu, B.F. Wang, H.F. Zheng, H. Ban, B.L. Miao, Ultrafiltration experiment of electrodialysis pretreatment for produced water desalination, Zhongguo Shiyou Daxue Xuebao (Ziran Kexue Ban)/Journal of China University of Petroleum (Edition of Natural Science). 30 (2006) 134–137.

[23]   Y. Oren, E. Korngold, N. Daltrophe, R. Messalem, Y. Volkman, L. Aronov, M. Weismann, N. Bouriakov, P. Glueckstern, J. Gilron, Pilot studies on high recovery BWRO-EDR for near zero liquid discharge approach, Desalination. 261 (2010) 321–330. doi:10.1016/j.desal.2010.06.010.

[24]   N. Cifuentes-Araya, G. Pourcelly, L. Bazinet, Impact of pulsed electric field on electrodialysis process performance and membrane fouling during consecutive demineralization of a model salt solution containing a high magnesium / calcium ratio, Journal of Colloid and Interface Science. 361 (2011) 79–89. doi:10.1016/j.jcis.2011.05.044.

[25]   N.A. Mishchuk, L.K. Koopal, F. Gonzalez-Caballero, Intensification of electrodialysis by applying a non-stationary electric field, Colloids and Surfaces A: Physicochemical and Engineering Aspects. 176 (2001) 195–212.

[26]   Y. V Karlin, V.N. Kropotov, Electrodialysis separation of Na+ and Ca2+ in a pulsed current mode, Russ. J. Electrochem. 31 (1995).

[27]   P. Malek, J.M. Ortiz, B.S. Richards, A.I. Schäfer, Electrodialytic removal of NaCl from water: Impacts of using pulsed electric potential on ion transport and water dissociation phenomena, Journal of Membrane Science. 435 (2013) 99–109. doi:10.1016/j.memsci.2013.01.060.

[28]   H.J. Lee, S.H. Moon, Enhancement of electrodialysis performances using pulsing electric fields during extended period operation, Journal of Colloid and Interface Science. (2005). doi:10.1016/j.jcis.2005.02.027.

[29]   H.K. Hansen, A. Rojo, Testing pulsed electric fields in electroremediation of copper mine tailings, Electrochimica Acta. 52 (2007) 3399–3405. doi:10.1016/j.electacta.2006.07.064.

[30]   H.J. Lee, S.H. Moon, S.P. Tsai, Effects of pulsed electric fields on membrane fouling in electrodialysis of NaCl solution containing humate, Separation and Purification Technology. 27 (2002) 89–95. doi:10.1016/S1383-5866(01)00167-8.

6

[31]   J.S. Park, H.J. Lee, S.H. Moon, Determination of an optimum frequency of square wave power for fouling mitigation in desalting electrodialysis in the presence of humate, Separation and Purification Technology. 30 (2003) 101–112. doi:10.1016/S1383-5866(02)00138-7.

[32]   B. Ruiz, P. Sistat, P. Huguet, G. Pourcelly, M. Araya-Farias, L. Bazinet, Application of relaxation periods during electrodialysis of a casein solution: Impact on anion-exchange membrane fouling, Journal of Membrane Science. 287 (2007) 41–50. doi:10.1016/j.memsci.2006.09.046.

[33]   N. Cifuentes-Araya, G. Pourcelly, L. Bazinet, Water splitting proton-barriers for mineral membrane fouling control and their optimization by accurate pulsed modes of electrodialysis, Journal of Membrane Science. 447 (2013) 433–441. doi:10.1016/j.memsci.2013.06.055.

[34]   P. Sistat, P. Huguet, B. Ruiz, G. Pourcelly, S.A. Mareev, V. V. Nikonenko, Effect of pulsed electric field on electrodialysis of a NaCl solution in sub-limiting current regime, Electrochimica Acta. 164 (2015) 267–280. doi:10.1016/j.electacta.2015.02.197.

[35]   A.R. Al-Hashmi, T. Divers, R.S. Al-Maamari, C. Favero, A. Thomas, Improving polymer flooding efficiency in Oman oil fields. Paper SPE-179834-MS, in: SPE EOR Conference at Oil and Gas West Asia Held in Muscat, Oman, 21–23 March 2016., SPE, Muscat, 2016: p. 18.

[36]   P. Długołecki, P. Ogonowski, S.J. Metz, M. Saakes, K. Nijmeijer, M. Wessling, On the resistances of membrane, diffusion boundary layer and double layer in ion exchange membrane transport, Journal of Membrane Science. 349 (2010) 369–379. doi:10.1016/j.memsci.2009.11.069.

[37]   S. Mulyati, R. Takagi, A. Fujii, Y. Ohmukai, H. Matsuyama, Simultaneous improvement of the monovalent anion selectivity and antifouling properties of an anion exchange membrane in an electrodialysis process, using polyelectrolyte multilayer deposition, Journal of Membrane Science. 431 (2013) 113–120. doi:10.1016/j.memsci.2012.12.022.

[38]   A.H. Galama, D.A. Vermaas, J. Veerman, M. Saakes, H.H.M. Rijnaarts, J.W. Post, K. Nijmeijer, Membrane resistance: The effect of salinity gradients over a cation exchange membrane, Journal of Membrane Science. 467 (2014) 279–291. doi:10.1016/j.memsci.2014.05.046.

[39]   S. Galier, H.R. De Balmann, The electrophoretic membrane contactor: A mass-transfer-based methodology applied to the separation of whey proteins, Separation and Purification Technology. 77 (2011) 237–244. doi:10.1016/j.seppur.2010.12.013.

[40]   K. Aoki, B. Wang, J. Chen, T. Nishiumi, Diffusion coefficients in viscous sodium alginate solutions, Electrochimica Acta. 83 (2012) 348–353. doi:10.1016/j.electacta.2012.08.004.

[41]   S. Peng, C. Wu, Light Scattering Study of the Formation and Structure of Partially Hydrolyzed Poly(acrylamide)/Calcium(II) Complexes, Macromolecules. 32 (1999) 585–589.

[42]   M.A. Andreeva, V. V. Gil, N.D. Pismenskaya, L. Dammak, N.A. Kononenko, C. Larchet, D. Grande, V. V. Nikonenko, Mitigation of membrane scaling in electrodialysis by electroconvection enhancement, pH adjustment and pulsed electric field application, Journal of Membrane Science. 549 (2018) 129–140. doi:10.1016/j.memsci.2017.12.005.

[43]   N. Lemay, S. Mikhaylin, L. Bazinet, Voltage spike and electroconvective vortices generation during electrodialysis under pulsed electric field: Impact on demineralization process efficiency and energy consumption, Innovative Food Science and Emerging Technologies. 52 (2019) 221–231. doi:10.1016/j.ifset.2018.12.004.

[44]   G. Dufton, S. Mikhaylin, S. Gaaloul, L. Bazinet, Positive impact of pulsed electric field on lactic acid removal, demineralization and membrane scaling during acid whey electrodialysis,

International Journal of Molecular Sciences. 20 (2019). doi:10.3390/ijms20040797.

[45]   P.A. Sosa-Fernandez, S.J. Miedema, H. Bruning, F.A.M. Leermakers, H.H.M. Rijnaarts, J.W. Post, Influence of solution composition on fouling of anion exchange membranes desalinating polymer-flooding produced water, Journal of Colloid And Interface Science. 557 (2019) 381–394. doi:10.1016/j.jcis.2019.09.029.

[46]   Y. Kim, W.S. Walker, D.F. Lawler, Competitive separation of di- vs mono-valent cations in electrodialysis: Effects of the boundary layer properties, Water Research. 46 (2012) 2042–2056. doi:10.1016/j.watres.2012.01.004.

[47]   L. Firdaous, J.P. Malériat, J.P. Schlumpf, F. Quéméneur, Transfer of monovalent and divalent cations in salt solutions by electrodialysis, Separation Science and Technology. 42 (2007) 931–948. doi:10.1080/01496390701206413.

[48]   M. Haddad, L. Bazinet, O. Savadogo, J. Paris, Electrochemical acidification of Kraft black liquor: Impacts of pulsed electric field application on bipolar membrane colloidal fouling and process intensification, Journal of Membrane Science. 524 (2017) 482–492. doi:10.1016/j.memsci.2016.10.043.

[49]   G. Dufton, S. Mikhaylin, S. Gaaloul, L. Bazinet, Systematic study of the impact of pulsed electric field parameters (Pulse/pause duration and frequency) on ED performances during acid whey treatment, Membranes. 10 (2020). doi:10.3390/membranes10010014.

[50]   D.A. Vermaas, D. Kunteng, M. Saakes, K. Nijmeijer, Fouling in reverse electrodialysis under natural conditions, Water Research. 47 (2013) 1289–1298. doi:10.1016/j.watres.2012.11.053.

[51]   V. Lindstrand, A.S. Jönsson, G. Sundström, Organic fouling of electrodialysis membranes with and without applied voltage, Desalination. 130 (2000) 73–84. doi:10.1016/S0011-9164(00)00075-8.

[52]   X. Guo, L. Liu, W. Wang, J. Zhang, Y. Wang, S.H. Yu, Controlled crystallization of hierarchical and porous calcium carbonate crystals using polypeptide type block copolymer as crystal growth modifier in a mixed solution, CrystEngComm. 13 (2011) 2054–2061. doi:10.1039/c0ce00202j.

[53]   N. Cifuentes-Araya, G. Pourcelly, L. Bazinet, How pulse modes affect proton-barriers and anion-exchange membrane mineral fouling during consecutive electrodialysis treatments, Journal of Colloid and Interface Science. 392 (2013) 396–406. doi:10.1016/j.jcis.2012.09.067.

[54]   N. Cifuentes-Araya, C. Astudillo-Castro, L. Bazinet, Mechanisms of mineral membrane fouling growth modulated by pulsed modes of current during electrodialysis: Evidences of water splitting implications in the appearance of the amorphous phases of magnesium hydroxide and calcium carbonate, Journal of Colloid and Interface Science. 426 (2014) 221–234. doi:10.1016/j.jcis.2014.03.054.

[55]   W. Wang, R. Fu, Z. Liu, H. Wang, Low-resistance anti-fouling ion exchange membranes fouled by organic foulants in electrodialysis, Desalination. 417 (2017) 1–8. doi:10.1016/j.desal.2017.05.013.

6

Appendix 6A. Supplementary material
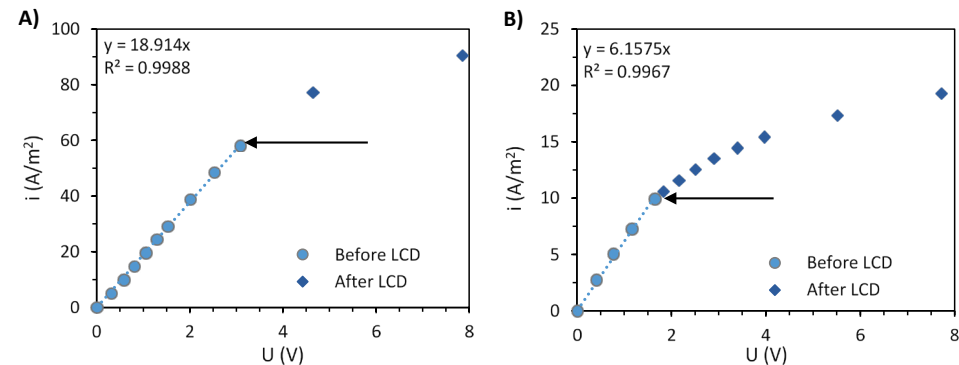
Figure A6.1. *Determination of the limiting current density (LCD) for BW+P solution of **A)** 7.8 mS/cm and, **B)** 1.5 mS/cm. The current density i is plotted versus the electric potential U. The LCD, signaled with the arrows, corresponds to the last data point falling within the linear trendline.*
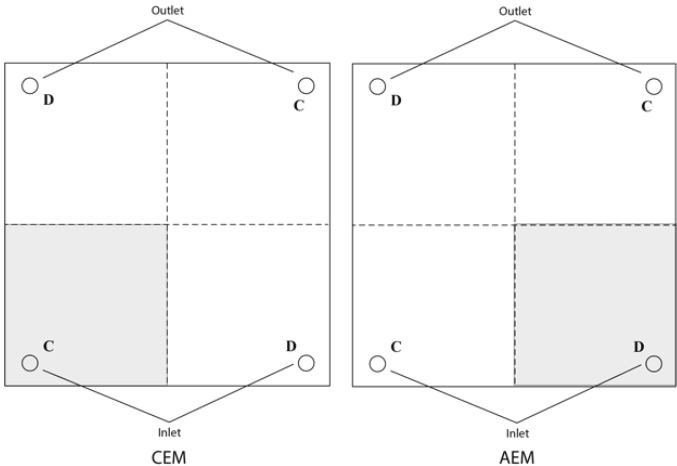

Figure A6.2. *Illustration of the cutting of the recovered membranes. SEM, EDX and rinsing water analyses were performed for the lower parts, were the inlets are located.*
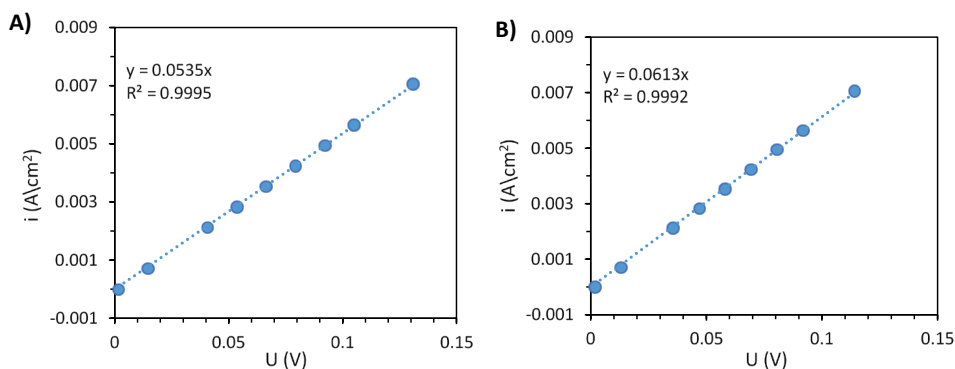
Figure A6.3. Examples of electrical resistance measurements. The current density i is plotted versus the measured voltage U, and the area resistance is calculated as the inverse of the slope of the trendline. A) i-U curve from the CEM recovered after the BW run, and B) blank i-U curve of solution without membrane.
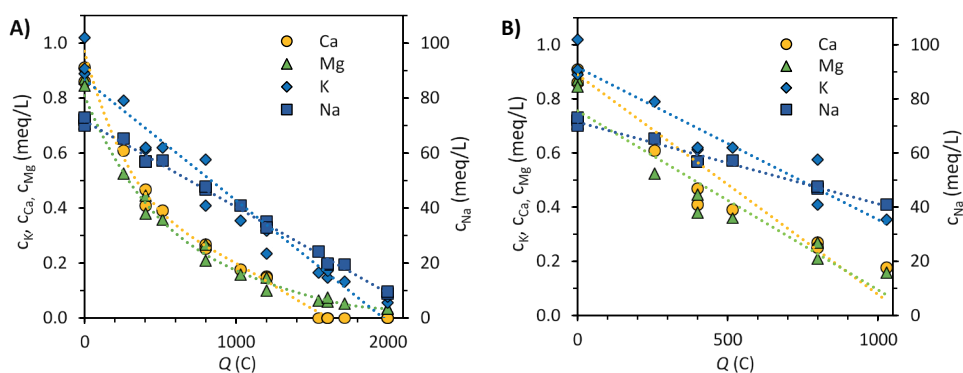
Figure A6.4. Concentration (c) of cations vs. transported charges Q in the diluate, taken from the ED runs with 3s/1s regime. c of K, Ca, and Mg is represented in the left axis, while c for Na is represented in the right one. In A), it is apparent that Na and K concentrations follow a lineal decrease, while Ca and Mg decrease as a 2nd order function. B) Same data but considering only samples taken before 1050 C fitted to linear trend-lines. The plots include data from 3 independent experiments.

6
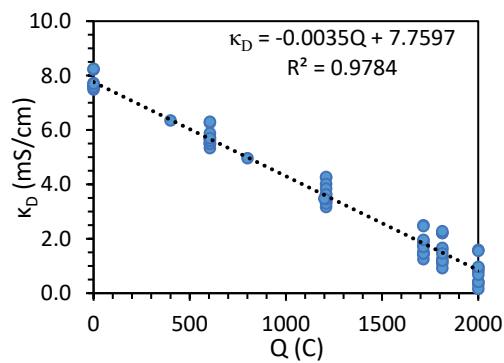
Figure A6.5. *Conductivity in the diluate κ_D as a function of transported charges Q. The plot allowed to obtain the linear equation relating both variables, which was later employed in the calculation of the displacement by electrophoresis.*
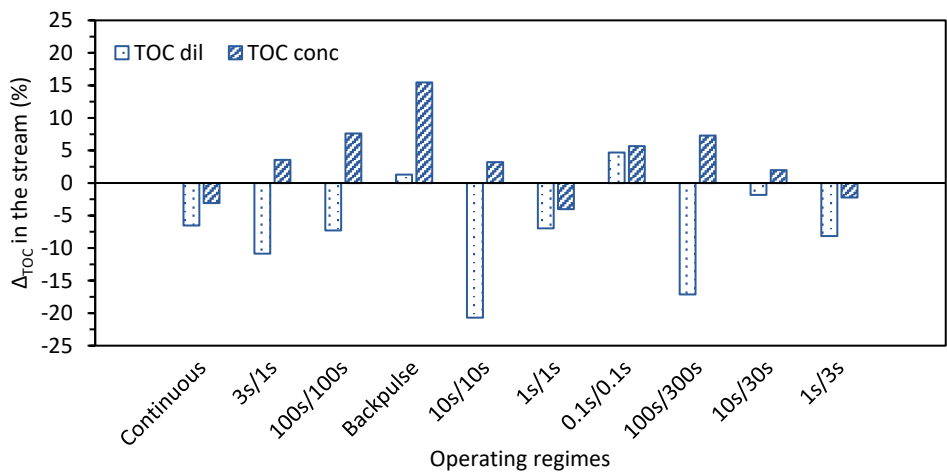
Figure A6.6. *Δ_{TOC} analysis for the experiments with BW+P+O feed solutions*
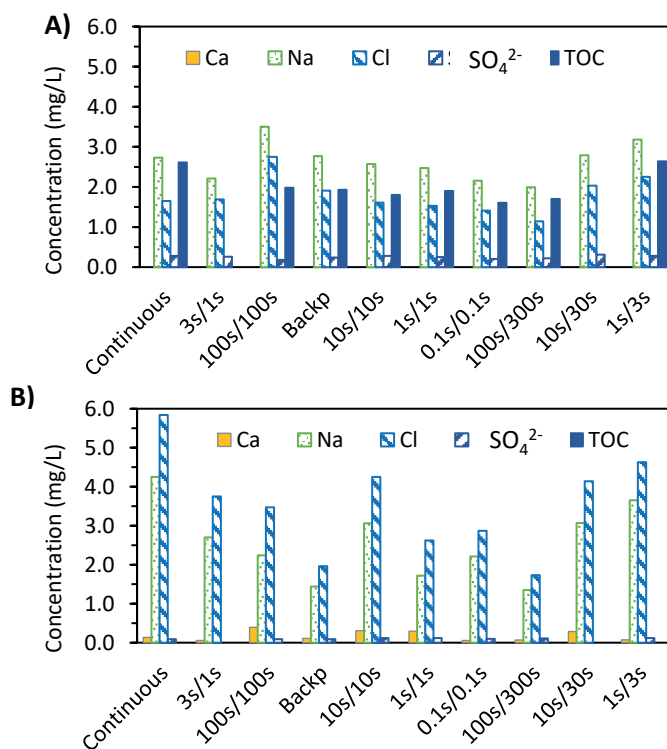
Figure A6.7. *Concentration of species in rinsing solution of membranes recovered after the ED of feed solutions BW+P+O. A) and B) show, respectively, the results from the CEMs and AEMs.*

Table A6.1. *EDX elemental analysis of CEMs recovered from selected ED experiments (sup. Table 6.4)*

Feed solution	Experiment	Side	Percentage (%)							
			C	N	O	Na	Mg	S	Cl	Ca
BW+P	Continuous	D	60.88	9.46	20.60	2.34	0.17	5.63	-	0.85
		C	58.50	9.95	21.49	2.90	0.15	5.67	0.37	0.90
	100s/100s	D	63.27	7.65	20.37	2.17	0.15	4.83	0.01	1.33
		C	61.85	8.92	20.35	2.47	0.17	5.24	0.06	0.78
	1s/1s	D	61.48	8.63	21.40	2.30	0.20	4.59	0.02	1.22
		C	61.02	8.68	20.80	2.75	0.21	5.71	0.05	0.62
	1s/3s	D	62.90	7.49	20.65	2.59	0.15	5.32	0.02	0.71
		C	61.94	8.02	21.17	2.62	0.15	5.25	0.01	0.66
	0.1s/0.1s	D	63.67	7.45	20.18	2.58	0.15	5.16	0.04	0.63
		C	61.39	7.99	21.44	2.62	0.15	5.48	0.03	0.78

Table A6.2. *EDX elemental analysis of AEMs recovered from selected ED experiments (sup. Table 6.5).*

Feed solution	Experiment	Side	Percentage (%)							
			C	N	O	Na	Mg	S	Cl	Ca
BW+P+O	Continuous	D	75.07	11.06	9.35	0.04	-	0.16	4.29	0.01
		C	75.58	10.93	8.51	0.04	-	0.22	4.67	-
	100s/100s	D	74.77	11.33	8.70	0.05	-	0.17	4.95	0.01
		C	76.02	10.67	8.92	0.04	0.01	0.16	4.16	-
	1s/1s	D	73.73	11.12	9.77	0.07	0.03	0.19	5.01	0.01
		C	72.99	11.67	9.93	0.13	0.04	0.19	4.99	0.02
	1s/3s	D	75.25	10.73	9.28	0.13	0.01	0.12	4.45	-
		C	60.39	7.38	22.84	2.84	0.20	5.49	0.04	0.58
	0.1s/0.1s	D	73.72	10.74	9.84	0.08	0.01	0.20	5.35	0.02
		C	74.15	10.35	10.64	0.10	-	0.14	4.56	0.02

Appendix 6B. Evaluation of fouling indexes methods

During this research, diverse fouling evaluation parameters were calculated and related to the obtained results, aiming to avoid opening the ED stack to determine if certain current regimes were being effective against fouling. The results are only presented for the BW+P solutions because the presence of crude oil did not seem to exert a significant influence in the ED performance.

Stack resistance

The stack resistance can provide an indication of fouling occurring during the electrodialysis. It was calculated from the potential and current data using Ohm's law, and the results for the BW+P solutions are shown in **Figure A6.8**. The resistance remained low and constant during the first half of the experiments, starting to increase only after approximately 1200 C had been transferred. The highest increase was computed for the backpulse regime, followed by the continuous one and the 100s/100s. The lower resistances were recorded for the regimes 10s/30s and 1s/3s, which indicates that pauses of 10s and 1s were not enough to eliminate the concentration polarization attained in the system during the pulses.
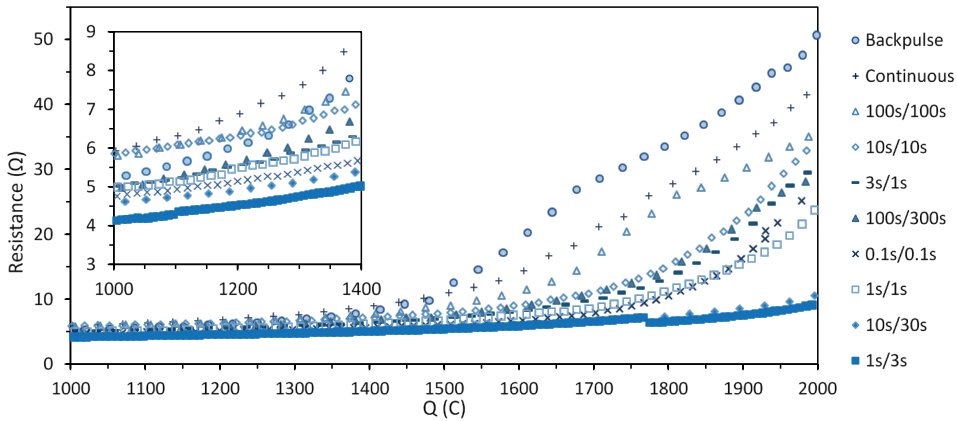
Figure A6.8. Calculated membrane stack resistance vs. transported charges Q during the electrodialysis of BW+P solution through different current regimes.

Electrodialysis Membrane Fouling Index (EDMFI)

The Electrodialysis Membrane Fouling Index (EDMFI) is another option to assess the effectiveness of anti-fouling treatments [30]. EDMFI derives from the model of formation of a gel layer on the IEM surface during electrodialysis. It considers that the concentration of deposited foulants on the surface increases proportionally to the time and forms a gel layer, which is then providing an additional resistance for the ED process. For a constant current, the EDMFI can be calculated by plotting the potential drop $U(t)$ over the squared current (I^2) against time [31]:

$$\frac{U(t)}{I^2} = \frac{R_m}{I} + (EDMFI)t \qquad \text{/6.9/}$$

Where R_m is the membrane resistance (Ω). The slope of the curve represents the EDMFI for the experiment, and higher index values imply a greater fouling potential.

Figure A6.9 shows the calculated values for a set of runs with BW+P solution. The application of PEF diminishes the fouling tendency of the system, as indicated by the lower slope. It shows that a shorter duration of applied current could lower the membrane index fouling. Furthermore, the application of long pauses is even more effective in reducing the EDMFI value, thus dropping the fouling tendency of ED. The operating regimes 10s/30s and 1s/3s resulted in the lowest fouling index.
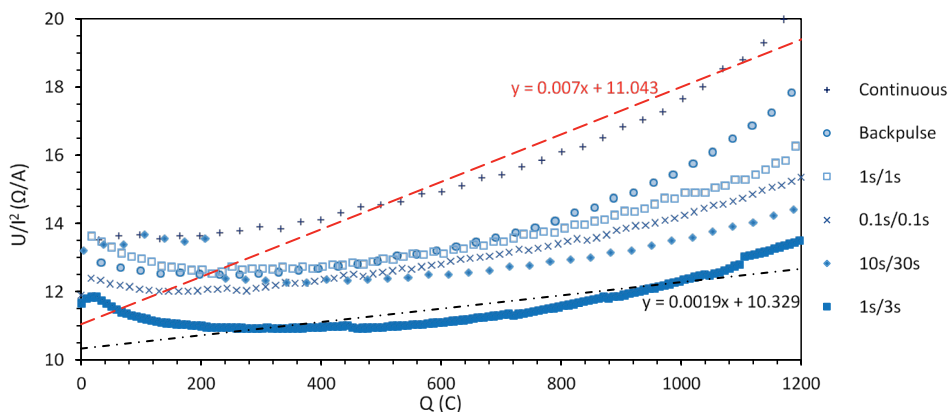
Figure A6.9. U over I^2 vs. transported charges Q for selected runs with BW+P solution. Linear trendlines are presented for the continuous (red) and for the 1s/3s intermittent regime (black). The slopes of the lines represent the Electrodialysis Membrane Fouling Index (EDMFI), as proposed by Lee et al. [30]. A greater slope means a higher EDMFI and a higher fouling tendency.

Normalized EDMFI

A modified version of the Membrane Fouling Index for Electrodialysis (EDMFI) proposed by Lee et al. [30] was employed as a quantitative indicator of the fouling tendency in the membrane system. The resulting plot is shown as **Figure A6.10.**
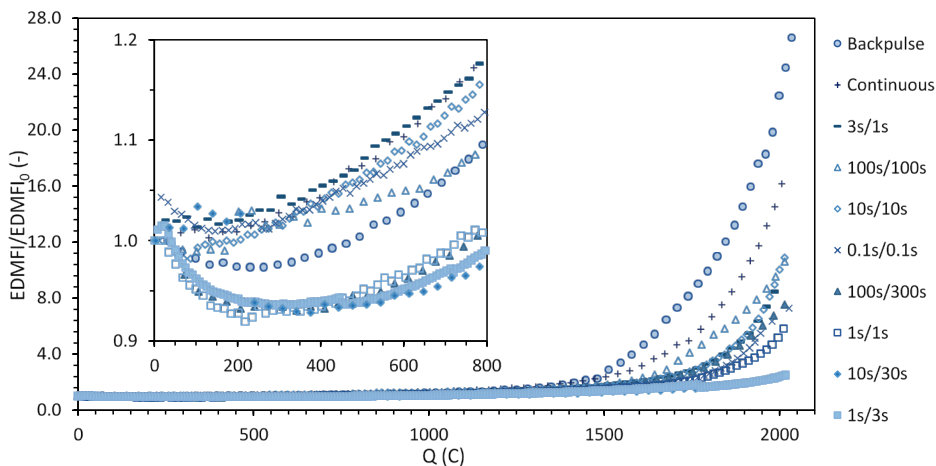
Figure A6.10. EDMFI over $EDMFI_0$ vs. transported charges Q for a set of electrodialysis experiments desalinating BW+P solutions.

6

Chapter 7

Electrodialysis reversal for desalination of (waste)water produced after polymer-flooding: performance related to anion exchange membrane characteristics
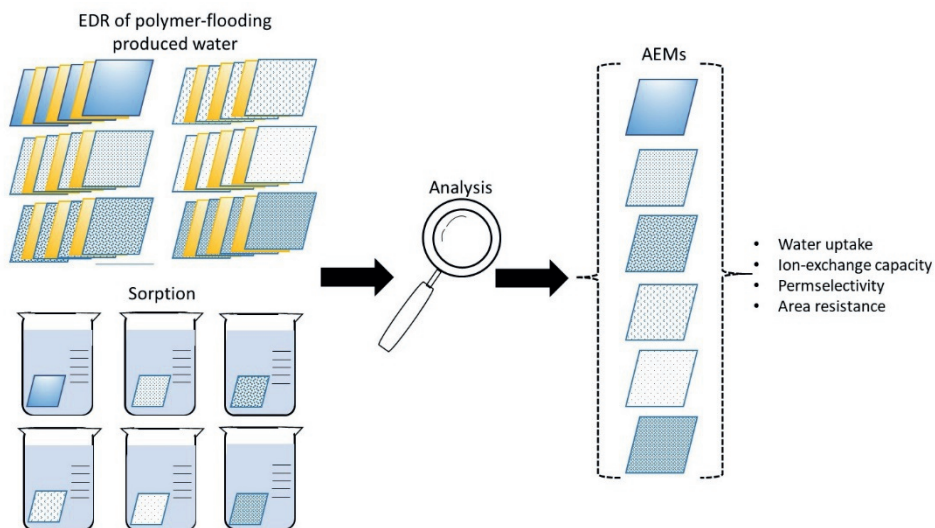
Abstract

Electrodialysis (ED) has been recently proposed to desalinate polymer-flooding produced water (PFPW), a byproduct stream from the oil and gas industry rich in charged polymers. However, process performance is limited by fouling occurring on the ion-exchange membranes, particularly on the anionic ones (AEMs). Thus, this study aimed to correlate the properties of different AEMs with their performance while desalinating PFPW, ultimately evaluating their significance when fouling is to be minimized and operation improved. Six stacks containing different homogeneous and commercially available AEMs were employed to desalinate synthetic PFPW during 8-days ED experiments operated in reversal mode. AEMs recovered from the stacks were analyzed in terms of water uptake, ion-exchange capacity, permselectivity, and area resistance, and compared against virgin AEMs. Relatively small changes were measured for most of the parameters evaluated. For most AEMs, the water uptake and resistance increased, while the IEC and permselectivity decreased during operation. Ultimately, AEMs with high area resistance were linked to the fast development of limiting current conditions in the stack, so this property turned out to be the most relevant when desalinating PFPW.

7.1 Introduction

Electrodialysis (ED) is a versatile electro-membrane process capable of removing ions and small charged particles from a stream by applying an electric potential over an arrangement of ion-exchange membranes (IEMs) [1,2]. One of its most recent applications is the treatment of polymer-flooding produced water (PFPW), an abundant stream from the oil and gas industry obtained after applying polymer flooding technology [3–5]. After reducing its salinity, PFPW could be reused to confect viscous flooding solution without the need to add excessive amounts of viscosifying polymer and chemicals, increasing chemical use efficiency, thus leading to environmental and economic benefits [6,7]. However, membrane fouling remains a recurrent issue that needs to be tackled to expedite the application of ED at an industrial scale [8,9].

Fouling denotes the undesirable attachment of species on the surface or the inner part of a membrane [10]. Fouling can appear as a consequence of concentration polarization, for example, due to the accumulation of salts beyond their maximum solubility (scaling), or propitiated by the local changes in pH when water dissociates on the surface of the IEMs [11]. Ultimately, fouling causes alterations in the membrane structure, decreased membrane permselectivity, water dissociation, and reduced process performance [10]. These complications also affect the desalination of PFPW, making fouling a critical issue to be resolved when treating such industrial water streams [12–14]. Since PFPW contains a mixture of organic compounds, dissolved gases, solid impurities, and minerals [15], fouling can be easily formed on the IEMs. The positively-charged anion exchange membranes (AEMs) are especially prone to be fouled by negatively-charged organic molecules, like partially hydrolyzed polyacrylamide (HPAM) [13,16,17], which is the most commonly employed viscosifier in polymer-flooding oil and gas reservoirs under exploitation [18].

Although the fouling nature of the feed solution is difficult to amend, there exist several strategies to control fouling during ED. A fundamental approach is the control of the hydrodynamic conditions to ensure the adequate mixing of the streams, and thus minimize concentration polarization. Adequate mixing is generally achieved by pumping at high flowrates, employing spacers designed to increase the turbulence, and by sparging air or other gases into the stack [19]. Besides, there are other strategies to prevent and control fouling during ED: application of electrodialysis with polarity reversal (EDR), incorporation of pretreatments, use of pulsed electric field, modification of the membranes, and the design of specific cleaning routines [10,20]. In EDR, the concentrating and diluting compartments are alternatively switched by periodically reversing the direction of the electric current [15,21]. In this way, ions for which the membranes are permeable pass through the membranes moving in the opposite direction, while impurities

adsorbed on the membranes are removed. However, one of the main disadvantages of EDR is the reduced efficiency due to the streams mixing every time that they are switched. Many of the other strategies have already been tested for desalinating PFPW. Ultrafiltration (UF) has been incorporated as a standard pretreatment since it reduced the severity of fouling on the IEMs. However, fouling still occurs since UF does not eliminate all the organic components present in the stream [16,22,23]. Cleaning routines have also been tested and optimized to remove the particular fouling caused by PFPW [12,14]. However, their use can also lead to potential negative impacts on membrane selectivity and performance [10,24].

Another of the strategies, the application of pulsed electric field (PEF), was recently tested by our research group for desalinating PFPW [25]. Besides concluding that concentration polarization caused most of the decreases in performance, it was surprising to observe that the fouling on the IEMs was minimal, especially considering our previous studies [6,13]. These observations included membranes utilized to desalinate PFPW with HPAM and crude oil in the continuous mode. Two reasons could explain the results: i) the duration of the experiments (2-6 hours) was too short for producing significant fouling, and ii) the type of membranes employed (FujiFilm type 10, based on an aliphatic matrix) also influenced the results.

In this line, recent investigations also suggest that the chemistry of the membranes and its water content are the main factors influencing the fouling of organic compounds [26]. When studying fouling by PFPW on PVDF membranes, Zuo et al. explained the antifouling characteristics of SiO_2/PVDF AEMs in terms of their hydrophilicity. They described that the mixture SiO_2/PVDF was more hydrophilic than PVDF alone, which allowed these membranes to interact stronger with the water molecules than with the organic and oily components in the feed [27]. Also, while performing electrodialysis on PFPW, Wang et al. concluded that the fouling on heterogeneous IEMs was more severe than the one on homogeneous IEMs due to physical blockage [16].

As presented, there are various indications that AEMs susceptibility to fouling when desalting PFPW, relates to material and matrix characteristics. Besides water content, it is desired to know which other membrane characteristics can be correlated to a high or low fouling incidence by treating PFPW. Thus, the general objective of this study is to determine which AEM properties are beneficial in terms of minimizing the effects of fouling and improving the performance when employed to desalinate PFPW. The research is focused on six commercially available homogeneous AEMs, which were employed to desalinate PFPW during relatively long term-experiments. To extend the process lifetime and increase membrane exposure, the EDR operation mode was employed, as it would be commonly used when desalinating industrial water. Then, the membranes were recovered, and their

properties evaluated. The results were compared against the properties measured for virgin membranes, and for membranes soaked in the feed solutions without the application of an electric potential (sorption experiments), aiming to improve the understanding of the role of membrane material on fouling.

7.2 Materials and methods

Experiments were planned to evaluate the performance of six different kinds of AEMs during long term electrodialysis runs with polarity reversal. After the ED experiments, the membranes were recovered from the stack, and their properties analyzed.

7.2.1 Materials

7.2.1.1 *Preparation of solutions*

The composition of the synthetic feed solution employed for all experiments was based on that of the brackish water (BW) in the Marmul field in Oman [28], as outlined in **Table 7.1**. All the salts employed (NaCl, KCl, $MgCl_2.6H2O$, $CaCl_2.2H2O$, Na_2SO_4, and $NaHCO_3$) were analytical grade, purchased from VWR (Belgium), and used without further purification.

Table 7.1. *Ionic composition of synthetic brackish water (BW) solution.*

Ion	Concentration (mM)
Na^+	73.92
K^+	0.72
Ca^{2+}	0.65
Mg^{2+}	0.46
Cl^-	56.24
HCO_3^-	15.59
SO_4^{2-}	2.51

Synthetic polymer-flooding produced water was prepared by adding the necessary amount of partially hydrolyzed polyacrylamide (HPAM) to 10.0 L of BW solution under fast stirring (~750 rpm). After pouring the HPAM, the stirring rate was reduced to 250 rpm, and the solution was left mixing overnight to assure complete HPAM hydration. The resulting solution is referred to as brackish water + polymer (BW+P) solution.

During the last part of the ED experiments, the feed PFPW contained emulsified crude oil. To prepare the emulsion, 2.0 g of crude oil was added to 2.0L of BW previously heated to 45 °C. The emulsification was done with an emulsifying mixer set at 15,000 rpm for 15 minutes. This stock solution was used to obtain 20 mg/L and

40 mg/L of oil emulsions employed in the 10L feed solution, also referred to as BW+P+O solution. The stock solution was immediately added to the feed to avoid separation of the non-soluble part when left unused for long periods.

The HPAM employed was AB-305-VLM (MW= 600-900 kDa and 30% hydrolyzed), kindly provided by SNF Floerger (France). The crude oil originated from the North Sea and was provided by Shell.

7.2.1.2   *Ion exchange membranes*

For this study, six different types of homogeneous anion exchange membranes were used, with properties summarized in **Table 7.2**. All membranes contain quaternary ammonium anion exchange groups and report high permselectivity. Type 1 and type 10 from FujiFilm were selected due to their different chemistry. The following membranes were either purchased or provided by the industry: Neosepta AMX from Eurodia (France); Fuji types 1, 10, and 12 by FujiFilm Manufacturing B.V. (The Netherlands); and Suez AR204E and Suez AR908E by Suez Water Technologies & Solutions (Canada).

The CEM employed was Neosepta CMX, a strong membrane that contains sulfonic acid groups as fixed charges. Its properties have been previously reported in the literature [29,30].

7.2.1.3   *Electrodialysis setup*

Experiments were performed using a cross-flow ED stack composed of five cell pairs. The stack contained six Neosepta CMX membranes plus five AEMs of the same type, as listed in **Table 7.2**. All membranes employed to assemble a stack were new, with an active membrane area of $0.01m^2$. The membranes were separated by 485 µm polyamide woven spacers (Sefar 06-700/53, Switzerland) with coated silicon rubber at the sides as gaskets (Aquabattery, The Netherlands). The cell contained electrodes made of titanium with mixed metal oxide coating from Magneto Special Anodes BV (The Netherlands). The housing of the stack was kindly provided by REDstack BV (The Netherlands). It consisted of polymethyl methacrylate side plates for the water distribution and end plates with the electrode compartments, plus the materials needed to close the assembly. A scheme of the stack is available in [19].

The electrical current was controlled by a potentiostat/galvanostat Ivium-n-Stat (Ivium Technologies, NL). The potential difference over the membrane stack was measured using two reference Ag/AgCl gel electrodes (QM711X, QIS, the Netherlands) placed at the inlet of each electrode compartment and connected to the Ivium-n-Stat.

Table 7.2. *Summary of chemical and physical properties of the six AEMs investigated as reported by the manufacturers.*

AEM type	Thickness (μm)	Area resistance* (Ω·cm²)	Chemistry	Description	Application
Neosepta AMX	135	2.4	Styrene-divinyl benzene	High crosslinking, high mechanical strength	Desalination of food, concentration of inorganic salt, hardness removal
Fuji type-1	110	0.9	3D-structure of inert polyolefin fibers filled with aliphatic polyamide [31]	Low power consumption & medium water permeating	Water softening by capacitive deionization
Fuji type-10	130	1.6	-	Low power consumption & medium water permeating	Purifying process/ wastewater/ brackish water/ food streams by ED
Fuji type-12	130	1.7	Same chemistry as Fuji type 10, but different support	-	-
Suez AR204E	550	5.5	Copolymers of vinyl monomers	medium	Water treatment
Suez AR908E	650	6.0	Copolymers of vinyl monomers	medium	Wastewater treatment

*Measured in 0.5M NaCl

The feed and electrolyte solutions were pumped by three independent peristaltic pumps from Cole-Parmer, Masterflex L/S Digital drive (USA). The conductivities of the diluate and the concentrate streams exiting the ED stack were continuously measured with conductivity probes (Orion DuraProbe 4-electrode conductivity cell 013005MD). A transmitter box (Orion Versastar Pro) connected to the probes corrected the measurements to the reference value at 25 °C and recorded them on the computer. The pH of the diluate and concentrate was also continuously measured by two pH probes (MemoSENS Endress+Hauser, pH range 1 to 12) placed after the ED stack. The pH probes were connected to a transmitter box (P862, QIS, Endress+Hauser). Two back-pressure valves, set at 0.25 bar, were placed at the outlet of electrolyte solution to ensure it was evenly distributed through the electrodes.

7.2.2 Methods for the EDR runs

7.2.2.1 *Electrodialysis reversal runs*

EDR experiments were conducted at a constant current in a batch recirculation mode, meaning that the diluate and concentrate streams were both fed from the same vessel, went through the ED stack, and returned to the feed container (**Figure 7.1**). The vessel contained 10.0 L of the feed solution, which composition and flowrate were varied for the different stages of the experiment, as specified in **Table 7.3**. Since the first stack assessed was the one containing Neosepta AMX, some operational parameters were determined based on its performance and later implemented on the subsequent experiments. For example, the switch to solution III (BW+ 50 mg/L HPAM) was done together with an increase in linear velocity to avoid operating at high voltages, and it was further increased when switching to stage IV (BW+ 100 mg/L HPAM). Since there was a rapid electric potential increase when stage V (BW+ 200 mg/L HPAM) started, the current density was reduced to 75 A/m^2.
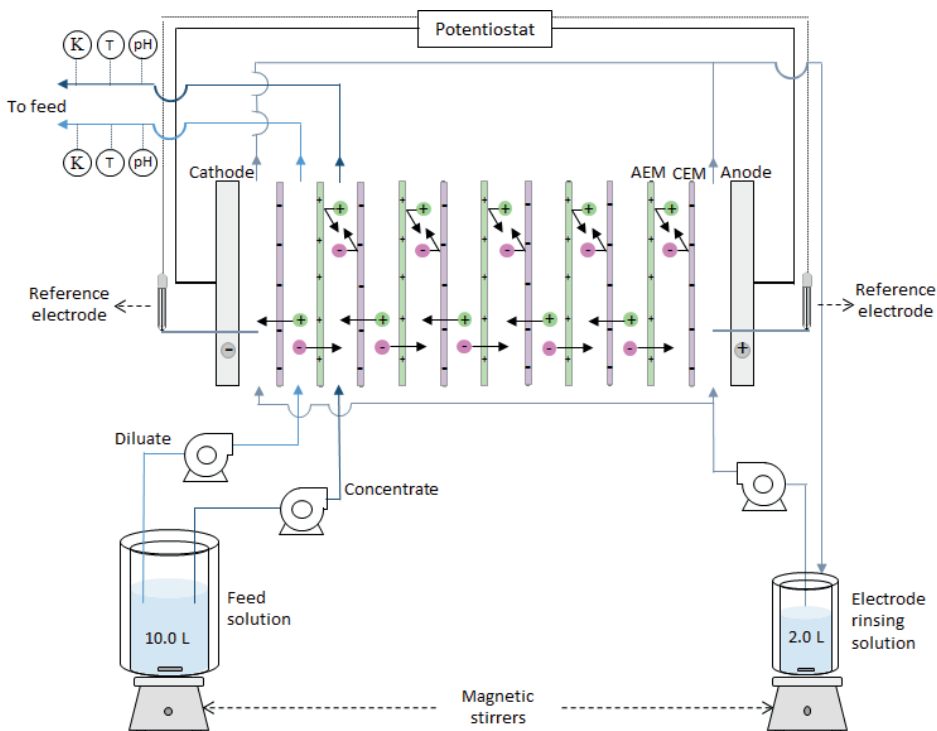
Figure 7.1. *Scheme of the setup employed. The experiments were run in a batch recirculation mode, in which two streams were taken from the same feed solution, circulated through the ED-stack, and returned to the same reservoir. Adapted from [6].*

Overall, the EDR was run at a constant current between 75 to 100 A/m^2 for nearly 200 hours with current reversal every hour (the lower current density was applied

to avoid reaching the 10 V limit of the potentiostat). The electrolyte solution, consisting of 0.14 M Na2SO4, was circulated at 170 mL/min and was replaced simultaneously with the feed solutions. The experiments were performed in a laboratory with controlled temperature at 23 ± 1°C.

Table 7.3. Feed compositions, current density, flow rate, velocity, and times of the different experimental stages

Stage	Feed solution (10 L volume)	Current density (A/m²)	Flow rate (mL/min)	Fluid velocity (cm/s)	t (h)
I	0.5 M NaCl	100	150	1.6	8+
II	BW	100	150	1.6	6
III	BW + 50 mg/L HPAM	100	180	1.9	24
IV	BW + 100 mg/L HPAM	100	210	2.2	24
V	BW + 200 mg/L HPAM	75	240	2.5	24
VI	BW + 200 mg/L HPAM +20 mg/L oil	75	240	2.5	48
VII	BW + 200 mg/L HPAM +40 mg/L oil	75	240	2.5	60
VIII	BW + 200 mg/L HPAM +40 mg/L oil	100	240	2.5	14

Each experiment started by running the electrodialysis for at least 12 hours with 0.5 M NaCl to ensure the optimum assembly of the stack. Then, the solution was substituted by BW, and the stack performance was measured to confirm that 100 A/m² could be supplied without reaching limiting current density (LCD) conditions. During the experiments, the applied current, stack voltage, conductivity, pH, and temperature were monitored continuously. Samples from all streams were periodically taken. After each experiment, the stack was disassembled, and all the membranes recovered for analysis.

7.2.2.2   *Degree of demineralization*

The degree of demineralization (D_{dem}, %) was calculated employing the initial conductivity of the feed solution c_0 (mS/cm) and the conductivity of the diluate solution c_d (mS/cm), according to equation 1 [32].

$$D_{dem} = \frac{C_0 - C_d}{C_0} * 100\% \qquad /7.1/$$

7.2.3   Methods for membrane characterization

7.2.3.1   *Water uptake and hydration number*

The water uptake (WU), also called swelling degree by some authors, indicates how the membrane mass changes when exposed to water [33]. For its determination, wet

membrane coupons were removed from 0.5M NaCl solution, their outer surface was smoothly wiped with a laboratory tissue, and their wet mass (m_w) recorded. Then, the coupons were placed in Petri dishes and left in a vacuum oven at 30°C to dry overnight. Then, the dry mass (m_d) of the coupons was measured, and the *WU* calculated as the mass of removed water divided by the dry mass [34,35]:

$$\text{WU} = \frac{m_w - m_d}{m_d} \qquad \text{/7.2/}$$

The hydration number (λ) [36] or water content [33] of the membranes was calculated by dividing the *WU* by the molecular weight of water and the ion exchange capacity (IEC, meq/g-dry) of the membrane. A factor of 1000 is necessary to report λ in mol H$_2$O/mol counterion.

$$\lambda = \frac{\text{WU} \times 1000}{MW_{H2O} \times \text{IEC}} \qquad \text{/7.3/}$$

7.2.3.2   *Ion-exchange capacity (IEC), charge density, and charge per area*

The ion-exchange capacity (IEC) of a membrane reports the number of ion-exchange equivalents per mass of dry membrane (meq/g-dry). It was determined by exchanging their counterion from chloride to nitrate and then measuring the amount of chloride released. First, AEM coupons were conditioned in 0.5M NaCl solution for at least 48 h. Then, they were rinsed with Milli-Q water (to ensure that excess chloride on the surface was removed) and soaked in 200 mL of 0.5M NaNO$_3$ while stirring at 300 rpm. In this way, the Cl$^-$ in the membrane is exchanged by NO$_3$. After 24 hours, samples of the solution were taken and analyzed for their chloride content via ion chromatography (see section 7.2.3.6). This concentration is proportional to the number of ionic charges present in the membrane sample, so once obtained, it was converted in meq and divided by the m_d to obtain the IEC [26,30,37].

The charge density (meq/g H$_2$O), which reflects the equivalents for the water-swollen membrane, was calculated by dividing the measured IEC by the *WU* [38].

7.2.3.3   *Permselectivity*

The permselectivity (α) of the AEMs was experimentally obtained by dividing the measured potential (ΔU_{meas}) over the theoretical one (ΔU_{theo}) for a 100% permselective membrane (Eq. 4), the last calculated through the Nernst equation. The activity coefficients of the 0.5M and 0.1M NaCl solutions were considered as 0.686 and 0.778, respectively [30].

$$\alpha = \frac{\Delta U_{meas}}{\Delta U_{theo}} \qquad /7.4/$$

ΔU_{meas} was determined by placing a membrane coupon in the middle of a two-compartment cell (Figure A7.1). Two solutions, 0.1M and 0.5M NaCl were circulated through each compartment of the cell at 300 mL/min. Both solutions were maintained at 25°C utilizing a recirculation bath. The potential difference across the membrane was measured using two Ag/AgCl reference electrodes, each placed inside one compartment, and connected to the Ivium potentiostat/galvanostat. The potentiostat was set in the open cell mode to register the potential generated from the sample membranes. The potential registered within the last 15 minutes of a running system was averaged to obtain the mean value after the system has stabilized.

7.2.3.4   *Electrical resistance*
The electrical resistance of the AEMs was measured in a six-compartment cell, as previously described [39]. The four inner compartments contained either 0.5M NaCl or BW solution, while the two outermost ones had 0.5M Na_2SO_4 as the electrolyte solution. The solutions were circulated at 170 mL/min using peristaltic pumps. The active area of the membrane under evaluation was 7.07 cm². The membrane was sided by two Habber-Luggin capillaries, each filled with a 3.0 M KCl solution and connected to an Ag/AgCl gel reference electrode, allowing to measure the potential drop across them. The measurements were performed at 25°C.

The measurements were performed on the same membrane coupons previously tested for permselectivity, which were conditioned in 0.5M NaCl. The area resistance was determined using chronopotentiometry: increasing values of current density were applied for two minutes each, while the electric potential was recorded. The current over the cell was provided by Autolab PGstat12 (The Netherlands). Three measurements were performed for each type of membrane, plus another time without it to obtain a blank measurement. The area resistances (Ω cm²), with and without membrane, were taken as the slope of the plot with the applied current density i (A/cm²) on the x-axis and the potential U (V) on the y-axis. Then, the membrane resistance r_m was calculated by subtracting the resistance of the blank r_s from the resistance with the membrane r_{m+s} as shown in Eq. 5.

$$r_m = r_{m+s} - r_s \qquad /7.5/$$

7.2.3.5   *Single AEM characterization in six-compartment cell*
The six-compartment cell was also employed to characterize the behavior of single AEMs when employed to desalinate the BW+P solution. The cell had the same

configuration as previously described, with compartments the four inner compartments filled with the BW solution. The AEM under study was placed in the middle of the cell and employed to desalinate the solution in compartment four at a constant current density of 28 A/m² [17]. After 30 minutes, the solution running through compartments 3 and 4 was substituted by BW+P solution containing 200 mg/L HPAM, after which the desalination continued for 90 minutes.

7.2.3.5.1.1   Sorption tests

Sorption tests were performed to evaluate the effect of exposing the membrane to HPAM-containing solutions, but without passing a current through them. The tests were performed by dipping virgin membrane coupons in 0.5L of BW+P solutions containing 200 mg/L HPAM. The solution was contained in plastic boxes that were kept closed and stored at lab temperature. After 48 hours, the membranes were recovered for analysis, and samples of the solution were collected and analyzed for Total Organic Carbon (TOC). The concentration of HPAM was related to TOC measurements through a standard curve (**Figure A7.2**).

7.2.3.6   *Solution analysis*

Samples taken during the ED and membrane characterization experiments were analyzed for their ionic and carbon composition. Cations were determined via inductive-coupled plasma optical emission spectroscopy (ICP-OES, Optima 5300DV, Perkin Elmer), and anions through ion chromatography (IC, 761 Compact IC, Metrohm). Total Carbon (TC), inorganic carbon (IC), and total organic carbon (TOC), were measured using a TOC analyzer (Shimadzu TOC-VCPH).

7.2.3.7   *Electrodialysis model*

The potential U required during the electrodialysis was calculated by modeling the system as an electric DC circuit with resistors in series. The area-specific resistance of a single cell-pair consists of four terms: the area-specific resistance of a CEM (r_{CEM}), that of the compartment filled with a spacer and a concentrated salt solution, that of the AEM (r_{AEM}), and that of the compartment filled with a spacer and a diluted salt solution. Since the feed solution was the same for both compartments and D_{dem} was relatively low, the resistances of the diluate and concentrate solutions can be calculated using the feed conductivity (κ_0), so the potential required by the stack can be calculated using Eq. 7.6:

$$U = I \cdot A_m \left[\frac{r_{CEM}}{1-\beta} + N \cdot \left(\frac{r_{CEM}}{1-\beta} + 2 \cdot \frac{h}{\kappa_0 \cdot (1-V_{sp})} + \frac{r_{AEM}}{1-\beta} \right) \right] \qquad /7.6/$$

Where I is the current (A), A_m is the membrane area (cm²), N is the number of cell pairs, β is the shadow factor, and V_{sp} is the volume fraction of the spacer [40]. The

equation considers the N number of cell pairs plus the extra CEM needed to close the stack.

7.3   Results and discussion

The first part of this section contains the results from the electrodialysis runs performed with the different AEMs. The second one includes the characterization of the membranes, including the virgin ones, and the ones recovered after the ED and the sorption experiments.

7.3.1   Desalination performance with different AEMs

After assembling each ED stack, its robustness was tested by desalinating 0.5M NaCl solution at 100 A/m² for approximately 16 hours (stage I). An example of the plots recorded during this stage is included in **Figure 7.2**, and the average absolute potential $\bar{U}$ recorded for each stack is summarized in **Table 7.4**. The lowest electric potential, and therefore the lowest stack resistance, was measured for the stack containing Fuji type 10 AEMs, which was approximately 30% lower than for the stack with Fuji type 12 AEMs, the one that registered the highest potential.
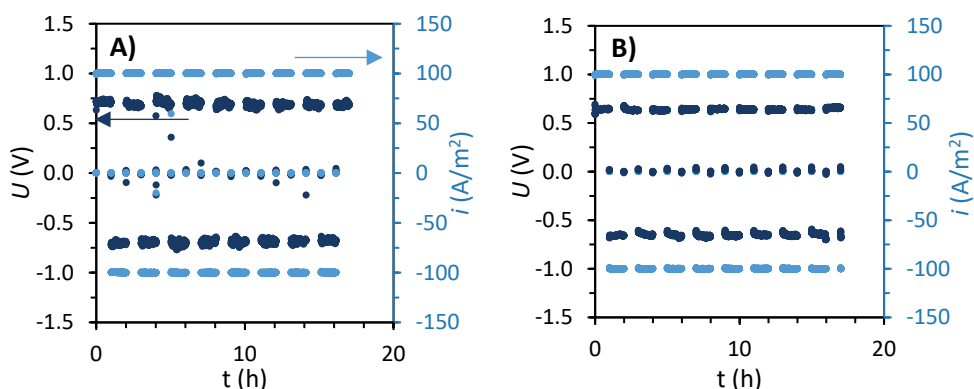
Figure 7.2. Electric potential U (marine) and current density i (light blue) versus time during the desalination of NaCl 0.5M (stage I) in EDR mode. Values measured for the stack composed by (A) Neosepta AMX and (B) Fuji type 10. The plots obtained from the other stacks can be found in the Appendix.

Table 7.4. Average absolute potential |Ū| measured while desalting NaCl 0.5M solution at 100 A/m².

Stack	$|\bar{U}|$ (V) stage A (0.5M NaCl)
Neosepta AMX	0.68
Suez AR204E	0.81
Fuji type 10	0.63
Suez AR908E	0.74
Fuji type 1	0.54
Fuji type 12	0.93

Next, the feed solution was switched to BW, and the stack rinsed for one hour. For the stack containing Neosepta AMX, the LCD was determined to be 180 A/m², corresponding to the inflexion point in the plot of current density versus stack voltage (**Figure A7.4**). For the rest of the stacks, a similar method was employed, but the measurement was stopped after ensuring that operating at 100 A/m² would still fall within the ohmic (linear) region. The only stack whose LCD was below 100 A/m² was the one containing FujiFilm type 12.

After the LCD tests, the stacks were employed for 6 hours to desalinate BW at 100 A/m² (stage II), as shown in **Figure 7.3**. Stages III and IV implied increases of the flow velocity, while in stage V the current density was decreased to 75 A/m² to avoid operating at high voltages. The figure shows that when crude oil was incorporated in stage VI no sharp increase in voltage was observed, the first time this occurred during the EDR runs. The relatively stable voltage profile was also observed during stage VII, whose feed solution contained 40 mg/L of crude oil, and allowed to switch back to a higher current density (100 A/m²) for stage VIII.

Figure 7.3 also shows that the measured potential fluctuated differently for each of the stacks. Still, it is possible to identify that the membranes Suez AR204E, Suez AR908E, and Fuji type 12 coincide in reaching higher voltages during the first hours of the experiments when desalinating at a current density of 100 A/m². The figure also shows that for the stages operated at 75 A/m², the voltage remained relatively stable, although slight increases occurred during stage VII for the Neosepta, Fuji 10, and Suez AR204 stacks.
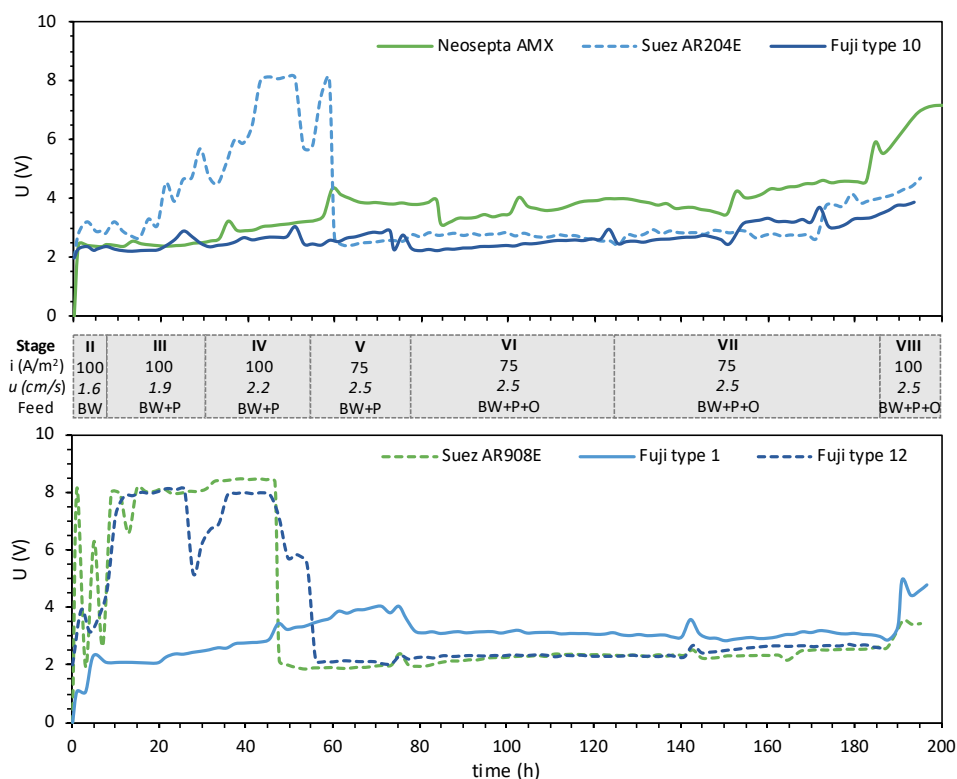
Figure 7.3. Electric potential U versus time during the EDR runs with stacks containing different AEMs. Chronologically, the experiments were performed in the following order: Neosepta AMX, Suez AR204E, Fuji type 10, Suez AR908E, Fuji type 1, and Fuji type 12.

The effects of multivalent ions were also observed in two stacks. First, the stack containing Suez AR908E presented some voltage peaks after changing from NaCl to BW solution, which was likely related to the presence of multivalent ions. This effect was further analyzed with the Fuji 1 stack since the first 4 hours of stage II desalinated a BW solution without divalent ions (Ca and Mg). As can be seen in **Figure 7.3**, this had a significant effect, since the recorded voltage was nearly half of that needed when desalting BW solution with all its components.

Figure 7.4 shows the degree of demineralization (D_{dem}) calculated from the measured conductivities of the solutions, according to Eq. 7.1. In general, the degree of desalination achieved with all the stacks was similar, as expected, given the operation at constant current, with values ranging between 10 and 30%. For the stacks composed by Neosepta AMX and Fuji type 1, the initial D_{dem} was slightly higher than for the rest, but it leveled at 20% around hour 60, when the current density was lowered to 75 A/m² (stage V). The lower plot also shows the moment when limiting current conditions were reached for the Suez AR908E and the Fuji

type 12 stacks at hour 6, when stage III started, as indicated by their lower demineralization performance.
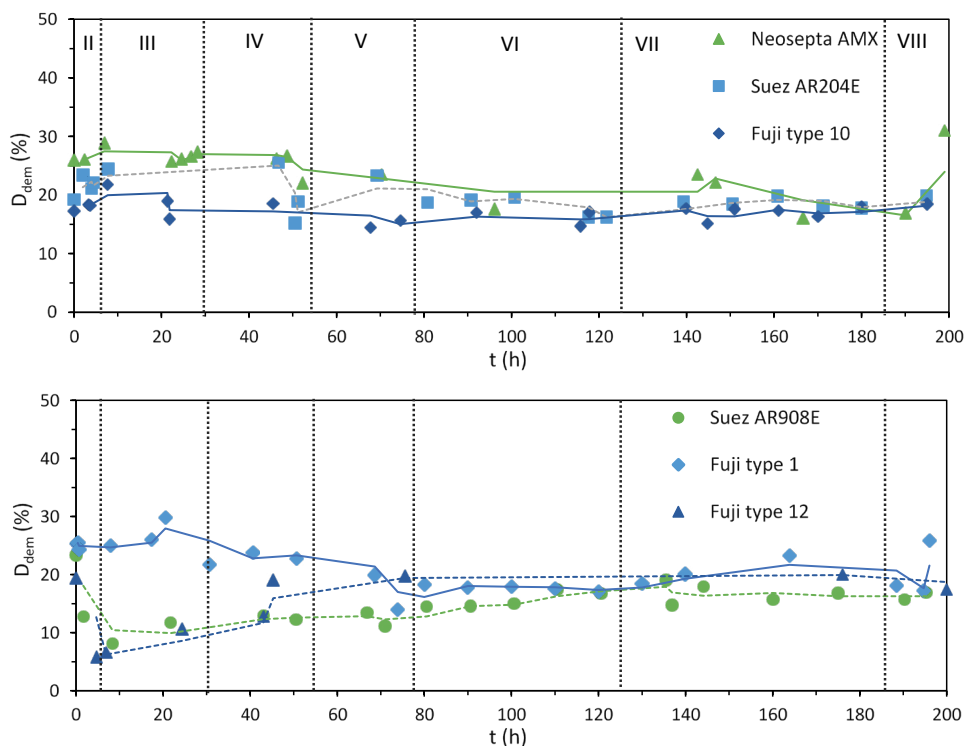
Figure 7.4. Demineralization after a single pass (%) vs. time during the EDR runs performed with different AEMs. Calculated values are represented by the symbols, and continuous trendlines (calculated as moving average) are included only for guiding the eye. The change of stage is represented by the horizontal lines.

Among the anions present in the feed solution, the removal of sulfate is particularly interesting because it is the only divalent, and it is usually transported with more difficulty than the monovalent ones [41]. **Figure 7.5** shows the sulfate removal, which was calculated from the diluate and concentrate samples taken during the runs. The initial SO_4^{2-} removal values of the stacks varied significantly, from almost 50% for Suez AR204E to 10% for Fuji type 12, with most values around 30%. The SO_4^{2-} removal above 30% in the initial stage is expected since this anion was not present in the solution before, so the membranes are still conditioning in the BW solution. Once the membranes are conditioned, the SO_4^{2-} removal further stabilizes.
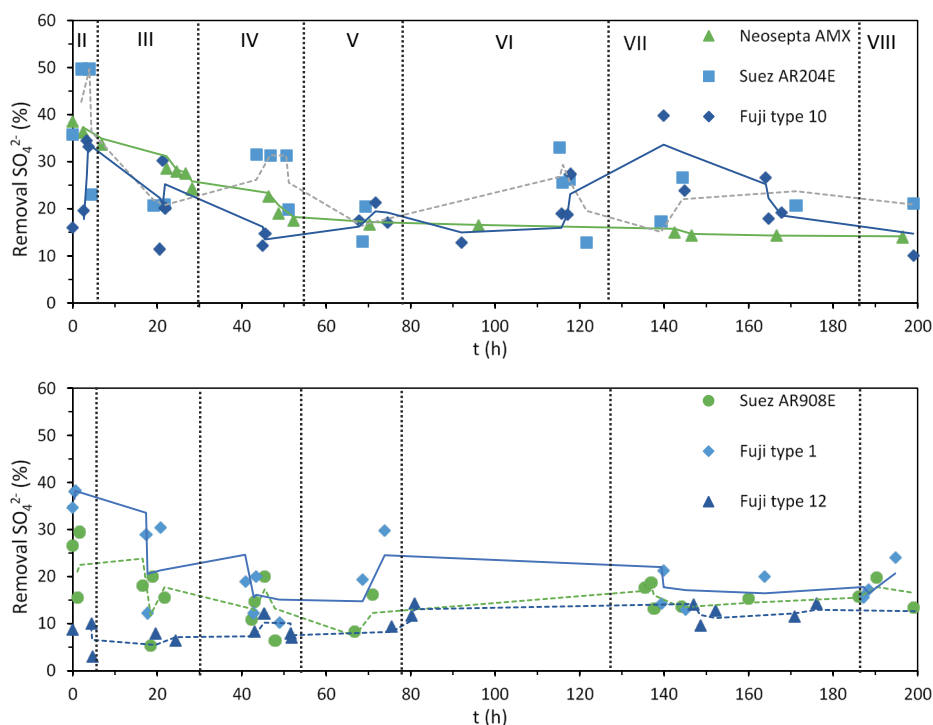
Figure 7.5. Measured sulfate removal vs. time for each stack. Each data point was calculated from the average changes in sulfate concentration in both the diluate and the concentrate stream. Continuous trendlines (calculated as moving average) are included only for guiding the eye.

7.3.2 Evaluation of the anion exchange membranes

Membrane properties (thickness, water uptake, IEC, permselectivity, and area resistance) were determined for virgin and fouled AEMs. There were two kinds of fouled membranes: the ones recovered from the ED-stack (photography's of these membranes are included in **Figure A7.5**), and the ones recovered from the sorption tests. The sorption experiments were performed to assess if the changes measured were caused by PFPW being transported, or if similar behaviors were observed when the AEMs were soaked in BW+P solution. We refer to sorption and not to adsorption tests because, although it has been noticed that the HPAM molecule is too big to go through the IEMs [6], it is possible that segments of the linear chains of the polymer can get inside the membranes.

The properties measured for the virgin membranes are included in **Table 7.5**, together with some values reported in the literature.

Table 7.5. *Values measured and reported in the literature for membrane properties. Typical repeat errors for permselectivity are below 0.02*

AEM type	Wet thickness (μm)	IEC (meq/g dry AEM)	Water uptake (g H_2O/g dry AEM)	Hydration number λ (mmol H_2O/meq)	Perm-selectivity (-)	Area resistance in 0.5M NaCl (Ω.cm²)	Area resistance in BW (Ω.cm²)
Neosepta AMX	137 ± 2 141 [26], 138 [29]	1.3 ± 0.03 1.4 [26], 1.3 [29]	0.25 ± 0.02 0.23 [26], 0.16 [29]	10.6 ± 0.9	0.94 0.94 [26], 0.91 [29]	2.39 ± 0.05 2.77 [26], 2.35 [29]	9.92 ± 0.14
Fuji type 1	127 ± 2 139 [25]	1.49 ± 0.24 1.8 [26]	0.40 ± 0.03 0.56 [26]	17.1 ± 1.4	0.86 0.90 [26]	1.24 ± 0.01 1.05 [26]	8.77 ± 0.11
Fuji type 10	151 ± 3	2.16 ± 0.12	0.63 ± 0.03	16.3 ± 0.8	0.91	1.56 ± 0.02	5.54 ± 0.12
Fuji type 12	148 ± 13	1.49 ± 0.18	0.21 ± 0.02	7.9 ± 0.23	0.90	5.13 ± 0.03	14.19 ± 0.26
Suez AR204E	616 ± 11	1.35 ± 0.18 2.34[a]	0.50 ± 0.03	14.8 ± 0.3 0.42[b]	0.90	4.73 ± 0.01 5.5	11.09 ± 0.18
Suez AR908E	655 ± 14	1.84 ± 0.19 1.97[a]	0.55 ± 0.04	16.7 ± 0.9 0.43[b]	0.92	4.96 ± 0.03 6.0	10.08 ± 0.19

[a] The manufacturer reports the IEC as meq/g of dry resin, so the values cannot be compared directly.
[b] Values reported by the manufacturer as % of the wet resin.

7.3.2.1 *Physico-chemical characterization of new membranes*

In general, the measured **thicknesses** correspond with the ones reported in the literature and by the membrane suppliers (**Table 7.2**). The only exception was Suez AR204E, which was over 60 μm thicker than reported by the supplier. Regarding the **IEC** of the AEMs, it ranged between 1.3 meq/g-dry for Neosepta AMX to 2.19 meq/g-dry for Fuji type 1. For the membranes for which data is available, the measured values do not deviate significantly from other values reported.

Water content is a function of the molar percentage of charged groups in the membrane. Charged groups in the membranes increase osmotic pressure hence increasing water uptake [42]. As presented in **Table 7.4**, the **water uptake** of the membranes under study covered a wide range, from 0.21 g H_2O/g dry AEM for the highly crosslinked Fuji type 12, to 0.63 g H_2O/g dry AEM for Fuji type 10. However, since the dry weight of the AEMs includes the thick support of the Suez membranes,

WU comparisons could be deceptive. To avoid this, the **hydration number λ** of the membranes was also calculated. This parameter shows that Neosepta AMX, Fuji type 1, and Fuji type 10 possess similar water content. Fuji type 12 is the least hydrated, corresponding with its measured *WU*. Regarding the Suez membranes, their hydration numbers are higher than for the rest of the AEMs and similar between each other. This observation agrees with the hydration reported by the manufacturer, which, although given in % of wet resin, indicates that the membranes are similar.

7.3.2.2 *Electrochemical characterization of new membranes*

The **permselectivities** of the evaluated membranes were similar, around 0.9. Neosepta AMX presented the highest value, 0.94, consistent with previous reports in the literature [26,29]. The high permselectivity of the membranes was expected since this property is directly related to the fixed charge concentration, which is high for all the evaluated AEMs.

The **area resistances** of the membranes were measured in two different solutions: 0.5M NaCl, which enables us to compare our measurements to others reported in the literature, and the BW solution employed during the desalination experiments. Among the six AEMs, Fuji type 12 exhibited the highest electrical resistance for both the NaCl solution (5.1 $\Omega \cdot cm^2$) and the BW one (14.19 $\Omega \cdot cm^2$). Despite Fuji type 12 is a thin membrane, the high resistance was expected since this property is highly dependent on water content, which is itself linked to the fixed charge concentration of the polymer [38]. Fuji type 12 presented a relatively low IEC, low hydration number, and, consequently, a high area resistance. Although much thicker than Fuji type 12, the Suez membranes presented similar resistance values, which can be explained given their higher water content. The other FujiFilm membranes (type 1 and type 10) show a low electrical resistance, as expected, given their thin support and elevated water content. The electrical of Neosepta AMX was slightly higher than for Fuji type 1 & 10, although they have similar thicknesses, which could be attributed to a higher crosslinking degree.

### 7.3.2.3 *Physico-chemical evaluation of fouled membranes*

The **water uptake** (WU) measured for the AEMs is displayed in **Figure 7.6A**. Compared to the virgin membranes, the fouled membranes after sorption and after electrodialysis presented similar changes; that is, they both increased or decreased depending on the type of AEM. Most of the membranes presented a net increase in WU, and only Neosepta AMX and Fuji type 10 membranes presented a decrease. The measured increases in WU are, at least partially, attributable to the presence of viscous solution being removed together with the AEM. The removal was evident because the fouled coupons had higher wet weights than the ones from virgin membranes, despite all being cut with the same surface dimensions. Although the

surfaces of the coupons were smoothly cleaned with a tissue, it is likely that some HPAM-containing solution remained on the AEM, especially on those with a rougher surface.

If the comparisons are made in terms of the **hydration number**, as shown in **Figure 7.6B**, the results indicate that the thin membranes (Neosepta and the Fuji ones), presented a decrease in hydration. In contrast, for the Suez ones, the tendency is still an increase in hydration. Other studies have also reported both increase and decrease of water content on aged membranes [43].

Figure 7.6C shows the **IEC** measured for the virgin and fouled membranes. With a few exceptions, the IEC of the AEMs did not significantly change when fouled, either by sorption or by ED. The exceptions were Fuji type 1 and Suez AR908E after ED, both of which presented a notorious increase of IEC compared to the virgin membranes. The increase in IEC could be caused by the presence of calcium ions, which could interact with the negatively charged HPAM to form a complex group with a positive net charge. The positive net charge group may provide extra charge carriers on the surface of the membranes hence increasing ion exchange capacity. Additional sorption tests were performed with only HPAM and NaCl solution (to exclude the effect of the divalent ions), and it was observed that the IEC of fouled AEMs dropped close to that of the virgin ones (data not shown).

The slight decreases in IEC are, on the contrary, commonly measured for aged or fouled membranes [43], and can have diverse causes. One is the foulant occupying the fixed charge group's sites, thus reducing the number of fixed charge carriers. The reduction of IEC is also typical when the membranes were exposed to high pH, for example, when reaching limiting current conditions and hydroxide anion was formed. When operated under high pH conditions, the functional groups of AEMs can decompose, and its functional property is reduced [24,37].
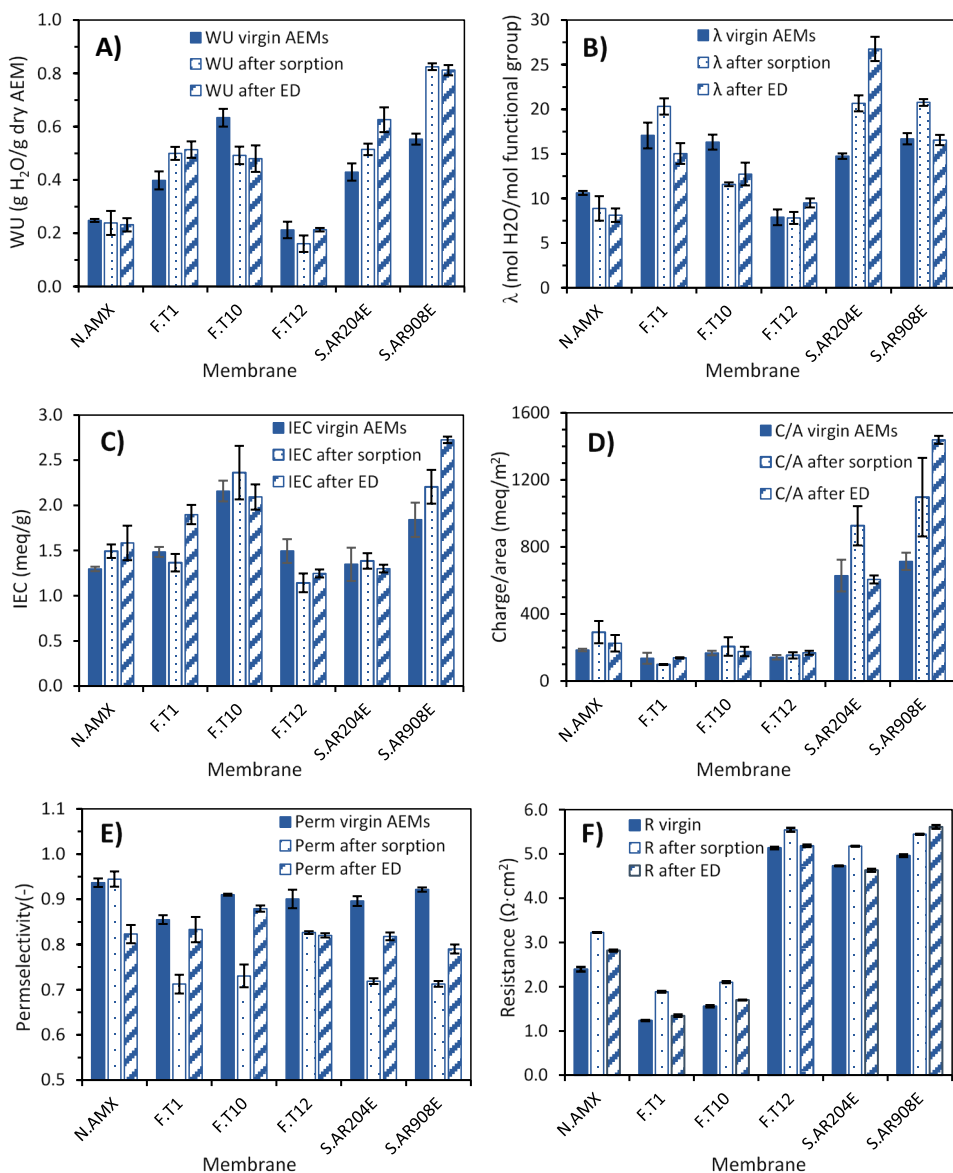
Figure 7.6. *Comparison of membrane properties for virgin, soaked, and membranes fouled after ED. (A) Water uptake (WU), B) hydration number (λ), C) ion exchange capacity (IEC), D) Charge per area, E) permselectivity and, F) area resistance (in 0.5M NaCl).*

7

7.3.2.4 *Electrochemical characterization of fouled membranes*

Figure 7.6E shows the **permselectivities** measured for all the AEMs. In this case, all fouled membranes presented the same behavior: their permselectivity decreased (except for Neosepta AMX after sorption, which remained the same). Two reasons can explain permselectivity reduction. First, HPAM and other charged molecules present in the solution probably interacted with the fixed charged groups of the AEMs and reduced their effective charge, therefore diminishing their ability to reject co-ions. A second reason is a permselectivity dependence on the binding affinity of the counterion with the polymer fixed charge groups [34]. Given the composition of the BW employed during the experiments, it is expected that varied counterions (Cl^-, SO_4^{2-} and HCO_3^-) would be present inside the AEM matrix, thus affecting membrane permselectivity.

The permselectivity also can be affected by the water content of the membrane, and the higher the water sorption, the lower the permselectivity of an AEM [38]. This relationship explains why the sharpest decreases in permselectivity (above 10%) were recorded for the Suez membranes, which presented the highest increase in water uptake (**Figure 7.6A**).

Furthermore, the permselectivity drops were more severe upon AEM sorption. Two factors might have influenced this result. First, the crude oil incorporated in the feed solutions from the last stages might foul the AEMs in a different form. Second, the dynamic operation in the ED-stack, particularly regarding fluid hydrodynamics, might have limited the amount of foulant remaining on the membranes.

Figure 7.6F shows the **electrical resistance**, measured in 0.5M NaCl, of the six AEMs. For most of the fouled membranes, there was a slight increase after fouling from both sorption and ED process, and even in a few cases, the resistance of the fouled membranes did not have a significant change. It must be recalled that the membrane coupons employed for resistance measurement were the same previously employed for measuring permselectivity (see section 7.2.3.4), so any foulant that was not firmly attached was removed by the fluid while measuring permselectivity. Therefore, the increase in resistance could be attributed to some firmly attached foulants (HPAM, oil), which attach to the membrane and reduce the available surface area for ion permeation. Resistance can also be affected by the presence of varied counterions on the AEM matrix, which affect the water content of the membrane [38].

7.3.3 Relationship between membrane properties and process behavior

In this section, we relate the performance of the stacks composed by different AEMs with the information gathered during the individual membrane characterization. Since the most considerable differences in stack performance were observed in terms of voltage increase, we first focused on explaining this behavior. To do so, we

modeled the ED stack as an analogous DC circuit in which the different components (CEM, AEM, diluate and concentrate compartments) are represented as a series of resistances, as explained in section 7.2.3.8. The parameters employed in the model are summarized in **Table 7.6**.

<p align="center">*Table 7.6. Parameters used for the ED model*</p>

Parameter	Value
CEM resistance (0.5M NaCl)	3.3 $\Omega \cdot cm^2$ [39]
CEM resistance (BW)	7.0 $\Omega \cdot cm^2$ [39]
AEM resistance (0.5M NaCl and BW)	Table 7.5
Shadow factor β	0.48 [40]
Spacer volume V_{sp}	0.2
Current density	100 A/m^2

Figure 7.7A shows that the modeled results are close to the ones measured during stage I, when a 0.5M NaCl was desalinated (**Table 7.4**). Furthermore, the same figure includes the results obtained after adjusting the model to estimate the potential required to desalinate the BW solution. For that case, CEM and AEM resistances had to be considered, as indicated in **Figure 7.6**. The voltages thereby obtained also approached the ones measured when the BW desalination was just started.
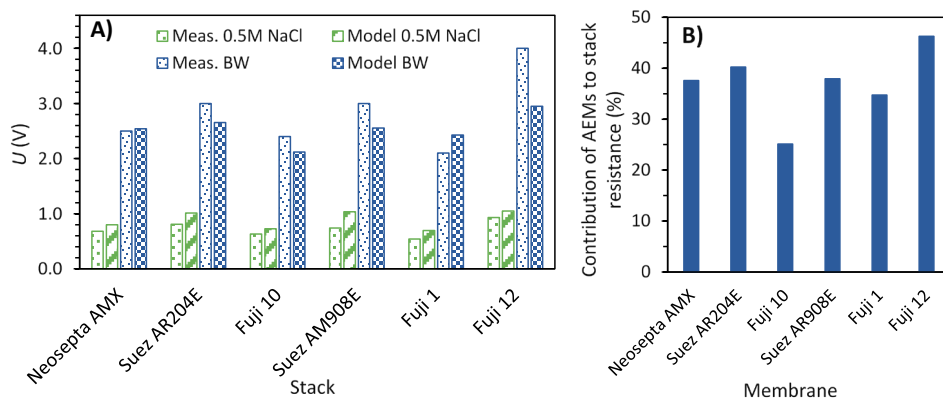
Figure 7.7. A) *Comparison of modeled and measured voltages for the different stacks operated at 100 A/m². **B)** Contribution of AEM resistance to the stack resistance according to the model for the BW solution.*

Besides reasonably predicting the voltages required by the different stacks, the model allowed us to weight the contribution of each of the cell pair's components. Focusing on the AEM's, we estimated that for the membrane with the lowest resistance, Fuji type 10, the AEMs represent 26% of the total stack resistance. In contrast, for the stack composed by Fuji type 12, the AEMs represent 48% of the resistance (**Figure 7.7B**).

Please note that the model is applied to the initial conditions of stage II, when only BW was being desalinated. However, not all stacks behaved the same during this stage. While for three of the stacks (Neosepta, Fuji type 1 and type 10), the applied voltage stabilizes very fast; for the other three membranes, it remains to fluctuate during the stage (see **Figure 7.3**). This difference could be attributed to the membranes still conditioning to the composition of the BW solution (given their thickness and high degree of crosslinking they take longer to do so), but also to the likely development of concentration polarization. This explains the differences between the modeled voltage values and the measured ones. Then, when the HPAM-containing solution is incorporated in stage III, concentration polarization increased and reduced the active area of the membranes, causing the surge in voltage. **Figure 7.3** shows that all stacks were somehow sensitive to the incorporation of BW+P solution, but the ones containing AEMs with lower electric resistance had smaller changes than the others.

In this regard, it appears that the other membrane properties analyzed in this study did not have much influence on the development of concentration polarization. **Figure 7.4** shows that lower desalination performances were recorded for the stacks composed by Fuji type 12 and Suez AR908E. Both AEMs coincide in having high area resistance, but their other properties differ significantly. Fuji type 12 has low WU, low IEC, and charge/area, while Suez AR908E combines a high WU with high IEC and charge/area.

Further tests were performed on single AEMs desalinating BW+P solutions at moderate current density (28 A/m^2) in the six-compartment cell (section 7.2.3.5). During the tests, the transmembrane electric potential (TMEP) was monitored continuously. Any sudden increase could be related to the development of concentration polarization and fouling on the different AEMs when exposed to the BW+P solution [17]. However, the results presented in **Figure 7.8** indicate that desalinating the BW+P solution did not cause a notorious increase of the TMEP, independently of the AEM under observation. For example, the membranes with low water content (Neosepta AMX and FujiFilm type 12), had similar behavior to those with high water content (Suez membranes). These results suggest that the high voltages achieved during the stack operation were not only driven by AEM fouling. Thus, it is likely that other factors were triggering the increase in voltage.
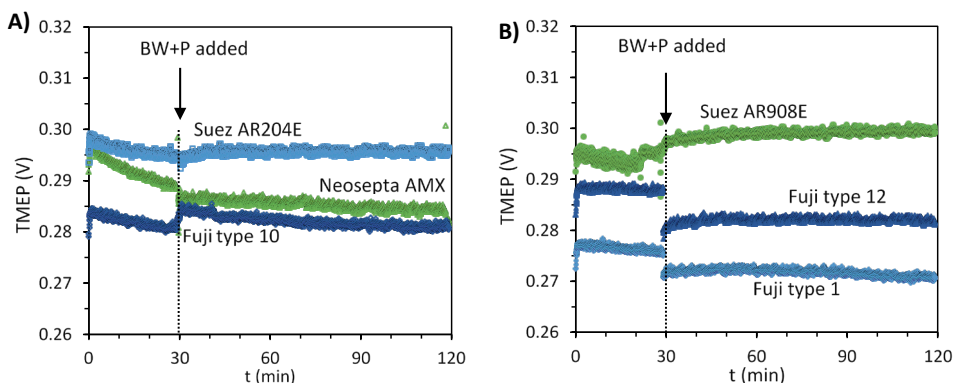
Figure 7.8. Measured transmembrane electric potential (TMEP) vs. time for fouling experiments in the 6-compartment cell. BW was desalinated at 28 A/m² for 30 minutes, after which the feed was substituted by the BW+P solution. Plot *A)* presents results for Neosepta AMX, Suez AR204E, and Fuji type 10, while plot *B)* includes Suez AR908E, Fuji type 1, and Fuji type 12. The jumps in TMEP are caused by small variations in the conductivity of the solution.

Then, it is interesting to pay attention to other phenomena happening in the cell, like concentration polarization and fouling of the spacer. The clean spacers already had a significant shadow factor, but this effect might have increased when they were exposed to HPAM-containing solution. The spacers, made of polyamide, had likely a high affinity with the polyacrylamide contained in the BW + P solution. Thus, the additive effects of higher solution viscosity plus the higher affinity with the spacer, the active area of the membranes in contact with the BW + P solution, was effectively reduced. For the stacks containing low-resistance membranes, this did not have a significant effect.

On the contrary, the stacks that contained AEMs with higher resistance reached LCD conditions almost immediately. According to the Nernst-Planck equation, higher resistance is due to lower diffusivity or thicker membrane. Ion transport by migration at high resistance can still be high by applying high voltage, but the driving force for diffusive ion transport cannot be compensated. Thus, the effect of high resistance is a change of transport mechanism, fewer diffusions, more migration. Then, the LCD occurs in the boundary layer next to the membrane due to the depletion of ions, causing water splitting phenomena and possibly damaging the AEMs due to the local increase of pH [24]. However, the pH meters placed after the ED cell registered relatively small changes (< 1.0), probably due to the bicarbonate in solution acting as a pH buffer.

Regarding the influence of the membrane chemistry, its role probed not to be as critical as expected [44]. While desalinating the BW + HPAM solution, the aromatic (Neosepta AMX) and some of the aliphatic membranes had relatively stable

performances. When adding crude oil to the feed and with it some aromatic compounds, the performance of all stacks stabilized (**Figure 7.3**). The pictures of the recovered AEMs (**Figure A7.5**) suggest similar degrees of fouling for all of them. It is also possible that surface properties non-measured in this investigation, like the roughness and hydrophilicity of the AEM, could have influenced their performance in the stack. However, these effects might have been small, as suggested by the single membrane experiments in **Figure 7.8**.

7.4 Conclusions

Six different ED stacks, each containing a different type of homogeneous strong AEM, were employed during 8-days experiments to desalinate PFPW. During three of the six EDR runs, limiting conditions were reached, which was attributed to the combination of high intrinsic area resistance of some of the AEMs and the development of concentration polarization when HPAM-containing solution was fed to the stack.

Operating the electrodialysis in reverse mode was only beneficial during some minutes after the switch, after which the required voltage increased again due to concentration polarization. Given the aim of this work of comparing the membranes after operating under similar conditions, the current density was maintained despite the higher voltage, which could have affected the membranes, like the reduction in charged functional group density. For other purposes, like operating the system during extended times, the current density should be adjusted according to the characteristics presented by each stack.

The incorporation of crude oil in the feed solution did not have a negative effect in terms of increasing the stack resistance, and, in some cases, it even caused its decrease and stabilization.

This experimental work proved the close relationship between membrane properties. Changes in their physico-chemical characteristics, like water content and IEC, were also reflected in their electrochemical behavior, namely permselectivity and area resistance. Membrane properties measured after ED and after sorption experiments generally followed the same trends, suggesting that most changes were mainly due to processes occurring on the surface of the membranes and not due to their internal poisoning. For some membrane properties, the measured changes were more substantial for the AEMs soaked in BW+P solution (without oil) than for the AEMs recovered from the ED stack, which suggests that even small concentrations of oil in solution influences the interaction between AEMs and the surrounding solution.

Although all tested AEMs operated smoothly after the operating current density was decreased to 75 A/m^2, this work evidenced the advantages of using membranes with low area resistance, which are operating at higher current densities and diminishing the risk of reaching limiting conditions. In that context, for future works, we would choose AEMs with a low resistance to desalinate PFPW. Since resistance is a consequence of material characteristics, the desired membrane would need to be relatively thin, have high IEC, and moderate to high water content. However, factors like mechanical and chemical stability, which were not analyzed in this investigation, could turn out to be more favorable for the reinforced membranes. Thus, for future studies, it would be desirable to i) evaluate the AEMs performance for reaching the final desalination objective, and ii) assess the long-term stability of different kinds of AEMs.

References

[1]   H. Strathmann, Electrodialysis, a mature technology with a multitude of new applications, Desalination. 264 (2010) 268–288. doi:10.1016/j.desal.2010.04.069.

[2]   T. Xu, C. Huang, Electrodialysis-based separation technologies: a critical review, Journal of the American Institute of Chemical Engineers. 54 (2008) 3147–3159. doi:10.1002/aic.

[3]   J. Guolin, W. Xiaoyu, H. Chunjie, The effect of oilfield polymer-flooding wastewater on anion-exchange membrane performance, Desalination. 220 (2008) 386–393. doi:10.1016/j.desal.2007.03.010.

[4]   G. Riethmuller, A. Abri, N. Al Azri, G. Stapel, S. Nijman, W. Subhi, R. Mehdi, Opportunities and Challenges of Polymer Flooding in Heavy Oil Reservoir in South of Oman, SPE EOR Conference at Oil and Gas West Asia. (2014). doi:10.2118/169737-MS.

[5]   S. Rellegadla, G. Prajapat, A. Agrawal, Polymers for enhanced oil recovery: fundamentals and selection criteria, Applied Microbiology and Biotechnology. 101 (2017) 4387–4402. doi:10.1007/s00253-017-8307-4.

[6]   P.A. Sosa-Fernandez, J.W. Post, H. Bruning, F.A.M. Leermakers, H.H.M. Rijnaarts, Electrodialysis-based desalination and reuse of sea and brackish polymer-flooding produced water, Desalination. 447 (2018) 120–132. doi:10.1016/j.desal.2018.09.012.

[7]   G. Jing, L. Xing, S. Li, C. Han, Reclaiming polymer-flooding produced water for beneficial use: Salt removal via electrodialysis, Desalination and Water Treatment. 25 (2011) 71–77. doi:10.5004/dwt.2011.1766.

[8]   H. Strathmann, Electromembrane Processes: Basic Aspects and Applications, in: Comprehensive Membrane Science and Engineering, Elsevier B.V., 2010: pp. 391–429. doi:DOI: 10.1016/B978-0-08-093250-7.00048-7.

[9]   S. Mikhaylin, V. Nikonenko, G. Pourcelly, L. Bazinet, Intensification of demineralization process and decrease in scaling by application of pulsed electric field with short pulse/pause conditions, Journal of Membrane Science. 468 (2014) 389–399. doi:10.1016/j.memsci.2014.05.045.

7

[10]   S. Mikhaylin, L. Bazinet, Fouling on ion-exchange membranes: Classification, characterization and strategies of prevention and control, Advances in Colloid and Interface Science. 229 (2016) 34–56. doi:10.1016/j.cis.2015.12.006.

[11]   E. Korngold, F. de Korosy, R. Rahav, M.F. Taboch, Fouling of anionselective membranes in electrodialysis, Desalination. 8 (1970) 195–220. doi:10.1016/S0011-9164(00)80230-1.

[12]   Q. Xia, H. Guo, Y. Ye, S. Yu, L. Li, Q. Li, R. Zhang, Study on the fouling mechanism and cleaning method in the treatment of polymer flooding produced water with ion exchange membranes, RSC Adv. 8 (2018) 29947–29957. doi:10.1039/c8ra05575k.

[13]   H. Guo, L. Xiao, S. Yu, H. Yang, J. Hu, G. Liu, Y. Tang, Analysis of anion exchange membrane fouling mechanism caused by anion polyacrylamide in electrodialysis, Desalination. 346 (2014) 46–53. doi:10.1016/j.desal.2014.05.010.

[14]   H. Guo, F. You, S. Yu, L. Li, D. Zhao, Mechanisms of chemical cleaning of ion exchange membranes: A case study of plant-scale electrodialysis for oily wastewater treatment, Journal of Membrane Science. 496 (2015) 310–317. doi:10.1016/j.memsci.2015.09.005.

[15]   J. Guolin, X. Lijie, L. Yang, D. Wenting, H. Chunjie, Development of a four-grade and four-segment electrodialysis setup for desalination of polymer-flooding produced water, Desalination. 264 (2010) 214–219. doi:10.1016/j.desal.2010.06.042.

[16]   T. Wang, S. Yu, L. an Hou, Impacts of HPAM molecular weights on desalination performance of ion exchange membranes and fouling mechanism, Desalination. 404 (2017) 50–58. doi:10.1016/j.desal.2016.10.007.

[17]   P.A. Sosa-Fernandez, S.J. Miedema, H. Bruning, F.A.M. Leermakers, H.H.M. Rijnaarts, J.W. Post, Influence of solution composition on fouling of anion exchange membranes desalinating polymer-flooding produced water, Journal of Colloid And Interface Science. 557 (2019) 381–394. doi:10.1016/j.jcis.2019.09.029.

[18]   D.A.Z. Wever, F. Picchioni, A.A. Broekhuis, Polymers for enhanced oil recovery: A paradigm for structure-property relationship in aqueous solution, Progress in Polymer Science (Oxford). 36 (2011) 1558–1628. doi:10.1016/j.progpolymsci.2011.05.006.

[19]   J. Moreno, N. de Hart, M. Saakes, K. Nijmeijer, CO2 saturated water as two-phase flow for fouling control in reverse electrodialysis, Water Research. 125 (2017) 23–31. doi:10.1016/j.watres.2017.08.015.

[20]   S. Mulyati, R. Takagi, A. Fujii, Y. Ohmukai, T. Maruyama, H. Matsuyama, Improvement of the antifouling potential of an anion exchange membrane by surface modification with a polyelectrolyte for an electrodialysis process, Journal of Membrane Science. 417–418 (2012) 137–143. doi:10.1016/j.memsci.2012.06.024.

[21]   D. Zhao, L.Y. Lee, S.L. Ong, P. Chowdhury, K.B. Siah, H.Y. Ng, Electrodialysis reversal for industrial reverse osmosis brine treatment, Separation and Purification Technology. 213 (2019) 339–347. doi:10.1016/j.seppur.2018.12.056.

[22]   S. Liu, X. Dong, H. Ban, T. Wang, W. Pan, H. Yu, C. Guo, C. Suo, Technology for confecting polymer solution with desalinated produced water, in: SPE (Ed.), 2007 SPE Annual Technical Conference and Exhibition Held in Anaheim, California, USA, SPE, Richardson, TX, 2007: pp. 1–5.

[23]   X.H. Zhen, S.L. Yu, B.F. Wang, H.F. Zheng, H. Ban, B.L. Miao, Ultrafiltration experiment of electrodialysis pretreatment for produced water desalination, Zhongguo Shiyou Daxue

Xuebao (Ziran Kexue Ban)/Journal of China University of Petroleum (Edition of Natural Science). 30 (2006) 134–137.

[24] Q. Xia, L. Qiu, S. Yu, H. Yang, L. Li, Y. Ye, Z. Gu, L. Ren, G. Liu, Effects of Alkaline Cleaning on the Conversion and Transformation of Functional Groups on Ion-Exchange Membranes in Polymer-Flooding Wastewater Treatment: Desalination Performance, Fouling Behavior, and Mechanism, Environmental Science and Technology. 53 (2019) 14430–14440. doi:10.1021/acs.est.9b05815.

[25] P.A. Sosa-Fernandez, J.W. Post, M.S. Ramdlan, F.A.M. Leermakers, H. Bruning, H.H.M. Rijnaarts, Improving the performance of polymer-flooding produced water electrodialysis through the application of pulsed electric field, Desalination. 484 (2020). https://doi.org/10.1016/j.desal.2020.114424.

[26] T. Rijnaarts, J. Moreno, M. Saakes, W.M. de Vos, K. Nijmeijer, Role of anion exchange membrane fouling in reverse electrodialysis using natural feed waters, Colloids and Surfaces A: Physicochemical and Engineering Aspects. 560 (2019) 198–204. doi:10.1016/j.colsurfa.2018.10.020.

[27] X. Zuo, L. Wang, J. He, Z. Li, S. Yu, SEM-EDX studies of SiO2/PVDF membranes fouling in electrodialysis of polymer-flooding produced wastewater: Diatomite, APAM and crude oil, Desalination. 347 (2014) 43–51. doi:10.1016/j.desal.2014.05.020.

[28] A.R. Al-Hashmi, T. Divers, R.S. Al-Maamari, C. Favero, A. Thomas, Improving polymer flooding efficiency in Oman oil fields. Paper SPE-179834-MS, in: SPE EOR Conference at Oil and Gas West Asia Held in Muscat, Oman, 21–23 March 2016., SPE, Muscat, 2016: p. 18.

[29] P. Długołecki, P. Ogonowski, S.J. Metz, M. Saakes, K. Nijmeijer, M. Wessling, On the resistances of membrane, diffusion boundary layer and double layer in ion exchange membrane transport, Journal of Membrane Science. 349 (2010) 369–379. doi:10.1016/j.memsci.2009.11.069.

[30] P. Długołecki, K. Nymeijer, S. Metz, M. Wessling, Current status of ion exchange membranes for power generation from salinity gradients, Journal of Membrane Science. 319 (2008) 214–222. doi:10.1016/j.memsci.2008.03.037.

[31] V. Sarapulova, I. Shkorkina, S. Mareev, N. Pismenskaya, N. Kononenko, C. Larchet, L. Dammak, V. Nikonenko, Transport characteristics of FujiFilm ion-exchange membranes as compared to homogeneous membranes AMX and CMX and to heterogeneous membranes MK-40 and MA-41, Membranes. 9 (2019) 1–23. doi:10.3390/membranes9070084.

[32] C. Casademont, P. Sistat, B. Ruiz, G. Pourcelly, L. Bazinet, Electrodialysis of model salt solution containing whey proteins : Enhancement by pulsed electric field and modified cell configuration, Journal of Membrane Science. 328 (2009) 238–245. doi:10.1016/j.memsci.2008.12.013.

[33] K.F.L. Hagesteijn, S. Jiang, B.P. Ladewig, A review of the synthesis and characterization of anion exchange membranes, Journal of Materials Science. 53 (2018) 11131–11150. doi:10.1007/s10853-018-2409-y.

[34] G.M. Geise, H.J. Cassady, D.R. Paul, B.E. Logan, M.A. Hickner, Specific ion effects on membrane potential and the permselectivity of ion exchange membranes, Physical Chemistry Chemical Physics. 16 (2014) 21673–21681. doi:10.1039/c4cp03076a.

[35] C. Klaysom, R. Marschall, L. Wang, B.P. Ladewig, G.Q.M. Lu, Synthesis of composite ion-

7

exchange membranes and their electrochemical properties for desalination applications, Journal of Materials Chemistry. 20 (2010) 4669–4674. doi:10.1039/b925357b.

[36]   X. Luo, A. Wright, T. Weissbach, S. Holdcroft, Water permeation through anion exchange membranes, Journal of Power Sources. 375 (2018) 442–451. doi:10.1016/j.jpowsour.2017.05.030.

[37]   F. Karas, J. Hnát, M. Paidar, J. Schauer, K. Bouzek, Determination of the ion-exchange capacity of anion-selective membranes, International Journal of Hydrogen Energy. 39 (2014) 5054–5062. doi:10.1016/j.ijhydene.2014.01.074.

[38]   M. Geise, M.A. Hickner, B.E. Logan, Ionic Resistance and Permselectivity Tradeoffs in Anion Exchange Membranes, Applied Materials and Interfaces. 5 (2013) 10294–10301. doi:dx.doi.org/10.1021/am403207w.

[39]   A.H. Galama, D.A. Vermaas, J. Veerman, M. Saakes, H.H.M. Rijnaarts, J.W. Post, K. Nijmeijer, Membrane resistance: The effect of salinity gradients over a cation exchange membrane, Journal of Membrane Science. 467 (2014) 279–291. doi:10.1016/j.memsci.2014.05.046.

[40]   J.W. Post, H.V.M. Hamelers, C.J.N. Buisman, Energy recovery from controlled mixing salt and fresh water with a reverse electrodialysis system, Environmental Science and Technology. 42 (2008) 5785–5790. doi:10.1021/es8004317.

[41]   P.A. Sosa-Fernandez, J.W. Post, F.A.M. Leermakers, H.H.M. Rijnaarts, H. Bruning, Removal of divalent ions from viscous polymer-flooding produced water and seawater via electrodialysis, Journal of Membrane Science. 589 (2019) 117251. doi:10.1016/j.memsci.2019.117251.

[42]   M. Higa, N. Tanaka, M. Nagase, K. Yutani, T. Kameyama, K. Takamura, Y. Kakihana, Electrodialytic properties of aromatic and aliphatic type hydrocarbon-based anion-exchange membranes with various anion-exchange groups, Polymer. 55 (2014) 3951–3960. doi:10.1016/j.polymer.2014.06.072.

[43]   R. Ghalloussi, W. Garcia-Vasquez, L. Chaabane, L. Dammak, C. Larchet, S.V. Deabate, E. Nevakshenova, V. Nikonenko, D. Grande, Ageing of ion-exchange membranes in electrodialysis: A structural and physicochemical investigation, Journal of Membrane Science. 436 (2013) 68–78. doi:10.1016/j.memsci.2013.02.011.

[44]   N. Tanaka, M. Nagase, M. Higa, Organic fouling behavior of commercially available hydrocarbon-based anion-exchange membranes by various organic-fouling substances, Desalination. 296 (2012) 81–86. doi:10.1016/j.desal.2012.04.010.
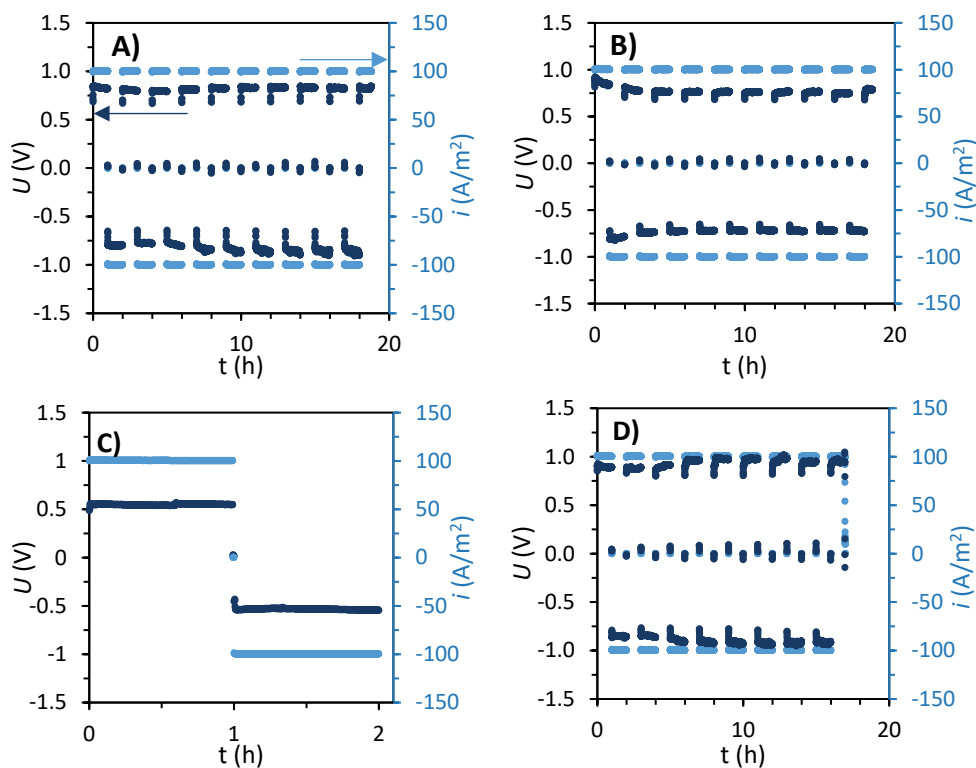
Appendix 7A. Supplementary material
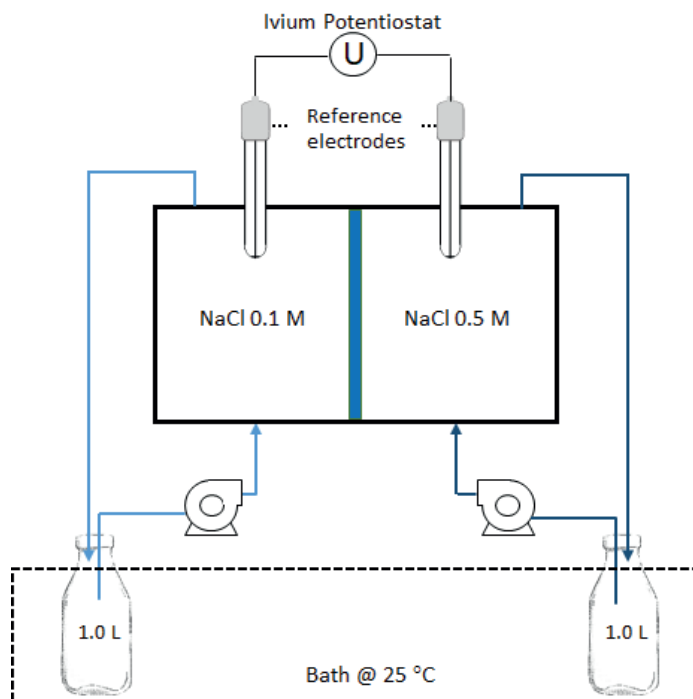
Figure A7.1. *Scheme of the two-compartment cell utilized for potential measurement, the potentiostat measures the open cell voltage. The solutions were stored in a warm bath at 25°C.*
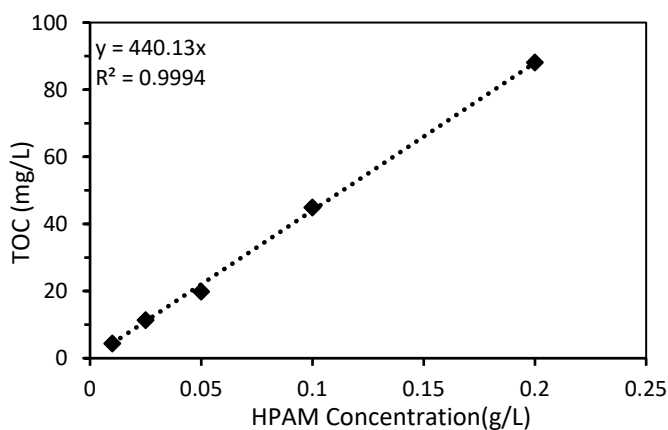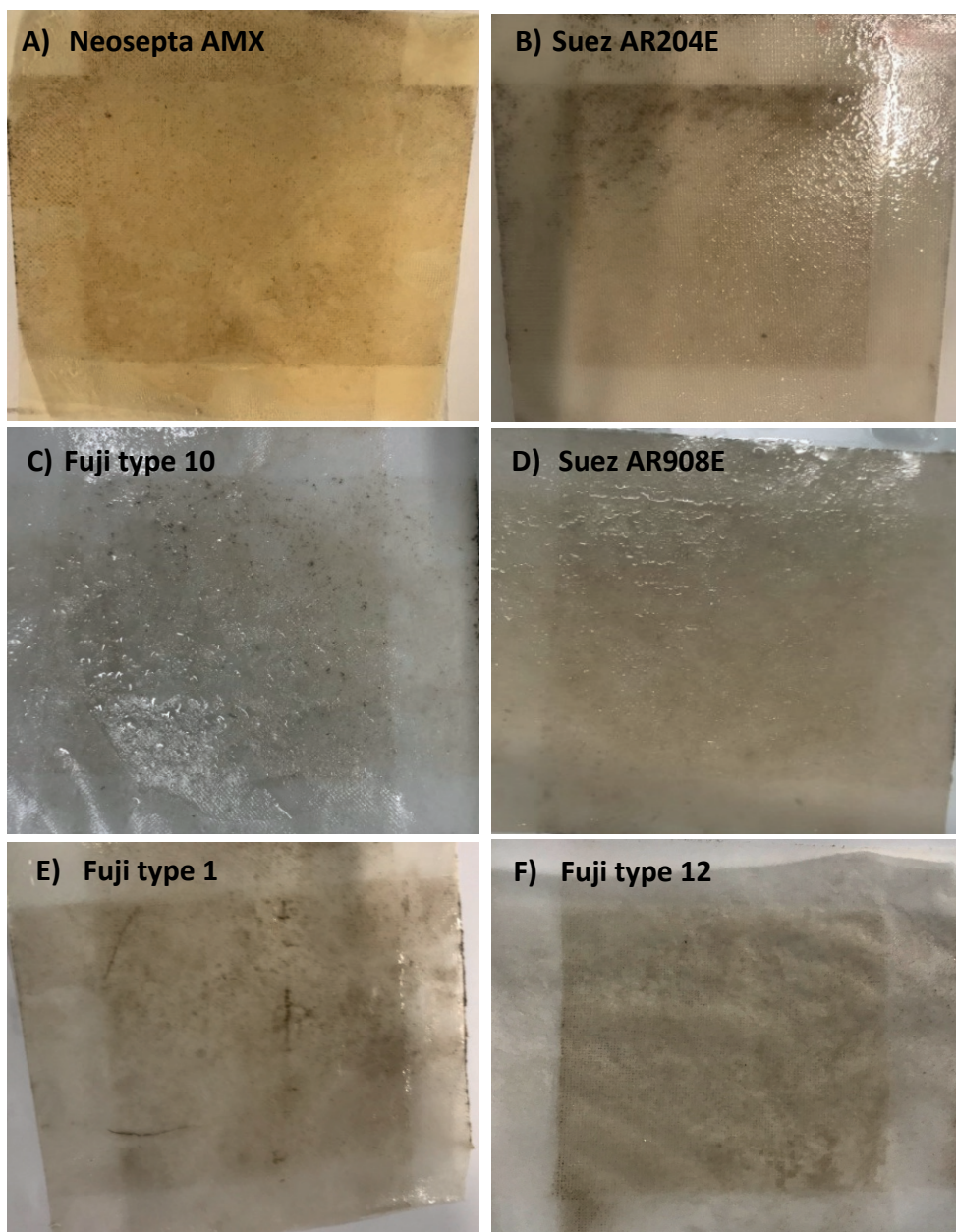

Figure A7.2. *Calibration curve relating the HPAM concentration to the measured TOC.*

Figure A7.3. *Electric potential U (marine) and current density i (light blue) versus time during the desalination of NaCl 0.5M (stage A) in the EDR mode (continuation of Figure 2). Values measured for the stack composed by (A) Suez AR204E, (B) Suez AR908E, (C) Fuji type 1 (incomplete data set due to a failure in the recording system), and (D) Fuji type 12.*
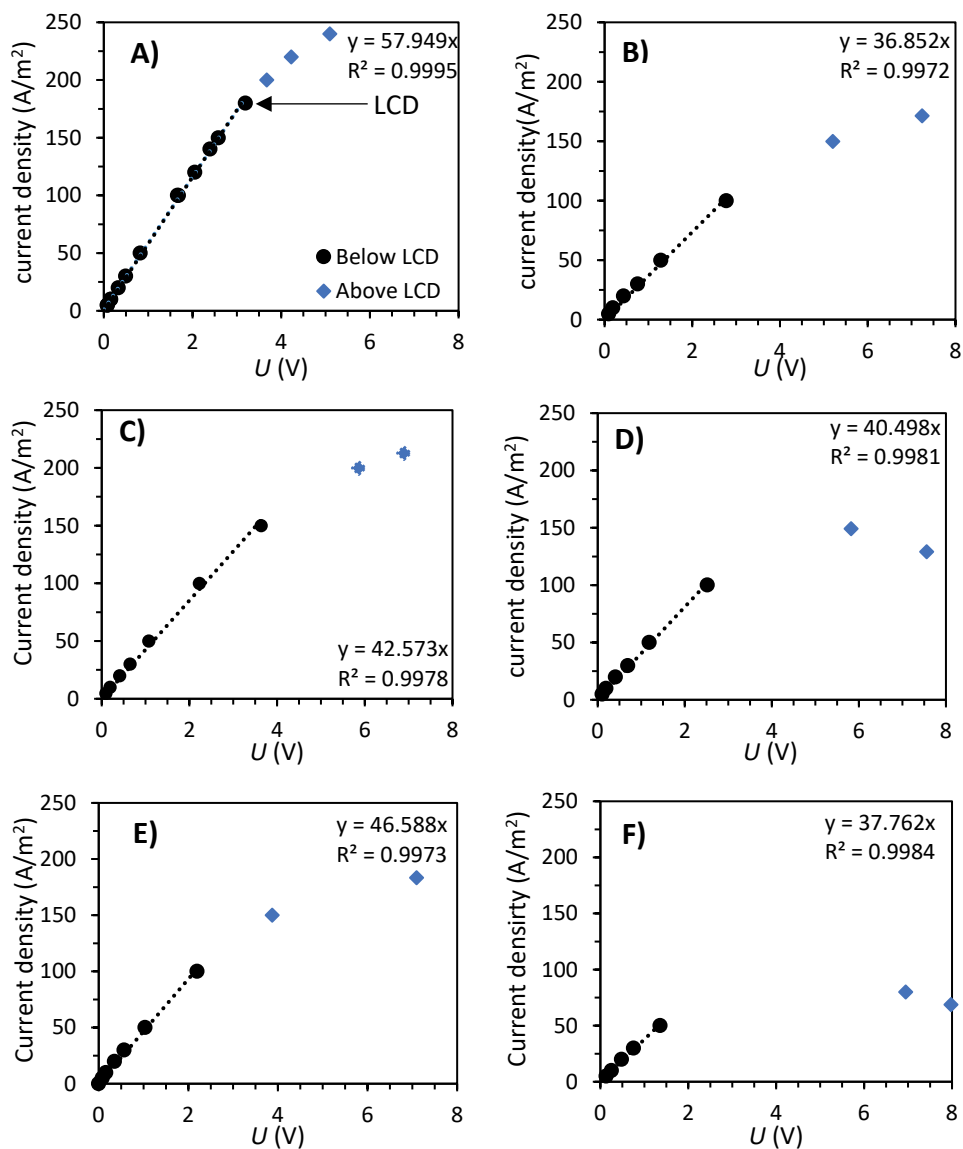
Figure A7.4. *Current density vs. voltage curves obtained when desalinating BW solution in stacks containing (A) Neosepta AMX, (B) Suez AR204E, (C) Fuji type 10, (D) Suez AR908E, (E) Fuji type 1, and (F) Fuji type 12. For Neosepta AMX, the LCD was calculated, while for the other AEMs, the test was only performed until enduring that the operation at 100 A/m² would follow ohmic behavior (linear trend).*

7

Figure A7.5. Photography's of anion exchange membranes recovered after the EDR runs

7

Chapter 8

Desalination of polymer-flooding produced water at increased water recovery and minimized energy
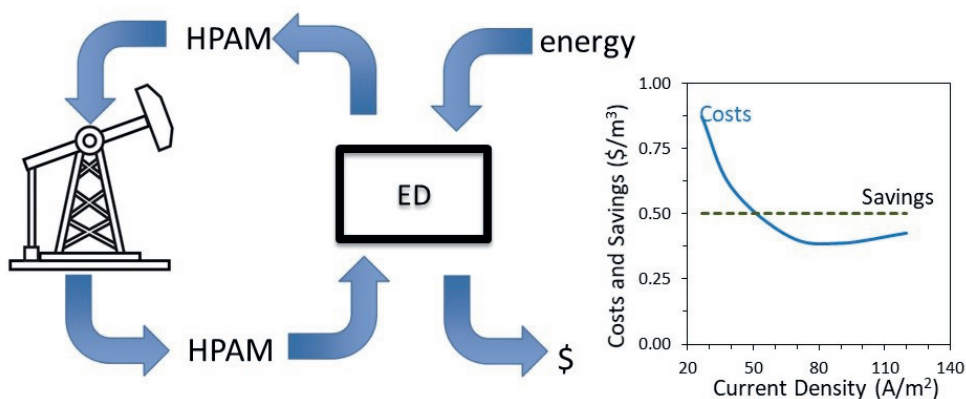
Abstract

When desalinating an industrial stream like polymer-flooding produced water via electrodialysis (ED), high water recoveries, low energy consumption, and reduced membrane area are all desirable. However, little effort has been done until now to experimentally achieve these goals. Encouraged by recent and promising results obtained using aliphatic membranes and pulsed electric field, this study experimentally evaluated different strategies and operational conditions to increase the water recovery while keeping a low energy consumption. The results obtained were analyzed to understand the tradeoffs in operative time, water recovery and energy consumption. At last, the experimental data was employed to perform an economic analysis, which indicated that although further optimization should be possible, current conditions already make ED desalination of polymer-flooding produced water a sound case from an economical point of view.

8.1 Introduction

Polymer-flooding produced water (PFPW) is a relatively new waste stream co-produced by the oil and gas industry when polymer flooding technology is applied to enhance oil recovery from a field. PFPW typically contains varying amounts of dissolved solids –mainly salts-, oil, and a viscosifying water-soluble polymer, typically partially hydrolyzed polyacrylamide (HPAM) or one of its derivatives [1]. To be reused in polymer flooding, PFPW should be partially desalinated, a goal that can be achieved by using electrodialysis (ED) [2,3]. However, the mixed composition of PFPW, and particularly the presence of the polyelectrolyte HPAM, makes the desalination by ED challenging due to concentration polarization and fouling [1,4,5].

An option to reduce concentration polarization and fouling incidences during ED is to use a pulsed electric field (PEF) [6]. This mode of operation consists in applying the electric current for a short time (pulse), followed by a resting period without current (pause), while the streams are continuously pumped through the ED stack. In this way the built up of polarization layers is prevented. In previous investigations, PEF and continuous modes were employed and compared in their performances to desalinate PFPW. Membrane surface analyses revealed that fouling was minimal, with negligible differences between both operation modes. In contrast, noteworthy reductions in energy consumption (above 30%) and desalination performance were found, especially when employing a pulse/pause regime of 1s/1s [7].

Although these results were encouraging, the small amount of fouling found on the IEMs was a surprise. Two explanations were put forward: either the duration of the experiments (2-8 hours) was too short to accumulate significant amounts of foulants, or the membranes employed (FujiFilm type 10) had superior antifouling properties than others previously employed in various studies [3,8,9].

Both hypotheses were addressed in a recent study, in which synthetic PFPW was desalinated continuously for 8 days employing stacks composed of different kinds of AEMs. The desalination performance and membrane analysis indicated more fouling than in the PEF study. Regarding the role of the membranes, it was found that the likelihood of the stacks reaching limiting conditions mainly depended on the resistance of the AEMs. Moreover, the stability in stack desalination performance, was smaller for aromatic AEMs than for aliphatic AEMs, suggesting that the latter were more adequate to desalinate PFPW [10].

The next step in operationalizing PFPW desalination by advanced ED is to operate the lab-scale system under relevant conditions to optimize energy consumption,

capital investment and water recovery, as well as the tradeoffs among these factors, as will be further elaborated.

First, the ED process needs to be designed to generate more product and less concentrate, that is, to achieve high water recoveries. This results from the purpose of desalinating PFPW is to reuse it, while minimizing the concentrate solution that needs to be further treated or disposed of. However, previous investigations have been conducted at constant water recoveries around 50%. Higher water recoveries could mean less waste, higher energy efficiency, and lower costs [11]. With ED very high water recoveries can be reached, above 90% for some industrial cases [12,13]. These high recoveries can be achieved by operating the ED in the feed and bleed mode [12], or in a batch process by splitting the feed disproportionately. Of course, achieving higher water recoveries may also affect energy consumption and likelihood of scaling, both of which could increase.

Another aspect to be considered when designing an electrodialysis process for PFPW is the number of hydraulic stages. Typically, the design values for salt removal in one hydraulic stage is 40-50%, meaning that to increase the amount of salts removed in an ED system, additional stages must be incorporated [13]. For example, Doornbusch et al. recently found that four stages would be needed to obtain drinking water (TDS<0.5 L) from seawater [14]. This is because the operating current density for an electrodialyzer is usually limited by the lowest salinity during the stage. If the process is divided in two or more stages, each stage can be operated at different current densities, which has a positive impact in the production rate, but implies more equipment and different energy consumption. In our case study (PFPW mimicking that from the Marmul field in Oman), the salinity of the feed is just below 5.0 g/L[15], while the desired salinity of the product is around 1.0 g/L[16], so 80% salt removal is needed. This means that, if PFPW is desalinated in a continuous process, at least two stages would be desirable to achieve the preferred product quality.

Another aspect that hasn't been addressed yet is the analysis of the cost-benefits of applying PEF at a larger scale. For a non-optimized system, we achieved energy savings of approximately 30% for a PEF regime of 1s/1s. Because of the pauses during operation, the time required to desalinate a fixed volume of solution was almost doubled. If a production rate is defined, a system operated in PEF with a 1s/1s regime would require twice the membrane area needed by an ED system operated in continuous mode. It might be possible to further reduce the pause time and still obtain beneficial results. For example, Mikhaylin et al. found their best results in terms of demineralization rate and low scaling by applying regime pauses four times shorter than the pulse (2s/0.5s) [17].

Summarizing, when selecting operational conditions for an ED system, the tradeoff between energy consumption, capital investment (including membrane area and staging) and water recovery should be considered. PFPW being highly viscous and containing high concentrations of polymers, does not behave like common brackish water, hence literature guidelines for designing and operating a system to minimize the total costs of regular brackish water desalination[18] might not be fully applicable and the costs and implications for PFPW desalination can be very different. For example, Thiel et al. estimated that, in practice, the minimum work necessary to desalinate produced water could be up to 9 kWh/m^3, nearly an order of magnitude higher than for seawater desalination [19].

Operational conditions for an ED system can vary quite significantly, and selection and design of an adequate ED configuration for a certain application requires a thorough understanding of the relationships among energy consumption – capital costs – water recovery. Furthermore, the possibility of using pulsed electric field has not been explicitly considered in the reports available in literature. Therefore, this study has two objectives: 1) to evaluate PFPW desalination at conditions close to the foreseen industrial application, specifically operating at high water recoveries, and at -close to- limiting current density, and 2) to use the collected data to relate performance in terms of energy consumption – capital costs – water recovery, and to identify strategies to cope with their tradeoffs.

To achieve these objectives, the study is subdivided in three sections. In the 1st section, the water recovery was systematically increased while evaluating the effects in energy consumption and water transport. In the 2nd part, the performance and fouling sensitivity of two ED-stacks composed of different IEMs was evaluated. Finally, the 3rd section employs the results from the previous two to scrutinize the energy–membrane area–water recovery tradeoffs, and to discuss the feasibility of using PEF during the process.

8.2 Materials and methods

8.2.1 Preparation of solutions and chemicals

The feed solutions consisted of a mixed salt solution, referred as brackish water (BW), plus viscosifying polymer (BW+P). The BW solutions were prepared in demineralized water, according to the composition of the Marmul field (Oman), by adding the following salts: 53.3 mM NaCl, 15.6 mM NaHCO$_3$, 2.51 mM Na$_2$SO$_4$, 0.72 mM KCl, 0.65 mM CaCl$_2$, and 0.46 mM MgCl$_2$ [15]. The pH of the fresh solutions was 7.7, and their conductivity 7.75 mS/cm.

All BW+P solutions had a concentration of 0.5 g/L of partially hydrolyzed polyacrylamide (HPAM). They were prepared by slowly pouring the polymer inside

the BW solution under fast agitation, after which the mixture was left stirring at low speed overnight.

The salts employed to prepare the solutions (NaCl, KCl, $MgCl_2·6H_2O$, $CaCl_2·2H_2O$, Na_2SO_4, and $NaHCO_3$) were analytical grade, purchased from VWR (Belgium), and employed without further purification. The HPAM employed was Flopaam 3130S (MW= 4.4 to 4.8 million Da and 30% hydrolyzed), kindly provided by SNF (France). NaOH and HCl solutions utilized for chemical cleaning were prepared from analytical grade reagents purchased from VWR.

8.2.2   Electrodialysis setup

Experiments were performed in ED stacks like the one previously described [7]. Two configurations were used:

i.   FujiFilm (FF) stack. Contained seven FujiFilm type 10 AEMs, six CEMs type 10, and two Neosepta CMX, which were placed at both ends of the stack as shielding membranes.

ii.   Neosepta stack. Consisted of seven Neosepta AMX membranes, six CMS CEMs, and two Neosepta CMX as shielding membranes.

The FujiFilm membranes were kindly provided by FujiFilm Manufacturing Europe B.V., while the Neosepta membranes were purchased from Eurodia (France). The working area of each membrane (104 cm^2), spacer, gasket, and electrode were the same as previously reported. A potentiostat/galvanostat Ivium-n-Stat (Ivium Technologies, NL) controlled the electrical current and measured the potential difference over the cell. The potential difference was measured using two reference Ag/AgCl gel electrodes (QM711X, QIS, NL) placed at the inlet of each of the electrode compartments.

The diluate, concentrate, and electrolyte solutions were pumped by three independent MasterFlex pumps. The conductivities of the diluate and concentrate were measured in line with two conductivity probes (Orion DuraProbe 4-electrode conductivity cell 013005MD) placed before the ED stack. The probes were connected to a transmitter box (Orion Versastar Pro), which corrected the measured values to the reference value at 25 °C. The pH of the solutions was measured with two pH probes (MemoSENS Endress+Hauser) connected to a transmitter box (P862, QIS). Two back-pressure valves (0.25 bar) were placed at the outlet of the electrolyte solution to guarantee the complete wetting of the electrodes.

8.2.3   Electrodialysis runs

The electrodialysis experiments were run in batch mode until the design conductivity of 2.0 mS/cm was reached in the diluate stream. Most of them were run at a constant current of 40 A/m², which was found to be the limiting current density when desalinating a 2.0 mS/cm solution prepared by diluting the BW solution with demi water (Figure A8.1). Diluate and concentrate feed solutions had the same composition. Both were pumped at 260 mL/min (linear velocity of 2.0 cm/s), while the electrolyte was circulated at 170 mL/min. The ED runs were performed at 23 ± 1°C in a controlled-temperature laboratory.

Two sets of experiments were performed during this study, summarized in **Table 8.1** together with their main conditions. For the water recovery set (#1), the only variable was the ratio between the volumes of diluate (V_D) and concentrate (V_C), which had different values depending on the volume of concentrate, which was varied between 5.0 to 0.5 L. The rest of the operational parameters, including the volume of the diluate (5.0L) and current density (40 A/m²), were kept constant. This set was run only with the FujiFilm stack.

8

Table 8.1. Summary of ED runs performed during this study

Run/set	Stack	V_D (L)	V_C (L)	Stages	Mode	i (A/m²)	Replicates
1a	FujiFilm	5.0	5.0	1	Continuous	40	3
1b	FujiFilm	5.0	3.0	1	Continuous	40	1
1c	FujiFilm	5.0	2.0	1	Continuous	40	1
1d	FujiFilm	5.0	1.0	1	Continuous	40	1
1e	FujiFilm	5.0	0.5	1	Continuous	40	3
2a	FujiFilm & Neosepta	4.0	0.4	1	Continuous	40	Set of 3
2b	FujiFilm & Neosepta	4.0	0.4	1	PEF 1s/0.5s	40	Set of 3
2c	FujiFilm & Neosepta	4.0	0.4	1	PEF 1s/0.5s	60	Set of 3

Before each ED run, the solutions were circulated through the cell for 10 minutes before starting the measurements. During the experiment, the applied current, stack voltage, and transported charges were recorded using the software provided by Ivium (IviumSoft). Samples were periodically taken. The final volumes of the solutions were measured with a graduated cylinder. Immediately after the runs, the ED stack was cleaned-in-place by circulating a sequence of solutions for 10 minutes each. The schedule included: HCl solution (pH = 2), NaCl solution (5.0 g/L), NaOH

solution (pH = 12), NaCl solution (5.0 g/L), and a final rinse of at least 15 minutes with BW solution [20,21].

8.2.4   ED for comparing the performance of two stacks through 3 sequential runs

For the second part of the study, two different ED-stacks were employed, one composed by FujiFilm membranes and one composed by Neosepta membranes (section 8.2.2). Besides the type of membranes, both stacks were identical, containing the same number of cell pairs, type of spacers, etc. Each of the stacks was employed to desalinate three sequential batches of 4.0L of BW+P solution, each set operated in a different mode. Three modes were tested: one in continuous, and two in PEF mode run at different current densities, as described in Table 8.1. The PEF regime was determined after performing preliminary experiments, included in **Appendix 8B**. After a set of three runs was finished, the stack was cleaned-in-place as explained in the previous section.

8.2.5   Analytical methods

8.2.5.1   *Solution analysis*

Diluate and concentrate samples were taken during the experiments. Their content of cations was analyzed with inductive-coupled plasma optical emission spectroscopy (ICP-OES, Optima 5300DV, Perkin Elmer), and that of anions with ion chromatography (761 Compact IC, Metrohm). Total Carbon, inorganic carbon, and total organic carbon (TOC) were measured using a TOC analyzer (Shimadzu TOC-VCPH).

8.2.5.2   *Water recovery and energy calculations*

The Water Recovery (WR) was calculated by dividing the final volume of diluate ($V_{D,f}$) by the sum of the initial volumes of diluate ($V_{D,i}$) and concentrate ($V_{C,i}$):

$$WR = \frac{V_{D,f}}{V_{D,i}+V_{C,i}} \times 100 \qquad \text{/8.1/}$$

The energy consumption (EC) was calculated by integrating the product of the current I (A) and the voltage U (V) [22]:

$$EC = \int I(t) \cdot U(t) \, dt \qquad \text{/8.2/}$$

The specific energy consumption (*SEC*) was obtained from dividing the EC by the final volume of diluate ($V_{D,f}$) in m^3.

8.2.5.3 *Osmotic and electro-osmotic transport*

The ionic composition of the streams, determined from the sample analysis, was used to calculate the flux of ions from the diluate to the concentrate stream and the concentrations in the bulk solutions. Then, the equations for osmotic and electro-osmotic water transport (Eqs. 2.1 and 2.2 in Chapter 2 [3]) were employed to estimate the amount of water transported. The parameters D_w (m²/s) and t_w (mol-H₂O/F) were simultaneously determined by employing a non-linear solving method that would minimize the square of the differences between the concentrations measured and the ones estimated. The constraints given to the program were $0 < D_w < 1$, and $4 < t_w < 20$.

8.3   Results and discussion

8.3.1   Water transport and energy consumption as water recovery is increased

The first objective of this work was to increase the water recovery (WR) of the process. The initial volume of concentrate solution ($V_{C,i}$) was systematically decreased from 1.0 to 0.1 times the volume of diluate ($V_{D,i}$) to achieve a higher water recovery. Since the rest of the parameters were maintained, including the volume and composition of the diluate solution, the amount of salts transferred from diluate to concentrate solution was essentially the same. This implied that for smaller volumes of concentrate, the resulting salt concentration was higher, as indicated by the measured conductivities in the bulk solution, presented in **Figure 8.1A**. This had a small effect on the electric potential required to maintain the desalination at constant current, as presented in **Figure 8.1B**.
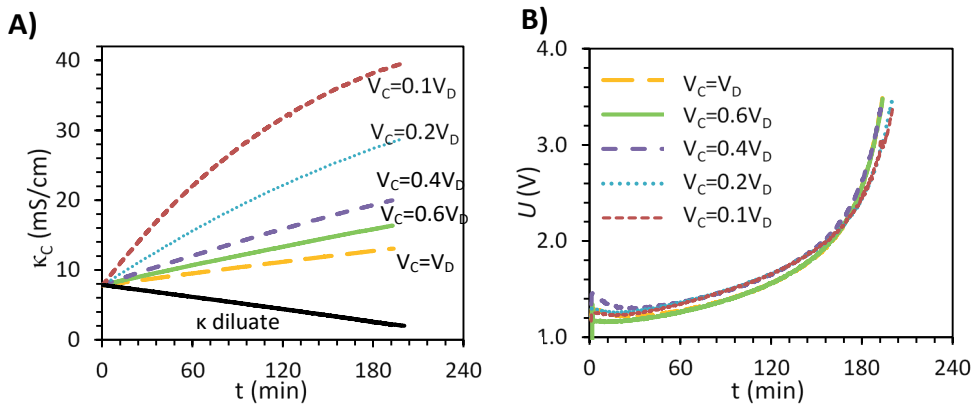
Figure 8.1. A) Conductivity of the bulk concentrate solution (κ_C) measured during batch ED experiments desalinating 5.0 L of diluate solution with different volumes of concentrate (V_C) solution. B) Electric potential (U) vs time (t) during the runs.

Another effect of increasing the water recovery was a higher amount of water transport, which can be inferred from differences in recovered diluate volumes (**Figure 8.2A**). Free water transport (osmosis) occurs due to the difference in osmotic pressure between the diluate and the concentrate streams, and the larger the difference is, the higher the water transport. The relation between the driving force and the flux of water transported by osmosis can be characterized by the water transfer or diffusion coefficient D_w (m²/s) [3]. However, water is also transported in the hydration shell of the ions that migrate from diluate to concentrate, commonly referred to as electro-osmosis. The water flux due to electro-osmosis is related to the flux of ions through the average water transport number for a specific membrane pair t_w (moles H₂O/F)[23]. By employing the method described in our previous work[3], the values of t_w and D_w for the pair of FujiFilm type 10 membranes were respectively estimated as 11 moles H₂O/F and 1.91×10⁻⁹ m²/s. Both values are higher than the ones previously determined for the membrane pair Neosepta CMX/AMX (t_w=8, and D_w=2.0×10⁻¹⁰ m²/s) [3], indicating that FujiFilm membranes allow higher osmotic and electro-osmotic transport. **Figure 8.3** shows how the modelled conductivity values, based on ion migration and water transport, compare with the experimental data for the runs with the lowest and the highest WR.

Finally, when plotting the specific energy consumption (*SEC*, calculated via Eq. 8.2), as a function of WR (**Figure 8.2B**), it can be noticed that by increasing the WR from 48% to 85%, the *SEC* was also higher, from 0.43 to 0.50 kWh/m³. This was caused by the combination of slightly higher electric potential required to transport the salts across the IEMs, plus the reduction in the volume of product due to water transport.
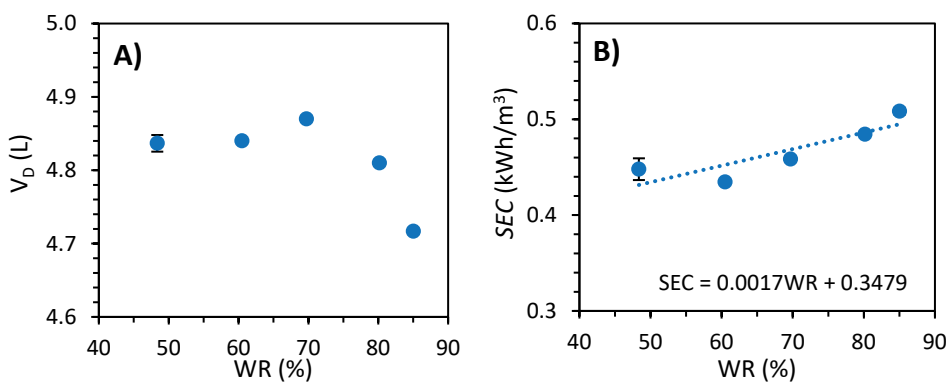
Figure 8.2. Diluate volume (A) and specific energy consumption (SEC) (B) both vs water recovery (WR) calculated from the ED runs with varying concentrate volume. The error bars were calculated from experiments performed by triplicate.
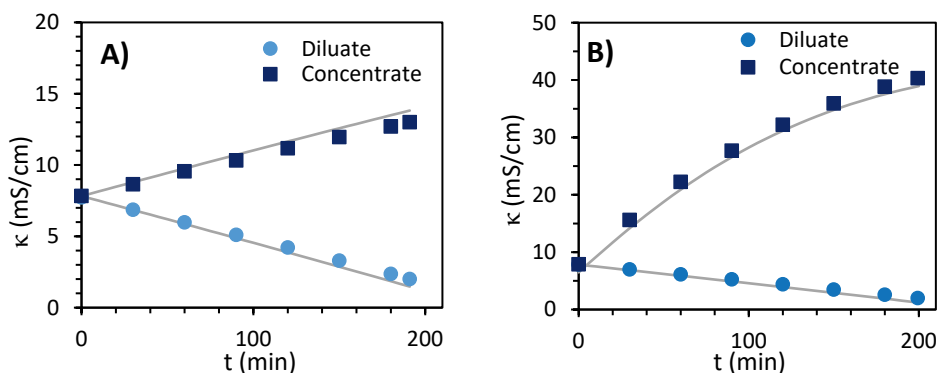
Figure 8.3. Average conductivities of the diluate and the concentrate streams vs time for experiments with 48% WR (A) and 85% WR (B). The modelled values consider 90% efficiency, t_w= 11, and D_w= 1.91 ×10^{-9} m^2/s.

8.3.2 Comparison of an aromatic (Neosepta) and an aliphatic (FujiFilm) stack in different operation modes

The second experimental part consisted in performing three batch desalinations in series without cleaning the ED-stack in between, with the aim of comparing their performance after fouling has occurred. As shown in **Figure 8.4**, three different operational scenarios were tested using the Neosepta and FujiFilm stacks: A) continuous (40 A/m^2); B) PEF mode (1s/0.5s) with 40 A/m^2 pulses (ī=26.7 A/m^2); and C) PEF mode (1s/0.5s) with 60 A/m^2 pulses (ī=40 A/m^2). There were considerable differences in the operative time and electric potential required to desalinate the three consecutive batches of PFPW depending on the stack and mode of operation. Among the several details that can be elaborated, our discussion will focus on three: time differences between runs, water transport, and energy consumption.

The time differences from run to run can be better appreciated in **Figure 8.5A**. Although the differences are small, it is curious to notice that while for the FujiFilm stack the 2nd and 3rd runs tended to be longer than the 1st one, the opposite occurred for the Neosepta stack. Based on our previous work[10], this could be an indication of some HPAM fouling the FujiFilm IEMs and reducing their permselectivity, which causes an increase in the transport of counter-ions and a decrease in efficiency, thus increasing the time of the run. In contrast, the duration of the experiments performed with the Neosepta stack was highly consistent from run to run, so apparently no changes in permselectivity occurred. The largest time difference for the Neosepta stack occurred between the 1st and 2nd run of the continuous experiments; this may be explained by the fact that the first run of the stack was done with new membranes, which were apparently still stabilizing during the 1st run.

8
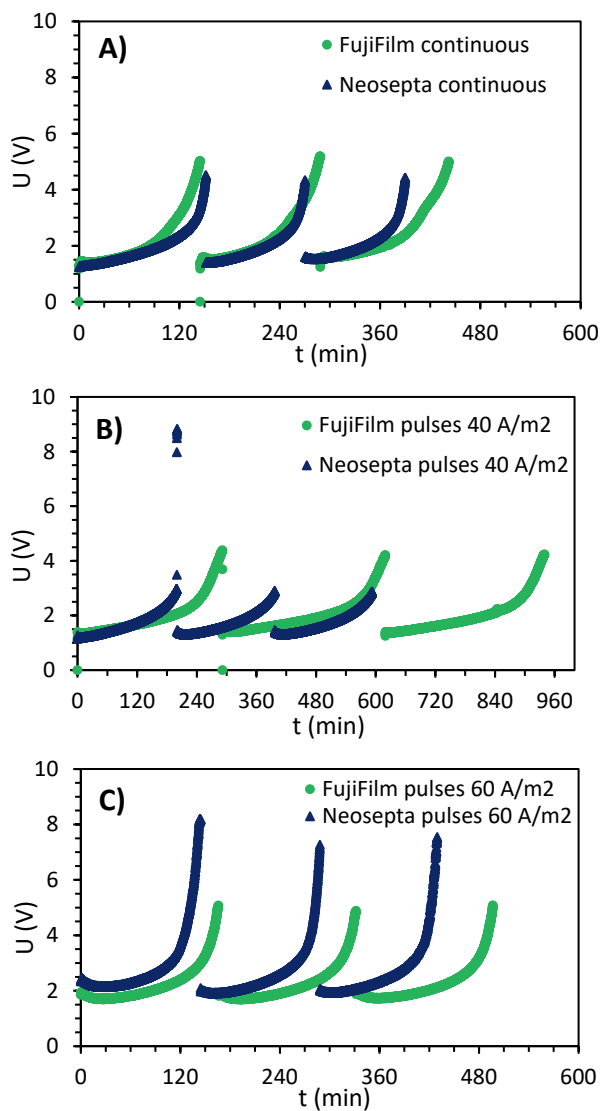
Figure 8.4. Electric potential (U) vs time during batch runs performed in sequence without cleaning-in-place. (A) Continuous operation at 40 A/m², (B) Pulsed operation 1s/0.5s, with 40 A/m² pulses, and (C) Pulsed operation 1s/0.5s, with 60 A/m² pulses.
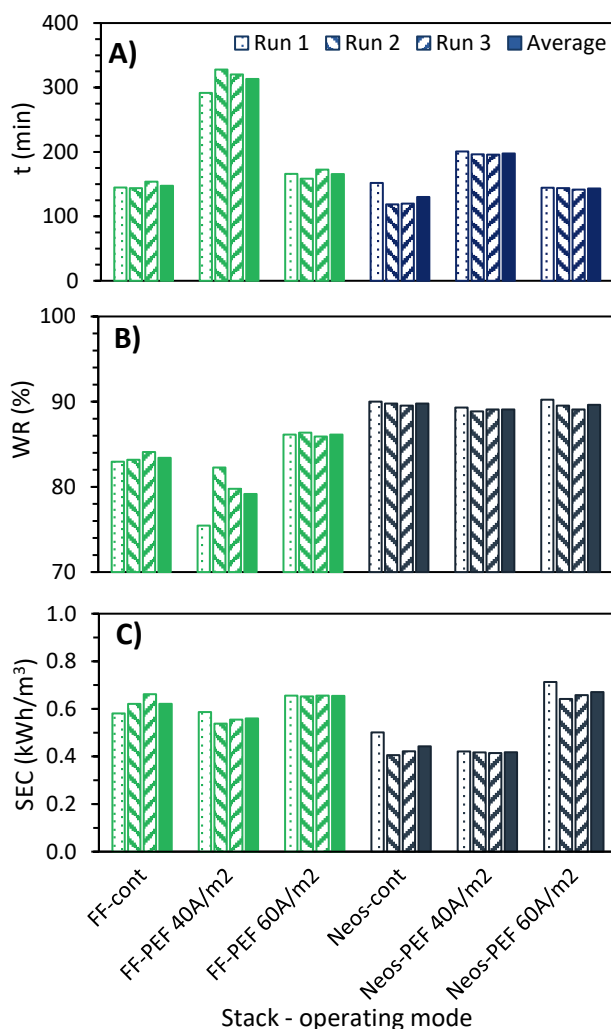
Figure 8.5. Running time (A), water recovery WR (B), and specific energy consumption SEC (C), obtained when operating the FujiFilm and Neosepta stacks in different modes to desalinate 3 batches of PFPW until reaching a conductivity of 2.0 mS/cm.

Water transport had also major consequences on the results presented in **Figure 8.4** and **Figure 8.5**. It did not only have implications in terms of reducing water recovery, but it also extended the operational time because it implies that the remaining salts are dissolved in a smaller volume, so more ions had to be transported to reach the desired quality in the diluate. Then, as shown in **Figure 8.4A**, when operated in continuous mode, the FujiFilm stack required roughly 50 more minutes over the 390 minutes used by the Neosepta stack to complete the three ED runs. Moreover, the average WR achieved by the FujiFilm stack was 83.4%, while for the Neosepta stack it was 89.8% (**Figure 8.5B**). These results can be related to the differences between the electro-osmotic and diffusion coefficients for both membranes, presented in

section 8.3.1. On average, 440 meq of ions were transported from diluate to concentrate during each of the runs, which implied an electro-osmotic transport of ~60 mL of water for the Neosepta stack and ~90 mL for the FujiFilm stack (considering t_w=8 mol H_2O/F and t_w=11 mol H_2O/F, respectively). For the Neosepta stack, that was practically all the water that was transported, meaning that water transport via diffusion did not play an important role, as expected from the low osmotic diffusion coefficient (D_w=2.0×10^{-10} m^2/s). On contrary, the osmotic diffusion coefficient calculated for the FujiFilm stack was one order of magnitude larger (D_w=1.9×10^{-9} m^2/s), and our measurements also indicated that most of the water transport (65%) can be attributed to osmosis.

Still addressing water transport, its effects were maximized during the pulsed operation at 40 A/m^2 (**Figure 8.4B**): while the total time required by the Neosepta stack was ~600 minutes, the operation with the FujiFilm stacks lasted more than 900 min. Similarly, the average duration of a run was under 200 minutes for Neosepta, and 300 minutes for FujiFilm (**Figure 8.5A**). For both stacks, the transport of water through electro-osmosis should have been the same as calculated for the continuous mode (since a similar number of salt equivalents were transported), but the osmotic transport increased due to the extended operational time. By comparing the conductivity measurements vs time (Sup. Material, Figure A8.2) it can be deduced that during the runs with the FujiFilm stack, forward salt transported during the pulse and backward water transported during the pause approached balancing values, which caused the extra operational time. However, these negative effects of elevated water transport in the FujiFilm stack were minimized by operating at 60 A/m^2 (**Figure 8.4C** and **Figure 8.5B**). In that case, the average operative time per run with the FujiFilm stack was 165 minutes, only 22 minutes longer than for the Neosepta stack, and the water recovery was 3% higher than for the continuous runs (**Figure 8.5B**).

In terms of energy consumption, **Figure 8.5C** shows that when operated in continuous mode or in PEF with low current density pulses (40 A/m^2), the Neosepta stack achieves the desired desalination with a lower *SEC*. However, the performance of the FujiFilm stack improves when operated at higher currents due to lower operative time (meaning lower water transport), and lower membrane resistance compared to the Neosepta membranes[10]. Thus, when operated in PEF mode with 60 A/m^2 pulses, the *SEC* of the FujiFilm stack is lower than that of Neosepta one. Additional experiments performed in PEF with 100 A/m^2 pulses ($\bar{\imath}$=66.7 A/m^2) resulted in 1.24 kWh/m^3 for the FujiFilm stack and 1.43 kWh/m^3 for the Neosepta one (plots included in Figure A8.3). This confirmed the tendency of improved performance of the FujiFilm stack when higher current densities are employed.

8.3.3 Inter-relative analysis of water recovery, energy use and implemented membrane area

The current densities employed in the previous sections fall in the lower-end of the recommended range to minimize costs for BW desalination[18]. However, this disadvantage could be compensated by the savings when reusing the desalted water, especially since they also imply savings in polymer. Thus, we performed an economic analysis to identify if the current process design would be satisfactory enough to move onwards to the scaling up of the process. **Table 8.2** includes the parameters and values employed for the calculations.

The costs were calculated by adding up the installed membrane costs plus the energy costs, both in $/m³. As can be observed in **Figure 8.6,** three cases were evaluated: low, moderate and high, depending on the price of the installed membrane area, which were assumed to be 100, 200 and 500 $/m², respectively. These values were determined based on the prices of different commercial IEMs and are in agreement with recent literature[27]. The energy cost was calculated by adding up the pumping cost (fixed at 0.4 kWh/m³), plus the energy for desalination cost. The desalination costs and membrane costs were calculated simultaneously, from the data presented in sections 8.3.1 and 8.3.2 of this study, as follows: a stack containing 0.146 m² of total membrane area (7 cell pairs x 104 cm²) produced approximately 4.0 L of diluate in 3h of operation at an average current density of 40 A/m². Hence, for this current density the apparent flux is 9.1 L/m²h. Assuming an annual utilization of 8,000 hours and a membrane lifetime of 6 years[24], each m² of installed membrane has a total production capacity of 437 m³ of diluate, or inversely, 2.28×10^{-3} m² of membrane area are needed per m³ of product. Similar calculations were performed for other current densities, some evaluated during this work (26.7, 66 A/m²), and some extrapolated (90 and 120 A/m²), resulting in energy costs ranging from 0.05 to 0.24 $/m³, and membrane costs between 1.71 and 0.11 $/m³. Thus, for most of the evaluated cases, the membrane cost dominates total costs, similar to previous calculations for brackish water desalination [18].

Table 8.2. Parameters used for cost estimation

Parameter	Value
Installed membrane cost	150, 250, 500 $/m³
Apparent flux with current stack @ 40 A/m²	9.1 L/m²h
Annual utilization	8,000 h
Membrane lifetime [24]	6 years
Energy consumption pumps & others	0.4 kWh/m³
Electricity cost	0.05 $/kWh
Amount of HPAM saved [3,25]	0.5 kg/m³
Price of HPAM [26]	1.0, 1.5, 2.5 $/kg

On the other hand, the only savings considered were those from a reduced polymer consumption. The reason for this is that the polymer is relatively costly, and the saving of water use and discharge are highly case dependent. In this generic assessment, these were not capitalized but could add case specific benefits on top of those assessed here. From our previous research, it was found that by desalinating the PFPW, at least 0.5 kg/m^3 of HPAM could be saved[3], an estimation supported by other studies [25]. For the calculations three cases were evaluated: low, moderate, and high savings, depending of the price of the polymer HPAM (1.0, 1.5 and 2.5 $/kg).

Finally, **Figure 8.6** shows that when moderate costs and savings are considered, the break-even point (indicated with an X in the figure) occurs at a relatively low current density of 30 A/m^2. At low membrane costs, even low end in polymer savings are offering a favorable business case at current densities of 35 A/m^2. Only when the membrane costs are in the high end, high polymer savings would be necessary to compensate for the operation at low current densities.
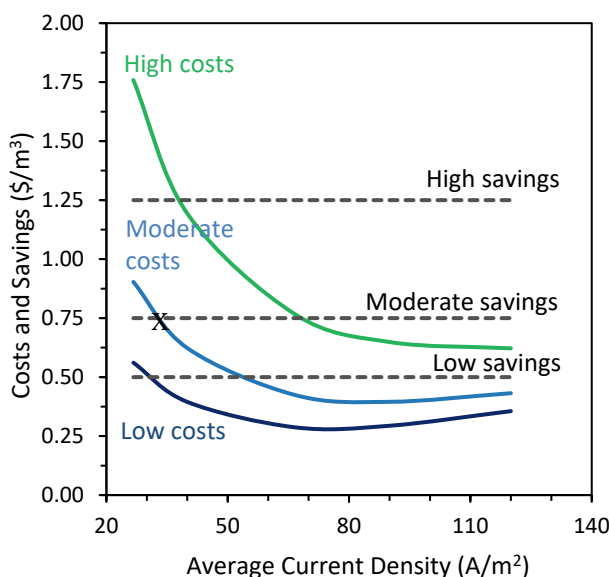
Figure 8.6. Estimation of costs and savings for polymer-flooding produced water desalination as a function of average current density. Low, moderate, and high costs and savings scenarios are based on the information supplied in Table 8.2.

8.4 Conclusions

During this study, the use of aliphatic versus aromatic membranes and the application of pulsed electric field were experimentally tested to increase the water recovery and reduce the energy consumption during PFPW desalination. Water

transport through the ion-exchange membranes tested showed significant differences. However, it was demonstrated how the high-water permeability of aliphatic FujiFilm-10 IEMs affected both energy consumption and the final water recovery of an electrodialysis-based process. However, it was also shown that most of the water transport could be attributed to the osmotic component, which becomes less significant when the ED was operated at higher current densities, so the performance of the stack containing aliphatic membranes equalized that of the stack containing the aromatic ones.

Regarding the application of pulsed electric field, comparisons made for same average current density showed a negative impact in SEC for the Neosepta stack and practically no impact in the case of the FujiFilm stack. Although fouling might have formed after desalinating three consecutive batches, its effect on the overall performance of the stacks was minimal.

The economic analysis demonstrated that the recovery of PFPW with ED at low current density offers a realistic business case with potential to be further improved if higher current densities are achieved. This could be achieved either by applying the PEF mode, or by employing stacks that allow operation with higher cross flow velocities and hence higher limiting current densities. Beyond savings in polymer use, additional, but case specific economic and sustainability benefits can be achieved by the reuse of water, which can be a significant factor in fresh water-scarce areas where many oil and gas production sites are located [28].

8

References

[1]   J. Guolin, W. Xiaoyu, H. Chunjie, The effect of oilfield polymer-flooding wastewater on anion-exchange membrane performance, Desalination. 220 (2008) 386–393. doi:10.1016/j.desal.2007.03.010.

[2]   G. Jing, L. Xing, S. Li, C. Han, Reclaiming polymer-flooding produced water for beneficial use: Salt removal via electrodialysis, Desalination and Water Treatment. 25 (2011) 71–77. doi:10.5004/dwt.2011.1766.

[3]   P.A. Sosa-Fernandez, J.W. Post, H. Bruning, F.A.M. Leermakers, H.H.M. Rijnaarts, Electrodialysis-based desalination and reuse of sea and brackish polymer-flooding produced water, Desalination. 447 (2018) 120–132. doi:10.1016/j.desal.2018.09.012.

[4]   P.A. Sosa-Fernandez, S.J. Miedema, H. Bruning, F.A.M. Leermakers, H.H.M. Rijnaarts, J.W. Post, Influence of solution composition on fouling of anion exchange membranes desalinating polymer-flooding produced water, Journal of Colloid And Interface Science. 557 (2019) 381–394. doi:10.1016/j.jcis.2019.09.029.

[5]   H. Guo, L. Xiao, S. Yu, H. Yang, J. Hu, G. Liu, Y. Tang, Analysis of anion exchange membrane fouling mechanism caused by anion polyacrylamide in electrodialysis, Desalination. 346 (2014) 46–53. doi:10.1016/j.desal.2014.05.010.

[6]   S. Mikhaylin, L. Bazinet, Fouling on ion-exchange membranes: Classification, characterization

and strategies of prevention and control, Advances in Colloid and Interface Science. 229 (2016) 34–56. doi:10.1016/j.cis.2015.12.006.

[7] P.A. Sosa-Fernandez, J.W. Post, M.S. Ramdlan, F.A.M. Leermakers, H. Bruning, H.H.M. Rijnaarts, Improving the performance of polymer-flooding produced water electrodialysis through the application of pulsed electric field, Desalination. 484 (2020). https://doi.org/10.1016/j.desal.2020.114424.

[8] T. Wang, S. Yu, L. an Hou, Impacts of HPAM molecular weights on desalination performance of ion exchange membranes and fouling mechanism, Desalination. 404 (2017) 50–58. doi:10.1016/j.desal.2016.10.007.

[9] X. Zuo, L. Wang, J. He, Z. Li, S. Yu, SEM-EDX studies of SiO2/PVDF membranes fouling in electrodialysis of polymer-flooding produced wastewater: Diatomite, APAM and crude oil, Desalination. 347 (2014) 43–51. doi:10.1016/j.desal.2014.05.020.

[10] P.A. Sosa-Fernandez, J.W. Post, H.L. Nabaala, H. Bruning, H.H.. Rijnaarts, Electrodialysis reversal for desalination of (waste)water produced after polymer flooding: performance related to anion exchange membrane characteristics, Manuscript Submitted for Publication. (2020).

[11] M. Turek, K. Mitko, K. Piotrowski, P. Dydo, E. Laskowska, A. Jakóbik-Kolon, Prospects for high water recovery membrane desalination, Desalination. 401 (2017) 180–189. doi:10.1016/j.desal.2016.07.047.

[12] H. Strathmann, Ion-Exchange Membrane Processes in Water Treatment, in: Sustainability Science and Engineering, Elsevier, 2010: pp. 141–199. doi:10.1016/S1871-2711(09)00206-2.

[13] F. Valero, A. Barceló, R. Arbós, Electrodialysis Technology. Theory and applications, in: M. Schorr (Ed.), Desalination, Trends and Technologies, InTech Europe, Rijeka, 2011: pp. 3–20. doi:10.1063/1.2717084.

[14] G.J. Doornbusch, M. Tedesco, J.W. Post, Z. Borneman, K. Nijmeijer, Experimental investigation of multistage electrodialysis for seawater desalination, Desalination. 464 (2019) 105–114. doi:10.1016/j.desal.2019.04.025.

[15] A.R. Al-Hashmi, T. Divers, R.S. Al-Maamari, C. Favero, A. Thomas, Improving polymer flooding efficiency in Oman oil fields. Paper SPE-179834-MS, in: SPE EOR Conference at Oil and Gas West Asia Held in Muscat, Oman, 21–23 March 2016., SPE, Muscat, 2016: p. 18.

[16] S.C. Ayirala, E. Uehara-Nagamine, A.N. Matzakos, R.W. Chin, P.H. Doe, P.J. van den Hoek, A Designer Water Process for Offshore Low Salinity and Polymer Flooding Applications, SPE Improved Oil Recovery Symposium. (2013). doi:10.2118/129926-MS.

[17] S. Mikhaylin, V. Nikonenko, G. Pourcelly, L. Bazinet, Intensification of demineralization process and decrease in scaling by application of pulsed electric field with short pulse/pause conditions, Journal of Membrane Science. 468 (2014) 389–399. doi:10.1016/j.memsci.2014.05.045.

[18] K.M. Chehayeb, D.M. Farhat, K.G. Nayar, J.H. Lienhard, Optimal design and operation of electrodialysis for brackish-water desalination and for high-salinity brine concentration, Desalination. 420 (2017) 167–182. doi:10.1016/j.desal.2017.07.003.

[19] G.P. Thiel, E.W. Tow, L.D. Banchik, H.W. Chung, J.H. Lienhard V, Energy consumption in desalinating produced water from shale oil and gas extraction, Desalination. 366 (2015) 94–112. doi:10.1016/j.desal.2014.12.038.

[20] H. Guo, F. You, S. Yu, L. Li, D. Zhao, Mechanisms of chemical cleaning of ion exchange

membranes: A case study of plant-scale electrodialysis for oily wastewater treatment, Journal of Membrane Science. 496 (2015) 310–317. doi:10.1016/j.memsci.2015.09.005.

[21]   Q. Xia, H. Guo, Y. Ye, S. Yu, L. Li, Q. Li, R. Zhang, Study on the fouling mechanism and cleaning method in the treatment of polymer flooding produced water with ion exchange membranes, RSC Adv. 8 (2018) 29947–29957. doi:10.1039/c8ra05575k.

[22]   B. Ruiz, P. Sistat, P. Huguet, G. Pourcelly, M. Araya-Farias, L. Bazinet, Application of relaxation periods during electrodialysis of a casein solution: Impact on anion-exchange membrane fouling, Journal of Membrane Science. 287 (2007) 41–50. doi:10.1016/j.memsci.2006.09.046.

[23]   A.H. Galama, M. Saakes, H. Bruning, H.H.M. Rijnaarts, J.W. Post, Seawater predesalination with electrodialysis, Desalination. 342 (2014) 61–69. doi:10.1016/j.desal.2013.07.012.

[24]   H. Strathmann, A. Grabowski, G. Eigenberger, Ion-exchange membranes in the chemical process industry, Industrial and Engineering Chemistry Research. 52 (2013) 10364–10379. doi:10.1021/ie4002102.

[25]   E.C.M. Vermolen, M. Pingo-almada, B.M. Wassing, D.J. Ligthelm, S.K. Masalmeh, H. Mohammadi, G.R. Jerauld, M. Pancharoen, IPTC 17342 Low-Salinity Polymer Flooding : Improving Polymer Flooding Technical Feasibility and Economics by Using Low-Salinity Make-up Brine, The SPE Imroved Oil Recovery Symposium-USA. (2014) 15. doi:10.2118/153161-MS.

[26]   A.M. AlSofi, M.J. Blunt, Polymer flooding design and optimization under economic uncertainty, Journal of Petroleum Science and Engineering. 124 (2014) 46–59. doi:10.1016/j.petrol.2014.10.014.

[27]   R.A. Tufa, Y. Noviello, G. Di Profio, F. Macedonio, A. Ali, E. Drioli, E. Fontananova, K. Bouzek, E. Curcio, Integrated membrane distillation-reverse electrodialysis system for energy-efficient seawater desalination, Applied Energy. 253 (2019) 113551. doi:10.1016/j.apenergy.2019.113551.

[28]   M. Nasiri, I. Jafari, B. Parniankhoy, Oil and Gas Produced Water Management: A Review of Treatment Technologies, Challenges, and Opportunities, Chemical Engineering Communications. 204 (2017) 990–1005. doi:10.1080/00986445.2017.1330747.

8

Appendix 8A. Supplementary material
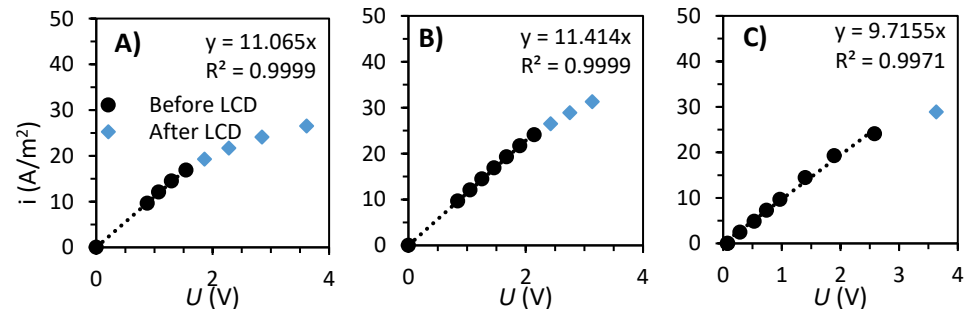
Figure A8.1. *Determination of limiting current density (LCD) for diluted BW solution (to 2 mS/cm) pumped at A) 170 mL/min, B) 260 mL/min, and C) 350 mL/min.*
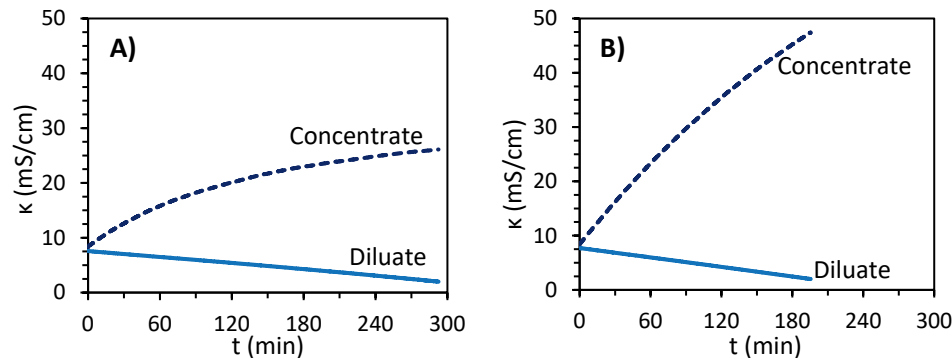
Figure A8.2. *Conductivities of the bulk diluate (––) and concentrate (- -) solutions vs time during the first desalination run (out of 3) performed under 1s/0.5s PEF regime, with pulses of 40A/m^2 (as presented in section 8.3.2).* ***A)*** *With the FujiFilm stack, and* ***B)*** *with the Neosepta stack.*
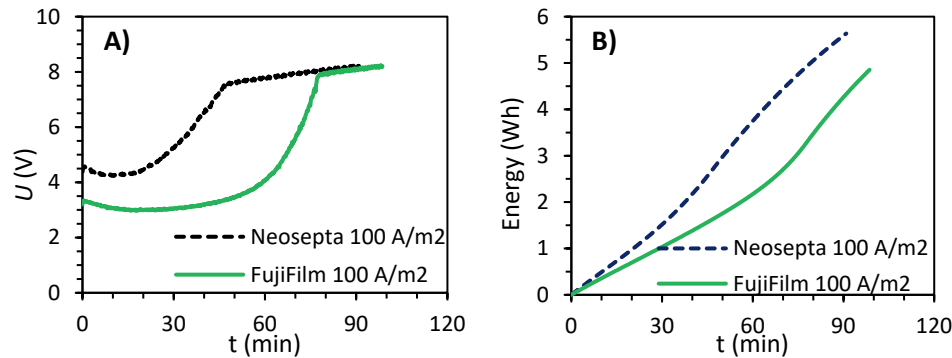
Figure A8.3. *Electric potential (A) and cumulative energy consumption (B) vs time for ED runs performed in PEF mode with pulses of 100 A/m^2 in regime 1s/0.5s ($\bar{\imath}$=66.7 A/m^2).*

Appendix 8B. Preliminary experiments to find optimal pause time during PEF with 1s pulses

Before carrying out the set of experiments presented in section 8.3.2, ED runs were performed to test the effect of reducing the pause period under 1s when applying a PEF regime with pulses of 1s. This PEF mode was the best performing in our previous investigation[7], but it was interesting to test if it could be further improved.

The desalination experiments were performed in two stages, divided in a way that each stage would remove around 50% of the salts [13]. The PEF mode was only applied during the second desalination stage since this is the most energy-intensive part of the process. The three PEF modes evaluated were: 1s/1s, 1s/0.5s, and 1s/0.33s. Given the different pause times, the runs had different durations, but also reached different electric potential, as can be observed in Figure A8.4. The *SEC* calculated for regimes with 1s, 0.5s and 0.33s pauses were, respectively, 12.0, 16.9 and 7.4% smaller than for the continuous case. Thus, further experiments were performed with a 1s/0.5s regime.
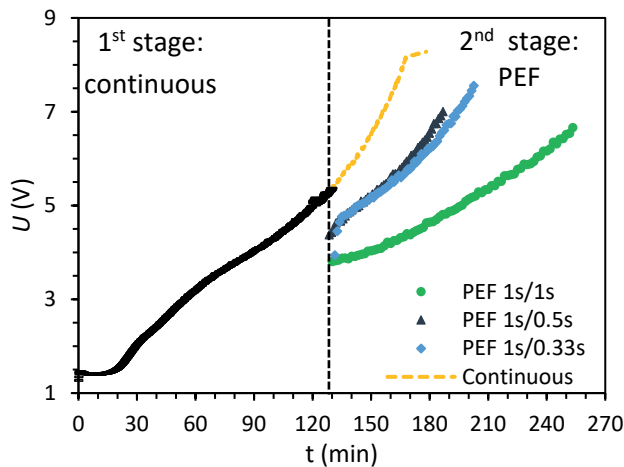
Figure A8.4. *Electric potential (U) vs time during the desalination of PFPW in two stages. The 1st stage is run in continuous mode, while the 2nd is run in PEF mode with different pause times (the continuous case is included as reference). The switch of stage was performed when the conductivity of the diluate decreased to 3.5 mS/cm and is roughly indicated by the vertical line. The curve presented in stage 1 is representative of the ones obtained in all the runs.*

Chapter 9

Energy consumption of an electrodialyzer desalting viscous solutions

Abstract

When performing electrodialysis to desalinate a stream, both the energy for desalination and the energy for pumping the solutions contribute to the total energy consumption, although usually the second term is much smaller than the first. This might differ when desalinating streams with high viscosities, i.e. above the one of water (1 cP). Accordingly, this experimental research focused on measuring the contribution of the desalination and the pumping energy to the total energy consumption when varying diverse parameters, namely the salinity and viscosity of the feed, and the type and thickness of the spacer. It was found that the type of spacer did not significantly influence the energy required for desalination. Regarding the pumping energy, it was higher than predicted by models found in the literature, but in most cases, it was minimal compared to the energy for desalination. Only when using very thin spacers (300 µm) and/or very viscous feeds (12 cP) energy for pumping equalized that of desalination of feeds with 1 g/L NaCl. Thus, it was concluded that the main contributor to the energy consumption of viscous solutions is still the desalination energy, and it is recommended to use spacers of a thickness between 450 and 720 µm to keep pumping energy low.

9.1   Introduction

Electrodialysis (ED) is a mature process applied in industrial scale for the production of potable water from brackish water sources for more than 50 years [1]. Since then, electrodialysis has been used in an increasing variety of applications, like production of table salt [2], recovery of organic acids [3], and for the desalination of industrial streams. Most of these industrial applications address the desalination of aqueous streams with low viscosity, so the operation of the electrodialyzer does not differ much from desalting brackish water. However, new applications are emerging, like removal of lactic acid from acid whey [4], desalination of glycerol [5], of fish sauce [6], and of viscous produced water from the oil and gas industry [7]. Besides their novelty, these applications have in common the high viscosity of the feed solutions, typically several times higher than sea or brackish water. In electrodialysis, the viscosity of the feed solution may influence not only the mass transfer between the solution and the membranes and hence the energy required for desalination [8,9], but also the energy required to pump the feed through the electrodialyzer. Since it is not known how the relative contributions for desalination and for pumping are in the total energy consumption, there is an evident need to study the electrodialysis of viscous feeds, focusing on the influence of several parameters in the energy consumption.

Electrodialysis uses an applied electrical potential difference as driving force to desalinate one of the streams circulating through an electrodialyzer, which consists of a series of anion and cation exchange membranes (AEMs and CEMs, respectively) placed alternately between two electrodes and separated by spacers. When operated, the electrodes generate an electrical field which allows the cations to migrate towards the cathode passing through the CEMs. Likewise, the anions migrate towards the anode passing through the AEMs while the desalting and concentrating solution flow between these membranes. Thus, the electrical potential difference at the electrodes allows ion transport in the electrodialyzer, resulting in a net transport of ions from the dilute compartment to the concentrate compartment [1,10].

The energy consumed by electrodialysis can be reduced to two main sources, i.e. pumping and desalination [11]. The energy required to separate ions in the solution (desalination energy) depends on the performance of the electrodialysis system, which is mainly determined by the electrical resistance of the membranes and the solutions. In most cases, the highest resistance in the system is due to the diffusive boundary layers close to the surface of the membranes in the diluate compartment. Due to the non-homogeneous mixing of the solutions at the proximities of IEMs, concentration polarization occurs, thus causing diffusive boundary layers of non-negligible thickness inside the channel. Concentration polarization phenomena in ED are enhanced when the current density increases. In particular, a limiting

condition is reached when the ion concentration at the membrane/solution interface approaches zero, and the corresponding current value is known as limiting current density [12–14].

Spacers play an important role for both energy contributions. They are placed between the ion-exchange membranes to create a constant intermembrane distance and to improve the mixing of the solutions in the stack. The use of spacers can also have some disadvantages, like covering part of the membrane and reducing the area available for ion conduction, a phenomenon called shadow effect [15]. On the one hand, thinner spacers are preferred to reduce the electric resistance caused by the ion migration through the solutions [16], but on the other hand thinner spacers also lead to increased pressure drop. Thus, it is important to have an optimal spacer thickness. Another option is the use of spacer-less cell design, by using profiled membranes [17,18], which allow to reduce pressure drops [19] and potentially minimizing the risk of fouling, though less effective than conventional spacers to promote mixing in the channels.

When fluids of viscosity above that of water, like the examples mentioned in the first paragraph of the introduction, flow in an electrodialyzer, their friction forces are higher than for non-viscous solutions. Hence, larger pressure losses than for other aqueous systems should be expected. However, assessing the pressure loss in an electrodialyzer is not an easy task. This has been recently pointed out by Wright et al. [20], who created a comprehensive model for brackish water desalination, but who admitted not being able to find a model that reliably predicted pressure drop in the flow channels. Because of this, the authors concluded that it is necessary to keep pressure drop and pumping power characterization for ED stacks as an ongoing area of research.

Therefore, it is of special interest to investigate what are the main constraints when employing ED to demineralize highly viscous solutions. For instance, in the case of viscous produced water from the oil and gas industry, the feed solution could initially have a water-like viscosity (i.e. in the range of 1-2 mPa·s) while increasing significantly (up to 20 mPa·s) after the ED step. Such a large increase of viscosity between inlet and outlet can remarkably impact the overall energy consumption of ED, as well as the optimal operating conditions of the process.

Accordingly, the aim of this work is to assess the energy consumption of electrodialysis with highly viscous streams (up to 12 mPa·s), by investigating the effect of different parameters, both on the feed conditions (flow rate, viscosity, salinity), and on the cell geometry (spacer thickness). We experimentally tested an ED unit composed by spacers of different thicknesses (between 300 to 720 μm) fed with solutions of NaCl (1 and 5 g/L) with different viscosities (1, 2, 5 and 12 mPa·s),

at different flowrates. Thus, in summary, the performance varied depending on the viscosity of the solution, the type of spacer, and the flowrate, as will be elaborated along the article.

## 9.2 Materials and methods

9.2.1 Materials

9.2.1.1 *Electrodialysis stack*

Desalination experiments were performed in an electrodialysis stack with cross-flow configuration for the feed streams (REDstack B.V, The Netherlands). The stack contained 10 membrane pairs, each one composed by one CEM, one AEM, and two spacers. The membranes in the stack were commercial CEMs and AEMs type 10 from FujiFilm B.V., while Neosepta CMX membranes (Astom Corp., Japan) were used as outer CEMs (close to the electrodes). Once placed in the stack, each membrane had a working area of 100 cm2. The outer membranes were separated from the electrode compartments by 300 µm gaskets. The electrodes, placed at the end plates, were made of titanium with mixed metal oxide coating from Magneto Special Anodes BV (NL). The stack was closed by the two end plates and tighten with bolts to 6 Nm. The complete seal in the stack was assured by using silicon glue. A scheme of the stack is available in [21].

The ion exchange membranes used were FujiFilm type 10 (AEMs and CEMs). These membranes are reinforced standard grade homogenous ion exchange membranes based on polyolefin with strong functional groups (quaternary ammonium for the AEM and sulfonic acid for the CEM). The membranes have low electric resistance, so low power consumption, and high permselectivity [22]. Before the experiments, the membranes were conditioned in a 0.1M sodium chloride solution for 5 days.

9.2.1.2 *Spacers*

Four different spacers were used in this research: one extruded and three woven, as shown in **Figure 9.1**. Their main properties are summarized in **Table 9.1**. All the thickness values reported in Table 9.1. were measured with a digital caliper (Mutitoyo 547-401, Japan). The extruded spacers, supplied by Deukum GmbH (Germany), were 300 µm thick. The woven spacers were 300, 450, and 720 µm thick. These spacers were manufactured by Aquabattery B.V. (The Netherlands) employing polyamide nettings from Sefar (Switzerland). The void fraction ε reported in Table 9.1. was calculated using the equation provided by Wright et al. [20] and the netting data.
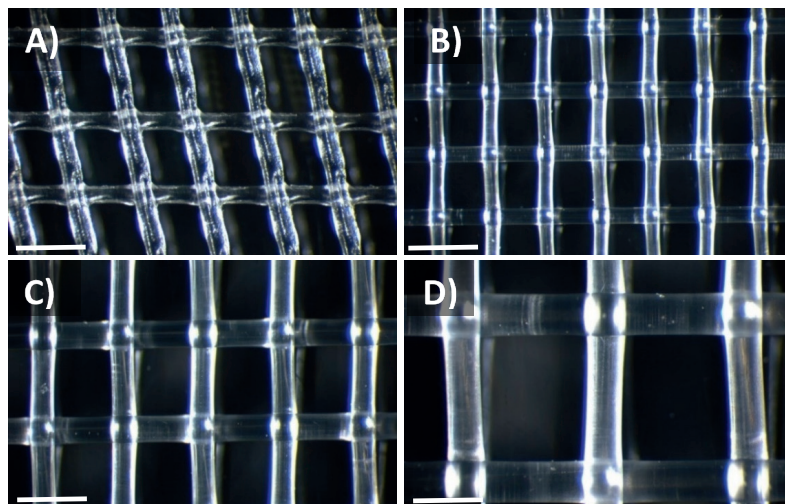
Figure 9.1. *The four spacers used during this study: **A)** 300 µm, extruded; **B)** 300 µm woven; **C)** 450 µm woven; **D)** 720 µm woven. The horizontal bars in the bottom left of the pictures indicate a length of 1 mm. The orientation presented here is the same as in the spacer.*

Table 9.1. *Characteristics of the spacers used during this investigation.*

Identifier	Thickness (µm)	Netting (code given by Sefar)[a]	Material	Void fraction ε	Supplier
300 extruded	300	-	Polypropylene	0.77	Deukum GmbH
300 woven	300	06-475/56	Polyamide	0.70	Aquabattery
450 woven	450	06-700/53	Polyamide	0.71	Aquabattery
720 woven	720	06-1320/59	Polyamide	0.76	Aquabattery

[a] The code indicates the material (06 for polyamide), mesh opening in µm (475, 700, 1320), and open area % (56, 53, 59).

9.2.1.3   *Solutions*

There were eight different solutions employed during this study, which comprised two different salinities and four viscosities. The salinities employed were 5.0 g/L NaCl, namely brackish water (BW), and 1.0 g/L NaCl, referred as low salinity water (LSW). The viscosities were 1, 2 5, and 12 cP, measured at 25 °C. The viscosities were attained by adding 1.0 to 4.0 g/L of non-ionic polyacrylamide (NPAM). Each experiment required 25L of concentrate and 25L of diluate solution. The polymer-containing solutions were prepared by first hydrating the NPAM in a flask containing 10L of salt solution, and then diluting it to reach 25L of feed solution with the desired viscosity. The experiment was executed within 2 days of preparing the feed solutions to avoid degradation of the polymer.

The sodium chloride was analytical grade, provided by VWR (The Netherlands). The non-ionic polymer NPAM was Flopaam FA920 (MW of 5-7 million Da), kindly provided by SNF (France). This non-ionic polymer was chosen over the hydrolyzed one used in previous studies [7,23] to limit the electrostatic interactions with the charged membranes. The electrode rinse solution (ERS) consists of an aqueous solution of sodium sulfate 20 g/L, which was continuously recirculated between anode and cathode for all the tests.

9.2.2   Methods

9.2.2.1   *Electrodialysis runs*

The electrodialysis experiments were conducted in continuous mode (single pass) at a constant voltage of 3.0 V supplied and controlled by a potentiostat (IVIUMnSTAT from Ivium Technologies, The Netherlands). Four different stacks, each one assembled with a different type of spacer, were employed to desalinate the eight solutions described in section 9.2.1.3. During each ED experiment, the diluate and concentrate solutions were circulated at the same flowrate, varied between 50 and 300 mL/min, by two independent pumps (Masterflex L/S). The electrode rinse solution was pumped by a third pump at a constant rate of 170 ml/min. The experiments were run in a laboratory with controlled temperature of $23 \pm 1°C$.

During each experiment, voltage, current, and conductivities of diluate and concentrate were continuously recorded. The pressure difference between the inlet and the outlet of the diluate stream was measured by means of two pressure sensors (Jumo, Germany) positioned immediately before and after the stack.

After each experiment, the stack was cleaned-in-place by circulating a sequence of solutions, each one during 10 minutes at a flow rate of 200 mL/min. The procedure comprised: HCl solution (pH=2), 0.1 M NaCl, NaOH solution (pH=12), 0.1M NaCl, and finally a 5.0 g/L NaCl solution. This cleaning procedure was chosen to guarantee the removal of polymer from the membranes [23].

9.2.2.2   *Composition analysis*

Samples from the feed and the desalted solutions were frequently taken. Their chloride concentration was measured by ion chromatography (IC, Compact IC, Metrohm), while sodium was measured by inductive-coupled plasma method (ICP-OES, Optima 5300DV, Perkin Elmer).

9.2.2.3   *Calculation of ion removal percentage*

For each flow rate, samples from the outlet of the diluate solution were taken by triplicate (approximately at minutes 15, 20 and 25) to independently measure their

Na$^+$ and Cl$^-$ content as previously described. Then, the average removal for each sample was calculated using the Na$^+$ and Cl$^-$ removal values, as expressed in Eq. 9.1:

$$\text{ion removal} = \left[\frac{\left(1 - \frac{n_{dil}^{Na}}{n_{feed}^{Na}}\right) + \left(1 - \frac{n_{dil}^{Cl}}{n_{feed}^{Cl}}\right)}{2} \right] \times 100\%$$ /9.1/

Where n_{dil}^{Na} and n_{dil}^{Cl} are, respectively, the number of moles of Na$^+$ and Cl$^-$ in the diluate of the sample; and $\overline{n_{feed}^{Na}}$ and $\overline{n_{feed}^{Cl}}$ are the average number of moles of Na$^+$ and Cl$^-$ in the feed solution, determined from 3 samples. As shown in the equation, the fraction of removed Na$^+$ and Cl$^-$ was calculated separately by dividing the number of moles in the diluate by the average number of moles of each ion in the feed and subtracting that number from the unit. Finally, the ion removal at each flow rate was averaged also from 3 independent samples.

9.2.2.4   *Linear velocity and Reynolds number*

The linear velocity of the fluid in the channel u (m/s) was calculated using eq. 2 [20]:

$$u = \frac{Q}{\epsilon whN}$$ /9.2/

Where Q is the total volumetric flow (m³/s), ε is the void fraction (-), w is the flow path width (m), h is the channel gap (m) and N is the number of cell pairs.

9.2.2.5   *Desalination energy consumption*

The desalination energy E_{des} (Wh/m³) required for each flowrate Q_d (m³/h) was calculated by dividing the average energy consumption $U \int_0^t I \cdot dt$ (Wh), by the product of the flowrate Q_d and the base time (1 hour). The current I (A) and voltage U (V) values were taken as recorded by the Ivium-n-Stat. Thus, the equation to calculate the desalination energy is:

$$E_{des} = \frac{U \int_0^t I \cdot dt}{Q_d \cdot t}$$ /9.3/

9.2.2.6   *Pressure drop models*

The pressure drops ΔP (Pa) between two parallel plates can be modelled by means of the Darcy-Weisbach equation, which relies on the fluid density ϱ, the Darcy friction factor f (-), the length of the channel's active area L (m), the fluid velocity in the channel u, and the spacer thickness h (m) [20]:

$$\Delta P = \frac{\rho f L u^2}{4h} \qquad\qquad \text{/9.4/}$$

The friction factor f was calculated using the models of Gurreri et al. [24] and Ponzio et al. [25] in the form that Wright [20] presented them. They were chosen based on the results presented by Wright et al., where these two models were the best in predicting the pressure drop of a bench-scale and a commercial stack, respectively. To perform this analysis, the Reynolds number was calculated as described by Wright et al., and using the viscosity values listed in section 9.2.1.3 .

9.2.2.7   *Pumping power consumption*

The energy consumed for pumping a fluid was determined from the flow rates and the pressure drop ΔP in each stream, expressed as:

$$E_{pump} = \frac{Q_d \cdot \Delta P_d + Q_c \cdot \Delta P_c}{Q_d \cdot k_{eff}} \qquad\qquad \text{/9.5/}$$

In which E_{pump} (Wh/m³) is the pumping power consumption for the diluate and concentrate streams [11], k_{eff} (-) is the efficiency of the pumps, while Q_d and Q_c are the flow rates (m³/h) and ΔP_d and ΔP_c are the pressure drops (Pa), of respectively the diluate and concentrate solutions. In this equation, the pressure drop in the electrode rinse is neglected due to the small volume of electrode rinse solution compared with the volumes of the diluate and concentrate solutions.

9.2.2.8   *Viscosity measurement*

Viscosity curves of the feed and diluate solutions were measured at different shear rates with a rheometer (RheoCompass, Anton Paar) using the bob and cup configuration. All samples were stored at 5 °C and measured at 25 °C within 5 days.

9.3   Results and discussion

9.3.1   Energy consumption for desalination

The electrodialysis experiments were run at constant voltage, so the first indication of differences in performance was the attained current density. An example of the initial data obtained is included in **Figure 9.2**, which presents the current densities recorded when desalting 1.0 g/L NaCl solutions with different viscosities and in the different stacks tested. The figure shows that the higher current densities were attained in the stack with extruded spacers. The current density also increased with time, since the flowrate was being increased. This can be explained by the fact that

less residence time will lead to less desalination (concentration gradients). In addition, higher flowrate would give slightly lower concentration polarization. The effect of both phenomena is less ohmic losses and hence higher current density with higher flow rate.
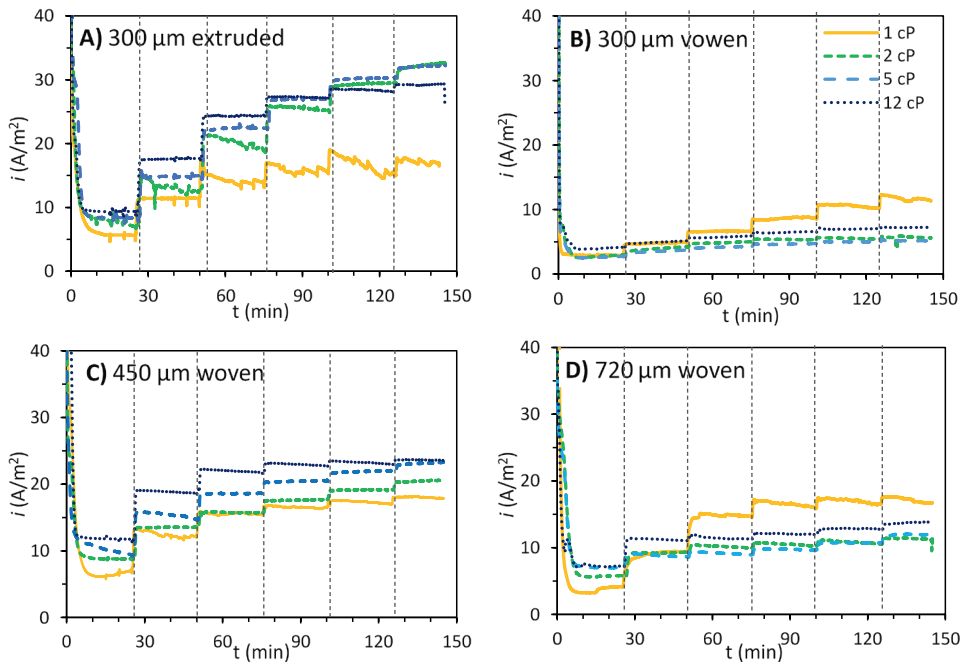

Figure 9.2. *Current density vs time for the ED runs performed to desalinate 1.0 g/L NaCl solutions of different viscosities in different stacks: A) 300 µm extruded, B) 300 µm woven, C) 450 µm woven, D) 720 µm woven. In each run six different flowrates were tested, starting from 50 until 300 mL/min, each one maintained for ~25 min.*

In most cases, higher current densities were obtained when desalting solutions with higher viscosity. This might be due to different flow regimes: on one hand one would expect higher concentration polarization with higher viscosity (i.e. a lower current density), but on the other side the higher viscosity may lead to a better flow distribution over the stack (i.e. a higher current density). Due to fouling or irregularities on the membrane surface, the flow through some areas of the electrodialyzer may become restricted, a phenomenon known as preferential channelling [26]. Apparently, in the stacks with the 300 um non-woven extruded spacer and the 450 um woven spacers, the latter effect is dominant.

For the experiments desalinating the solutions with 5.0 g/L NaCl (included in **Figure A9.1**), the current densities attained were higher than for the 1.0 g/L NaCl solutions, as would be normally expected.

Next, using the samples collected during the experiments and Eq. 1, the average ion removal was calculated for each stack, solution, and flow condition. The average fluid velocity in the stack was calculated using Eq. 9.2 and the spacer specifications. The results hereby obtained are presented in **Figure 9.3** as ion removal versus linear velocity u for the different spacers and solutions.

It is worth noticing that the ion removals included in **Figure 9.3** are consistent with the current densities shown in **Figure 9.2**, which suggest an also steady current efficiency during the runs. All plots in **Figure 9.3** also show decreased ion removal as the fluid velocity increases, which was also anticipated since at higher velocity the residence time decreases. The figure also shows that different spacers allowed very different ion removal percentages: while the 450 μm spacer yielded up to 90% ion removal, the 300 μm woven one did not allow to remove more than 20% of the ions present in the feed. When comparing the 300 μm spacers, it can be observed that the ion removal using extruded spacers was approximately 3 times higher than when using the woven one. This could be due to the fluid channelling and not wetting the entire membrane area available. The highest ion removals were achieved with the stack containing 450 μm woven spacers, which can be attributed to a better flow distribution in the stack, and consequently a higher current efficiency. It also results noteworthy that the percentages of ion removal only varied depending on the spacer and were very similar for solutions with the same viscosity and different salinity.

9
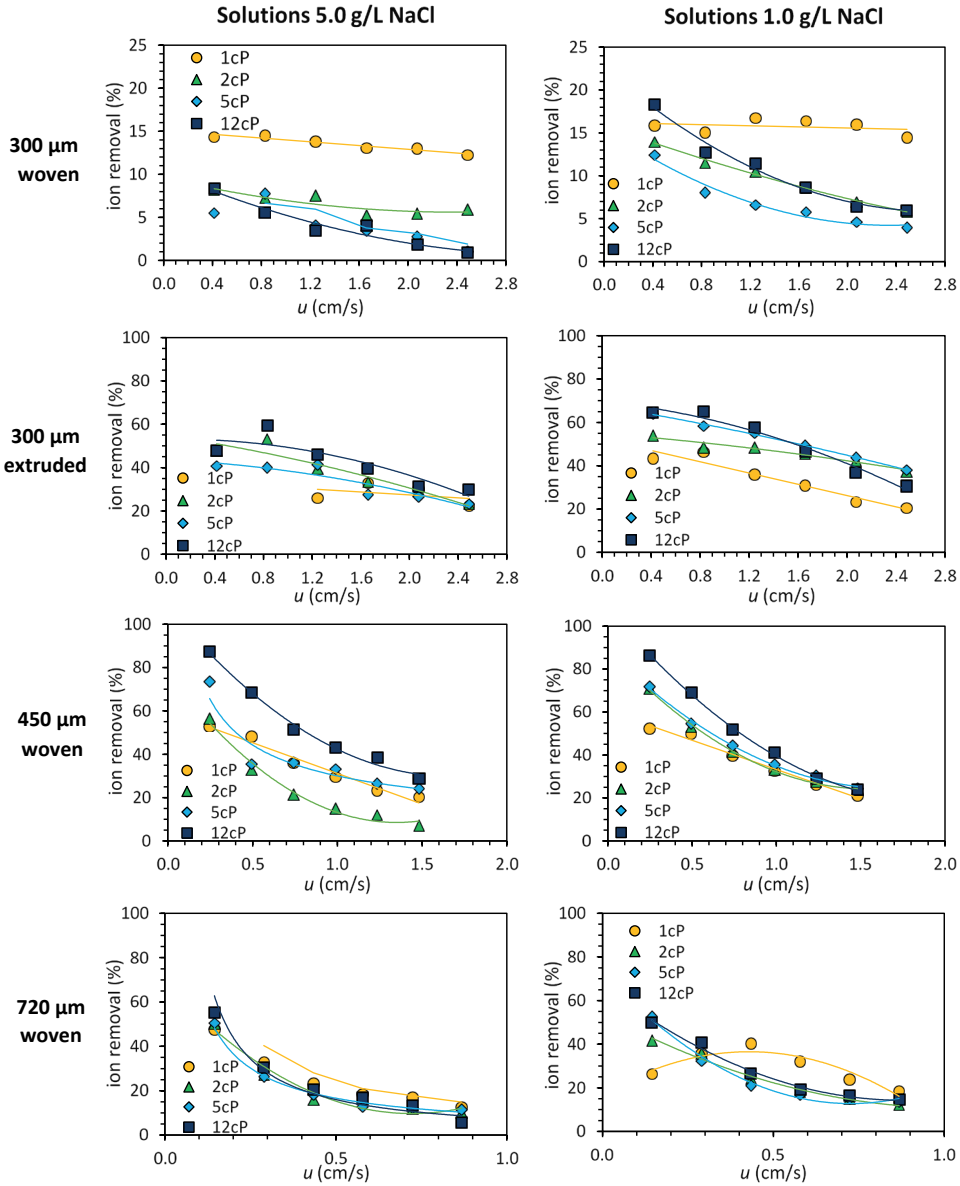
Figure 9.3. *Ion removal (%) versus linear velocity for desalination experiments of NaCl solutions with different viscosities performed in 4 different stacks.*

As was shown in **Figure 9.2** and **Figure 9.3**, different ion removals and current densities were obtained depending on the experimental conditions. Consequently, the desalination energy consumption E_{des}, calculated using Eq. 3, also varied. This can be observed in **Figure 9.4**, where the energy is plotted against the ion removal percentage.
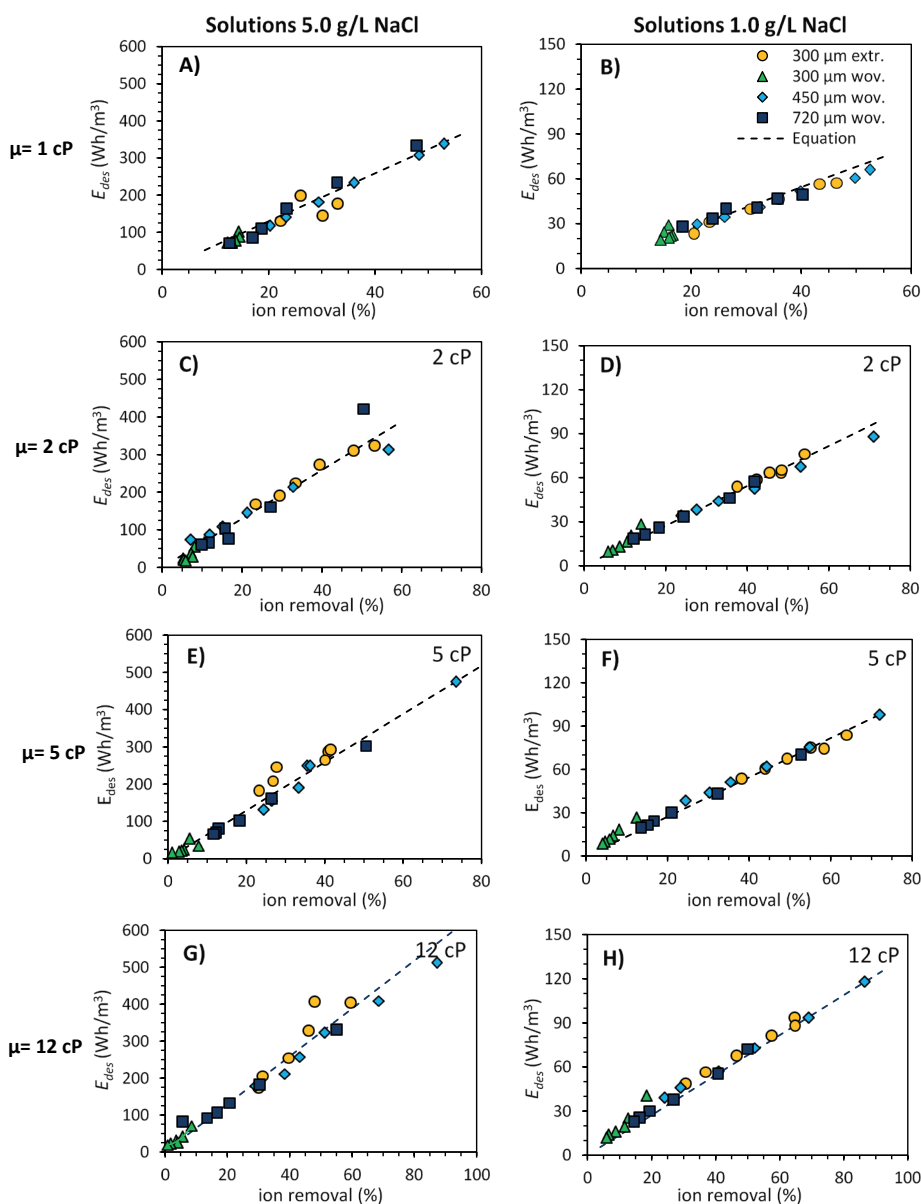
Figure 9.4. *Specific energy consumption vs. ion removal for electrodialysis experiments desalinating solutions containing 5.0 and 1.0 g/L NaCl.*

Figure 9.4 shows that the energy for desalination E_{des} is linearly dependent of the amount of the percentage of removed ions, independently of the viscosity of the solution or the spacer in the stack. In other words, the current efficiency remains constant in all the tests. This is expected to occur for experiments at constant voltage, because any increase in resistance does not lead to higher heat losses, but to a lower

current (density). Then, since the power consumption E_{des} is directly related to the current (Eq. 4) and the latter is linked to the number of ions transported, the relationship between E_{des} and ion removal should be linear. Then, as shown in **Figure 9.4**, experiments run with same salinity feed followed the same trend, which allowed to obtain the two empirical equations presented in **Table 9.2**.

Table 9.2. *Empirical equations relating the desalination energy (Wh/m³) to the ion removal (%)*

Salinity	Equation	R²
5.0 g/L	E_{des}= 6.4682*ion_removal	0.87
1.0 g/L	E_{des}= 1.3602*ion_removal	0.97

9.3.2 Pressure loss and energy for pumping

Figure 9.5 includes the experimentally measured pressure drops for the diluate side of the four stacks. Higher pressure drops occurred on the stacks with thinner spacers (smaller h) and for higher flow velocities, as expected when considering equation 5. The pressure drop was also higher when the viscosity of the diluate was higher, which causes a higher friction factor f.

Besides the experimental data, **Figure 9.5** also includes the pressure drop calculated by the models developed by Ponzio [25] and by Gurreri [24] and adapted by Wright et al. [20] (as described in section 9.2.2.6). It can be observed that both models underestimate ΔP, most notoriously for the 720 µm spacer and for the higher viscosities. Indeed, Wright also reported an underestimation of the pressure drop when using these and other models, although in their case the differences were less significant [20]. Still, it must be considered that the models were developed mostly for low-viscosity solutions, so it is understandable that they do not accurately predict the pressure loss when a fluid with higher viscosity is being pumped. Furthermore, the polymer solution is a non-Newtonian fluid which apparent viscosity increases as the shear rate increases, making more difficult to predict the pressure loss due to friction. In this case, the friction factor calculated by any of the models would need to be approximately three times higher in order to predict more accurately the experimental data here presented.
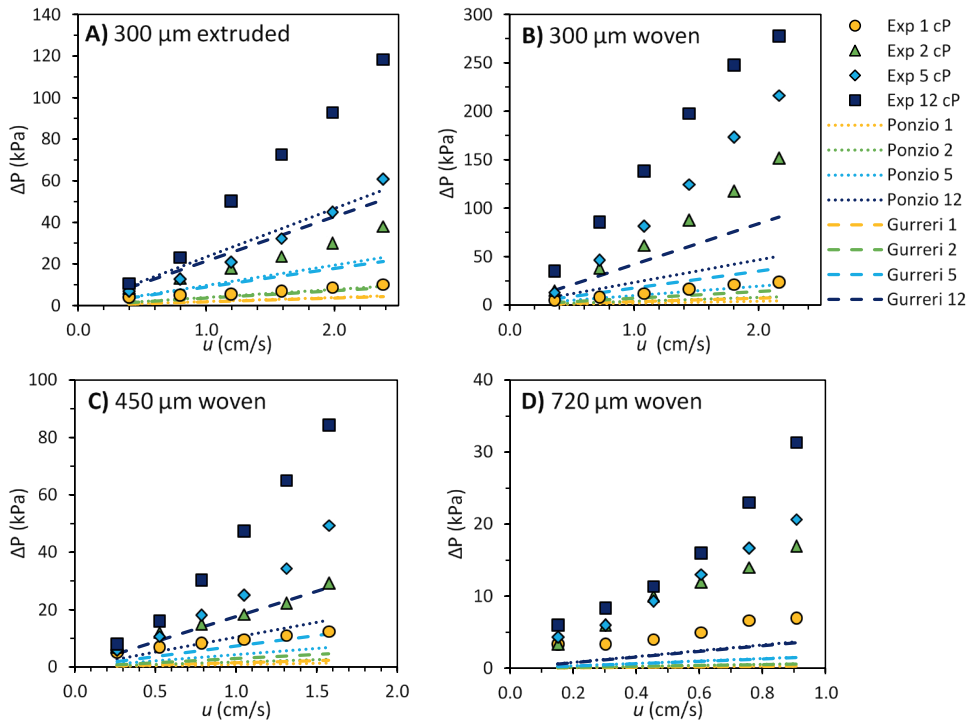
Figure 9.5. Model and experimental pressure drop for the 4 stacks tested with solutions of 1, 2 5, and 12 cP.

The energy needed to pump the diluate and concentrate solutions through the electrodialyzer was calculated using Eq. 9.5 (ΔP_d, Q_d, ΔP_c, Q_c and k_{eff}= 0.9). Then, the results obtained for the low salinity case are presented in **Figure 9.6** as a function of the linear velocity u. The results are closely related to those presented in the previous figure: larger pumping energies were required when treating fluids with higher viscosity, as well as when using thinner spacers. It is worth noticing that the pumping energy for the 450 and the 720 μm spacers is very similar, while the one obtained for 300 μm woven spacer is significantly different from the other two, especially for viscosities of 2 cP or higher.

9
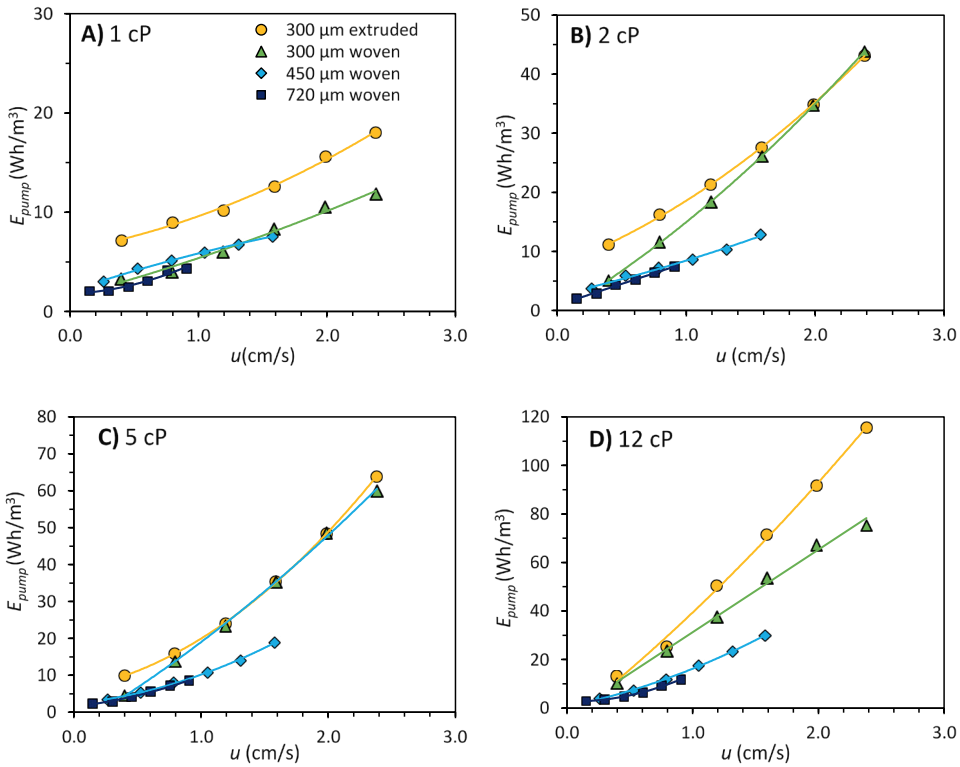
Figure 9.6. *Pumping power as a function of linear velocity u for the LSW.*

9.3.3 Total energy consumption

Figure 9.7 presents the total energy consumption needed to remove 50% of the ions from the low salinity solutions (1.0 g/L), calculated by adding the desalination and pumping energy consumptions. It shows that, for all studied cases, E_{des} is larger than E_{pump}, and when using 450 or 720 µm spacers to desalinate solutions with viscosities up to 5 cP, the pumping energy can still be considered negligible. However, when employing any of the 300 µm spacers, or when desalting the streams with higher viscosity (12 cP) the E_{pump} value becomes more relevant, even equalizing the E_{des} value in the case of the 12 cP solution with the 300 µm extruded spacer.

When analysing the results obtained for the BW solution it should be considered that the desalination energy is approximately 5 times larger than for the LSW, while the energy for pumping is the same. Therefore, for the BW solution the main contribution to energy consumption was in all cases the desalination energy. These results are included in the supplementary material.
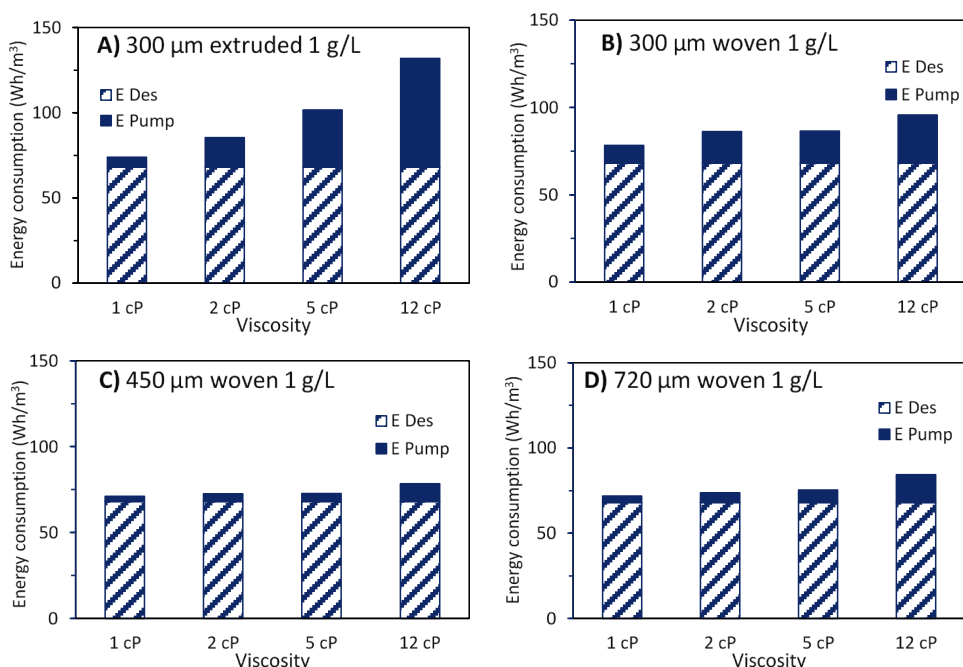
Figure 9.7. *Total energy consumption to remove 50% of the salt from 1.0 g/L NaCl solutions, calculated for each viscosity and spacer.*

9.3.4 Evaluation of fluid viscosity after ED

Besides the main energy requirements of the process, there is another constraint when pumping viscous solutions: the sensitivity of the materials to shear. In the case of polymer-containing solutions, high shear rates can cause breaking of the polymer and reduction of the viscosity. To evaluate this effect, the viscosity of the feed and the diluate solutions was determined after all the experiments.

The viscosity measurements are presented in **Figure 9.8** as a function of shear rate. It shows that all the diluate solutions had the same viscosity as the initial feed solution, independently of the stack or fluid velocity at which they were treated. This is a positive result, since it suggests that the shear forces inside the stack do not become high enough to break the polymer chains. There could be the possibility that due to the decrease in the salt content, the viscosity of the diluate increases and was compensated for the possible polymer degradation. However, even the solution that had minimal ion removals, like those that went through the 300 μm woven stack, presented the same viscosity as the feed.
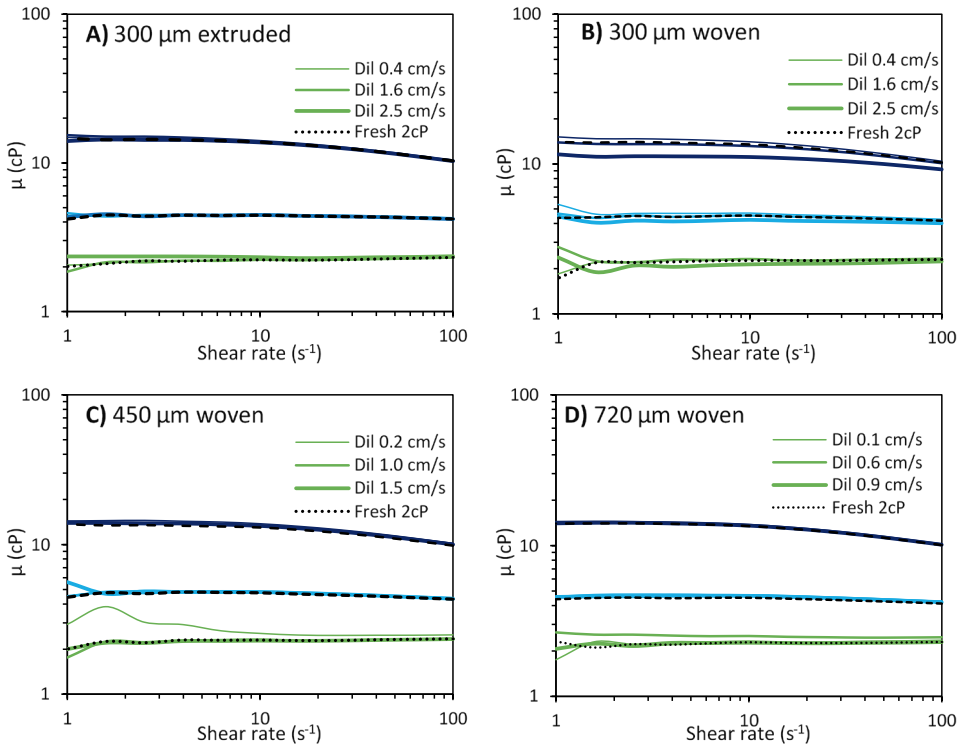
Figure 9.8. *Viscosity curves of the feed and diluate solutions. The plots show the measurements for LSW solutions (1 g/L NaCl) viscosified at 2, 5 and 12 cP. The viscosity was measured for each of the flowrates tested, but only 50, 200 and 300 mL/min (expressed as fluid velocity) are included. The data is divided by stack A) 300 um extruded, B) 300 um woven, C) 450 um woven and D) 720 um woven.*

9.4   Conclusions

In this investigation, we assess the energy consumption for the desalination and pumping of viscous fluids using ED-stacks with different spacers. The combination of stacks using different spacers and varying fluid viscosities resulted in different current densities and ion removal percentages. However, when compared for the same output of 50% ion removal, results indicated practically equal energy consumption for all viscosities and spacer configurations tested, indicating no additional energy needs for pumping.

Still, the results showed an evident effect of spacer configuration and fluid viscosity on the pumping energy consumption. The pumping energy became a significant component in the total energy need when solutions of viscosity above 1 mPa·s (1 cP) were desalinated, especially when desalting 12 mPa·s solutions. Nevertheless, the only case in which the measured pumping energy consumption equalized the

desalting energy consumption was when desalting a 1 g/L NaCl solution of 12 mPa·s in a stack containing 300 μm-thick spacers.

The results obtained indicated that the effect of spacer thickness on the energy for desalination E_{des} is insignificant, but that it is wise to use spacers of thicknesses between 450 and 720 μm to keep the pumping energy E_{pump} limited and to achieve enough molar salt removal.

References

[1]   H. Strathmann, Electrodialysis, a mature technology with a multitude of new applications, Desalination. 264 (2010) 268–288. doi:10.1016/j.desal.2010.04.069.

[2]   T. Kawahara, K. Suzuki, Utilization of the waste concentrated seawater in the desalination plants, Desalination. 38 (1981) 499–507.

[3]   C. Huang, T. Xu, Y. Zhang, Y. Xue, G. Chen, Application of electrodialysis to the production of organic acids: State-of-the-art and recent developments, Journal of Membrane Science. 288 (2007) 1–12. doi:10.1016/j.memsci.2006.11.026.

[4]   G.Q. Chen, F.I.I. Eschbach, M. Weeks, S.L. Gras, S.E. Kentish, Removal of lactic acid from acid whey using electrodialysis, Separation and Purification Technology. 158 (2016) 230–237. doi:10.1016/j.seppur.2015.12.016.

[5]   P. Vadthya, A. Kumari, C. Sumana, S. Sridhar, Electrodialysis aided desalination of crude glycerol in the production of biodiesel from oil feed stock, Desalination. 362 (2015) 133–140. doi:10.1016/j.desal.2015.02.001.

[6]   J. Chen, M. Li, R. Yi, K. Bai, G. Wang, R. Tan, S. Sun, N. Xu, Electrodialysis Extraction of Pufferfish Skin (Takifugu flavidus): A promising source of collagen, Marine Drugs. 17 (2019) 1–15. doi:10.3390/md17010025.

[7]   P.A. Sosa-Fernandez, J.W. Post, H. Bruning, F.A.M. Leermakers, H.H.M. Rijnaarts, Electrodialysis-based desalination and reuse of sea and brackish polymer-flooding produced water, Desalination. 447 (2018) 120–132. doi:10.1016/j.desal.2018.09.012.

[8]   O. Kuroda, S. Takahashi, M. Nomura, Characteristics of flow and mass transfer rate in an electrodialyzer compartment including spacer, Desalination. 46 (1983) 225–232.

[9]   T. Huang, I. Yu, Correlation of ionic transfer rate in electrodialysis under limiting current density conditions, Journal of Membrane Science. 35 (1988) 193–206. doi:10.1016/S0376-7388(00)82443-6.

[10]   R. Valerdi-Pérez, M. López-Rodríguez, J.A. Ibáez-Mengual, Characterizing an elecrodialysis reversal pilot plant, Desalination. 137 (2001) 199–206. doi:10.1016/S0011-9164(01)00219-3.

[11]   H. Strathmann, Assessment of Electrodialysis Water Desalination Process Costs, Proceedings of the International Conference on Desalination Costing, Lemassol, Cyprus, December 6-8, 2004. (2004) 32–54.

[12]   V. V. Nikonenko, A. V. Kovalenko, M.K. Urtenov, N.D. Pismenskaya, J. Han, P. Sistat, G. Pourcelly, Desalination at overlimiting currents: State-of-the-art and perspectives, Desalination. 342 (2014) 85–106. doi:10.1016/j.desal.2014.01.008.

[13]   A.M. Peers, General discussion, Discussions of the Faraday Society. 1956 (1956) 124–125.

9

[14]   M. La Cerva, L. Gurreri, M. Tedesco, A. Cipollina, M. Ciofalo, A. Tamburini, G. Micale, Determination of limiting current density and current efficiency in electrodialysis units, Desalination. 445 (2018) 138–148. doi:10.1016/j.desal.2018.07.028.

[15]   H. Strathmann, Ion-Exchange membrane separation processes, First, Elsevier B.V., Amsterdam, 2004.

[16]   D.A. Vermaas, M. Saakes, K. Nijmeijer, Doubled power density from salinity gradients at reduced intermembrane distance, Environmental Science and Technology. 45 (2011) 7089–7095. doi:10.1021/es2012758.

[17]   S. Pawlowski, J.G. Crespo, S. Velizarov, Profiled ion exchange membranes: A comprehensible review, International Journal of Molecular Sciences. 20 (2019). doi:10.3390/ijms20010165.

[18]   C. Larchet, V.I. Zabolotsky, N. Pismenskaya, V. V. Nikonenko, A. Tskhay, K. Tastanov, G. Pourcelly, Comparison of different ED stack conceptions when applied for drinking water production from brackish waters, Desalination. 222 (2008) 489–496. doi:10.1016/j.desal.2007.02.067.

[19]   D.A. Vermaas, M. Saakes, K. Nijmeijer, Power generation using profiled membranes in reverse electrodialysis, Journal of Membrane Science. 385–386 (2011) 234–242. doi:10.1016/j.memsci.2011.09.043.

[20]   N.C. Wright, S.R. Shah, S.E. Amrose, A.G. Winter, A robust model of brackish water electrodialysis desalination with experimental comparison at different size scales, Desalination. 443 (2018) 27–43. doi:10.1016/j.desal.2018.04.018.

[21]   J. Moreno, N. de Hart, M. Saakes, K. Nijmeijer, CO2 saturated water as two-phase flow for fouling control in reverse electrodialysis, Water Research. 125 (2017) 23–31. doi:10.1016/j.watres.2017.08.015.

[22]   P.A. Sosa-Fernandez, S.J. Miedema, H. Bruning, F.A.M. Leermakers, H.H.M. Rijnaarts, J.W. Post, Influence of solution composition on fouling of anion exchange membranes desalinating polymer-flooding produced water, Journal of Colloid And Interface Science. 557 (2019) 381–394. doi:10.1016/j.jcis.2019.09.029.

[23]   P.A. Sosa-Fernandez, J.W. Post, M.S. Ramdlan, F.A.M. Leermakers, H. Bruning, H.H.M. Rijnaarts, Improving the performance of polymer-flooding produced water electrodialysis through the application of pulsed electric field, Desalination. 484 (2020). https://doi.org/10.1016/j.desal.2020.114424.

[24]   L. Gurreri, A. Tamburini, A. Cipollina, G. Micale, M. Ciofalo, Flow and mass transfer in spacer-filled channels for reverse electrodialysis: a CFD parametrical study, Journal of Membrane Science. 497 (2016) 300–317. doi:10.1016/j.memsci.2015.09.006.

[25]   F.N. Ponzio, A. Tamburini, A. Cipollina, G. Micale, M. Ciofalo, Experimental and computational investigation of heat transfer in channels filled by woven spacers, International Journal of Heat and Mass Transfer. 104 (2017) 163–177. doi:10.1016/j.ijheatmasstransfer.2016.08.023.

[26]   D.A. Vermaas, M. Saakes, K. Nijmeijer, Early detection of preferential channeling in reverse electrodialysis, Electrochimica Acta. 117 (2014) 9–17. doi:10.1016/j.electacta.2013.11.094.

Appendix 9A. Supplementary material
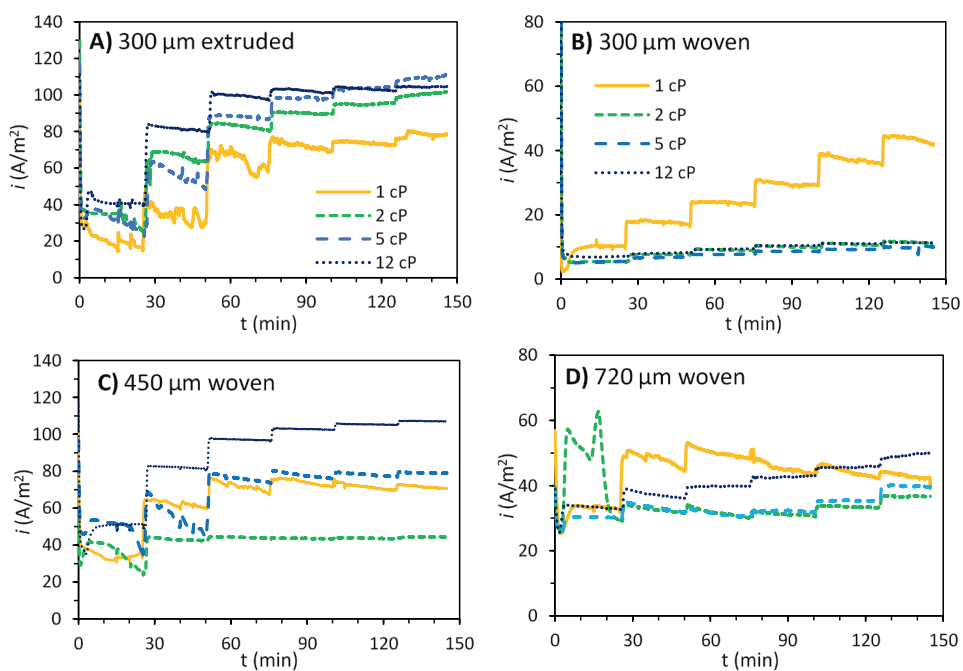
Figure A9.1. *Current density vs time for the ED runs performed to desalinate 5.0 g/L NaCl solutions of different viscosities. In each run six different flowrates were tested, from 50 to 300 mL/min, each one maintained for ~25 min.*

Chapter 10

General discussion and outlook

This chapter is divided in three sections. In section 10.1, we recall the main areas of investigation that were defined in the first chapter (influence of polymer-flooding produced water composition and conditions, removal of multivalent ions, fouling, preservation of polymer integrity) and discuss the findings presented in this thesis. Then, section 10.2 introduces a polymer flooding case with brackish water and evaluates the feasibility of introducing a produced water desalination step. Finally, section 10.3 includes some last remarks about the outlook and recommendations for future research.

10.1 Main findings for the electrodialysis of polymer-flooding produced water

10.1.1 Influence of PFPW temperature, composition, and HPAM size on ED performance

Polymer-flooding produced water (PFPW) can have very different compositions and be recovered at diverse temperatures depending on the geographic location of the oilfield. Despite these extensive variations, in **Chapter 2** we proved that electrodialysis (ED) can be used to desalinate PFPW at salinities ranging from 5,000 to 32,000 mg/L, and at temperatures ranging from 10 to 40°C. In terms of energy consumption and polymer loss, the process proved to be more attractive when operated at higher temperature (40°C), due to faster diffusion of the ions and less concentration polarization [1,2]. This means that although ED and polymer-flooding could be employed at most oil production locations in the world, those where PFPW is available at higher temperatures would are more attractive for its implementation.

In many of the chapters of this thesis, the process performance was assessed utilizing the desalination energy consumption (E_{des}). For the brackish water desalination, the energy consumption was reduced from 1.8 kWh/m³ (at 20°C, **Chapter 2**) to 0.6 kWh/m³ (at 23 °C, **Chapter 8**). The improvement was achieved by 1) increasing the linear flow velocity in the stack, and 2) stopping the desalination earlier in the process (when reaching 2.0 mS/cm instead of 1.0 mS/cm). Furthermore, to dissipate the doubt of elevated pumping power consumption when desalinating viscous feeds, **Chapter 9** compared the energies consumed by desalinating and by pumping in diverse scenarios. The results indicated that the energy for desalination E_{des} was the main contributor (> 90%) to the total energy consumption when using 450 μm thick spacers, for solution viscosities ranging from 1 to 12 mPa·s. Since the rest of the experimental work in this thesis made use of this kind of spacers, it is safe to suppose that the E_{des} presented in the different chapters comprise most of the total energy consumption by the ED system.

By measuring the concentration of polymer in the desalinating solution, in **Chapter 2** it was found that a sharp loss of polymer occurred when the salinity of the stream decreases to approximately 2.5 g/L or lower, independently from the starting salt concentration (and thus of the duration of the ED runs). This observation indicated that, when addressing fouling, the most critical part of the desalination process was the one at lower salinity.

Another variable to be considered during PFPW desalination is the size of the partially hydrolyzed polyacrylamide (HPAM) molecules. When the fresh solution for injection is prepared, HPAM molecules of large MW are used, normally 20 million Da or more. However, during the polymer flooding process the shear forces cause the HPAM molecules to break down in smaller sizes. Accordingly, during this research the synthetic PFPW was prepared with HPAM molecules of three different MW, all of them for 30% hydrolyzed. **Chapters 2** to **5** employed HPAM with an average MW of 5-8 million Da (Flopaam 3230S). In the research described in chapters 6 and 8, HPAM with 4.4-4.8 million Da (Flopaam 3130S), and **Chapter 7** HPAM with 0.6-0.9 million Da (AB-305-VLM) were utilized, respectively. The first experiments were performed with the higher MW HPAM to evaluate likely polymer breakage during the electrodialysis process, and possible effects of the smaller fragments on the ED by penetration of Ion Exchange Membranes (IEMs). Contrary to these expectations, LC-OCD measurements did not show any significant polymer degradation, at least within its recognition range. Thus, the lower MW HPAM was used to study the possibility of some smaller molecules to go through the IEMs, but no evidence of such a behavior of these smaller polymer fragments was observed, both observed phenomena to be important for PFPW treatment.

It must be pointed out that the HPAM analyses presented in the previous chapters, consisting in TOC and LC-OCD measurements, could not be used to verify the MW of the HPAM supplied by SNF Floerger. The experimental determination was recently done thanks to a new method developed to determine the MW of polymers above 1 million Da. The method, fully described by Ajao et al. [3], makes use of the same LC-OCD apparatus, but equipped with a tandem column consisting of an Agilent BioSec5 5 μm 1000 A (7.8 mm*300 mm) and a Toyopearl HW-50S 30 μm (20 mm*250 mm). By using this method, BW solutions containing 0.5 g/L of each kind of HPAM were analyzed, finding slightly higher MW for Flopaam 3130S and AB-305-VLM, as shown in Table 10.1.

Table 10.1. *Molecular weight of HPAM used to prepare the viscous solutions to desalinate*

| Commercial name	Nominal MW	Measured MW
Flopaam 3230S	5-8 million Da	5.54 million Da
Flopaam 3130S	4.4-4.8 million Da	5.54 million Da
AB-305-VLM	0.6-0.9 million Da	1.40 million Da

Contrary to the LC-OCD characterization, viscosity measurements confirmed that Flopaam 3230S had indeed a larger MW than Flopaam 3130S, as reported by the supplier. It is known that HPAM of larger MW has a stronger viscosifying effect, so, for solutions with an equal HPAM concentration and hydrolysis degree, the viscosity is expected to be proportional to the MW of the polymer. To quantify this effect, BW solutions containing 0.5 g/L HPAM were prepared and their viscosity measured. As can be observed in Figure 10.1, the viscosity of the BW solution containing Flopaam 3230S was approximately 2 times higher than that containing Flopaam 3130S, and the viscosity of this solution was also twofold the one of the solution containing AB-305-VLM.
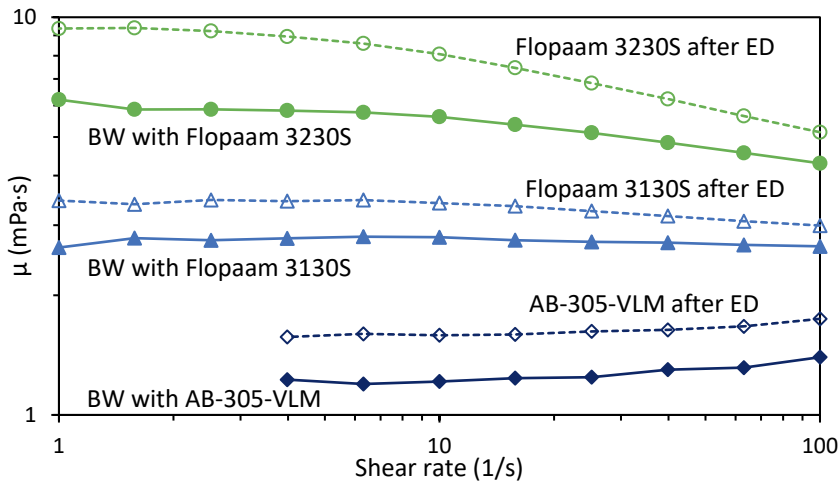
Figure 10.1. *Viscosity vs shear rate for BW solutions prepared with 0.5 g/L HPAM of different MW: 5-8 million Da (Flopaam 3230S), 4.4 to 4.8 million Da (Flopaam 3130S), and 0.6-0.9 million Da (AB-305-VLM). Measurements performed at 25°C.*

Likewise, the effect of using HPAM of different MW on the desalination performance had not been explicitly tested in the literature and studies described in previous chapters, so the last ED runs executed had this objective. These were performed with the FujiFilm stack and setup described in **Chapter 8**, at a constant current of 60 A/m². The desalination was carried out in batch mode, until a conductivity of 2 mS/cm was reached in the diluate solution (approximately 80% TDS removal). The diluate solutions consisted in BW solutions containing 0.5 g/L of HPAM with different MW. Then, as presented in **Figure 10.2**, the two runs with high MW HPAM showed no difference in terms of electric potential or energy consumption. However, the ED run performed with the smallest HPAM behaved somewhat different, displaying a slightly higher electric potential, operational time, and energy consumption. This is the opposite of the results reported by Wang et al. [4] when comparing the impact of 0.3, 0.8 and 3.0 million Da HPAM on energy

consumption and current efficiency. Thus, despite the results suggest that there could be a minor influence of the MW of HPAM in solution, these results must be considered as preliminary since each ED test was only performed once, and these might be still influenced by the order of execution, i.e. a decreasing HPAM size over experimental time.
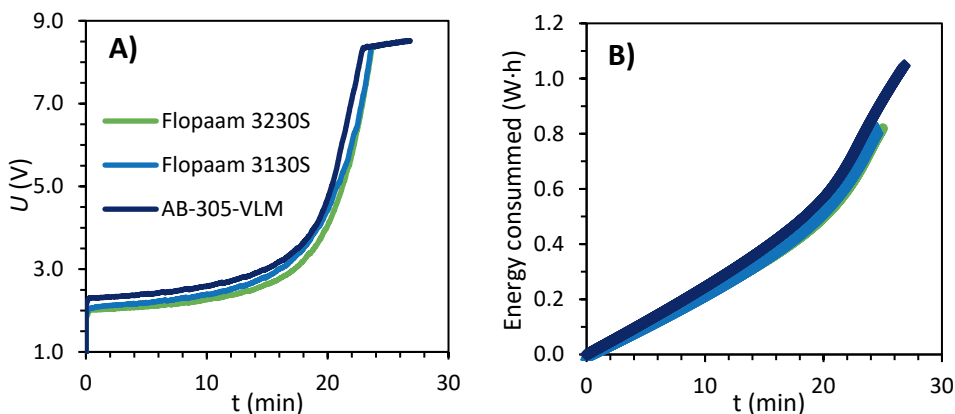
Figure 10.2. Electric potential U (A) and consumed energy (B) vs time for ED runs desalinating 1L of BW solution containing 0.5 g/L of HPAM of different MW

Finally, as can be observed in **Figure 10.1**, the viscosity of the diluate recovered after ED was tested again, increasing between 20% (Flopaam 3130S) and 40% (Flopaam 3230S).

From this section, three conclusions can be obtained: i) the higher the temperature of PFPW, the lower the energy consumption during electrodialysis; ii) ED can be used to desalinate PFPW with salinities ranging from 5,000 to 32,000 mg/L; and iii) the size of the HPAM molecule does not exert a significant influence in ED performance, this being valid for nominal HPAM sizes between 0.6 and 8 million Da.

10.1.2 Removal of multivalent ions

In **Chapter 3**, it was demonstrated that by using low current densities and higher temperatures, it is possible to accelerate the removal of the most abundant divalent cations in PFPW, namely calcium and magnesium. The transport of divalent cations was also reported in **Chapter 6**, where an increase in the transport number of Ca^{2+} was measured during the application of pulsed electric field (PEF) modes, coinciding with previous literature reports [5]. In both chapters, the faster transport of divalent cations was related to the reduction of concentration polarization. Less concentration polarization of ions in the diluate side facilitates for those with slower diffusion coefficients, like Ca^{2+} and Mg^{2+}, to reach the surface of the cation exchange

membrane (CEM). Furthermore, the results from **Chapter 3** showed that calcium and magnesium were not transported equally. The transport of Ca^{2+} is facilitated compared to that of Mg^{2+}, most likely because the latter has to overcome a larger energy barrier due to the partial dehydration required to be transported through the CEMs [6].

Regarding the divalent anions, only sulfate was included in the PFPW formulation applied in **Chapter 3**. In this chapter, it was observed that its removal rate was only increased as an effect of temperature and not as a result of current density. Later, as described in **Chapter 7**, the removal of sulfate was also measured while employing different AEMs, finding only small differences in the removal percentage when the same current density was applied.

To summarize, multivalent cations (Ca^{2+} and Mg^{2+}) can be preferentially removed over Na and K when concentration polarization is minimized, either by applying low current densities or by increasing the temperature. Sulfate removal, on the other hand, only increased when higher temperatures were applied.

10.1.3 Fouling

Since the beginning of this investigation, the literature suggested that membrane fouling would be an important issue when desalinating PFPW [7,8]. The first evidence of fouling was described in **Chapter 2**, when organic carbon concentration (TOC) was found to decrease mainly during the last part of the ED process, when the conductivity of the diluate was under 5 mS/cm.

Later in this thesis, fouling was specifically addressed in **Chapters 4** and **5**. We recognized the difference between HPAM adsorption and the formation of gel layers, since our experimental work was mainly suited to study the latter phenomena. It was found that thick gel layers were formed on the diluate side of the AEMs and on the concentrate side of the CEMs, which lead us to realize that the main driving force was the electrophoresis of HPAM moving towards the positive electrode under the influence of the applied electric field. It was also found that when the feed solution contained divalent cations, the gel layers were thicker and caused larger increase of resistance that for feed solutions containing only sodium chloride and HPAM. However, the membrane resistances measured during these experiments were extremely large, especially in the case of the AEMs, making us realize that the hydrodynamic conditions in the 6-compartment cell were likely enhancing the fouling phenomenon.

Consequently, the next study addressing fouling (**Chapter 6**) was performed in an ED-stack. In this case, a membrane pair was recovered from the stack after performing ED runs using different operational conditions in terms of pulsed

10

electric field (PEF). Compared to the study presented in **Chapter 2**, the desalination was finished earlier, when reaching a conductivity of 1.5 mS/cm instead of 1.0 mS/cm, but the flow velocity was the same, 1.3 cm/s. Besides the improvements in process performance, it was surprising to find through TOC analysis that the loss of HPAM during the desalination had been minimal, independently of the operation mode. Although small amounts of polymer were released from the CEMs rinsed in pure water, SEM photographs of non-rinsed pieces showed minimal amounts of fouling on both, the CEMs and AEMs. We considered two possible explanations: either the duration of the experiments (2-8 hours) was too short to accumulate significant amounts of foulants, or the membranes employed (from FujiFilm) had superior antifouling properties than the ones used in **Chapter 2** (Neosepta membranes).

The previous results leaded us to design our next study (**Chapter 7**). In it, stacks composed by different AEMs were used continuously for 200 hours to desalinate brackish water with increasing amounts of HPAM and crude oil. Despite faster flow velocities were employed (up to 2.5 cm/s), three of the six stacks evaluated reached limiting conditions, which was related to the higher area resistance of the AEMs they contained. It was also found that a more stable operation was obtained when the feed solution contained crude oil, even if the concentrations were minimal, which was already observed in the previous studies. This suggested once more that the main fouling mechanism involved formation of HPAM gel layers that are resistant to moderate shear forces. It was proposed that when oil is present the gel layers are easier to be removed, thus causing less operational problems.

Finally, in **Chapter 8**, three consecutive batch desalinations were performed, showing practically the same behavior in the first and the last run, suggesting that fouling was not severe, independently of the set of IEMs employed. Thus, by comparing the results obtained in **Chapter 2** and in **Chapter 8**, can be concluded that the operation performance was improved, and fouling reduced by 1) increasing the flow velocity, and 2) aiming for slightly higher salinities/conductivities (2.0 mS/cm instead of 1.0 mS/cm) for the final product.

### 10.1.4 Reusability of the desalinated water

The reusability of the desalinated water was tested in **Chapter 2**. When measured after the desalination, the viscosity of the solution did not increase as much as expected, which was attributed to the decrease in pH during electrodialysis. For situations where the pH of the solution is not brought back to neutrality, the amount of fresh polymer needed to reach the desired viscosity of 40 mPa·s was reduced by approximately 60% compared to that required when brackish and seawater were used as a basis. However, to further increase the viscosity of the desalted solutions, the pH of these solutions had to be brought back to neutrality by adding a strong

base, which is inconvenient due to the use of additional chemicals. Thus, it was needed to gain understanding why the pH changes occurred and how they could be minimized so the desalinated solution could be reused without extra pH adjustment.

In **Chapter 2**, the pH changes were most significant for seawater and not so much for brackish water, which helped to identify two variables affecting pH changes. The first one, is that the used brackish water recipe included a relatively large amount of bicarbonate, which acted as a buffer and minimized pH variations. The second one was that the batch electrodialysis of seawater took 5 times longer time, meaning that more protons could migrate from the electrode compartments towards the diluate solution, decreasing its pH. However, from the electric potential curves it was also possible to identify that the limiting conditions were reached during the last moments of the runs, likely causing water splitting and the consequent pH alteration.

Considering these observations, the conditions set for subsequent experiments were improved in terms of reducing concentration polarization and pH changes. Two actions were taken: increasing the flow speeds (from 1.3 in **Chapter 2** to 2.0 cm/s in **Chapter 8**) and lowering the desalination goal (from 1.0 to 2.0 mS/cm, comparing the same chapters). Although the last conditions were not tested for the desalination of seawater, for brackish water they meant a significant reduction in the pH change of the diluate solution: the solutions recovered during the experimentation for Chapter 8 had a final pH of 7.5, instead of the 6.9 measured after the runs of **Chapter 2** (**Figure 2.9**).

Then, as presented in **Figure 10.3**, the desalinated solution at pH=6.9 was as viscous as required without any added HPAM, while the one at pH=7.5 still needed the addition of 0.2 g/L of HPAM 20M Da, which means 84 to 100% polymer savings. The small viscosity difference is attributable to the amount of residual polymer in the solutions, which was 1.0 g/L for the first and 0.5 g/L for the second. Still, there are other rheologic and mechanical properties to be considered when injecting viscous solutions [9,10], so it is likely that HPAM 20M Da or other particular viscosifier would still be required.

10
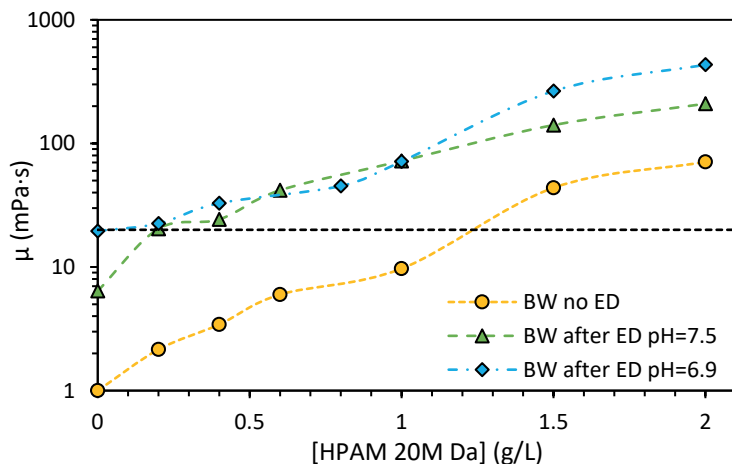
Figure 10.3. Comparison of the viscosities of polymeric solutions vs the concentration of HPAM 20M Da when using different water sources for the preparation. The BW no ED represents the BW formulation without being desalinated, "BW after ED pH=6.9" is the diluate produced in Chapter 2, and "BW after ED pH=6.9" is the diluate produced in Chapter 8. The viscosities were measured at 40°C, and the horizontal line represents a viscosity goal of 20 mPa·s.

Summarizing the findings on reusability of the desalinated water, the results obtained indicate that it would be fit to be reused in the same process without any major complication. As presented in **Figure 10.3**, the residual polymer may or may not contribute significantly to the viscosity gain, but the most relevant feature is that it does not interfere with the hydration of the fresh polymer.

10.2 Case study for electrodialysis application: polymer flooding in a field in the south of Oman

This case study has been addressed during most of the chapters included in this thesis because it is a good example of a polymer-flooding project in a water-scarce area. Since 2014, Riethmuller et al. [11] identified the use of low-salinity makeup water as the most important opportunity when implementing Enhanced Oil Recovery in the area of South Oman, as it had the potential to substantially improve the project economics by reducing polymer consumption.

10.2.1 General information

Oman is the largest oil producer in the Middle East that is not a member of the Organization of the Petroleum Exporting Countries (OPEC). Its national oil company, Petroleum Development Oman (PDO), implemented in 2010 polymer flooding to increase the oil recovery from Marmul field, in the South of Oman (**Figure 10.4.**).

Figure 10.4. Marmul field, located in the South of Oman, approximately 60 km from the nearest coast.

The required polymer injection rate is approximately 13 000 m^3/d at 15 mPa·s polymer viscosity at the wellhead. On site, there is a water-treatment plant which treats the produced water to reduce the amount of oil and the total suspended solids to a prescribed limit to ensure that the optimum polymer-injectivity rate is maintained. The water-treatment plant consists of a two-stage treatment. Primary treatment uses induced-gas-flotation units to remove oil and solids by droplet coalescence, while secondary treatment uses nutshell filters to further remove oil [12,13]. Once treated, the produced water is mixed with the viscosifying polymer and reinjected (**Figure 10.5A**).

The optional process path, as presented along this thesis, is to include a desalination step with electrodialysis. However, the pre-treatment necessary to perform the ED might be different for each situation. For this thesis, it was assumed that an ultrafiltration stage preceded the ED, as has been documented for the pilot plant operating in the Daqing field, in China [14,15]. The UF reduces the concentration of oil, HPAM, and solids suspension in the feed, which helps to reduce the fouling incidence in the IEMs [14]. However, recent literature suggests that it might be possible to perform the ED immediately after the media filtration [16], without the need of UF. This optionality of the UF step has been included in the process diagram included as **Figure 10.5B** and will be therefore considered for the economic analysis.

10
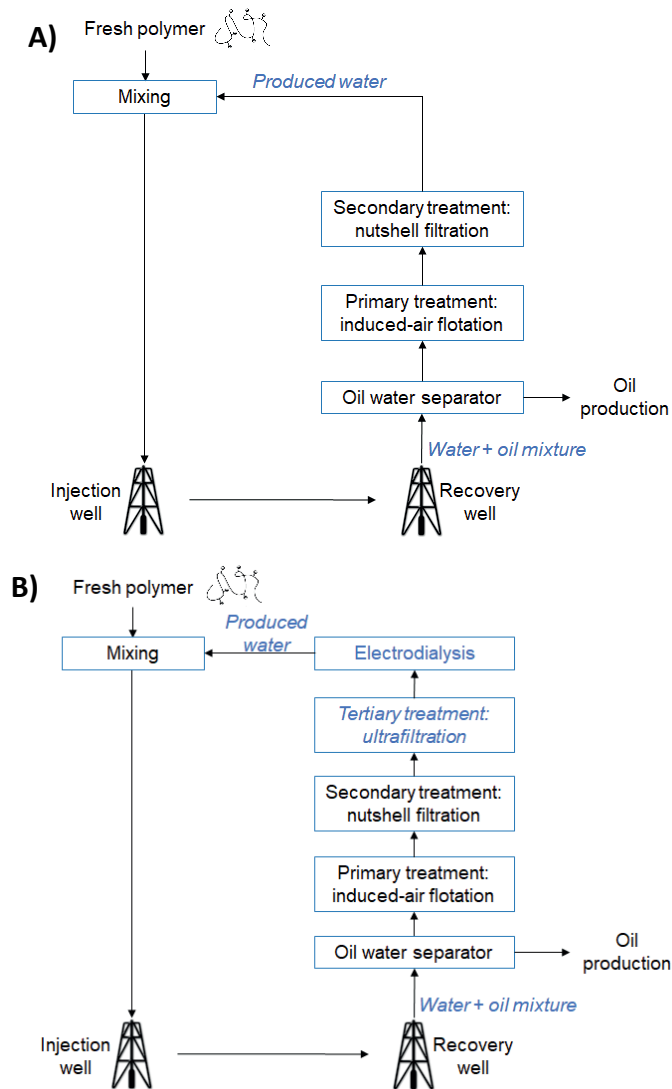
Figure 10.5. *Process diagrams for polymer flooding A) using produced water after secondary treatment, and B) including a desalination step to reduce the salinity of the produced water.*

10.2.2 Economic analysis

The economic analysis was done for 3 case scenarios (A, B, and C), and is presented in **Table 10.2**. These analyses differ in the calculations for ED and UF equipment but consider the same values for polymer savings. For this last aspect, it was assumed that a cubic meter of BW water would need approximately 1.0 kg of HPAM (18-20 million Da) to reach the viscosity goal of 15 mPa·s [17,18]. Considering the injected volume of 13,000 m³/d, and a conservative polymer price of USD $1.5/kg [19], the yearly cost of polymer is estimated as 7.14 million USD (operating 330 days per

year). By reducing the salinity of the water, the amount of polymer needed can be halved, so the polymer savings were estimated as 3.57 million $/year.

Scenario A is based on the results presented in **Chapter 8**, in which electrodialysis was performed at an average current density of 40 A/m², yielding a product flux of 9.1 Lm⁻²h⁻¹, or 0.22 m³m⁻²d⁻¹. This value served to calculate the membrane area of 59,500 m², which would be required to treat the 13,000 m³/d for polymer injection in Marmul. The investment for ED was calculated using this value and assuming a membrane installed cost of $150/m². Then, the CAPEX for ED was obtained by dividing the investment by 6 years, the assumed useful life of the membranes [20]. The OPEX cost was calculated from the energy consumption, as in **Chapter 8**, and the price of electricity in the Dhofar region, in Oman, which is USD $0.05/kWh [21]. The other operational costs are estimated as fixed annual prices for staff ($80k/y) and cleaning chemicals ($100k/y). The result, as can be observed in Table 10.2, is a positive annual balance, with a return-of-investment of 19% (a payback in about 5 years).

Table 10.2. *Economic analysis for 3 scenarios of polymer-flooding implementation*

	Scenario A	Scenario B	Scenario C
Membrane area ED (m²)	59,500	59,500	15,000
Energy consumption ED (kWh/m³)	1.05	1.05	4.2
Investment ED	8,928k	8,928k	2,232k
Investment UF		1,450k	1,450k
Total Investment	**8,928k**	**10,378k**	**3,682k**
CAPEX ED	1,488k	1,488k	372k
CAPEX UF		242k	242k
OPEX ED	405k	405k	1,081k
OPEX UF		204k	204k
Annual polymer saving	3,571k	3,571k	3,571k
Total annual benefit	**1,678k**	**1,232k**	**1,672k**
RoI (%)	**19%**	**12%**	**45%**

Scenario B uses the same values as A for the ED, but also includes the cost of UF. The CAPEX for UF were calculated using information from a commercial supplier website with an investment of 100$/(m³.d) for UF membrane installations (Nanostone, US [22]), and for simplicity a similar lifetime as ED membranes (note: lifetimes may be much longer when ceramic UF membranes are applied). As presented in Table 10.2, the CAPEX and OPEX for the UF plant are adding to the ED one, causing a negative impact for the RoI in this scenario. It is likely that the OPEX costs for UF in Oman would be lower than the one calculated given the relatively

low cost of electricity, but even if it was negligible the scenario would remain less feasible.

Scenario C also includes UF, but the ED calculations are based on optimized process conditions to reduce the CAPEX. According to Chehayeb et al. [23], the costs of BW ED can be minimized by using high flow speeds which would allow to operate at high current densities, thus minimizing the required membrane area. Accordingly, scenario C assumed an ED operation at 160 A/m^2, which remains within the possibilities of commercial electrodialyzers [16], and would reduce the required membrane area to nearly 15,000 m^2, one fourth compared to the previous scenarios. The energy costs for ED was calculated to increase fourfold, a value determined from an extrapolation of our own measurements in **Chapter 8** (8x increase for 160 A/m^2) and the power requirement presented in Fig. 7 of Chehayeb et al. [23] as a function of the applied current density (2x increase). Nevertheless, due to the very high savings in CAPEX for ED, this scenario concludes with very positive numbers for potential annual savings, and an RoI of 45%.

The analysis shows that the economic viability of desalinating PFPW via ED can be subject to some constraints, especially if a pre-treatment is included. All the scenarios would result more positive if the polymer savings were USD $1.2/m^3, which is still a realistic value, for example considering the savings of USD $2.5/m^3 reported by Sparrow et al [16]. Furthermore, it is likely that the operative life of the equipment could be extended to at least 10 years by considering a membrane replacement after 5 or 6 years, which would lower the CAPEX for both UF and ED. The most interesting case, both economically and scientifically, would be to utilize ED without a previous UF stage. Sparrow et al. report that the electrodialyzer Flex EDR Organix E200 from Saltworks, containing hydrocarbon-resistant Ion-Flux membranes, successfully treated PFPW from a Canadian oilfield containing up to 1000 ppm oil-in-water during 60 days [16]. Although the highest oil content of the PFPW fed during this thesis was 40 ppm (**Chapter 7**), its presence did not show negative effects during the ED runs, opening the possibility to test the treatment of feeds with elevated oil content.

Hence, for practical applications two main conclusions coming forward from the research of this thesis and need to be considered:

i. PFPW ED treatment with a UF pretreatment unit. The main advantage is that the fouling on the ion exchange membranes would be minimal. The con is that the economic feasibility of the process becomes more constrained and dependent on the OPEX savings by reducing polymer consumption.

ii. PFPW ED treatment without a UF pretreatment unit. The main advantage of this treatment train is the economical since the CAPEX would be halved.

However, the challenge would be ensuring that the ED plant, and mainly the ion exchange membranes, can operate for long times in the presence of oil and other organic compounds without suffering of major complications.

10.3 Last remarks and outlook

10.3.1 Concerns about fluid velocity

Typical fluid velocities for an electrodialyzer range between 6 to 12 cm/s [24]. However, during the present work, flow velocities were lower, between 1 and 2 cm/s. Still, when the effect of increased velocity was tested in Chapter 8, it did not show further improvement of the limiting current density. This was probably due to the design of the ED-stacks used for that and for most of the research described in this thesis, relying in only two inlets of 0.7mm diameter for feeding both the diluate and concentrate compartments. Still, the fact that promising results were obtained with this stack just emphasizes the opportunities of applying the technology on a larger scale.

10.3.2 Options to treat the concentrate and increase the sustainability of the process

A frequent concern when desalination processes like electrodialysis are employed is what to do with the concentrated solution, i.e. what would be the most adequate brine management approach [25]. Water management technologies and pollution prevention strategies suggest the following hierarchy regarding environmental preferences: i) Minimization, ii) Recycle/reuse and, iii) disposal [26]. In the present case, minimization is addressed by designing the ED process to 90% water recovery, but still the volume of concentrate would be significant. Considering an inland project in which the disposal to the sea/ocean is not an option, the most suitable options would be:

- *Reinjection.* This is the first choice for most of the projects. The concentrated solution could be reinjected in the reservoir, or in deeper wells not connected to it, also known as deep-water injection. In deep well injection, the waste streams are permanently stored in the injection zone, and is a very common technique used by the desalination water treatment plants [27].

- *Evaporation ponds*. The salty solutions are placed in specially designed ponds which are open to the environment, allowing the natural evaporation of the water. Dry salt is the final waste product, which must be characterized and disposed of accordingly as solid waste. This technique is considered as a common solution for brine disposal, especially for inland desalination plants in arid and semi-arid areas [27,28], as well as for the treatment of produced water onsite and offsite [29]. Although evaporation ponds are typically economical,

10

they have the disadvantage of requiring large land areas, of not recovering the water, and having a low process productivity [28]. In addition, their implementation is being even more restricted due to environmental concerns and new legislation being applied worldwide.

- *Thermal treatments to reduce volume until zero-liquid discharge.* There are several thermal processes capable of further concentrating the streams and even achieve zero-liquid discharge goals. One of the most promising from the industrial point of view is the use of falling-film evaporators, which use a vertical tube heat exchanger bundle where the brine is distributed in a falling film along the inside of the tube wall, where condensing steam causes a portion of the salty water to evaporate [30]. An option that is still under development, is the use of super-critical water desalination [31]. The main disadvantage is the energy consumption and CO_2 and other greenhouse gases footprint associated to this [32] which is becoming a major issue for all oil industries.

- *Constructed wetlands*. In onshore locations, where space is available, constructed wetlands are an option to treat industrial effluents and make them fit for reuse or for surface discharge [33,34]. However, in this case the salinity of the water cannot be as high as for the other treatment options due to the sensitivity of the plants. High levels of monovalent ions (especially sodium [35–37]) and remaining polymer or oil related [38] are problems that need to be resolved before the water can be released in open natural systems.

Although all the presented options are widely accepted, they must be selected not only considering the economical but also the sustainability point of view. In **Chapter 8** of this thesis it was discussed how higher recoveries would be beneficial in terms of equipment investment, but the higher salinities in the concentrate might also require the addition of anti-scalants and other chemicals, increasing the environmental impact of the desalination. Therefore, to ensure the sustainability of any project, it is better if the evaluation is performed as a whole, considering both the electrodialysis and the disposal of the brine. By doing so, it might be found that moderate water recoveries are better since the brines produced could be discharged with less or no environmental damage.

The options to perform this analysis are varied. A relatively simple way of analyzing a desalination and concentrate-disposal train would be to calculate its total emissions in CO_2 equivalents [39], although this method might overlook some sustainability aspects. Another option is to perform a life-cycle assessment, which would allow to determine the total emissions during the life-cycle of a project, thus aiding in the selection process [40]. Finally, there are new tools, modelling frameworks, which are being designed for evaluating and comparing desalination treatment trains from both the economical and sustainable points of view [41].

10.3.3 Outlook

The results from this investigation have shown that electrodialysis is a suitable technology to treat synthetic PFPW. Since the experiments were performed far from the producing sites and PFPW would possibly degrade during transport, real produced water could not be tested. However, for the next stage of investigation, it can be suggested to treat real PFPW, and to do so as close as possible to the production site to prevent any polymer or oil degradation during the transport.

Further research would also be advisable for understanding the adsorption of HPAM on ion-exchange membranes with different chemistries. One possibility for doing so would be to use reflectometry [42]. However, meaningful results could only be obtained if the silicon wafers needed to perform this technique can be successfully modified with the same polymers and ion-exchange groups as used in the ion-exchange membranes. Another possibility to use the adsorption of foulants on surfaces is to use self-assembled monolayers with different ending chemical functionalities [43].

Moreover, the balance between water recovery and brine production/brine quality and the use of chemicals (polymer, antiscalants, anti-corrosives, and pH adjustments), UF and other equipment, and total energy (carbon footprint) of the whole treatment train needs to be addressed to fully assess the sustainability of PFPW treatment variants.

10

References

[1]   A.M. Benneker, T. Rijnaarts, R.G.H. Lammertink, J.A. Wood, Effect of temperature gradients in (reverse) electrodialysis in the Ohmic regime, Journal of Membrane Science. 548 (2018) 421–428. doi:10.1016/j.memsci.2017.11.029.

[2]   T. Huang, I. Yu, Correlation of ionic transfer rate in electrodialysis under limiting current density conditions, Journal of Membrane Science. 35 (1988) 193–206. doi:10.1016/S0376-7388(00)82443-6.

[3]   V. Ajao, S. Millah, M. Cristina, H. Bruning, H. Rijnaarts, H. Temmink, Valorization of glycerol / ethanol-rich wastewater to bio fl occulants : recovery , properties , and performance, Journal of Hazardous Materials. 375 (2019) 273–280. doi:10.1016/j.jhazmat.2019.05.009.

[4]   T. Wang, S. Yu, L. an Hou, Impacts of HPAM molecular weights on desalination performance of ion exchange membranes and fouling mechanism, Desalination. 404 (2017) 50–58. doi:10.1016/j.desal.2016.10.007.

[5]   C. Casademont, P. Sistat, B. Ruiz, G. Pourcelly, L. Bazinet, Electrodialysis of model salt solution containing whey proteins : Enhancement by pulsed electric field and modified cell configuration, Journal of Membrane Science. 328 (2009) 238–245. doi:10.1016/j.memsci.2008.12.013.

[6]   L. Firdaous, J.P. Malériat, J.P. Schlumpf, F. Quéméneur, Transfer of monovalent and divalent cations in salt solutions by electrodialysis, Separation Science and Technology. 42 (2007) 931–948. doi:10.1080/01496390701206413.

[7]   H. Guo, L. Xiao, S. Yu, H. Yang, J. Hu, G. Liu, Y. Tang, Analysis of anion exchange membrane fouling mechanism caused by anion polyacrylamide in electrodialysis, Desalination. 346 (2014) 46–53. doi:10.1016/j.desal.2014.05.010.

[8]   H. Guo, F. You, S. Yu, L. Li, D. Zhao, Mechanisms of chemical cleaning of ion exchange membranes: A case study of plant-scale electrodialysis for oily wastewater treatment, Journal of Membrane Science. 496 (2015) 310–317. doi:10.1016/j.memsci.2015.09.005.

[9]   B. Wei, L. Romero-Zeron, D. Rodrigue, Mechanical Properties and Flow Behavior of Polymers for Enhanced Oil Recovery, Journal of Macromolecular Science Part B-Physics. 53 (2014) 625–644. doi:Doi 10.1080/00222348.2013.857546.

[10]   E.C.M. Vermolen, M. Pingo-almada, B.M. Wassing, D.J. Ligthelm, S.K. Masalmeh, H. Mohammadi, G.R. Jerauld, M. Pancharoen, Low-Salinity Polymer Flooding : Improving Polymer Flooding Technical Feasibility and Economics by Using Low-Salinity Make-up Brine, The SPE Imroved Oil Recovery Symposium-USA. (2014) 15. doi:10.2118/153161-MS.

[11]   G. Riethmuller, A. Abri, N. Al Azri, G. Stapel, S. Nijman, W. Subhi, R. Mehdi, Opportunities and challenges of polymer flooding in heavy oil reservoir in south of Oman, Society of Petroleum Engineers - SPE EOR Conference at Oil and Gas West Asia 2014: Driving Integrated and Innovative EOR. (2014) 799–808. doi:10.2118/169737-ms.

[12]   F. Plans, B.A. Amri, S. Nofli, J. Van Wunnik, H.F. Jaspers, S. Harthi, K. Shuaili, K. Cherukupalli, R. Chakravarthi, P. Development, G.W. Asia, Polymer Flooding in a Large Field in South Oman — Results and Plans, (2013) 82–85.

[13]   G. Jing, X. Wang, H. Zhao, Study on TDS removal from polymer-flooding wastewater in crude oil: extraction by electrodialysis, Desalination. 244 (2009) 90–96. doi:10.1016/j.desal.2008.04.039.

[14]   J. Guolin, W. Xiaoyu, H. Chunjie, The effect of oilfield polymer-flooding wastewater on anion-exchange membrane performance, Desalination. 220 (2008) 386–393. doi:10.1016/j.desal.2007.03.010.

[15]   X. Qiao, Z. Zhang, J. Yu, X. Ye, Performance characteristics of a hybrid membrane pilot-scale plant for oilfield-produced wastewater, Desalination. 225 (2008) 113–122. doi:10.1016/j.desal.2007.04.092.

[16]   B. Sparrow, A. Ebsary, D. Mandel, M. Man, An advanced electrochemical system for EOR produced water desalination and reduced polymer consumption, in: Proceedings - SPE Symposium on Improved Oil Recovery 2018, SPE, Tulsa, Oklahoma, 2018.

[17]   A.R. Al-Hashmi, T. Divers, R.S. Al-Maamari, C. Favero, A. Thomas, Improving polymer flooding efficiency in Oman oil fields. Paper SPE-179834-MS, in: SPE EOR Conference at Oil and Gas West Asia Held in Muscat, Oman, 21–23 March 2016., SPE, Muscat, 2016: p. 18.

[18]   P.A. Sosa-Fernandez, J.W. Post, H. Bruning, F.A.M. Leermakers, H.H.M. Rijnaarts, Electrodialysis-based desalination and reuse of sea and brackish polymer-flooding produced water, Desalination. 447 (2018) 120–132. doi:10.1016/j.desal.2018.09.012.

[19]   A.M. AlSofi, M.J. Blunt, Polymer flooding design and optimization under economic uncertainty, Journal of Petroleum Science and Engineering. 124 (2014) 46–59. doi:10.1016/j.petrol.2014.10.014.

[20]   H. Strathmann, A. Grabowski, G. Eigenberger, Ion-exchange membranes in the chemical process industry, Industrial and Engineering Chemistry Research. 52 (2013) 10364–10379. doi:10.1021/ie4002102.

[21]   Authority for Electricity Regulation Oman, Permitted tariffs, (2020). https://www.aer.om/en/tariffs (accessed April 18, 2020).

[22]   Nanostone, Nanostone membranes, (2017). https://www.nanostone.com/ceramic-membranes-gwi-ad-2017 (accessed May 16, 2020).

[23]   K.M. Chehayeb, D.M. Farhat, K.G. Nayar, J.H. Lienhard, Optimal design and operation of electrodialysis for brackish-water desalination and for high-salinity brine concentration, Desalination. 420 (2017) 167–182. doi:10.1016/j.desal.2017.07.003.

[24]   H. Strathmann, Ion-Exchange Membrane Processes in Water Treatment, in: Sustainability Science and Engineering, Elsevier, 2010: pp. 141–199. doi:10.1016/S1871-2711(09)00206-2.

[25]   A.S. Sánchez, Â.P. Matos, Desalination Concentrate Management and Valorization Methods, Elsevier Inc., 2018. doi:10.1016/B978-0-12-809240-8.00009-5.

[26]   S. Jiménez, M.M. Micó, M. Arnaldos, F. Medina, S. Contreras, State of the art of produced water treatment, Chemosphere. 192 (2018) 186–208. doi:10.1016/j.chemosphere.2017.10.139.

[27]   A.G. (Tony) Fane, R. Wang, Y. Jia, Membrane Technology: Past, Present and Future, in: L.K. Wang, J.P. Chen, Y.-T. Hung, N.K. Shammas (Eds.), Membrane and Desalination Technologies, Humana Press, 2011: pp. 1–45. doi:10.1007/978-1-59745-278-6.

[28]   A. Pérez-González, A.M. Urtiaga, R. Ibáñez, I. Ortiz, State of the art and review on the treatment technologies of water reverse osmosis concentrates, Water Research. 46 (2012) 267–283. doi:10.1016/j.watres.2011.10.046.

[29]   E.T. Igunnu, G.Z. Chen, Produced water treatment technologies, International Journal of Low-Carbon Technologies. 9 (2014) 157–177. doi:10.1093/ijlct/cts049.

[30]   D.P. Bjorklund, D. Kersey, G.J. Mandigo, C. Tiwari, Method for recycling deoiled water using counterflow falling-film evaporators, US9120685B2, 2015.

[31]   S. van Wyk, S.O. Odu, A.G.J. van der Ham, S.R.A. Kersten, Design and results of a first generation pilot plant for supercritical water desalination (SCWD), Desalination. 439 (2018) 80–92. doi:10.1016/j.desal.2018.03.028.

[32]   T. Tong, M. Elimelech, The Global Rise of Zero Liquid Discharge for Wastewater Management: Drivers, Technologies, and Future Directions, Environmental Science and Technology. 50 (2016) 6846–6855. doi:10.1021/acs.est.6b01000.

[33]   S. Wu, S. Wallace, H. Brix, P. Kuschk, W.K. Kirui, F. Masi, R. Dong, Treatment of industrial effluents in constructed wetlands: Challenges, operational strategies and overall performance, Environmental Pollution. 201 (2015) 107–120. doi:10.1016/j.envpol.2015.03.006.

[34]   G. Ji, T. Sun, Q. Zhou, X. Sui, S. Chang, P. Li, Constructed subsurface flow wetland for treating heavy oil-produced water of the Liaohe Oilfield in China, Ecological Engineering. 18 (2002) 459–465. doi:10.1016/S0925-8574(01)00106-9.

[35]   Z. Qian, H. Miedema, L.C.P.M. de Smet, E.J.R. Sudhölter, Modelling the selective removal of sodium ions from greenhouse irrigation water using membrane technology, Chemical Engineering Research and Design. 134 (2018) 154–161. doi:10.1016/j.cherd.2018.03.040.

10

[36]   J.M. Pardo, F.J. Quintero, Plants and sodium ions: keeping company with the enemy, Genome Biology. 3 (2002) 1–4.

[37]   A. Läuchli, S.R. Grattan, Plant growth and development under salinity stress, in: M.A. Jenks (Ed.), Advances in Molecular Breeding Toward Drought and Salt Tolerant Crops, Springer, 2007: pp. 1–32.

[38]   T. V Wagner, J.R. Parsons, H.H.M. Rijnaarts, P. De Voogt, A.A.M. Langenhoff, T. V Wagner, J.R. Parsons, H.H.M. Rijnaarts, P. De Voogt, Technology A review on the removal of conditioning chemicals from cooling tower water in constructed wetlands, Critical Reviews in Environmental Science and Technology. 48 (2019) 1094–1125. doi:10.1080/10643389.2018.1512289.

[39]   P.G. Youssef, R.K. Al-dadah, S.M. Mahmoud, Comparative Analysis of Desalination Technologies, Energy Procedia. 61 (2014) 2604–2607. doi:10.1016/j.egypro.2014.12.258.

[40]   R. Salcedo, E. Antipova, D. Boer, L. Jiménez, G. Guillén-gosálbez, Multi-objective optimization of solar Rankine cycles coupled with reverse osmosis desalination considering economic and life cycle environmental concerns, Desalination. 286 (2012) 358–371. doi:10.1016/j.desal.2011.11.050.

[41]   J.M. Wreyford, J.E. Dykstra, K. Wetser, H. Bruning, H.H.M. Rijnaarts, Modelling framework for desalination train comparison, Under Revision. (2020) 1–35.

[42]   J.C. Dijt, M.A.C. Stuart, G.J. Fleer, Reflectometry as a tool for adsorption studies, Advances in Colloid and Interface Science. 50 (1994) 79–101. doi:10.1016/0001-8686(94)80026-X.

[43]   A.E. Contreras, Z. Steiner, J. Miao, R. Kasher, Q. Li, Studying the role of common membrane surface functionalities on adsorption and cleaning of organic foulants using QCM-D, Environmental Science and Technology. 45 (2011) 6309–6315. doi:10.1021/es200570t.

10

Summary

This thesis explores the use of electrodialysis, an electrical and membrane-based technology, to partially desalinate polymer-containing produced water (PFPW) generated in the oil and gas industry. **Chapter 1** includes an introduction to polymer flooding, explains its water needs in terms of quality and quantity, and enlists some possible treatments to reach the desired water quality. It is also explained how, by partially desalinating PFPW while retaining the viscosifying polymer, electrodialysis would allow reusing the water for polymer flooding, while significantly decreasing the amount of new polymer to be added when preparing viscous solutions. The chapter also includes some possible constraints for the implementation and enlists the research questions that are answered in the subsequent chapters.

In **Chapter 2,** we assessed electrodialysis to desalinate PFPW generated in different scenarios and evaluated the reuse of the desalted water to confect the polymer-flooding solution. The experimental work involved desalting two kinds of synthetic PFPW solutions, one with relatively low salinity (TDS=5000 mg/L, brackish PFPW), and another with high salinity (TDS= 32,000 mg/L, sea PFPW), at two different temperatures, and later reusing the desalted solution to prepare viscous solutions. The analysis for the ED-step included the effects of feed composition and temperature on water transport, energy consumption, and current efficiency. It was found that the presence of polymer did not significantly influence the water transport rate nor the specific energy consumption for the seawater cases, but had a measurable effect when desalting brackish water at 20°C. It was also found that some polymer remained in the stack, the loss occurring faster for the brackish PFPW. Still, both kinds of reused PFPW probed adequate to be employed as a basis for preparing polymer solutions.

Chapter 3 addressed the selective removal of divalent cations from PFPW through a variety of operational conditions. The chapter starts by explaining how the presence of multivalent ions in PFPW hampers its recycling mainly because i) they increase the risk of scaling and reservoir souring (sulfate), ii) they interfere with the viscosifying effect of the fresh polyelectrolyte. Then, the chapter explains the experimental work, which consisted of batch experiments run in an electrodialysis-stack. Synthetic PFPW solutions containing a mixture of monovalent and divalent ions were desalted at four different current densities and three different temperatures. Additionally, the effect of the dissolved polymer on the removal was assessed by performing half of the experiments on polymer-containing solutions and half of them on solutions without it. The results demonstrated that it is possible to achieve preferential removal of divalent ions (calcium, magnesium, sulfate) through electrodialysis, especially when employing low current densities (24 A/m²)

and high temperature (40°C). The presence of polyelectrolyte did not significantly affect the removal rate of divalent ions. It was concluded that the precise application of ED to minimize concentrations of divalent ions in PFPW is a possible a more effective way for water and polymer recycling in enhanced oil recovery situations, then the use of other non-selective desalination technologies.

Chapters 4 and **5** address the influence of the feed composition on the fouling formed on anion and cation exchange membranes, respectively. The composition of the solution, which includes various dissolved salts, partially hydrolyzed polyacrylamide (HPAM), crude oil, and surfactants. Electrodialysis experiments were performed to desalinate feed solutions with different compositions, aiming to distinguish between their individual and combined effects. The solutions contained diverse mono- and divalent ions. The analysis included data collected during the desalination and characterization of the fouled AEMs by diverse analytical techniques. **Chapter 4** shows that HPAM produced the most severe effects in terms of visible fouling and increase of resistance. This polyelectrolyte fouls the AEM by adsorbing on its surface and by forming a viscous gel layer that hampers the replenishment of ions from the bulk solution. Ca and Mg have a large influence on the formation of thick HPAM gel layers, while the oily compounds have only a minimal influence acting mainly as a destabilizing agent. The membranes showed scaling consisting of calcium precipitates. The effects of the gel layer were minimized by applying current reversal and foulant-free solutions. Regarding the CEMs, **Chapter 5** showed that fouling was detected on most CEMs and occurred mainly in the presence of the viscosifying polyelectrolyte. Under normal pH conditions (pH~8), the polyelectrolyte fouled the concentrate side of the CEMs, as expected due to electrophoresis. Precipitation occurred mostly on the opposite side of the membrane, with different morphology depending on the feed composition.

In **Chapter 6**, we evaluated the application of pulsed electric field (PEF) during the electrodialysis of PFPW, that is, to supply a constant current during a short time (pulse) followed by a period without current (pause). This operation mode aimed to improve process performance by reducing fouling incidences. The experimental work consisted of ED batch runs in a laboratory-scale stack containing commercial ion-exchange membranes. Synthetic PFPW was desalinated under different operating regimes until a fixed amount of charges was passed. After each experiment, a membrane pair was recovered from the stack and analyzed through diverse techniques. The application of PEF improved the ED performance in terms of demineralization rate and energy consumption, the latter having reductions of 36% compared to the continuous mode. In general, the shorter the pulses, the higher the demineralization rate, and the lower the energy consumption. Regarding the application of different pause lengths, longer pauses yielded lower energy consumptions but also lower demineralization. Amorphous precipitates composed

of polymer and calcium fouled on the anion and cation exchange membranes, independently of the applied current regime, but in a moderate amount. Finally, the chapter related the observed effects of PEF application to the electrophoresis and diffusion of HPAM. It showed that PEF is a sound option to enhance the desalination of PFPW.

Under the premise that process performance is limited by fouling occurring on the anion-exchange membranes, **Chapter 7** aimed to correlate the properties of different AEMs with their performance while desalinating PFPW. The study made use of six stacks containing different homogeneous, commercially available AEMs, which were employed to desalinate synthetic PFPW during 8-days ED experiments operated in reversal mode. The AEMs recovered from the stacks were analyzed in terms of water uptake, ion-exchange capacity, permselectivity, and area resistance, and compared against virgin AEMs. Relatively small changes were measured for most of the parameters evaluated. For most AEMs, the water uptake and resistance increased, while the IEC and permselectivity decreased during operation. Ultimately, AEMs with high area resistance were linked to the fast development of limiting current conditions in the stack, so this property turned out to be the most relevant when desalinating PFPW.

Considering the most favorable conditions assessed in previous chapters, **Chapter 8** addresses the experimental evaluation of different operational conditions to increase water recovery while keeping a low energy consumption. The experimental work included the evaluation of applying a continuous constant voltage operation versus the use of PEF, as well as comparing the performance of stacks composed by either aromatic or aliphatic membranes. The results were analyzed in terms of operative time, water recovery, and energy consumption and serve to indicate under which conditions specific types of membranes would be preferred. At last, the collected data was used to perform an economic analysis. It indicated that although further optimization should be possible, achieved settings already made ED desalination of polymer-flooding produced water, a sound case from an economic point of view.

Chapter 9 assessed the contribution of the desalination and the pumping energy to the total energy consumption desalinating streams with high viscosities, i.e., above the one of water (1 cP). The assessment included the influence of other important parameters, namely the salinity of the feed and the type and thickness of the spacer. It was found that the type of spacer did not significantly influence the energy required for desalination. Regarding the pumping energy, it was higher than predicted by models found in the literature, but in most cases, it was minimal compared to the energy for desalination. Only when using very thin spacers (300 μm) or very viscous feeds (12 cP) energy for pumping equalized that of desalination of feeds with 1 g/L NaCl. Thus, it was concluded that the main contributor to the

energy consumption of these viscous solutions is still the desalination energy, and it is recommended to use spacers of a thickness between 450 and 720 μm to keep pumping energy low.

At last, **Chapter 10** starts by recalling the main areas of investigation that were defined in **Chapter 1** (influence of polymer-flooding produced water composition and conditions, removal of multivalent ions, fouling, preservation of polymer integrity) and discuss the findings presented in this thesis. Then, a full-scale polymer flooding case is introduced and based on the results of the previous chapters, an economic analysis performed. In the three scenarios analyzed, introducing a produced water desalination step would have a positive return on investment. In two of them, the payback time is sooner than six years. Finally, the chapter includes some last remarks about the investigation and recommendations for future research.

Acknowledgments

My dear officemates from the "Office of Love", going to work was a pleasure mostly because of you. It was great to come and always having someone to hug (joyful times before corona). **Rik**, thanks for taking me on my first cycling adventures outside Leeuwarden. **Jaapie**, thanks for letting me take awkward pictures of you and for making me laugh, a lot. **Karine**, thanks a lot for organizing many enjoyable office dinners and other nice evenings, and for preparing Tres Leches and sharing ;-). **Maarten**, thanks a lot for increasing the scientific interest in the office, for the telescope nights, and for being blond :D. **Stan**, thanks for always sharing your happiness, enthusiasm, and beers with us. **Steffen**, thanks a lot for making my desk look clean and ordered, and for the very warm hugs. (**Nimmy**)x20, I enjoyed our talks about underwear and going together to zumba classes. But above all thanks a lot for introducing us to **Haniel** and his cooking skills :D. **Mariana the II**, thanks for encouraging me and Maarten to learn Dutch, and for sharing your delicious Portuguese food. **Ricardo** and **Chris**, thanks for keeping the work environment in balance and for sharing fresh plant fertilizer. **Cao Vinh**, **Alicia** and **Tallie**, I wish you can enjoy your office time as much as I did. And to my officemates for the last months, **Casper**, **Rebe**, and **Yang**, thanks for keeping the spirit up.

I am also very grateful to the students who chose to work in my project. I hope you enjoyed and learnt as much as I did. **Sjirk**, your fast-paced way of working forced me to be more efficient, thanks a lot for that. **Biw**, thanks a lot for being so dedicated and thoughtful. To **Said**, for always keeping your enthusiasm. **Loc**, for being resourceful in solving all kinds of issues, and for teaching me a bit about your culture. **Harrison**, thanks for being very patient when I had low motivation to work. Thank you **Apurva** for the hard work, and to you **Maria** for not letting my "flojera" to invade you :p.

This thesis exists also thanks to the work of the technical team. **Harm**, you are the best. Thanks a lot for not letting me worry about the electronics in my setup. I am also very thankful to **Jan T.**, **Ernst**, **John**, and **J.J.** for supporting me always that I needed. However, I acknowledge that I gave much more work to the analytical team. I understand that you don't miss the PSOS samples. I am very grateful to **Mieke**, **Marianne**, **Lisette**, **Jelmer**, and **Jan Willem** for all the effort you put on running those analyses. And thanks also to **Wim**, **Janneke**, and **Gerrit** for making sure that all the resources were always available.

Something I really appreciate from Wetsus was the will of many people to help in different projects. I want to acknowledge to the people organizing and participating in the fouling meetings: **Caroline**, **Michel**, **Antoine K.**, **Natascha**, **Barbara**, **Rose**, **Xiaoxia**, **Diego**, **Ettore**, **Victor A.**, for listening to my presentations and sharing their interesting ideas. I also would like to thank to the members of the Desalination

theme, especially to **Willem van Baak**, **Albert Verver** and **Lucian Boels** for their valuable input for the project.

Some people had the (bad) luck to be positioned close to my setup. I hope I did not distract you too much. **Victor T.** and **Qingdian**, I am sorry for scaring you sometimes. There must be something in your spot. **Gosia**, thanks a lot for sharing your ED-tips and especially for getting a new 6-compartment cell. **Gijs**, thanks for all your practical advice, especially during the first months when I had no idea of what equipment I would need. **Diego**, thanks a lot for your help with Autolab. My files are still saved inside your folder. **Hakan**, I am glad you were using auditive protection while experimenting with the ultrasound. I wasn't. **Victor A.**, thanks a lot for the time and patience when teaching me how to use new equipment, but especially for not invading my setup table ;-). And to my dear friend **Louis**, thanks a lot for the nice talks while running our experiments, for the morning coffees, the late piano concerts, and for your genuine interest in understanding and helping me with my project. Your friendship has been one of the highlights of my PhD period.

I also would like to thank to the people who gave me reasons to leave the Wetsus buildings during the evenings and try new things. **Marianne** and **Natascha**, thanks a lot for inviting me to do sports with you and encouraging me to go out my comfort zone. Thanks also **Hakan** and **Gijs** for pushing me to experience a bit of speed in the racing bike. **Nimmy**, **Geert-Jan**, **Chris** and **Qingdian**, thanks a lot for the exciting squash matches. **Louis**, I really enjoyed our few but intensive tennis trainings, but my favorite sportive moment with you was doing pull-ups. I think of it and I cry with laughter again. And in the last year, I finally found my perfect gym-mates: **Sebastian Castaño** and **Amiga**, it was sooo fun to train with you. Many thanks for pulling me to stay active even during winter and in the busiest months of my PhD.

I also have many nice memories with my Wetsus colleagues outside the working hours. **Rebe**, thanks for inviting me to your birthday parties despite I did not always follow the dress-code ;-). **Sandra**, I enjoyed baking colorful cakes and cookies with you. We still need to figure out where we actually met. **Sebastian**, thank you for letting me use your laundry machine when mine broke. We also had good laughs while editing Hector's stukje, thanks a lot for that. **Gonçalo**, it was fun to discover our communication style by analyzing our shopping behavior. **Thomas**, thanks for the fun game-evenings. Maybe next time you won't have to explain the rules again. **Carlo**, I really enjoy your sense of humor ;-). **Catarina**, thanks a lot for the tomato plant, it is still alive :D. **Zexin**, it was so fun to explore Perth and Sydney with you. I am very sorry I did not take better pics :(. **Rita** and **Angel**, thanks for the hilarious moments while filming, specially the toilet scene. And many thanks also to **Fabian**, **Philipp W.**, **Philipp K.**, **Wokke**, **Ettore**, **Caspar**, **Prashant**, **Michele**, **Jan de Groot**

and **Roel** for many other fun moments outside Wetsus, either at house-parties or Scooters or at the city center.

I would like to have a special mention for the Mexican people. **Hectorito**, I had so much fun with you. It did not matter if we were exploring the Netherlands, or planning the trip to Mexico or just watching movies together, I always had a great time with you. It was an honor being your paranymph. **Mariana the I**, thanks a lot for the good advices and for sharing your positive energy and enthusiasm. **Lucia**, thanks a lot for starting the "Mexican lunch" tradition, for my poblano plant, but above all, for my birthday piñata. And **Sara**, thanks a lot for your invaluable help in times of need.

I want to thank specially to the Wetsus people who dared to go to Mexico with Héctor and me. I really appreciate your trust and enthusiasm. For me it was a dream come true to share a bit of our country and culture. And it also made me very happy to remain close to all of you during the rest of my PhD.

I am also grateful to my ETE colleagues **Dainis**, **Joeri**, **Rosanne**, **Farzaneh**, **Ilse**, **Laura** (alarm), **Tania**, **Adrian**, **Thomas** and **Carlos** for the organization of our exciting study-trip. I enjoyed meeting you and feeling the connection to ETE. I also want to thank to **Liesbeth** for her support during my PhD time.

I would also like to thank to my new colleagues and friends from EMI and the MST cluster. Thank you **Tymen**, **Heleen**, **Alberto** and **Monica** for the warm welcoming. **Harmen**, it was a real pleasure to work together during the quarantine. You have no idea how much I enjoyed and value our long video-chats that covered everything from scientific work to finding the right emoji for a meeting. **Andrew**, you showed up at the right time. Thanks a lot for approaching, for your friendship and for including me in your weekend plans. It has meant a lot to me. **Angela**, thanks a lot for welcoming me so warmly and infecting me with your passion and enthusiasm. **Arputha** and **Julia**, thanks a lot for distracting me and at the same time cheering me up.

And, of course, my dear paranymphs. Did you think I would forget you? **Raquelita**, you were my first friend in Leeuwarden. We went cycling to the lakes and it rained on us 2 or 3 times. And although that was an accurate indication of how our future adventures would be, you always stayed by my side. I am very happy you will also do on the day of my defense. **Shu**, I guess our thing started with an orange pullover. It was a sweet gesture that I did not expect but meant something to me. From there our relationship flourished, sometimes with violence involved, but you resisted and even liked it. In the last months of my PhD, our roles inverted and instead of me pulling you to the classes it was you who pulled me to go. Thanks a lot for all the

fun moments, for the very long talks, for the advices and for constantly keeping an eye on me. Las quiero amigas.

Esta tesis no existiría sin el apoyo constante de mi familia y amigos. **Ma**, **pa**, muchas gracias por darme todas las herramientas necesarias para vivir haciendo lo que me gusta. **Gus**, gracias por apoyarme en todas mis aventuras. A todos mis tíos, tías, primos y primas, de Puebla y de Santiago, muchas gracias por estar ahí para mí. Aún a la distancia siento su cariño que me motiva a seguir superándome. Y a **Andrés**, que estuvo conmigo desde que decidí cambiar el rumbo y retomar los estudios, también te doy mi más sincero agradecimiento. Sentí tu apoyo constante durante todo el curso de mi PhD, y nuestros viajes juntos fueron una constante fuente de inspiración. Esta tesis también existe gracias a ti.

About the author

Paulina Abigail Sosa Fernández was born on October 15, 1986 in Puebla, México. She obtained her bachelor's degree in Chemical Engineering in 2009 from the Universidad de las Americas, Puebla, after defending her thesis work about the dynamic behavior of Petlyuk distillation columns. She began her professional career by joining Schlumberger, a leading company in the oil and gas industry. During her 4+ years in the company she was based in Villahermosa, Mexico, where she performed first as field cementing engineer and later as engineer in charge of operations.

Pursuing her desire to perform as a downstream processing engineer, in 2013 she obtained a full scholarship and joined the Erasmus Mundus Master in Membrane Engineering (EM3E). Her track included studies in Montpellier (France), Prague (Czech Republic) and Lisbon (Portugal), specializing in biotechnology, food and health applications. She performed her thesis work at the Universidade Nova de Lisboa, where she experimented with various technologies for the recovery and purification of bio-succinic acid.

In 2016, Paulina started her PhD in the Environmental Technology (ETE) department of Wageningen University, but carrying out her work at Wetsus, in Leeuwarden. The results of her investigation are presented in this thesis. In March 2020, she started working as researcher at the European Membrane Institute (EMI) in Enschede.

List of publications

1. **P.A. Sosa-Fernandez**, J.W. Post, H. Bruning, F.A.M. Leermakers, H.H.M. Rijnaarts, Electrodialysis-based desalination and reuse of sea and brackish polymer-flooding produced water, Desalination. 447 (2018) 120–132. doi:10.1016/j.desal.2018.09.012.

2. **P.A. Sosa-Fernandez**, J.W. Post, F.A.M. Leermakers, H.H.M. Rijnaarts, H. Bruning, Removal of divalent ions from viscous polymer-flooding produced water and seawater via electrodialysis, J. Memb. Sci. 589 (2019) 117251. doi:10.1016/j.memsci.2019.117251.

3. **P.A. Sosa-Fernandez**, S.J. Miedema, H. Bruning, F.A.M. Leermakers, H.H.M. Rijnaarts, J.W. Post, Influence of solution composition on fouling of anion exchange membranes desalinating polymer-flooding produced water, J. Colloid Interface Sci. 557 (2019) 381–394. doi:10.1016/j.jcis.2019.09.029.

4. **P.A. Sosa-Fernandez**, J.W. Post, M.S. Ramdlan, F.A.M. Leermakers, H. Bruning, H.H.M. Rijnaarts, Improving the performance of polymer-flooding produced water electrodialysis through the application of pulsed electric field, Desalination. 484 (2020). https://doi.org/10.1016/j.desal.2020.114424.

5. **P.A. Sosa-Fernandez**, J.W. Post, A. Karemore, H. Bruning, H.H.M. Rijnaarts, Desalination of polymer-flooding produced water at increased water recovery and minimized energy, Industrial & Engineering Chemistry Research (2020). https://dx.doi.org/10.1021/acs.iecr.0c02088.

SENSE

Netherlands Research School for the
Socio-Economic and Natural Sciences of the Environment

D I P L O M A

for specialised PhD training

The Netherlands research school for the
Socio-Economic and Natural Sciences of the Environment
(SENSE) declares that

Paulina Abigail
Sosa Fernández

born on 15 October 1986 in Puebla, México

has successfully fulfilled all requirements of the
educational PhD programme of SENSE.

Leeuwarden, 11 September 2020

Chair of the SENSE board

Prof. dr. Martin Wassen

The SENSE Director

Prof. Philipp Pattberg

The SENSE Research School has been accredited by the Royal Netherlands Academy of Arts and Sciences (KNAW)

K O N I N K L I J K E   N E D E R L A N D S E
A K A D E M I E   V A N   W E T E N S C H A P P E N

The SENSE Research School declares that **Paulina Abigail Sosa Fernández** has successfully fulfilled all requirements of the educational PhD programme of SENSE with a work load of 46.2 EC, including the following activities:

SENSE PhD Courses

o   Environmental research in context (2016)
o   Research in context activity: 'Organization of consultancy trip to Chile' (2019)

Other PhD and Advanced MSc Courses

o   Brain training, Wageningen Graduate Schools (2016)
o   Presentation skills, Wetsus (2016)
o   Supervision of students, Wetsus (2016)
o   Communication styles, Wetsus (2016)
o   Illustrations for scientific publications, Wetsus (2016)
o   Bath Electrochemistry Winter School, University of Bath (2017)
o   Water Treatment Workshop, University of Kentucky (2017)
o   Design of Experiments, Wetsus (2017)
o   Talents, Wetsus (2017)
o   Scientific Writing, Wageningen Graduate Schools (2019)

Management and Didactic Skills Training

o   Organisation of the International Conference on Membranes in the Production of Drinking and Industrial Water (MDIW), Wetsus (2017)
o   Supervising three MSc students with thesis (2017-2018)

Selection of Oral Presentations

o   *Preferential removal of multivalent cations in the desalination of polymer-flooding produced water via electrodialysis*. International Congress on Membranes and Membrane Processes, 29 July 29 -4 August 2017, San Francisco, United States of America
o   *Electrodialysis-based desalination and reuse of polymer flooding produced water*. Conference on Membrane and Electro-membrane Processes (MELPRO), 20-23 May 2018, Prague, Czech Republic
o   *Desalination of produced water via electrodialysis*. Technological approaches for future (waste) water treatment and resource recovery, 6 March 2019, Santiago, Chile
o   *Application of pulsed electric field during the electrodialysis of polymer-flooding produced water: effects on performance and fouling*. 4th International Conference on Desalination using Membrane Technology, 1-4 December 2019, Perth, Australia

SENSE coordinator PhD education

Dr. ir. Peter Vermeulen